Award Number:	**DE- NT0003894**
Submitting Organization:	**UTC Power Corporation**
Organization Address:	**195 Governor's Highway** **South Windsor, CT 06074**
Sub-recipient Organization:	**Delphi Automotive Systems, LLC**
Organization Address:	**2151 W. Thompson Road** **Fenton, MI 48430**

Project Title:	**SECA Coal-Based Systems – UTC Power**
Principal Author:	**Michael Gorman – UTC Power**
Principal Author :	**Rick Kerr – Delphi Automotive Systems LLC**

Report Title:	**UTC Power/Delphi SECA CBS Final Report**
Type of Report:	**Final Scientific/Technical Report**
Reporting Period Start Date:	**1 Oct 2008**
Reporting Period End Date:	**31 Mar 2013**
Date of Report:	**June 2013**

Acknowledgment
This Final Report and results described herein were prepared with the support of the U.S. Department of Energy, under Award No. DE-NT0003894.

Abstract

The subject report summarizes the results of solid oxide fuel cell development conducted by UTC Power in conjunction with Delphi Automotive Systems under a cost-share program with the Department of Energy's National Energy Technology Laboratory from October 2008 through March of 2013. Over that period Delphi Automotive Systems developed a nearly four times larger area solid oxide fuel cell stack capable of operating on pre-reformed natural gas and simulated coal gas with durability demonstrated to 5,000 hours and projected to exceed 10,000 hours. The new stack design was scaled to 40-cell stacks with power output in excess of 6.25kW. Delphi also made significant strides in improving the manufacturability, yield and production cost of these solid oxide fuel cells over the course of the program.

Concurrently, UTC Power developed a conceptual design for a 120 MW Integrated Gasification Fuel Cell (IGFC) operating on coal syngas with as high as 57% Higher Heating Value (HHV) efficiency as a measure of the feasibility of the technology. Subsequently a 400 kW on-site system preliminary design with 55% Lower Heating Value (LHV) efficiency operating on natural gas was down-selected from eighteen candidate designs. That design was used as the basis for a 25kW breadboard power plant incorporating four Delphi cell stacks that was tested on natural gas before the program was discontinued due to the sale of UTC Power in early 2013.

Though the program was cut short of the endurance target of 3,000 hours, many aspects of the technology were proven including: large-area, repeatable cell manufacture, cell stack operation on simulated coal gas and natural gas and integrated power plant operation on natural gas. The potential of the technology for high efficiency stationary electric power generation is clear. Acceptable production costs, durability, and reliability in real world environments are the remaining challenges to commercialization.

Table of Contents

1. Executive Summary

Objectives:

In October of 2008, UTC Power, in conjunction with subcontractors Delphi Automotive Systems LLC, United Technologies Research Center and Battelle/Pacific Northwest National Lab started a development effort under DOE Award #DE- NT0003894 with the following primary objectives:

1. Scale-up a Solid Oxide Fuel Cell (SOFC) area to a size suitable for use in a 25 to 50 kW stack
2. Assemble large area fuel cells into 25 to 50 kW stacks
3. Develop a test stand capable of testing a fuel cell stack up to 50 kW
4. Develop preliminary design of a 250-1,000 kW solid oxide fuel cell (SOFC) power module operating on either pre-reformed natural gas or coal syngas
5. Develop conceptual design of a >100 MW baseload SOFC power plant operating on coal syngas with a target efficiency of 50 percent (HHV) that separates greater than 90 percent of the carbon in the coal feedstock

The effort to complete the above objectives continued through March 31, 2013 from Phase I to Phase II and finally Phase IIb with results that follow.

Results:

1. Scale-up a Solid Oxide Fuel Cell (SOFC) area to a size suitable for use in a 25 to 50 kW stack

   Delphi developed a Generation 4 stack design in 2009 with a more commercially attractive cell area of 403 cm2 compared with the previous generation cell area of 105 cm2. The Generation 4 cell design was shown to have equivalent performance to the previous generation cell design. The increased cell area is a decided advantage for manufactured

cost of the cell stacks by lessening the amount of repeating and non-repeating unit support hardware for a given power (e.g. end plates, tie rods, manifolding, etc.).

2. Assemble large area fuel cells into 25 to 50 kW stacks

   A 40-cell Gen 4 stack demonstrated a maximum initial power of 6.4 kW at an average power density of 398 mW/cm2 and average cell voltage of 0.7 volts, utilizing the SECA simulated coal gas blend. A four stack module was projected to exceed the SECA requirement of >25 kW.

   Four new 40-cell Gen 4 stacks were installed by Delphi personnel into the 25 kW breadboard at UTC Power toward the end of January 2013. The breadboard was tested with the new stacks in early February, achieving greater than 6.5 kW aggregate DC output on natural gas before the program was terminated due to the sale of UTC Power.

3. Develop a test stand capable of testing a fuel cell stack up to 50 kW

   The design of the 50 kW SOFC stack test stand was started in calendar year 2009. Designs were complete in 2010 and fabrication was complete at the end of 2010. In the first calendar quarter of 2011, the 50 kW capable test stand was first commissioned using a debug stack and later run with multiple stacks. The stand would later demonstrate both forming gas and natural gas operation testing both stacks and ultimately a natural gas fueled breadboard power plant in early 2013.

4. Develop preliminary design of a 250-1,000 kW solid oxide fuel cell (SOFC) power module operating on either pre-reformed natural gas or coal syngas

   UTC Power performed conceptual trade-studies of 18 different system concepts for the SOFC power module and selected the Duo P concept as the final configuration based on high scores for system efficiency, system reliability, controllability, development cost and cost of future product. The completed preliminary design of a 400 kW power module operating on syngas achieved a projected efficiency of 55 percent (LHV).

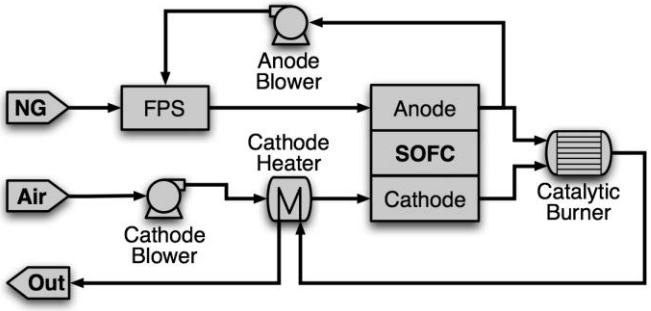

Figure 1-1: Process flow diagram of conceptual 400 kW NG-fueled SOFC power module.

The team subsequently completed the design and build of a 25 kW breadboard based on the Duo P concept.

5. Develop conceptual design of a >100 MW baseload SOFC power plant operating on coal syngas with a target efficiency of 50 percent (HHV) that separates greater than 90 percent of the carbon in the coal feedstock

   Three Integrated Gasification Fuel Cell (IGFC) system conceptual designs were completed meeting the desired efficiency and carbon separation targets: an atmospheric SOFC/steam turbine (ST) cycle; an atmospheric SOFC/gas turbine (GT)/ST cycle; and a pressurized SOFC/GT/ST cycle. All three systems are designed to produce greater than 120 MW net AC power at greater than 50 percent HHV efficiency. The IGFC system with steam turbine and air blower achieves approximately 51 percent HHV efficiency, while the gas turbine systems achieve greater than 57 percent HHV efficiency.

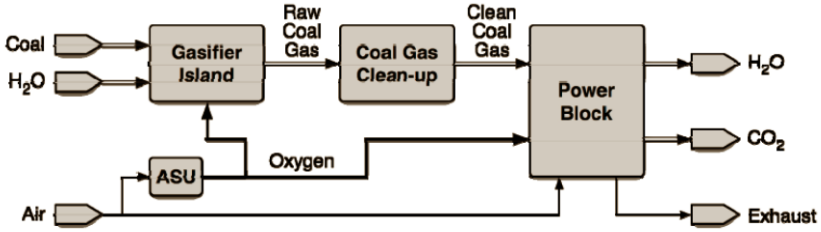

Figure 1-2: One of UTC Power's concepts for a coal-based Integrated Gasification Fuel Cell (IGFC) system.

Primary Reporting Topics

2. Cell and Stack Technology – Delphi

Cell Development

The objectives of this subtask are to 1) continue the discrete cell and cell component accelerated testing to characterize and confirm electrochemical performance stability 2) develop more stable, durable, lower-cost cathodes, anodes and electrolytes and 3) fabricate and test a significant number of cells of various sizes to assess the performance impacts of cell material, design, and process changes on electrochemical stability and durability.

Cell Testing

1) Develop the appropriate accelerated testing to characterize cell performance (power, long term stability, durability)
2) Determine the contribution(s) of the cell to the overall stack electrochemical performance stability

3) Validate low cost, production sources of anode, cathode, and electrolyte powders capable of meeting the cell performance targets

Standard cell production continues with the larger 403 cm^2 active area footprint (Gen 4), while the former, smaller cells (Gen 3, 105 cm^2 active area) are still typically fabricated for product and process development purposes. Button cells (2.5 cm^2) continue to be fabricated for testing at the R&D/proof-of-concept level. Gen 4, Gen 3 and button cells are used to evaluate complete electrochemical performance. Finally, measuring the resistance (including complex impedance of "half-cells" occasionally is used to characterize cathode side performance. Figure 2-1 shows a photograph of the standard Gen 4 cell along with the smaller Gen3 cell. After bilayer sintering (anode and electrolyte co-fire) and before cathode side processing, multiple Gen 3 bilayers can be fabricated from one Gen 4 bilayer for testing purposes.

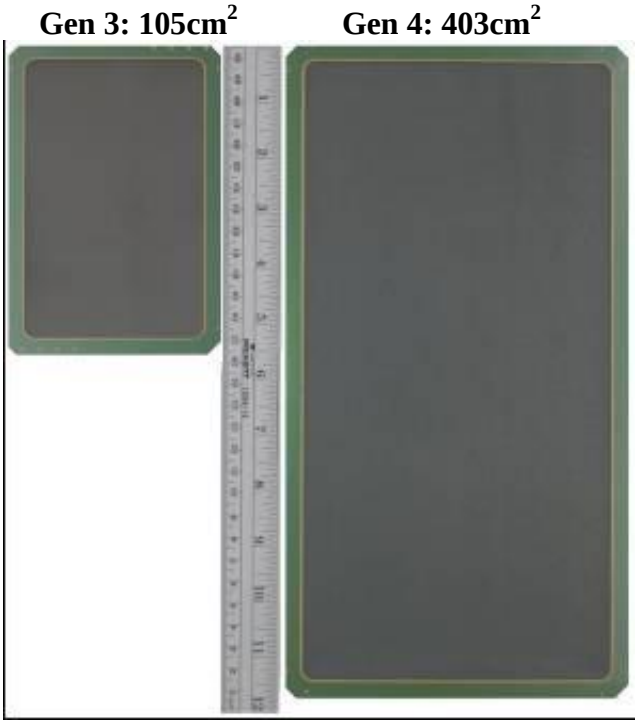

Figure 2-1: Delphi Gen 3 and Gen 4 Solid Oxide Fuel Cells

At Delphi, short stack testing continues to be developed and utilized as a lower cost alternative to full size Gen 4 stack testing to assist in SOFC product development. Short stacks consist of 1 to 5 cells that contain the same material sets, components, interconnect scheme and repeating unit design as full size stacks, and simply built on a smaller scale. They allow for complete electrochemical testing, including performance and durability, and the individual cells can be tracked throughout the test period in terms of voltage, current, and complex impedance. This platform is now being used to evaluate stack performance relative to fuel composition, sulfur tolerance, internal reforming, material stability, interconnect design, and other factors that affect performance and durability.

Button cells continue to be used for "proof of concept" testing and also serve as the first phase of testing for the evaluation of new raw materials in the form of powders, tapes, and pastes. Delphi has continued to evaluate anode and cathode powders, and pastes from production sources in search of low cost, high quality, capable suppliers. The goal is to qualify at least two (2) productive sources for each material. Button cell testing has served as the platform for initial screening tests for these commercially supplied materials.

High Performance Cathode Development

1) improved cathode stability to meet the long-term SECA durability and degradation targets
2) increased overall electrochemical performance of the cathode (thereby improving cell and stack performance)
3) continued cost reduction activities by developing low cost, qualified, production capable material supply to meet the SECA stack cost target

LSCF Paste Supplier

Delphi has qualified two paste suppliers for LSCF cathode paste. The new supplier has provided a paste that meets our specifications for a high solids loading paste that is screen printable and achieved the specified fired thick thickness with a single print operation. Electrochemical testing results on the button cell (Figure 2-2) shows that the performance is comparable to the paste currently being made in house by Delphi. The single print operation and having a supplier supply the cathode paste has potential to reduce cost to Delphi as we scale up the volume of cells manufactured.

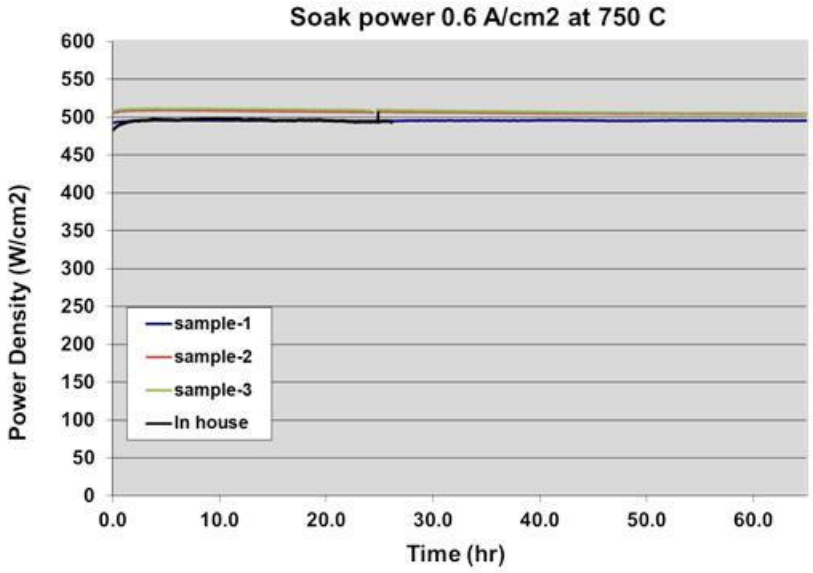

Figure 2-2: Comparison of Cathode Paste from Supplier to Delphi In-House

An in-house binder vehicle development project for high performance cathodes is complete. Using this material we have developed a single print HPC (High Performance Cathode) process, with the cathode sintered to achieve the proper microstructure. Similarly, interlayer films have

been prepared with reduced defects. A comparison of the microstructure with current standard cathode shows a reduction in as-printed and as-sintered film defects. Figures 2-3(a-d) show cathode structures from a current commercially available vehicle while Figures 2-4(a-c) show cathode structures with the new, improved in-house developed vehicle.

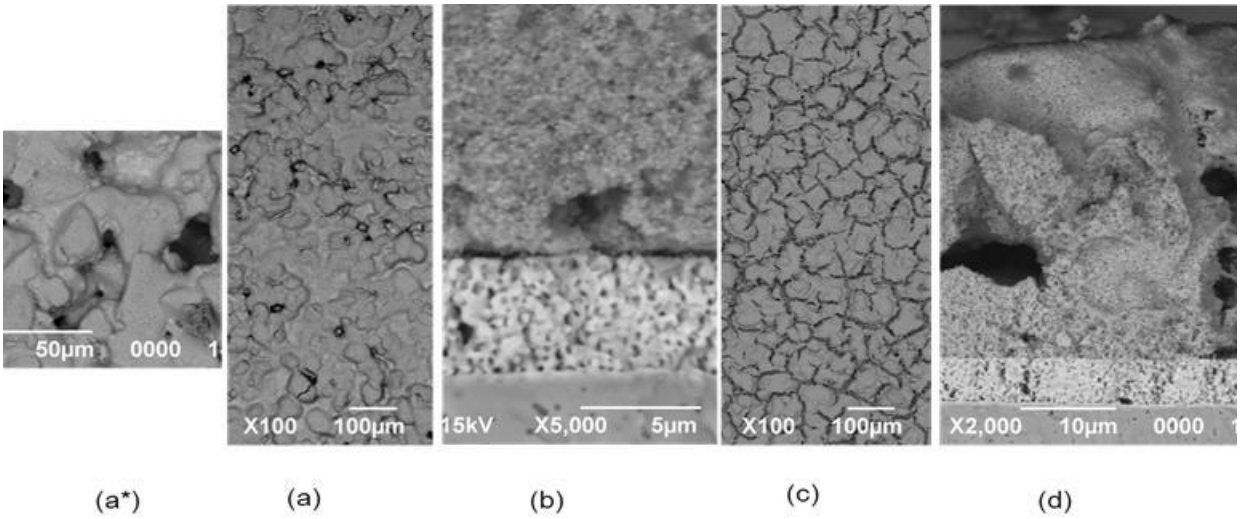

Figure 2-3: SEM images of screen printed LSCF film prepared from a commercial vehicle, dried at 150°C (a*). After drying (a) plan view - unfired, (b) cross section –unfired, (c) plan view – fired, (d) cross section - fired

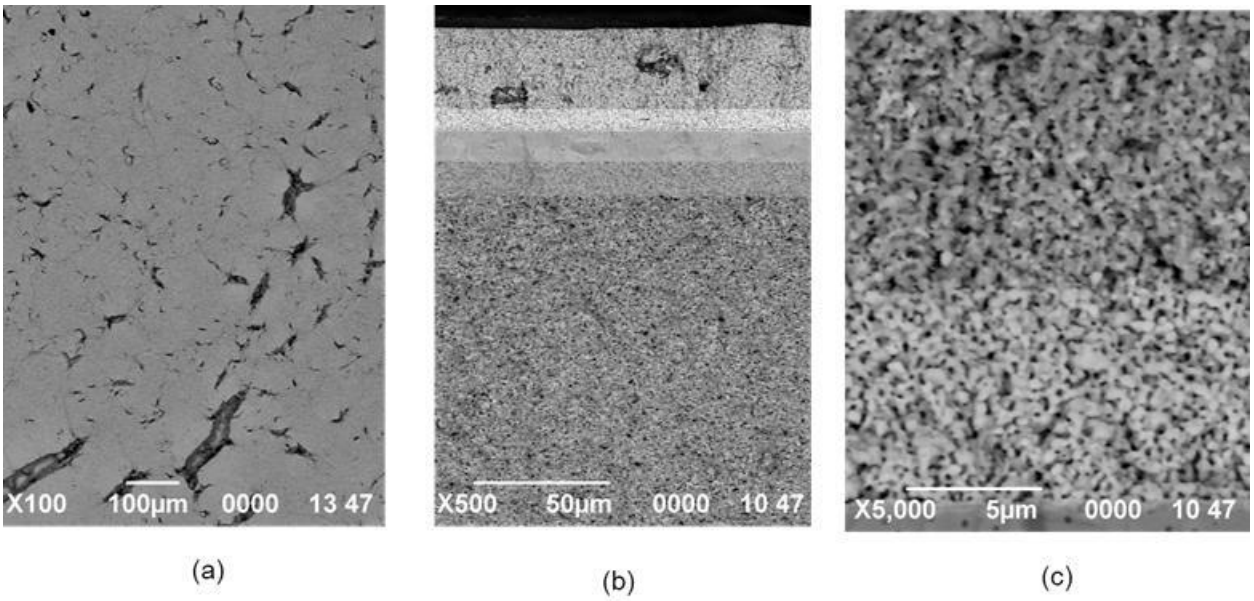

Figure 2-4: SEM images of a screen printed high performance single print cathode prepared from the new vehicle, (a) plan view - fired, (b) cross section - fired, (c) cross section - fired.

Binder vehicle development was further expanded to include metal current collecting layers and improved microstructures as shown in Figures 2-5(a-b).

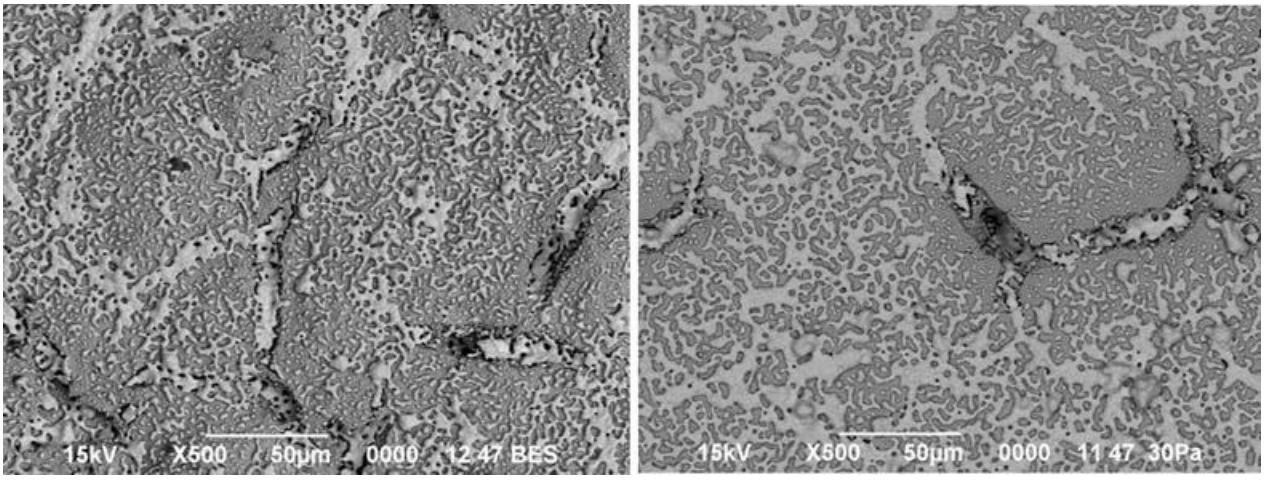

Figure 2-5: SEM images of screen printed current collector film prepared from the proposed vehicle (after sintering), (a) plan view commercial binder, (b) plan view from new in-house vehicle.

A Robust Engineering is being conducted on the optimization of the cathode electrode. The results will provide information necessary for a production intent materials specification and a manufacturing process plan. LSCF powders have been chosen from two commercial suppliers, pastes have been prepared by a third commercial supplier, and Delphi has fabricated the samples and has developed the test plan for each treatment combination. Control factors in the L-4 Designed Experiment are surface area and fired thickness. Other paste characteristics that will be recorded are rheology, fineness of grind (FOG), and solids loading used to achieve the desired levels for the control factors. Finally, firing temperature is being evaluated as a noise factor. Table 2-1 shows a table of the basic setup of the experiment including the treatment combinations and levels.

Table 2-1: L-4 Design Experiment for Cathode Optimization

Treatment Combination	Surface Area	Fired thickness (µm)	Noise Level: Firing Temperature
1	Low	20	Low
2	High	20	Low
3	Low	30	Low
4	High	30	Low
Baseline	Mid	Mid	Low
1	Low	20	High
2	High	20	High
3	Low	30	High
4	High	30	High
Baseline	Mid	Mid	High

Part of the high performance cathode (HPC) development has been focused on optimizing the commercial vehicle systems used to prepare ceria interlayer and LSCF cathode pastes. Figure 2-6 shows the defects observed in the plan views of screen printed and sintered ceria interlayer. Similar defects are also observed in LSCF sintered films. We are working to develop a vehicle system to address powder agglomeration, wetting, leveling, surface tension, & air bubble inclusion issues. This binder system will reduce paste costs and improve the overall cell performance and power density. Preliminary laboratory results are very promising and are shown in Figure 2-6 and Figure 2-7.

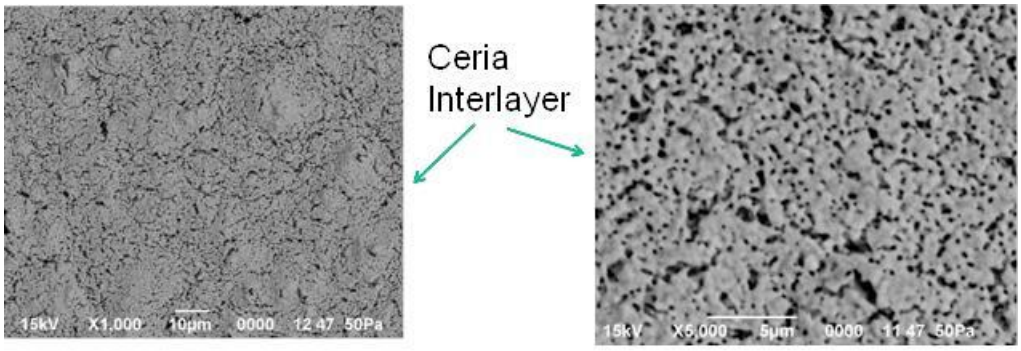

Figure 2-6: Defects in Interlayer using Current Commercial Binder System

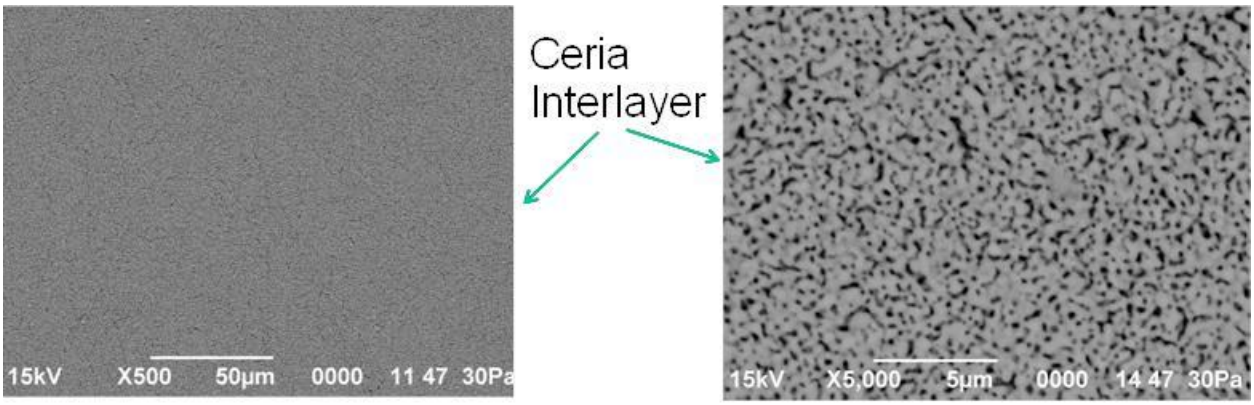

Figure 2-7: Ceria Interlayer Using a New Binder System

Development efforts have also been continued to develop an economical process to make a dense barrier layer (or a barrier layer with closed porosity) using an infiltration technique. Currently, a ceria layer is used as a barrier to prevent the reaction between LSCF cathode and zirconia electrolyte. However, this ceria-based barrier layer, applied using screen printing, is quite porous due to the constrained sintering and the limited firing temperature necessary to avoid the formation of resistive phase created by a reaction between ceria and YSZ. To decrease the ohmic loss of SOFCs by maximizing the conductivity of the barrier layer, it is desirable to have a dense barrier layer. In this study, we evaluated cells with dense ceria layers which were deposited on high-performance active anode bilayers by the University of Houston using a pulsed-laser deposition technique. Figure 2-8 shows the electrochemical performance of LSCF cells containing a dense ceria barrier layer under the constant voltage condition of 0.7 V at 750°C with a 50/50 H_2/N_2 fuel. Compared to a cell with a standard porous ceria layer, an LSCF cell with a dense ceria layer revealed >400 mW/cm^2 increase in power. To measure the ohmic contribution of a standard porous ceria layer, a porous ceria layer was also applied on top of a dense ceria layer using screen printing, followed by firing at the standard condition (at 1225°C for 2 hrs). A cell containing both a dense ceria and a porous ceria layer still exhibited a higher power (>200 mW/cm^2) than the standard cell with only a porous ceria layer, even though it had an additional layer of dense ceria. This result indicates that the effect of a dense ceria layer on the electrochemical performance is not limited to the improvement in conductivity of the barrier layer due to the removal of porosity. The results of impedance measurements conducted on these cells are shown in Figure 2-9.

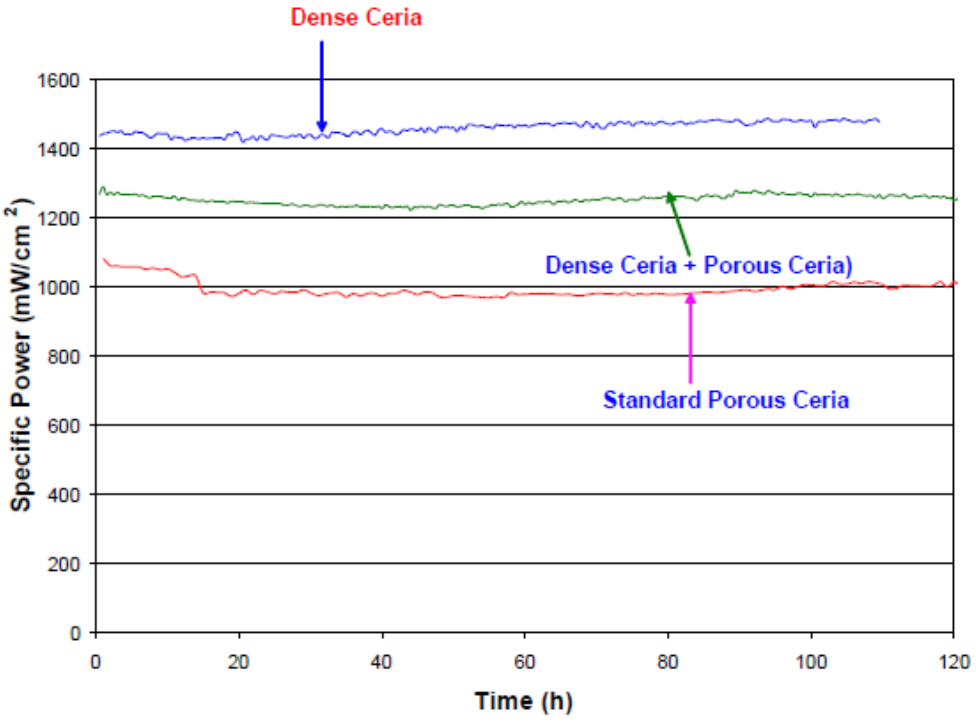

Figure 2-8: Effects of dense barrier of ceria cells: specific power vs. time

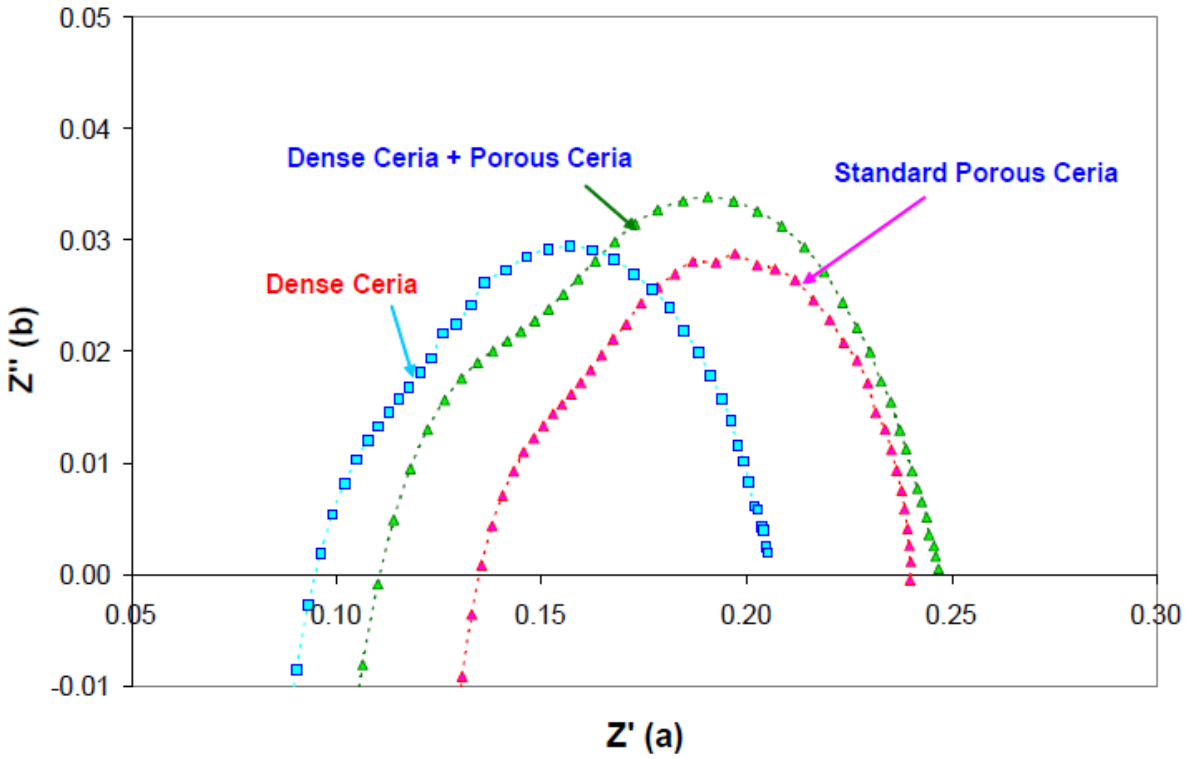

Figure 2-9: Effects of dense barrier of ceria cells: Impedance results

The replacement of a porous ceria barrier with a dense ceria layer caused ~400 mW/cm^2 increase in power, shown in Figure 2-10. The impedance results shown in Figure 2-11 also indicate that this power increase is mainly due to the decrease in ohmic resistance. Figure 2-12 shows the SEM micrographs and the EDS analysis results of infiltrated ceria cells. In the case of the infiltrated porous barrier layer, the reaction of Sr with YSZ electrolyte is clearly observed at the electrolyte/barrier interface, possibly due to the higher of mobility of Sr from the infiltrant compared to LSCF and its higher firing temperature. On the other hand, no Sr was detected at the electrolyte/barrier interface of the cell with a dense ceria layer. Thus, the dense barrier layer was effective to prevent Sr migration through the barrier layer and hence to suppress the formation of resistive phases such as strontium zirconate.

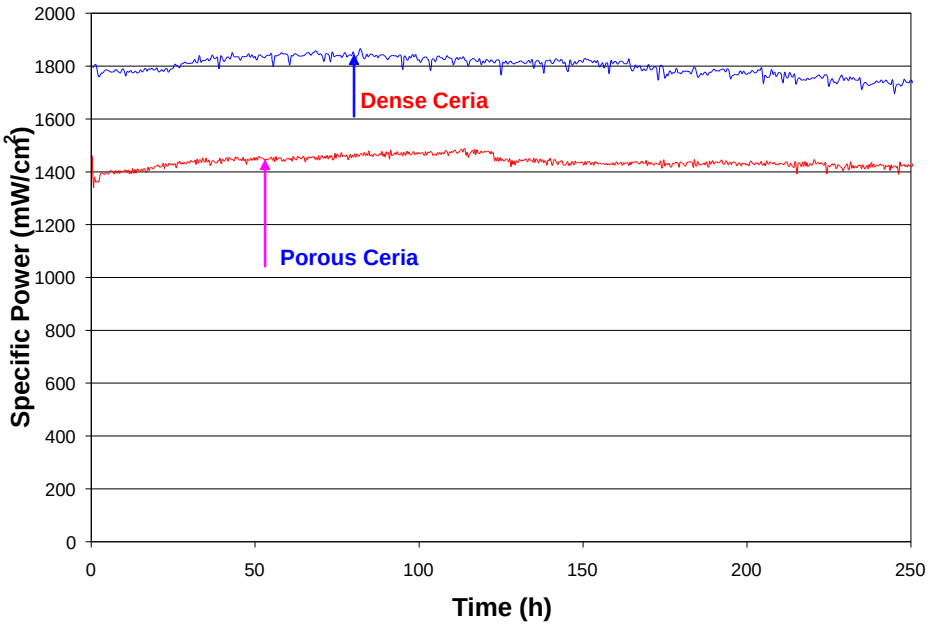

Figure 2-10: Effects of dense barrier: specific power vs. time

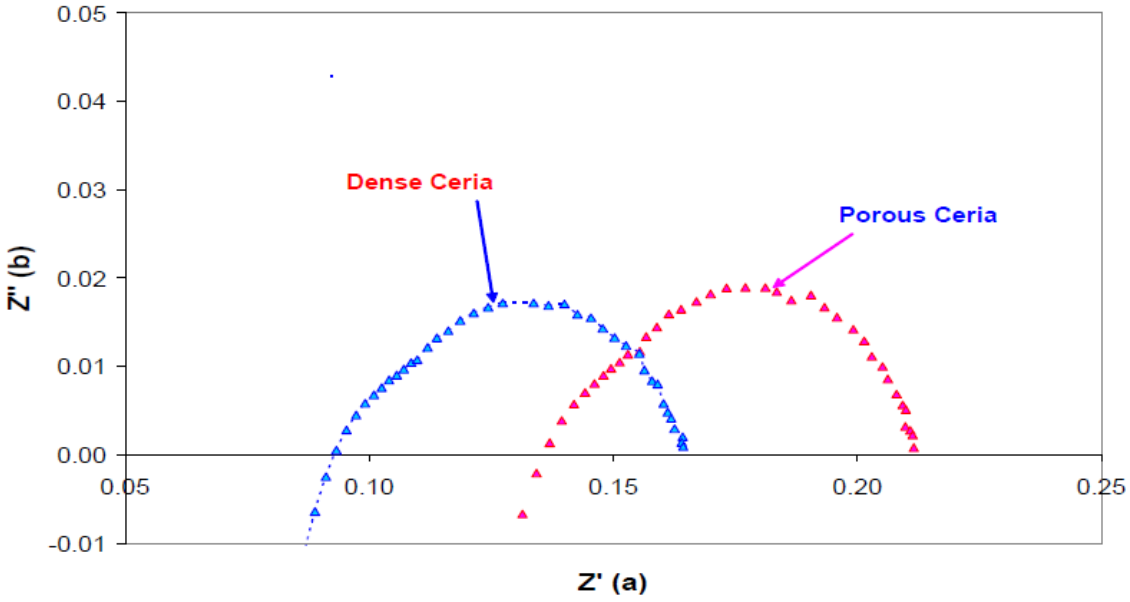

Figure 2-11: Effects of dense barrier: Impedance results

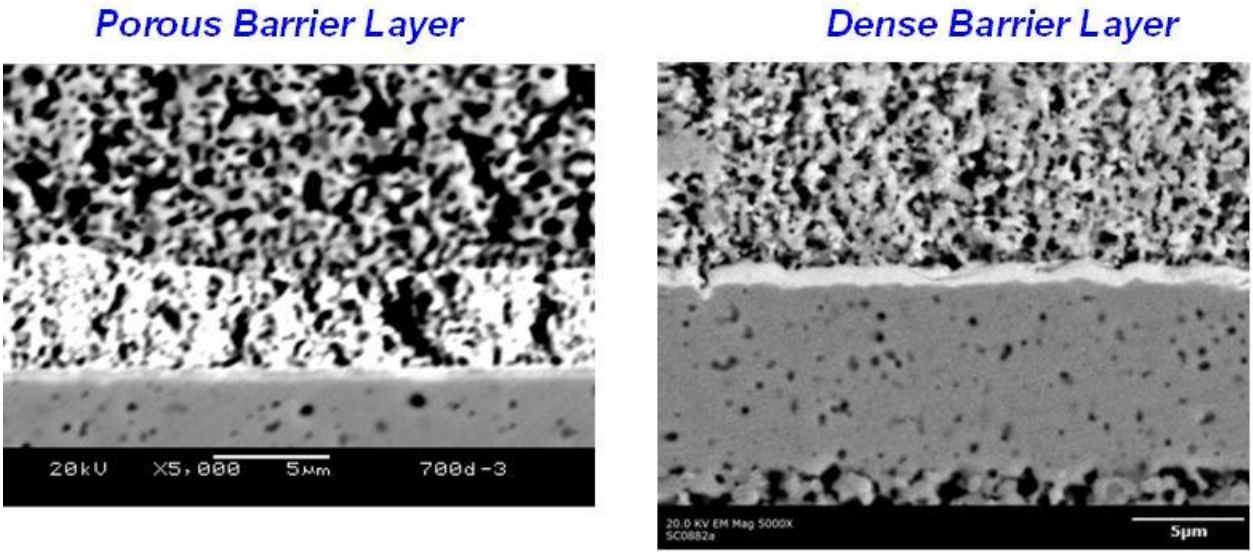

Figure 2-12: SEM micrographs of cells: porous barrier vs. dense barrier

To improve the power of LSCF cells further, the LSCF cell containing a dense barrier layer was infiltrated. This cell exhibited the power over 1.8W/cm^2 at 0.7 V. Therefore, more than 2 times increase in power can be achieved compared to a standard LSCF cell (~800 mW/cm2 at 0.7V) by incorporating all the power ingredients such as a doped active anode, a dense barrier layer, and cathode infiltration. The contribution of each power ingredient to the power at 0.7V was shown in Figure 2-13. The future research will be focused to develop economical ways to achieve the benefits of each power ingredient.

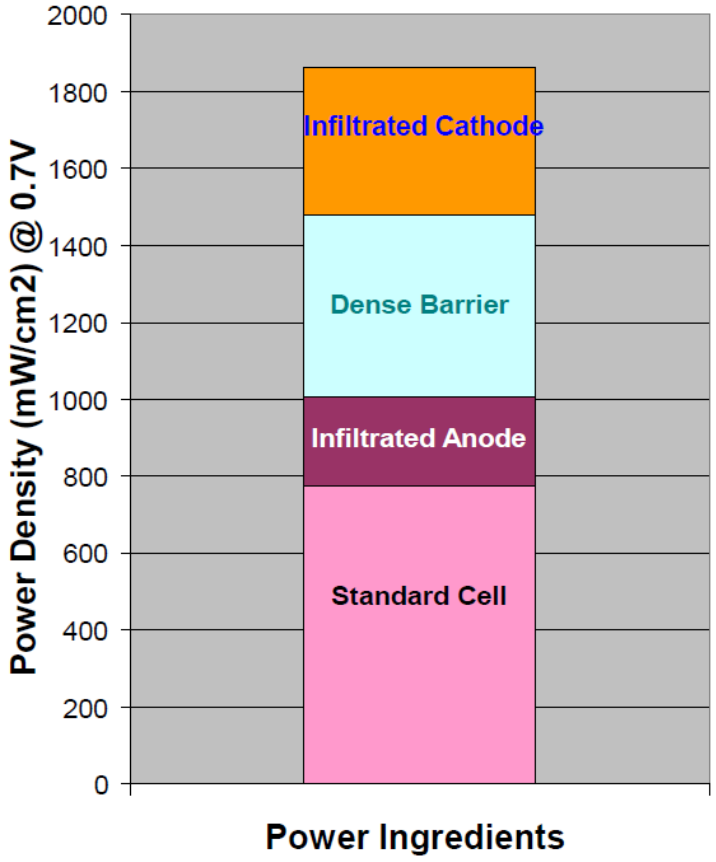

Figure 2-13: Contribution of each power ingredient to high power cells

To reduce the cost of SOFCs further, we have evaluated the low-cost ceria powders synthesized by a solid-state process. Two low-cost powders were evaluated. These powders were prepared using the same solid-state reaction technique, but were milled in two different ways to meet the specification of particle size and specific surface area. Overall, solid-state processed powders were more refractory than the standard powder. Cells with solid-state processed, water-milled ceria revealed similar power compared to a cell with standard ceria, while cells with IPA-milled ceria exhibited slightly lower power (refer to Figure 2-14). The refractory nature of IPA-milled ceria also resulted in slightly higher ohmic resistance compared to a standard cell and a cell with water-milled ceria (see Figure 2-15). These results and the results of the accompanying microstructural study demonstrate the feasibility of low-cost, solid-state processed ceria as a substitute for more expensive standard ceria. More validation tests will be conducted to verify the long-term stability, reproducibility and mechanical integrity of these powders.

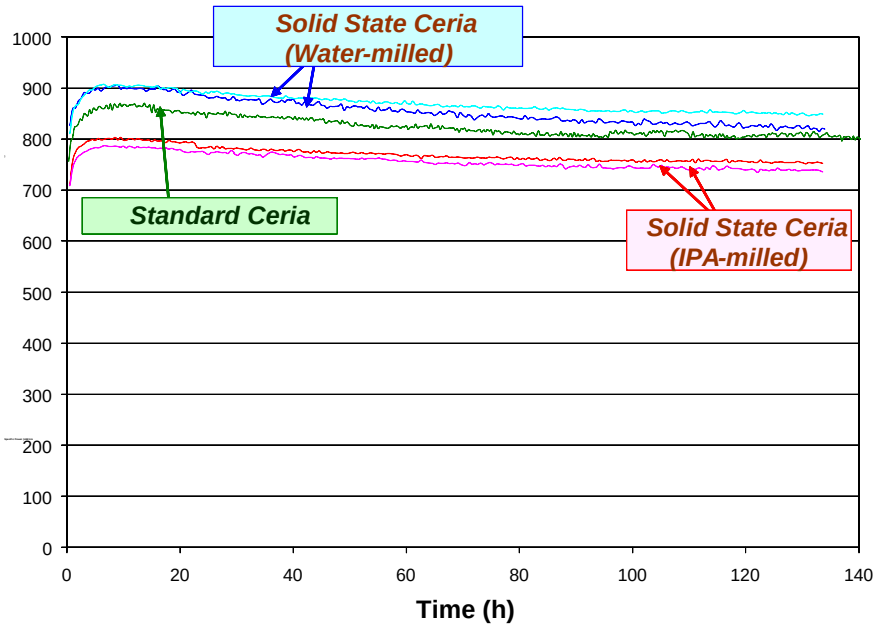

Figure 2-14: Specific Power vs. time of cells with solid-state processed ceria

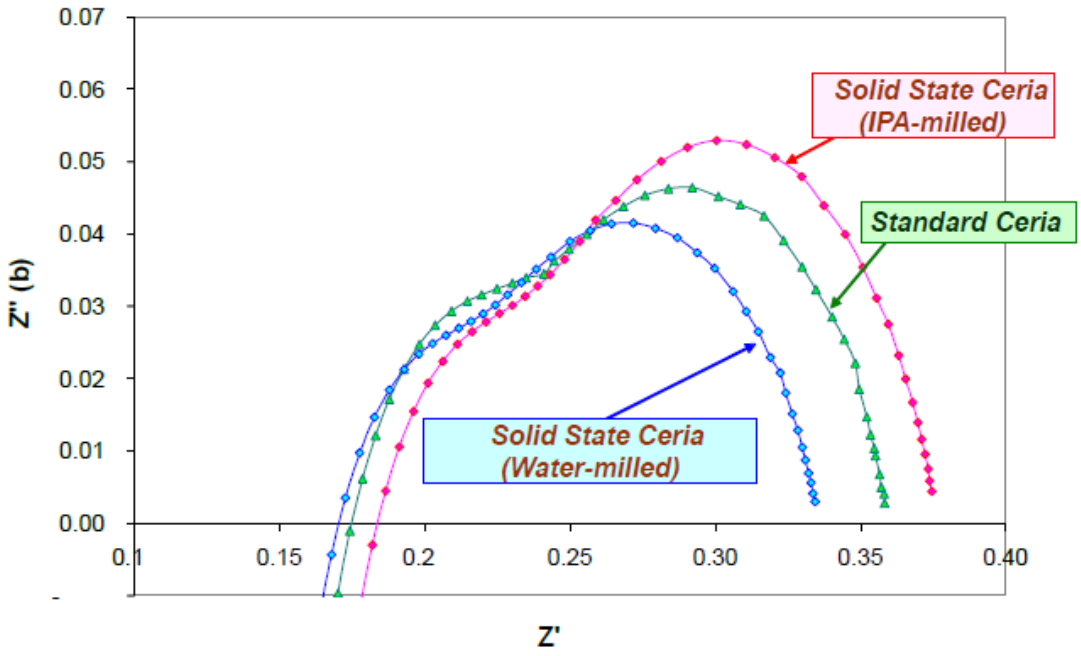

Figure 2-15: Impedance results of cells with solid-state processed ceria

Interlayer Firing Processing Window

Currently, interlayer fire is completed in a batch furnace since the peak firing temperature exceeds the capability of metal belt continuous furnaces. However, for high volume manufacturing, continuous furnaces are essential to show reasonable manufacturing costs. For example, a roller hearth continuous furnace could be used to fire interlayer.

Cells with interlayer were fired at various ramp rates and firing temperatures. A voltage-current curve for the various conditions is shown in Figure 2-16. The data shows that interlayer could be fired at much faster ramp rates, such as 44C/min ramp up to the peak temperature, than currently used. This proves that interlayer could be fired in a continuous furnace, with much faster ramp rates possible compared to a batch furnace. Interlayer firing temperature, in the range investigated did not have significant effect on electrochemical behavior at anticipated voltage operating ranges.

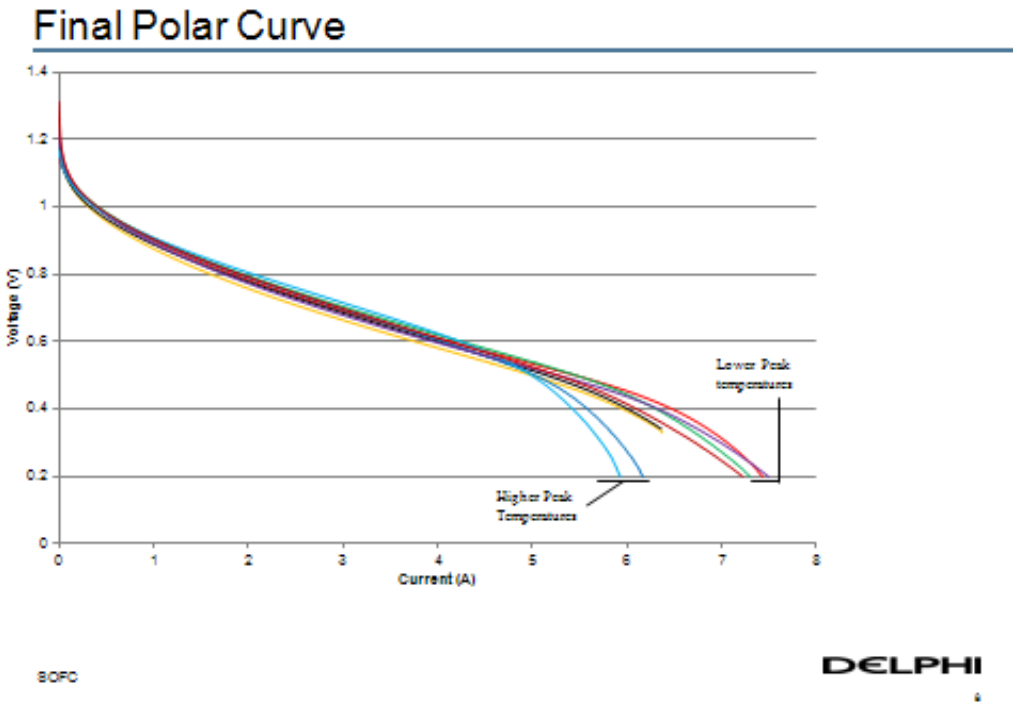

Figure 2-16: Button Cells with Interlayer Fired at Various Temperatures and Ramp Rates

High-Performance Anode and Electrolyte Development

1) improved long-term durability and performance stability to meet the SECA Phase II targets for continuous operation
2) continued cost reduction activities to meet the SECA stack cost deliverable
3) improved overall electrochemical performance of the cell

An anode development effort is the development of an economical process to fabricate high-performance doped active anode bilayers. Figure 2-17 shows the electrochemical performance of cells with doped active anode bilayers. These cells exhibited improved performance compared to standard, un-doped cells. Impedance results (Figure 2-18) also indicate that the use of a dopant is effective in reducing total cell polarization as well as ohmic resistance. Future research will be to optimize the composition and the process of doping and to understand the fundamental causes of power improvement associated with doping.

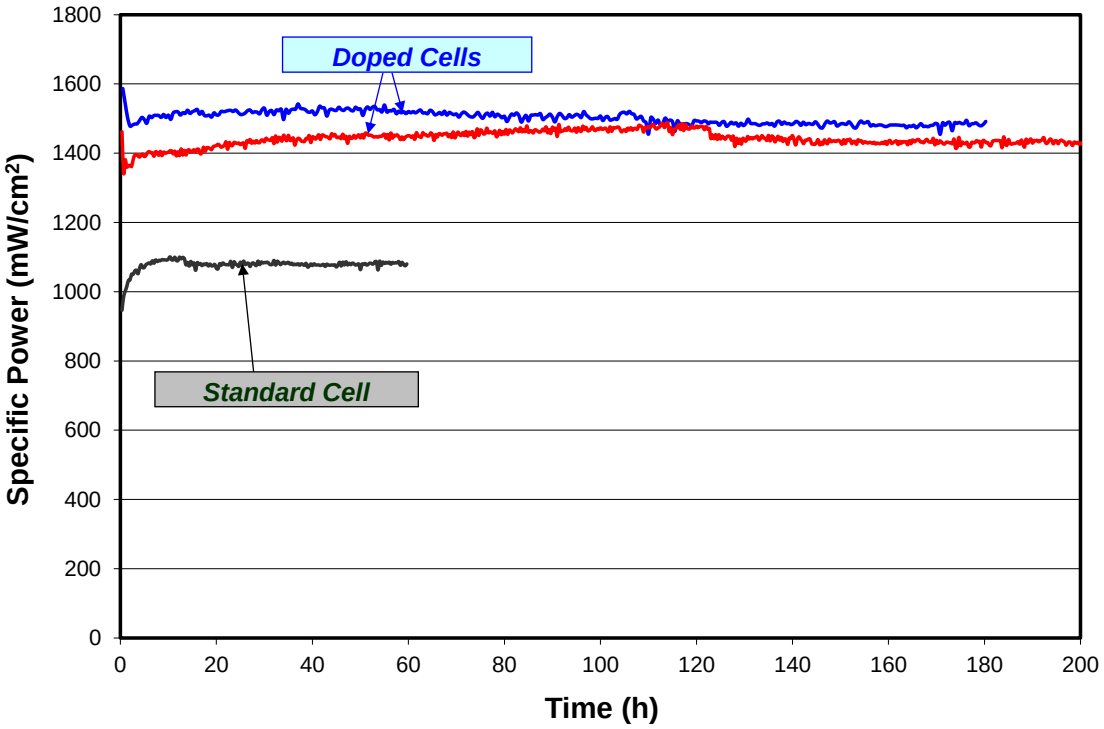

Figure 2-17: Specific power vs. time: Doped vs. non-doped active anode

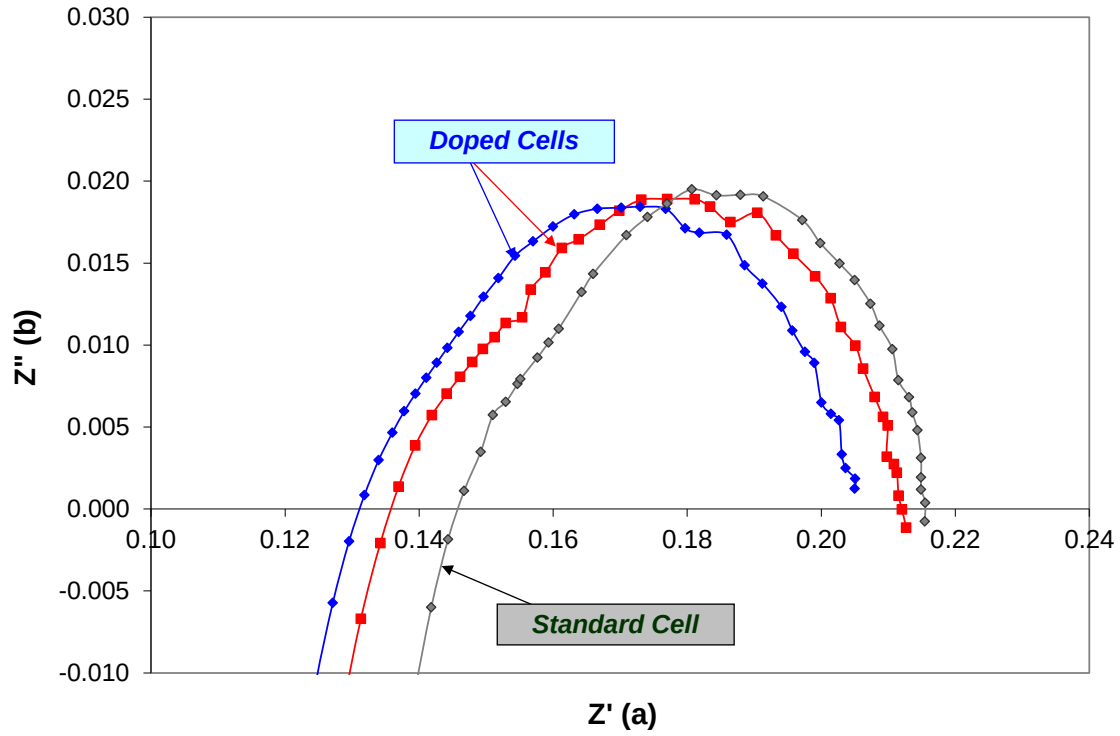

Figure 2-18: Impedance results: doped active anode

Delphi is currently working on a new cost reduction concept that relates to a change in the anode electrode of the cell. This concept, called active bulk, involves reducing the number of tape cast film layers in the build design from 6 to 5. This change eliminates one layer of bulk anode (approximately 200 microns thick in the unfired state) but does include an increase in the thickness of the active anode layer. Figure 2-19 shows schematics of the standard (baseline) design compared to the new active bulk design being investigated.

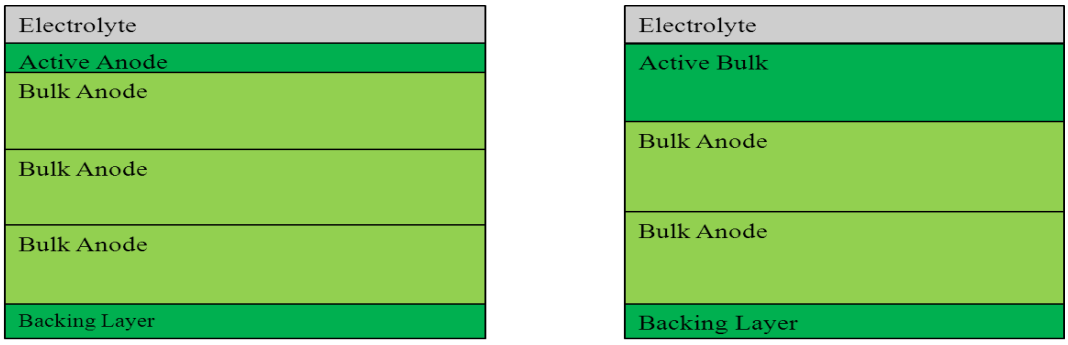

Figure 2-19: Standard 6 Layer Design vs. Active Bulk 5 Layer Design

Figure 2-20 shows an SEM image of the standard 6 layer design with an active anode layer of approximately 10 microns in the fired state, compared to the 5 layer design with an active bulk layer of approximately 100 microns in the fired state.

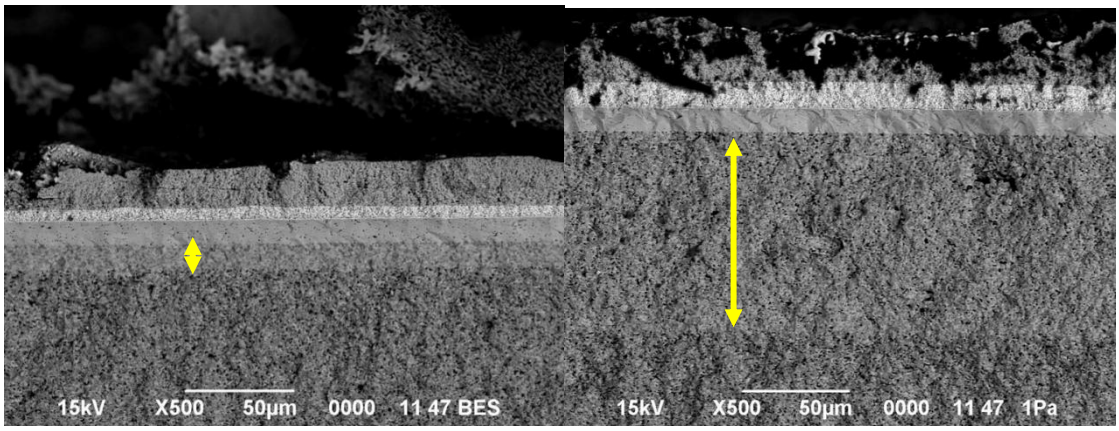

Figure 2-20: Active Anode (~10µm) vs. Active Bulk (~100µm)

The impact of this change to the anode side of the cell was evaluated by testing the electrochemical performance of button cells. Figure 2-21 shows the IV curve results of active bulk samples versus baseline samples when tested on 50%H2:50%N2.

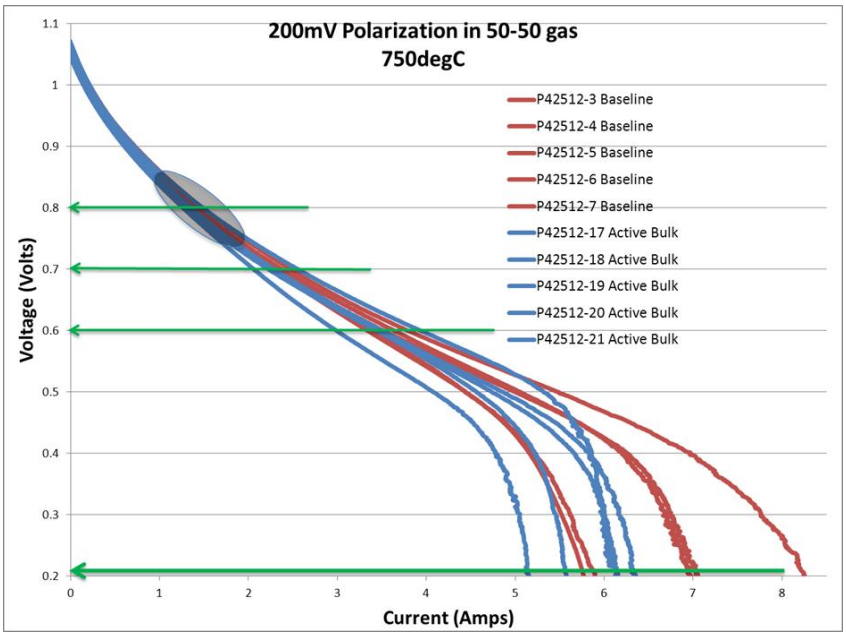

Figure 2-21: Polarization Curve Comparison in 50H2:50N2

The dark oval represents a normal operating range, while green arrows are points which were t-tested for difference in means. The ohmic and total resistances were also measured at 800mV by AC impedance spectroscopy to see if the thicker active bulk layer causes a higher resistance than the thinner active anode layer of the baseline cell. Figure 2-22 shows this impedance comparison at 800mV and 750°C.

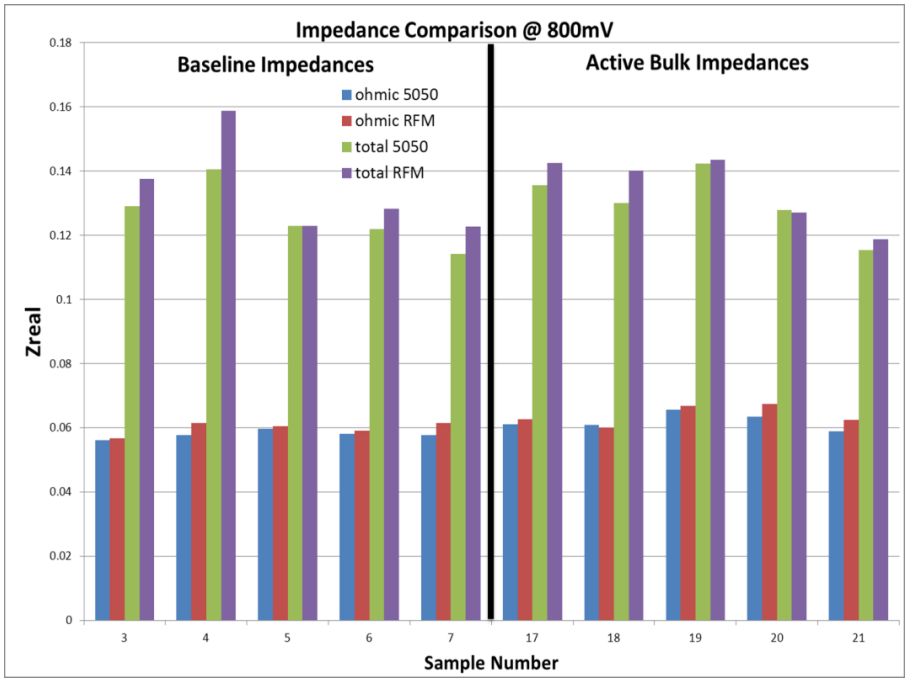

Figure 2-22: Impedance Comparison at 800mV and 750°C

Upon reduction of the data, it was concluded that the only significant difference between the baseline and active bulk experimental cast occurred in ohmic impedances where there appears to be a small increase in ohmic resistance with the thicker/denser active bulk. It was determined that there were no differences in means for the IV curves and total resistance.

Electrolyte Inspection

A Nordson YESTECH, a system for Inline Automated Optical Inspection, has been installed and is operational at our cell fabrication facility in Fenton, Michigan. This equipment will be used in identifying, classifying and eliminating defects in the cell prior to printing, and it eliminates the need for manual visual inspection (Figure 2-23).

Figure 2-23: Nordson YESTECH Inline Automated Optical Inspection System (AOI)

High Volume Isostatic Lamination/Firing Process Development

An operation search of the bilayer build process had identified and confirmed that the predominant bilayer defect is caused by a contaminant on the incoming tape. As a result, we have moved the problem solving focus to the supplier's process in an effort to either eliminate the source of the contaminant or remove the contaminant post-processing. The bilayer build process has been revised to minimize the exposure to the environment once the material has been received from the supplier.

Ongoing investigations into reduction of visual defects on the electrolyte surface which are found in the inspection step after perimeter scribe have resulted in significant First Time Quality (FTQ) improvement through implementation of process adjustments. Pictures in Figures 2-24 and 2-25 show the appearance of these defects:

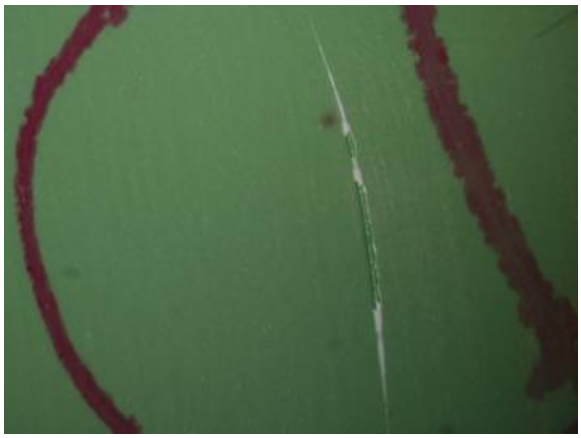

Figure 2-24: Optical Microscope Image of Defect on Electrolyte Surface

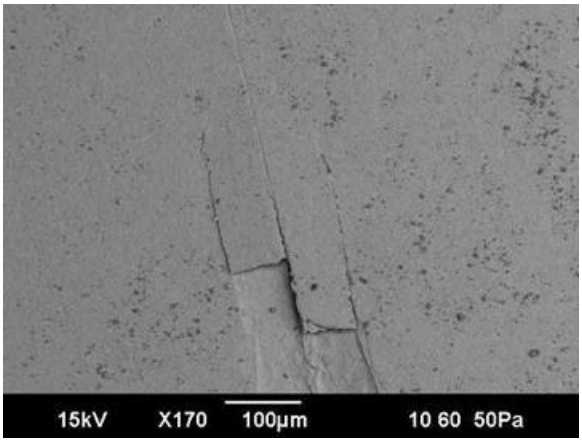

Figure 2-25: SEM Image of Defect on Electrolyte Surface

It was found that stray particles from the support refractories used in bilayer and creep flattening were present on a wooden-surface table that was used to serialize bilayers on the anode side with the electrolyte surface down. This made them very susceptible to scratching and proved to be the major cause of two of our highest categories of inspection defects. The support refractory material is harder than zirconia, so any relative movement can cause scratches if a particle is trapped between the electrolyte surface and the table during serialization. When these defects were sectioned, it was found they only penetrated partially through the electrolyte as shown in Figure 2-26. Process changes were implemented to address these defects. The lossses due to these defects have been reduced to near zero.

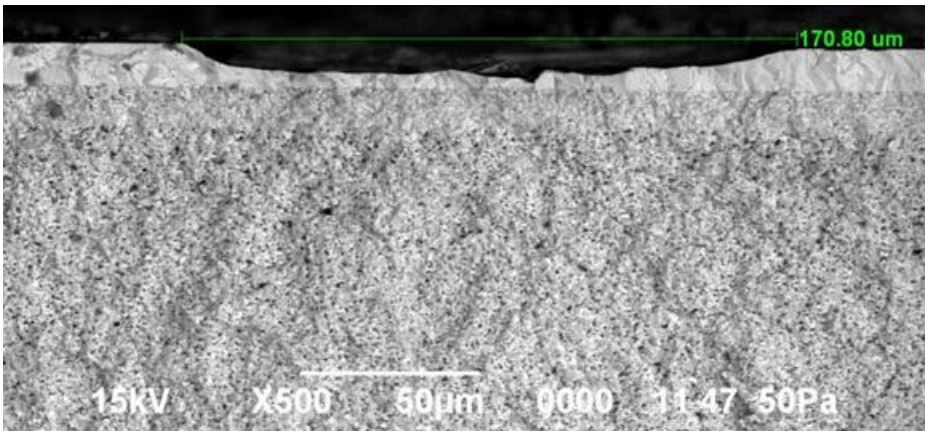

Figure 2-26: Partial Penetration of Defect through Electrolyte Layer

Stack Development

The work included as a part of this subtask will be focused on optimizing the Gen 4 stack for stable electrochemical durability performance in continuous operation and thermal cycling operation. Specifically, stack level development will include interconnects and repeating unit to repeating unit seals.

Gen 4 Design Update

While we continue to build and test 40-cell Gen 4 stacks and evaluate performance, we have made refinements to several component designs to improve performance and manufacturability, as well as to facilitate the assembly process. We have resized the cathode interconnect to accommodate the cell to retainer seal joint and to allow for additional assembly tolerance. Likewise, we have reconfigured the perimeter extrusions on the anode plate to accommodate for assembly tolerance stack-ups. In addition, as a result of extensive CFD studies, the repeating unit cathode outlet ports have been resized. In addition to component optimization, we continue several development efforts.

A design of experiment, utilizing computational fluid dynamics, was conducted to optimize the flow from repeating unit to repeating unit, as the number of repeating units is increased. When increasing the number of repeating units in a stack assembly the performance is negatively affected due to mal-distribution. The overall stack performance is defined by the lowest performing repeating unit and if it is assumed each repeating unit is the same, then only mass distribution of anode and cathode gases can affect the performance. The design of the repeating unit is defined by the cell geometry and the inlet and outlet port design for both the anode and cathode flows, among other features. The inlet port(s) have been maximized to reduce pressure restrictions and to achieve maximum flow volume. The outlet ports are designed to balance pressure across the cell and minimize the pressure drop on the outlet chimneys as the repeating units are stacked on each other. The design of experiment was structured around optimization of the outlet ports to maximum mass distribution while minimizing the pressure drop of the stack assembly. In Figure 2-27, the baseline data of the cathode flow can be reviewed, along with the optimized data. The data displays three different stack sizes, 32, 64, and 100 repeating units, and how each stack's performance to distribution is affected by the optimized outlet port diameter. It

can be concluded, from the data, that a 100 repeating unit stack is possible with the optimization of the outlet port. In Figure 2-28, the baseline and optimized data of the anode flow can be reviewed, very similar to the cathode data. The anode target limit is a stricter limit, because of the utilization of the anode flow within the stack. Again the data suggests the capability of building a 100 repeating unit stack would not be limited by the flow characteristics. With both cases, the anode and cathode, the uniformity of the mass distribution was greatly increased while little to no effect to the pressure characteristics.

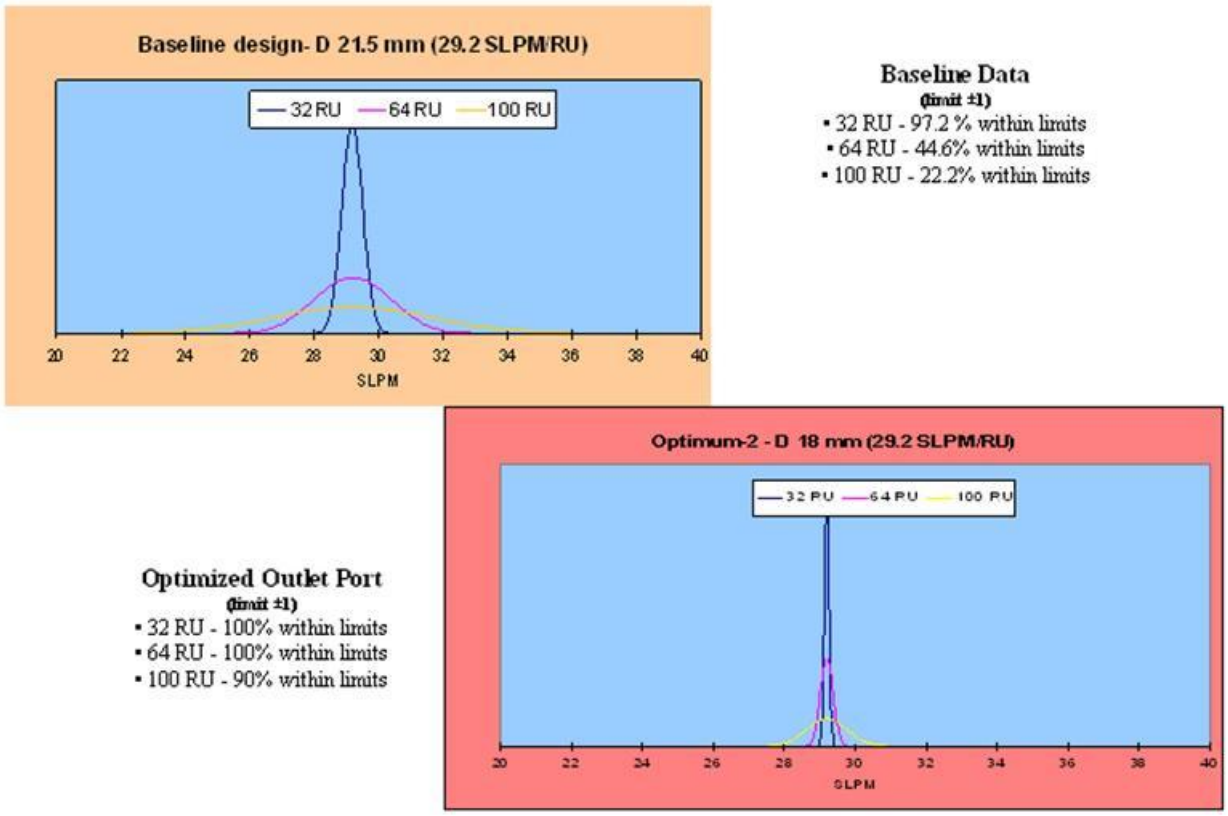

Figure 2-27: Cathode Flow Optimization

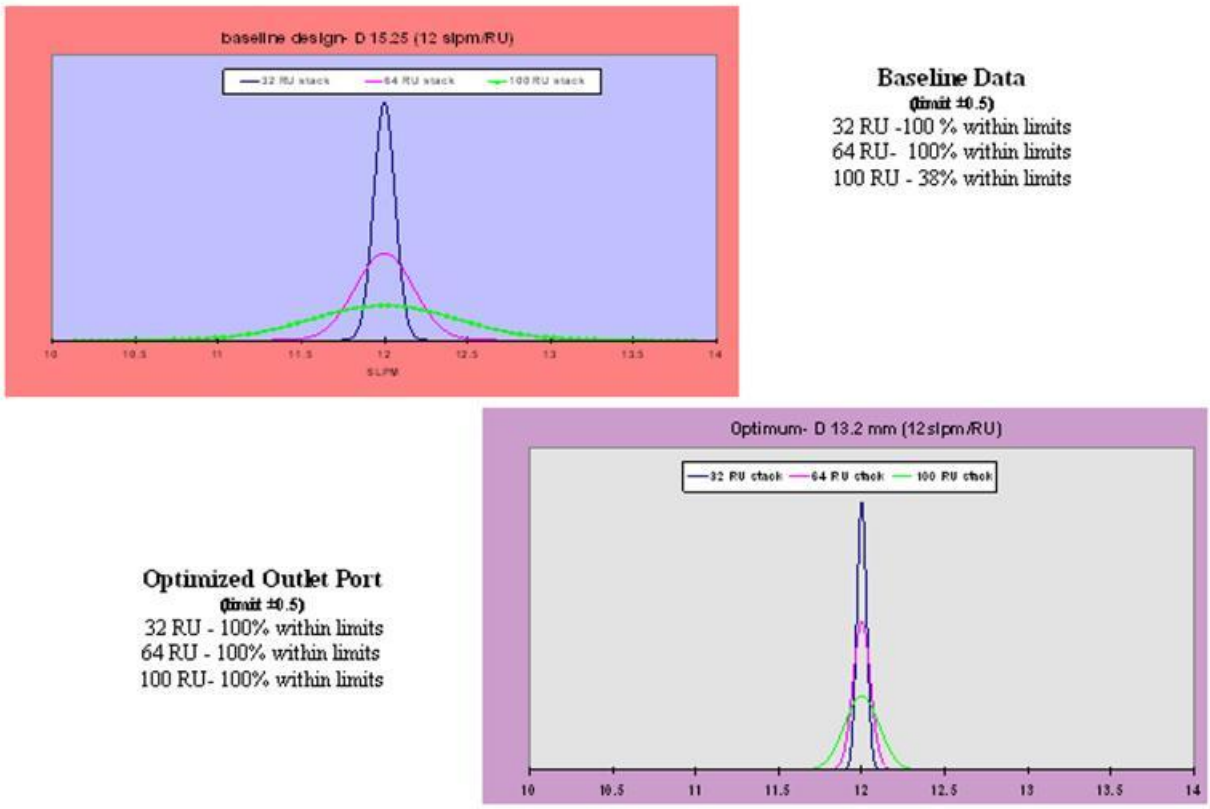

Figure 2-28: Anode Flow Optimization

We have implemented the larger footprint diaphragm assembly and the compliant bottom current collector design in our recent stacks. The larger diaphragm assembly provides a more uniform load across the repeating unit seal, and the compliant current collector limits the stress transmitted to the repeating unit seals.

Our plan to improve the compressive load applied to the stack continues to move forward. The new "leaf spring" component to our stack load mechanism has now been procured. This high temperature alloy component will help keep the desired compressive load on the stack at all times. Once the testing is complete, we will evaluate the spring on a stack.

Finally, through FEA, we have validated that our design intent repeating unit seal geometry is better able to withstand shear forces versus a repeating unit seal which does not sinter to the desired profile. Our analysis showed that a seal which sintered down to the designed thickness and completely filled the gland created by features on the retainer and separator plate outperformed a glass seal which was thicker than nominal and did not fill the gland. Therefore, further work is required in sintering to achieve our design intent repeating unit seal geometry.

Interconnect Technology Development

1) improved interconnect stability to meet the long-term SECA Phase II durability targets
2) improved interfacial ASR performance of the interconnect (thereby improving cell and stack performance stability)
3) continued cost reduction activities by developing low cost, production manufacturable interconnect coating processes to meet the SECA stack cost target
4) development of accelerated bench testing for performance evaluation of interconnects and interconnect surface modifications

Development of the interconnect coatings is part of the cost reduction plan for the stack. The anode interconnects are fabricated from SS441 and are electroplated. Currently, the perimeter of the anode interconnect requires masking to reduce plating thickness around the perimeter. Cost reduction is focused on eliminating the masking process. In addition to removing masking, the plating adhesion is also being optimized.

The cathode interconnects are also stamped and electroplated. After plating, they are processed through a hydrogen furnace for diffusion. Some initial bend testing of revealed flaking of the plating. Pre-treatment prior to electroplating bath has been demonstrated to be an important process for improving adhesion, as shown in Figure 2-29.

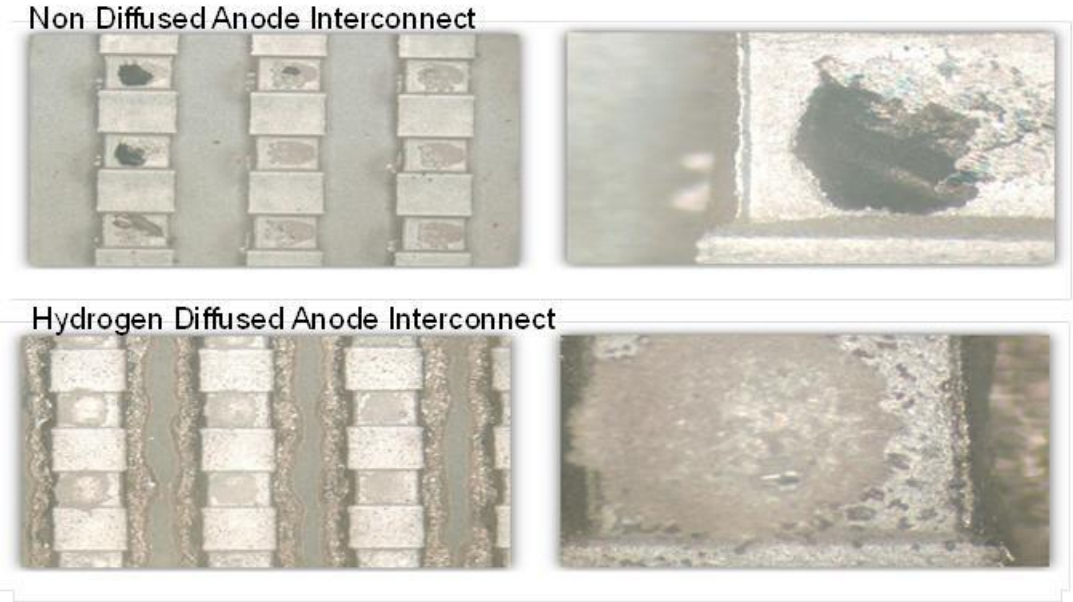

Figure 2-29: Hydrogen diffused plated anode interconnects compared to non-diffused parts after stack test

Delphi is working on cost reduction electroplating by evaluating an alternative coating supplier. Currently we are at the dimensional study stages of evaluating the new supplier. In addition,

coating thickness is also being evaluated. The study will also look at thickness variation at center and edges, plating uniformity, and plating adhesion.

Interconnects for Gen 3.2 stacks were designed as patterned columns of contact, where Gen 4 interconnects were designed with contact along supporting ribs. The ribbed designs have open channels for a more uniform distribution of flow. The Gen 3.5 interconnect design will simulate the Gen 4 design into the Gen 3 size (Figure 2-30). Stacks have been built and performance verified with the ribbed designs, which are the current standard for all future stack builds.

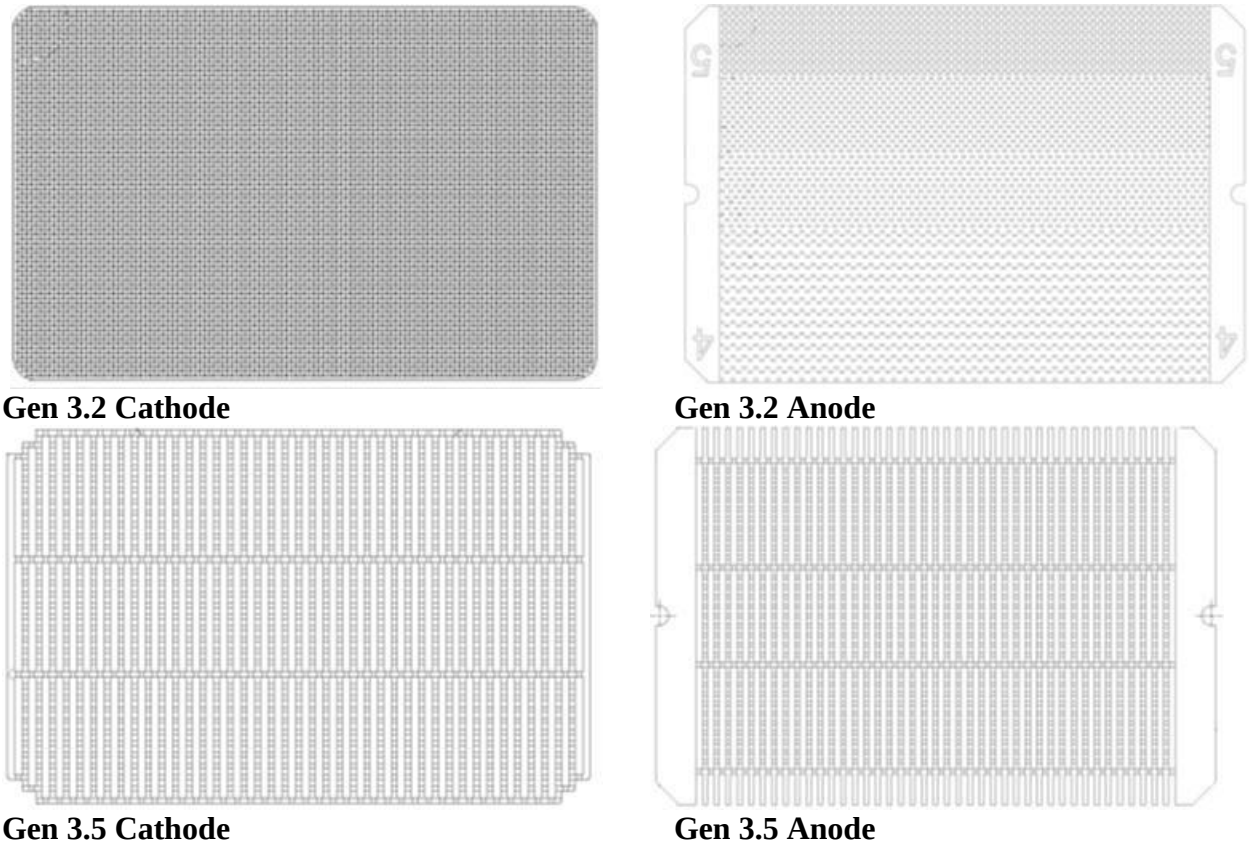

Figure 2-30: Gen 3.2 vs. Gen 3.5 interconnects

One interconnect project was to reduce the pressure drop on the cathode side of the Gen 4 repeating unit. Simulation of the proposed design change indicated that a 50% increase in air flow could be achieved at the same level of restriction of the current design, by increasing the width of the flow channels in the cathode interconnects. Figure 2-31 indicates the areas of focus for decreasing flow restriction for the Gen 4 cathode interconnect. Note there are six rows of solid material termed Y-bars. Each Y-bar has notches coined in to allow air flow to pass along the cathode. The flow restriction was reduced by increasing the size of the coin, creating a wider notch.

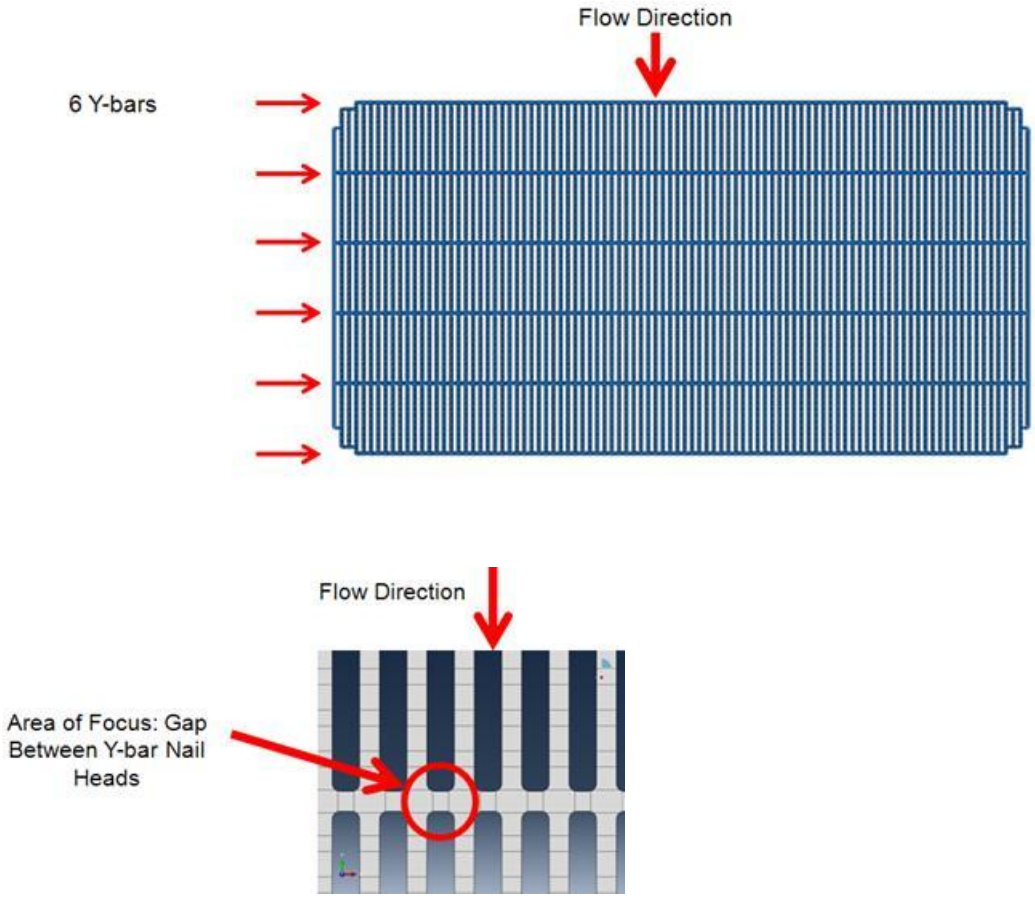

Figure 2-31: Gen 4 Cathode Interconnect

Figure 2-32 shows photographs of the original stampings and the low restriction stampings. Note the change in the width of the coined notches on the Y-bar.

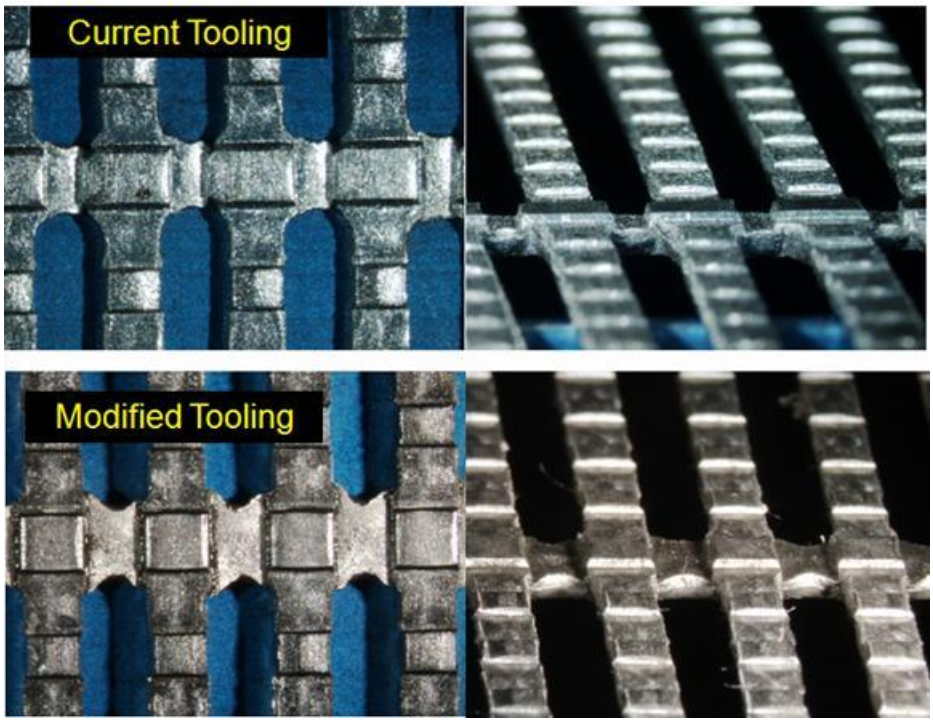

Figure 2-32: Gen 4 cathode interconnects with reduced flow restriction

Cold flow restriction testing of the cathode interconnect stampings agrees with the simulation and is shown in the plot of Figure 2-33.

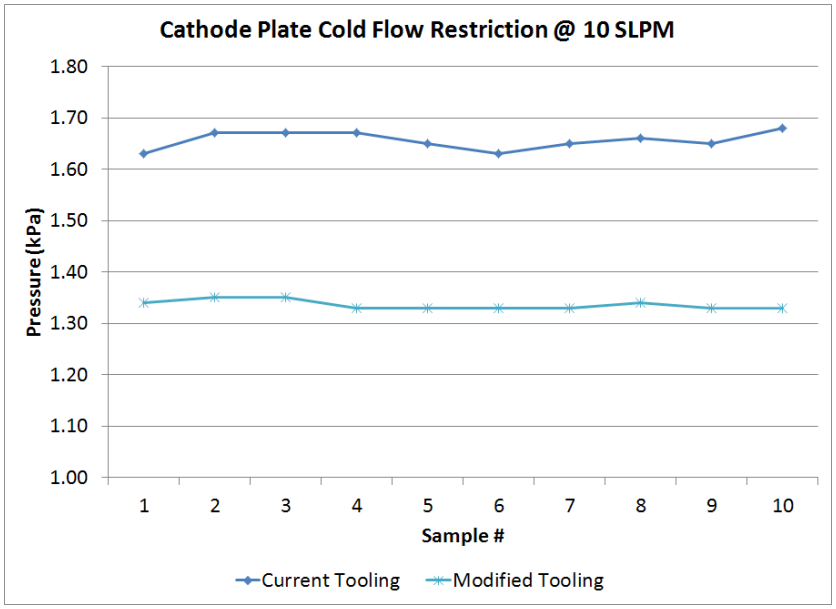

Figure 2-33: Cold flow restriction of Gen 4 cathode interconnects

Stack Confirmation Testing

Confirmation testing of the low-restriction cathode interconnects was completed on two (2) Gen 4 stacks, resulting in a 20% reduction in stack cathode flow restriction. Figure 2-34 compares ten (10) previously built Gen 4 stacks with the two low-restriction stacks.

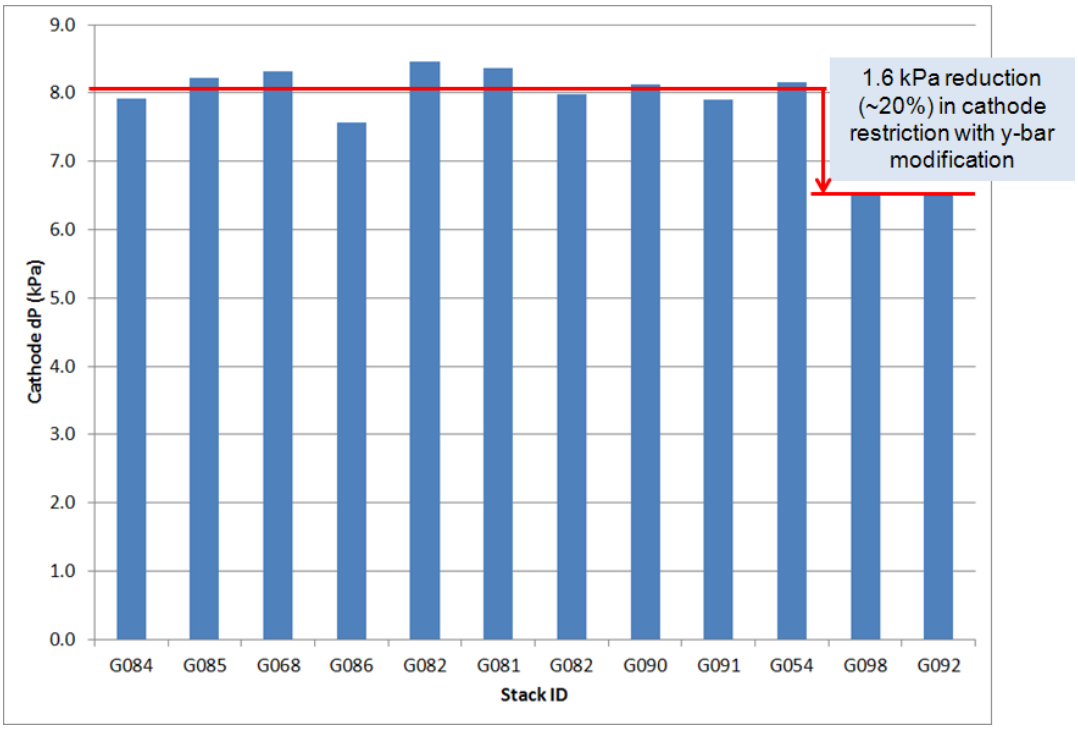

Figure 2-34: Gen 4 Cathode Interconnect

The benefits of the reduced restriction are evident in Figure 2-35 (under constant current testing) where the power was increased by 22% while the increased air flow rate maintained a peak cell temperature within the allowable limits.

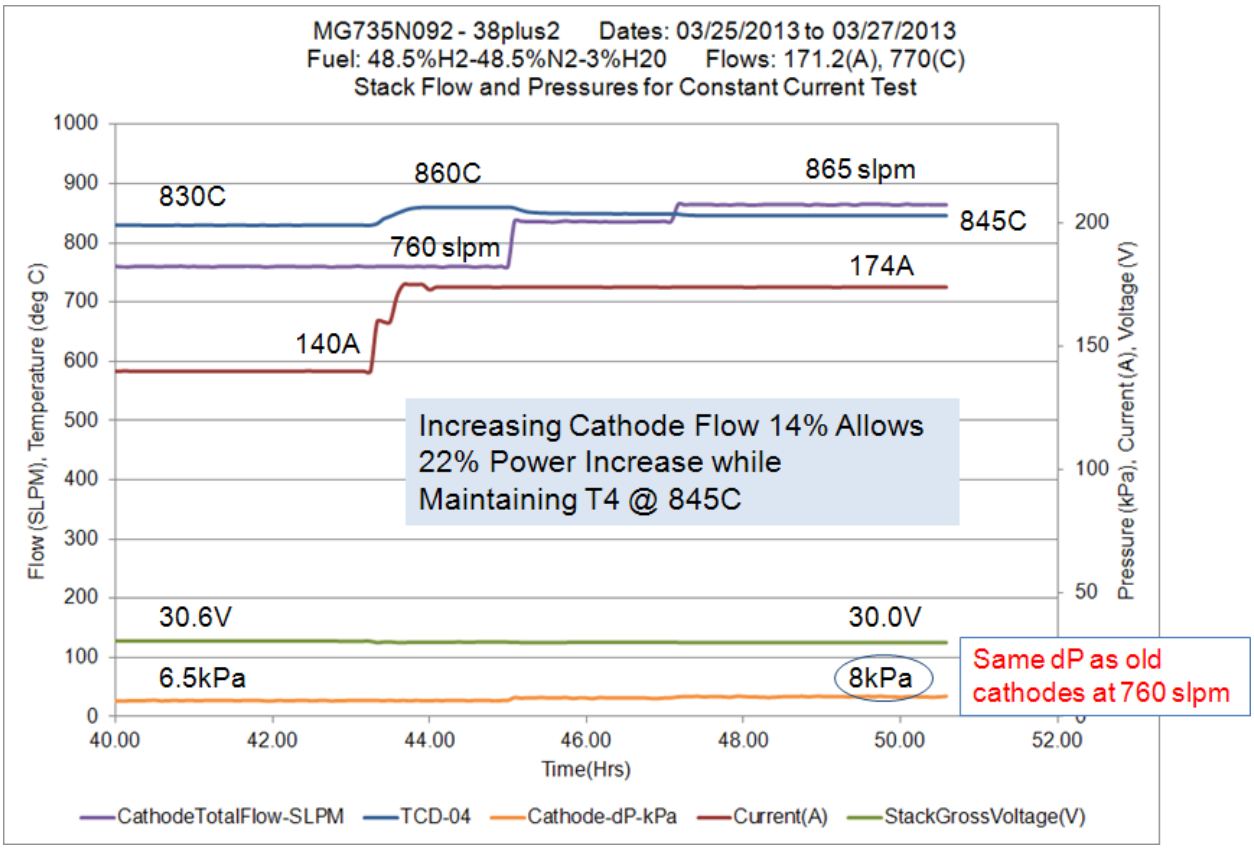

Figure 2-35: Constant current testing with low restriction cathode interconnects

Performance and Durability Evaluation of Stacks

A new, inexpensive anode contact paste has now replaced the previously utilized contact pastes, which had a number of specific issues to overcome and has been implemented in all stack builds. The new contact paste has the benefits of reduced cost and improved dimensional stability during the stack sintering and reduction process. Figure 2-36 is a cross section of a Gen 4 stack built with the new anode contact paste. Good bonding is evident between the anode interconnect and the paste applied to the separator plate and the cell anode.

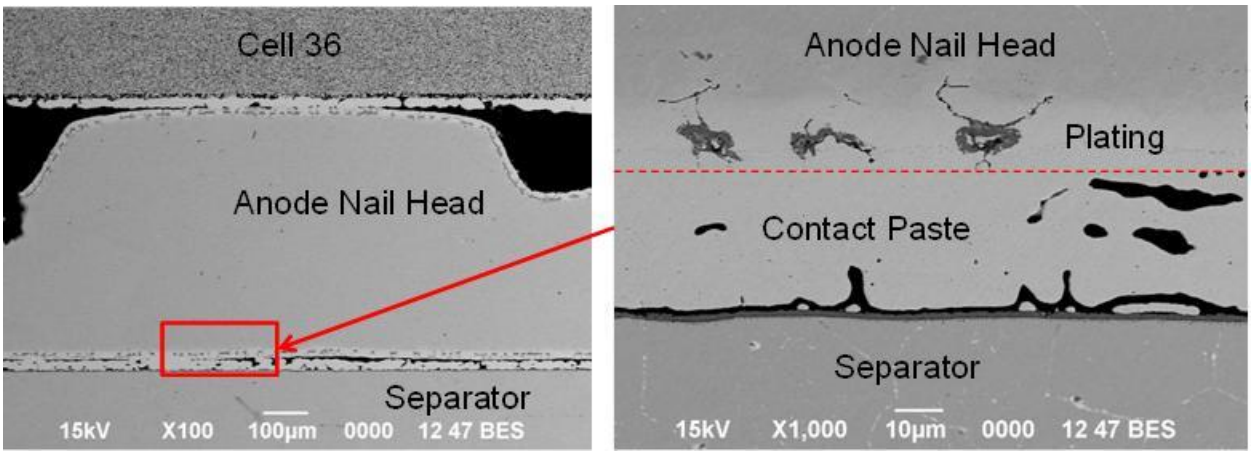

Figure 2-36: New anode paste interface

Constant current testing of a Gen 4 stack using the new anode paste yielded the expected performance at normal operating conditions, as shown in Figure 2-37.

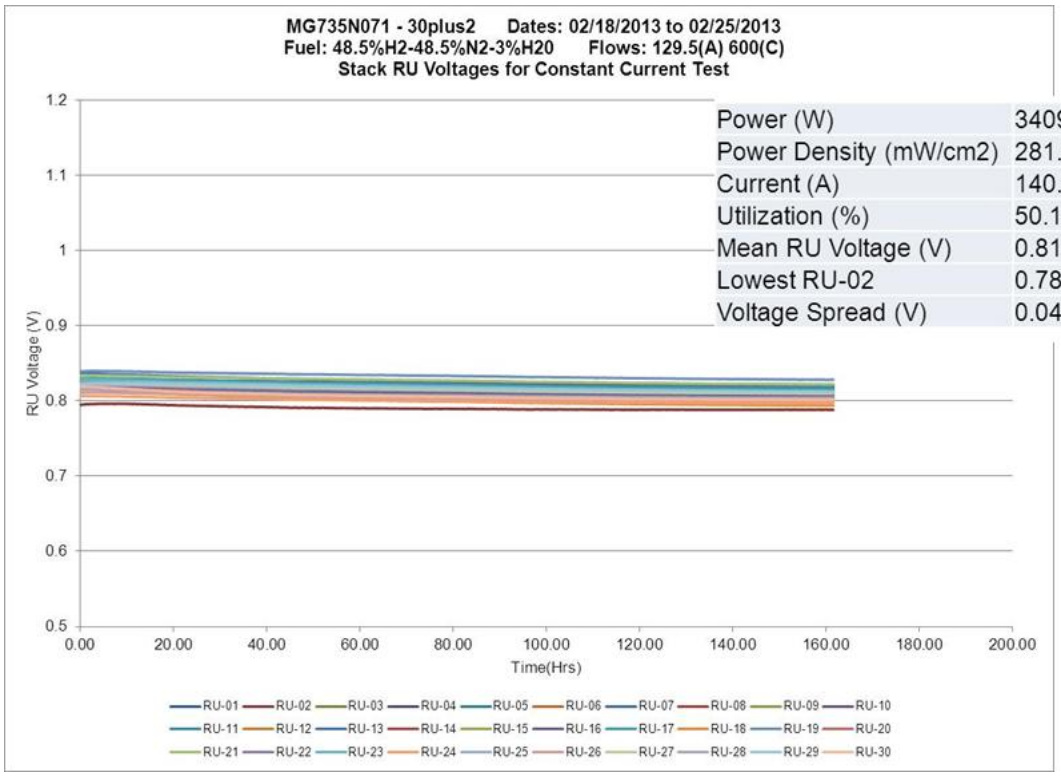

Figure 2-37: Constant current testing of Gen 4 stack utilizing new anode paste

Repeating Unit Seal Development

1) Develop stand requirements and accelerating factors, then develop and build dual atmosphere accelerated test stand(s) for seal testing
2) Conduct accelerated bench testing of repeating unit to repeating unit seals
3) Engineer new seals using the accelerated test platform as a test platform
4) Provide analytical support for the characterization of new seal materials

Delphi has developed rapid thermal test stands that have the capability to thermal cycle coupon level hardware at a much higher rate than previous test stands. The rapid thermal cycling test stand has the capability to thermal cycle coupon level hardware at a maximum rate of forty two cycles per day. Figure 2-38 as an example of the temperature data acquired during test development of the rapid thermal test stand. A significant amount of thermal cycling testing has been completed to determine the test protocol required to correlate the test stand results to stack test results and not introduce any foolish failures.

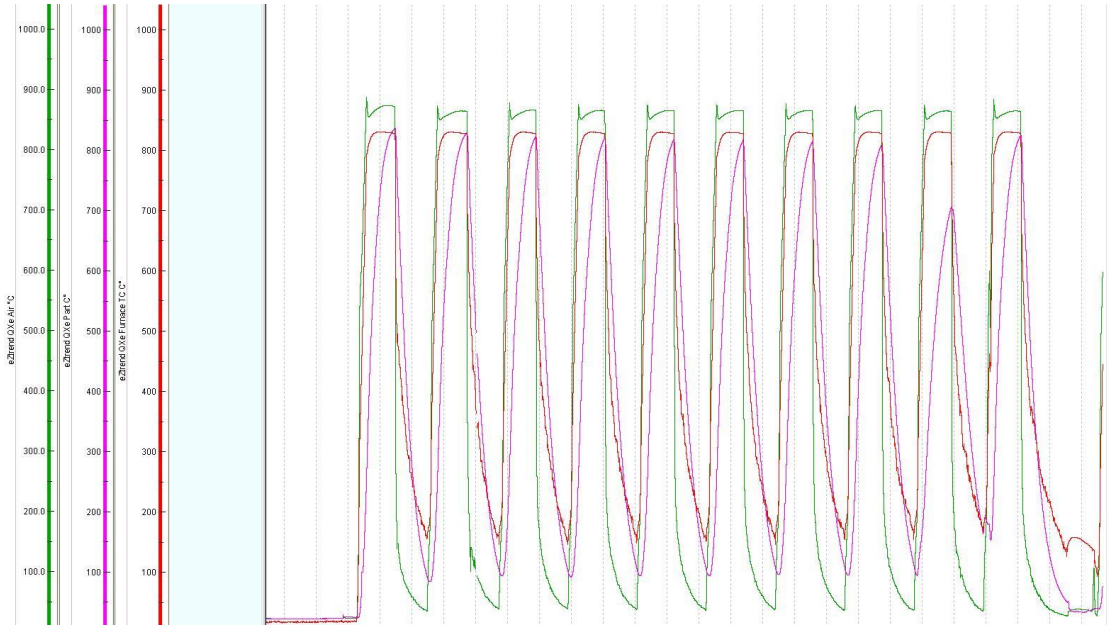

Figure 2-38: Thermal Cycle Temperature Data

An abbreviated set of screening tests were started in the fall of 2011 on novel coatings. The thermal cycle portion of this test has completed 200 thermal cycles using 441 and the standard repeating unit seal material. Refer to Figure 2-39.

Long term thermal cycle testing on a number of different shear coupons is complete. This test utilized shear coupons primarily of SS441, with several Crofer samples. Compatibility tests with novel sealing glasses, substrates and after-treatments have been completed. As a cost reduction, maximum reclaim of repeating unit seal material (termed “100% recycle”) was investigated as

well as newer, doped seal materials. 100% recycle seems to have a lower crystalline content then the current glass ceramic seal (at 30% recycle content). Lower crystalline contents improve reliability of the glass ceramic seal.

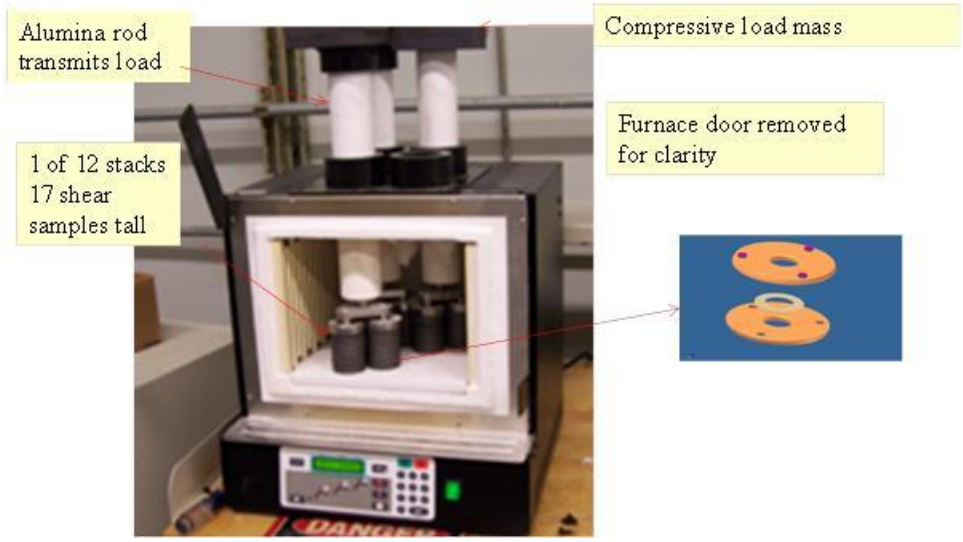

Figure 2-39: Thermal Cycle Test Setup

Repeating unit seal material development efforts have continued to be investigated utilizing a number of metrics, including DMA (dynamic mechanical analysis), phase development, residual glass level, pop gun strength, and thermal expansion, as a function of thermal cycling at elevated temperatures (850-875°C). Three specific compositions of glasses have been chosen for in-depth testing and characterization studies. G18 has been compared to G18-based glasses with chemistry modifications to reduce the formation of hexacelsian and monocelsian phases (which have thermal expansion coefficients lower than the bulk glass, other crystalline phases, and other cell components). By reducing or eliminating these celsian phases, stresses within the glasses should be reduced, thereby improving the seal strength and durability over long times at temperature. Better matching the thermal expansion should also improve the ability of the seal to be thermal cycled without significant stress build-up and eventual failure.

Radar or spider plots have been developed with targeted glass properties. The properties examined include change in XRD patterns and % residual glass from after the glass is set and thermally cycled 100 times at 850°C (this also includes undesired formation of monocelsian phases), popgun strength after glass set, popgun strength after thermal cycling 100 times at 850°C, thermal expansion value after glass set, thermal expansion value after thermal cycling 100 times at 850°C, and DMA response after glass set with applied load of 10 psi. The results of the three glass compositions with varying second phase additions are on-going. Table 2-2 shows the glass properties examined and the targets.

Table 2-2: Glass properties investigated and targets

	Target
DMA (10 psi) glass set profile	>70
XRD as set 100TC @ 850°C	minimal or no hexacelsian monocelsian
Pop Gun Strength as set 850°C-100TC	> 40
Thermal Expansion as set 850°C-100TC	≥ 10.5

The results from the above battery of property measurements have helped identify a compositional change to the base G18 glass formulation and to the amount of the second phase to be added which, taken together, results in a more stable coefficient of thermal expansion and a more stable microstructure during hundreds of thermal cycles. This composition is currently being tape cast and scaled up for stack testing.

Performance and Durability Evaluation of Stacks

1) electrochemical performance evaluations in continuous current extended durability
2) electrochemical performance in thermal and load cycling operating modes
3) electrochemical testing in accelerated aging conditions, such as elevated current density

Delphi continues to test Gen 3 and Gen 4 stacks. Figure 2-40 shows data from a 40 repeating unit Gen 4 stack. The initial IV curve showed a power density of 490 mW per cm^2 at an average voltage of 0.81 V (current density of 595 mA per cm^2, 750°C, 48.5% H_2, 3% H_2O, balance N_2). This stack was used for evaluating the peak power using simulated coal gas reformate. Figure 2-41 shows data from the steady state operation for one hour at a peak power of 6.42 kW (power density of 399 mW per cm^2, 0.7 V average per cell, 50% utilization).

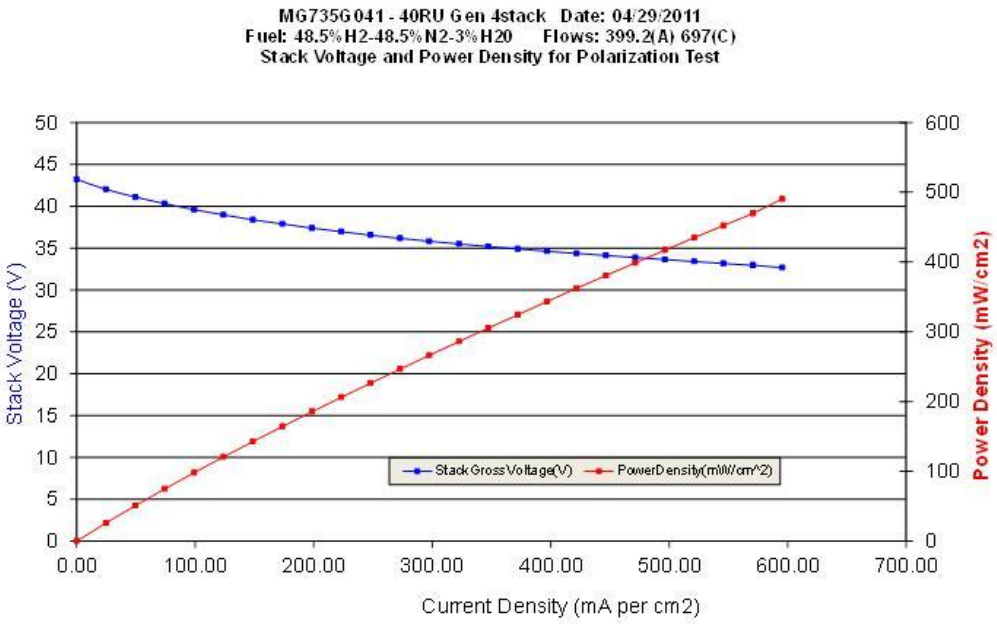

Figure 2-40: IV data from a 40 RU Gen 4 stack

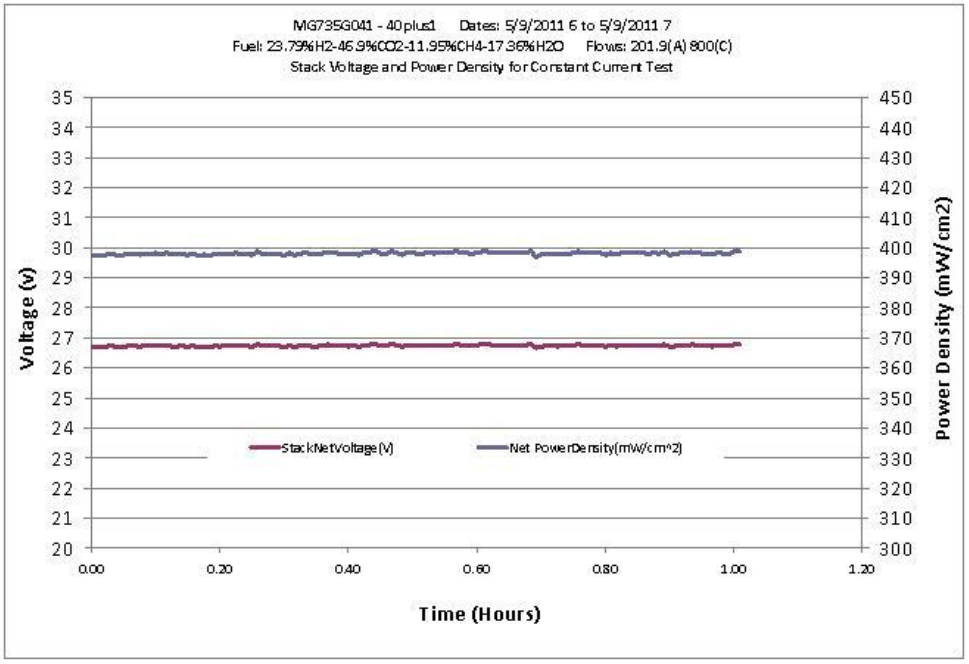

Figure 2-41: Steady state operation at peak power conditions with 40 RU Gen 4 stack

Previously, Delphi reported poisoning of the nickel anode was determined to be the root cause of a stack's initial (approximately) 10% power degradation. Since the discovery of the poisoning mechanism, several Gen 4 stacks have been constructed using the newest anode conductive paste. Figure 2-42 confirms the change in the anode conductive paste eliminates the 10% power loss in the first hours of testing, and stack performance is stable.

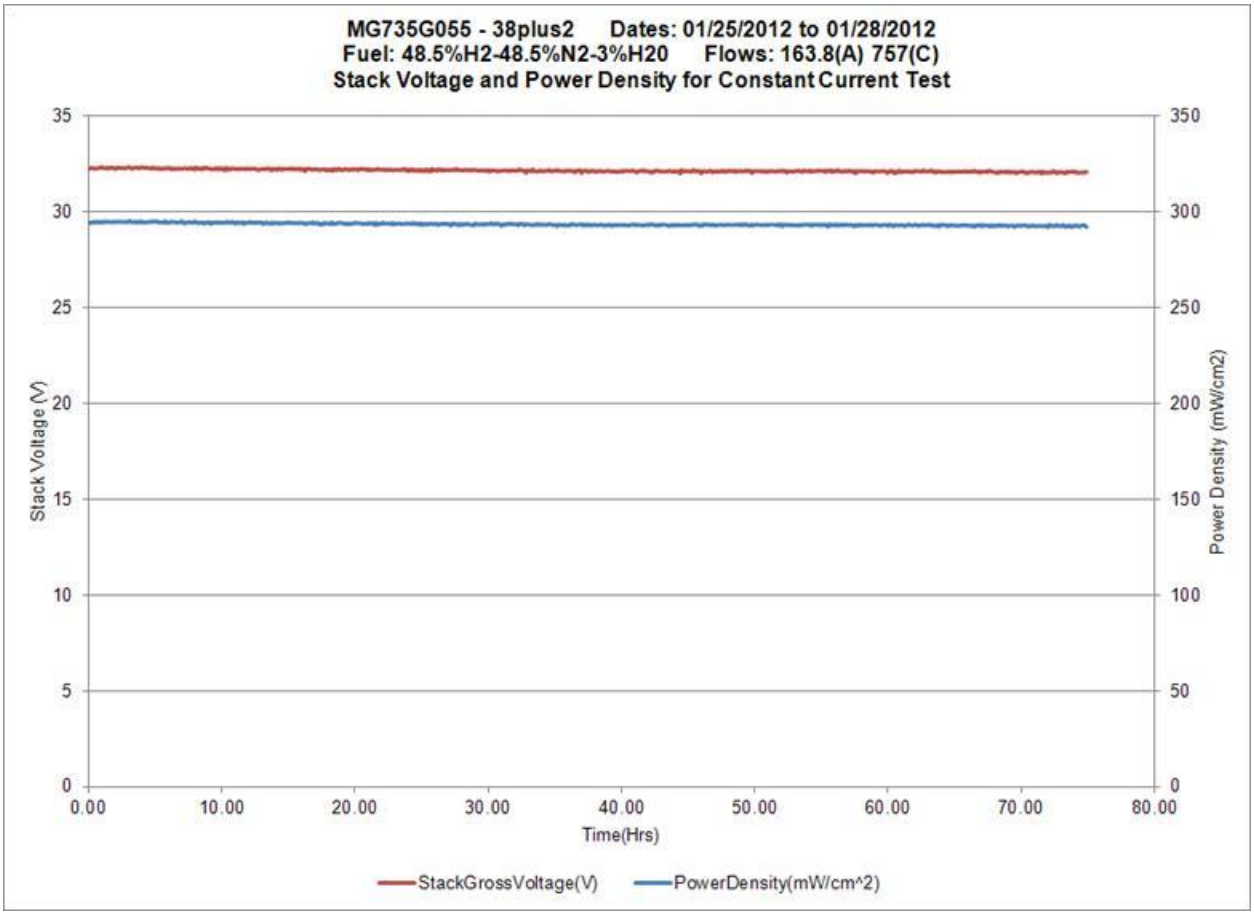

Figure 2-42: Constant current durability data for 70 hours

Thermal cycling of full-sized stacks has intermittently occurred over this contractual period. Three 30-cell Gen 3 stacks have each been deep thermal cycled (~ 100C to stack operating temperature) for long periods with stable performance results. Two stacks were each thermal cycled over 120 times, and one stack was cycled over 200 times. The mean voltage performance of the stack cycled over 200 times is shown in Figure 2-43. When tested at 299 mA/cm2, this stack exhibited an end of test voltage degradation of only 4%. Additionally, the end of test voltage degradation of the two stacks tested 120+ cycles were calculated as 3% and 7% (tested at 283 and 288 mA/cm2)

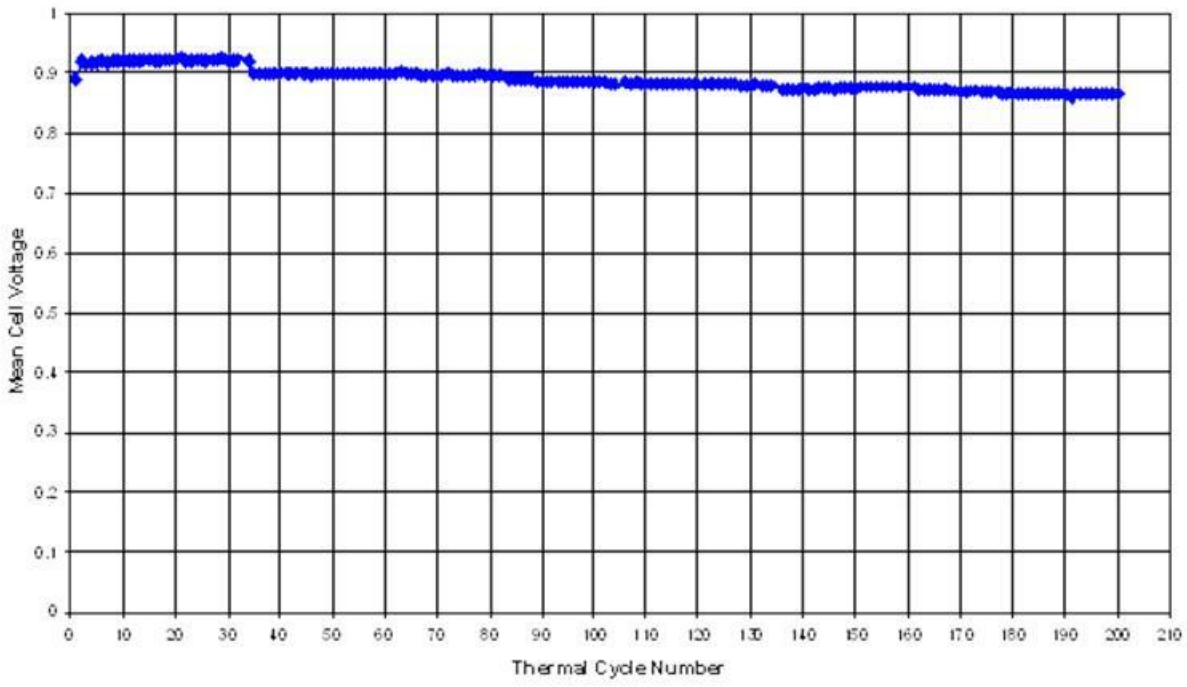

Figure 2-43: Thermal Cycling Performance of 30-Cell Gen 3 Stack

Thermal cycling evaluation of Gen 4 stacks continues. Results are shown in Figure 2-44. A 30-cell Gen 4 stack with a number of different configurations of interconnect-cell-separator plate interface material combinations was removed from testing after 72 thermal cycles. Current level was adjusted twice during the testing, as one of the treatment combinations approached the low voltage cut-off limit set for this test. The stack voltage remained very constant through the entire course of the thermal cycling.

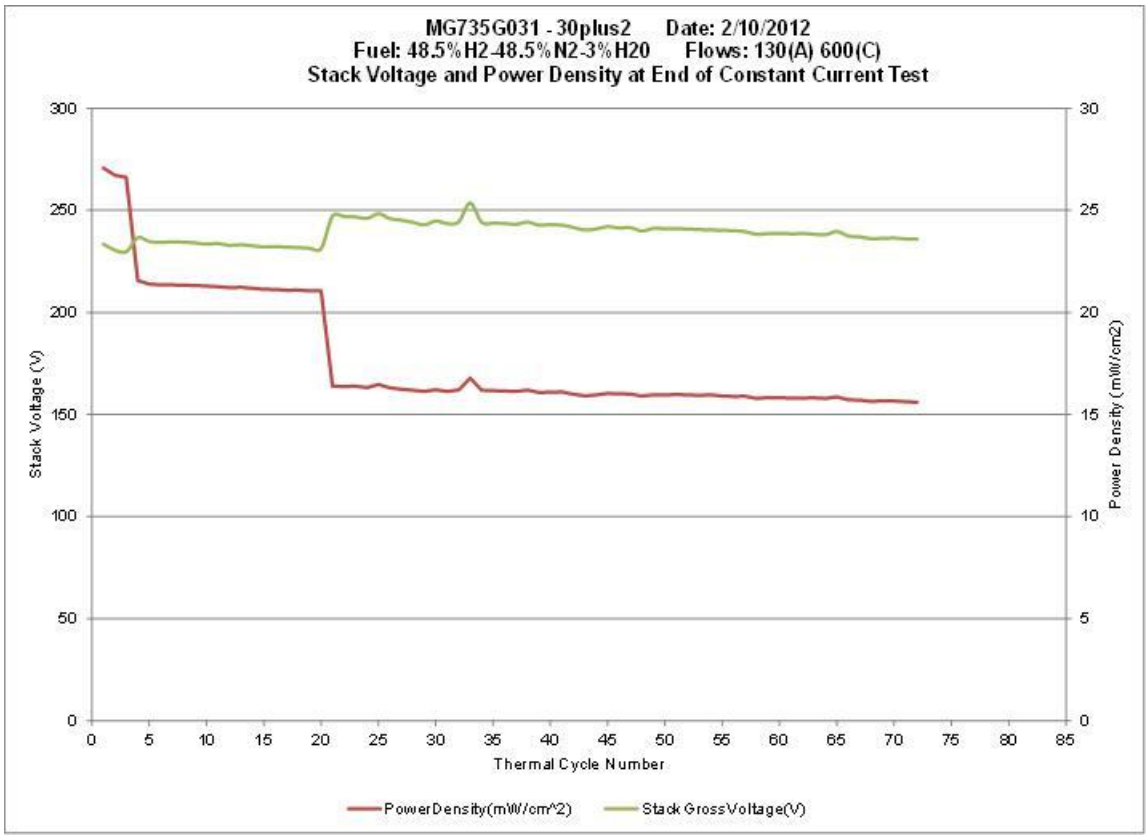

Figure 2-44: Thermal cycling of 30-cell Gen 4 stack

A second 30-cell Gen 4 stack was also thermal cycled and completed 130 deep thermal cycles prior to completing the test. The results from this stack test are shown in Figure 2-45 below.

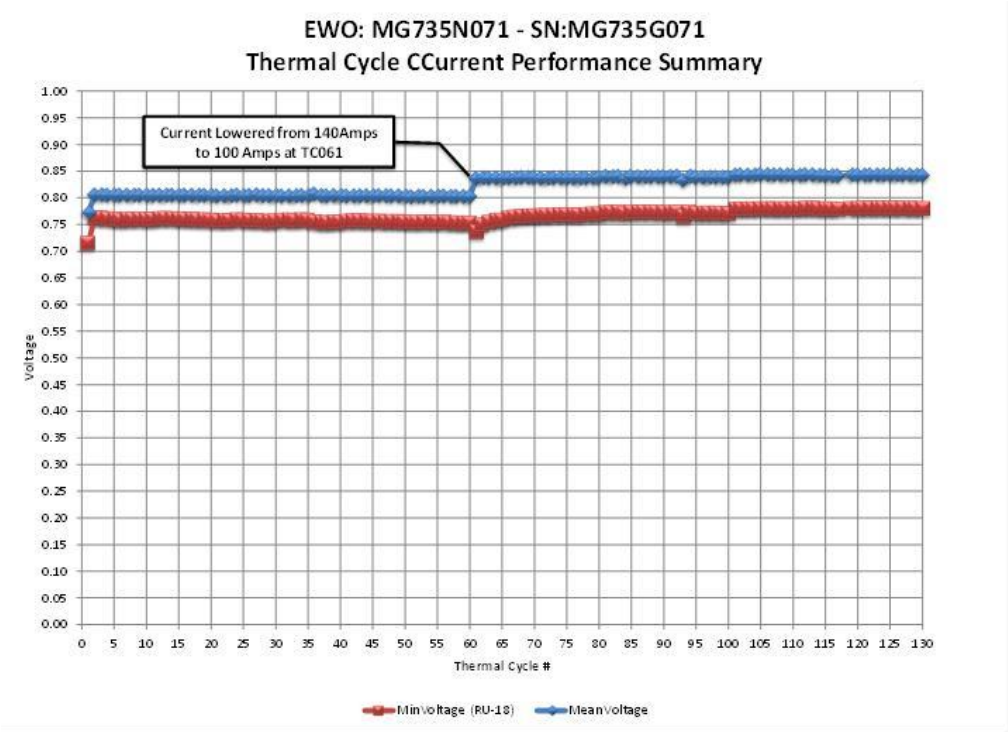

Figure 2-45: Thermal cycling of 30-cell Gen 4 stack

Gen 3 stacks have also been shock and vibration tested to determine their robustness for multiple applications. First, using a step over-stress strategy, Delphi completed vibration testing on a 30-cell Gen 3 stack based on a modified Mil Std 810G, "Truck and Transportation Over US Highways" standard. The testing was conducted at ambient temperature, and the stack was subjected to random vibration in 3 distinct axes, as shown in Figure 2-46.

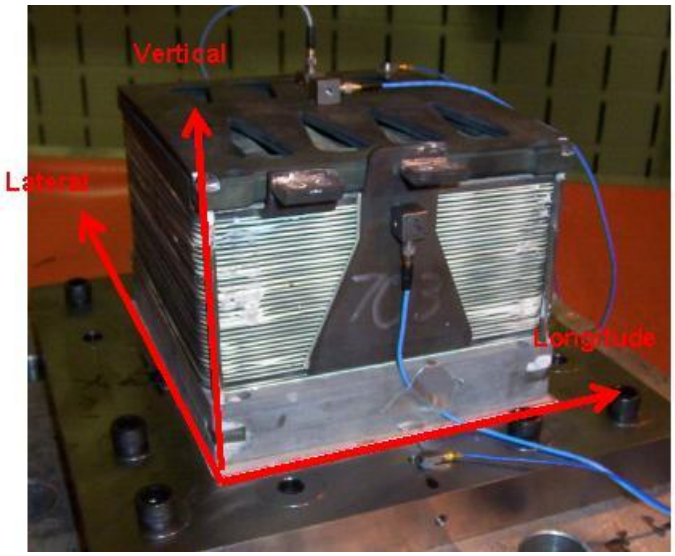

Figure 2-46: Gen 3 Stack Mounted on Vibration Platform

The stack was evaluated for performance after each axis of testing. As shown in Figure 2-47, the stack successfully completed 3.75 million vehicle miles equivalent vibration with no measurable performance degradation.

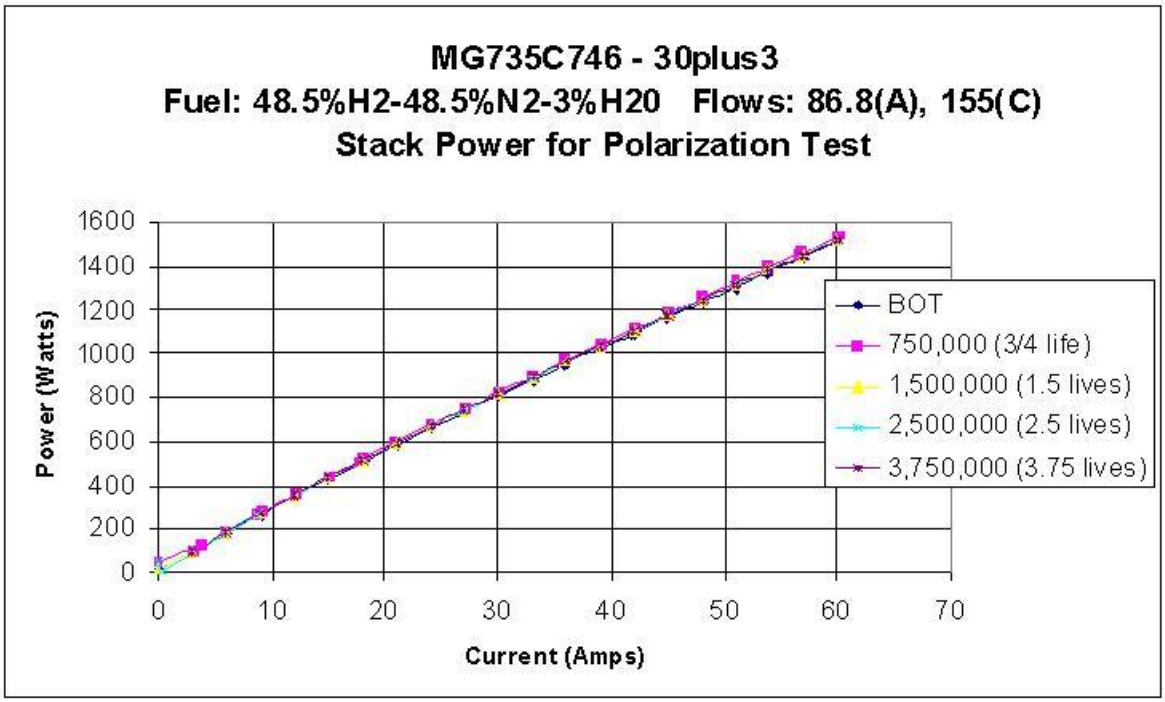

Figure 2-47: Performance from 30-cell stack after 3-axis vibration test

In addition to vibration testing, a 30-cell Gen 3 stack was also subjected to an ambient temperature dynamic shock test schedule. The testing simulates a high percentile (96th %) Class 8 truck user at 4 years/1M miles of ambient dynamic shock. The Delphi validation team developed the test profile based actual Class 8 semi-truck road conditions. The profile was generated from data taken at a truck OEM's test track in spring of 2009. A Semi Truck/Trailer was instrumented with accelerometers and driven over several different open and closed track road conditions, as shown in Figure 2-48. The profile also incorporated Class 8 long haul user profiles from ATRI driver surveys.

Figure 2-48: Development of Dynamic Shock Test Profile

The Dynamic Shock Test consisted of a Gen 3 stack mounted to a shaker via an adaptor then exposed to four scenarios, which, taken together, constituted greater than 1400 shock events. The events included:

- Low G Truck to Trailer Hook-ups
- Moderate G Speed Bumps
- High G 20mph Speed Bumps
- Severe G 30 mph Chuck Holes

After each of the dynamic shock events listed, the stack leakage and electrochemical performance were measured. As shown in Figure 2-49, no stack cross leak (anode to cathode) was identified throughout the test. Also, anode and cathode external leakage increased slightly, but remained within specification after a representative lifetime of one million equivalent miles.

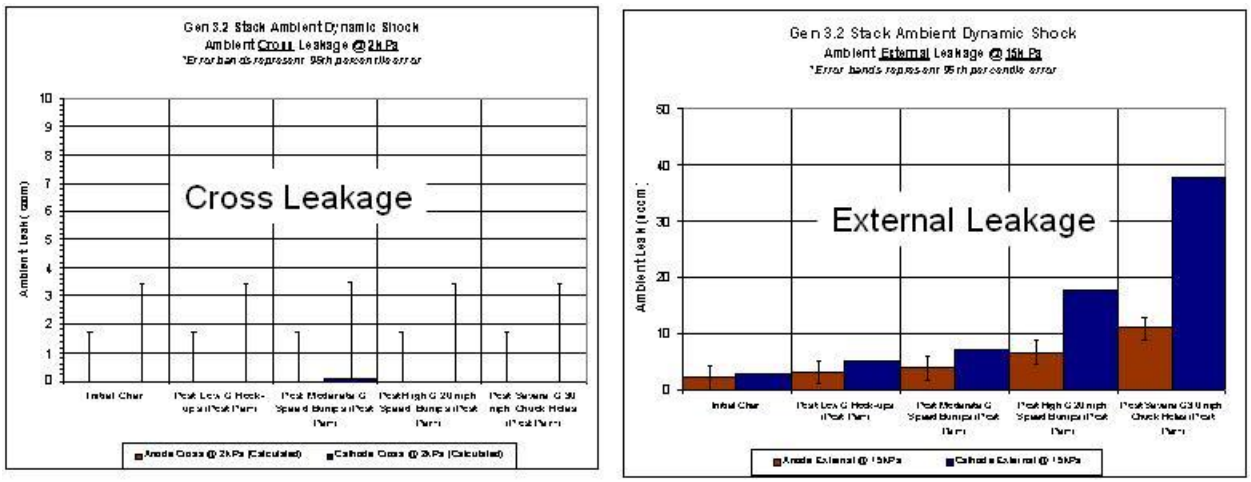

Figure 2-49: Dynamic Shock Leakage Performance

As mentioned above, stack electrochemical performance was also characterized after each series of dynamic shock events. As shown in Figure 2-50, no significant change to the 30A mean stack voltage occurred during testing, and the mean stack voltage at 570 mA/cm2 remained within 2% throughout the test.

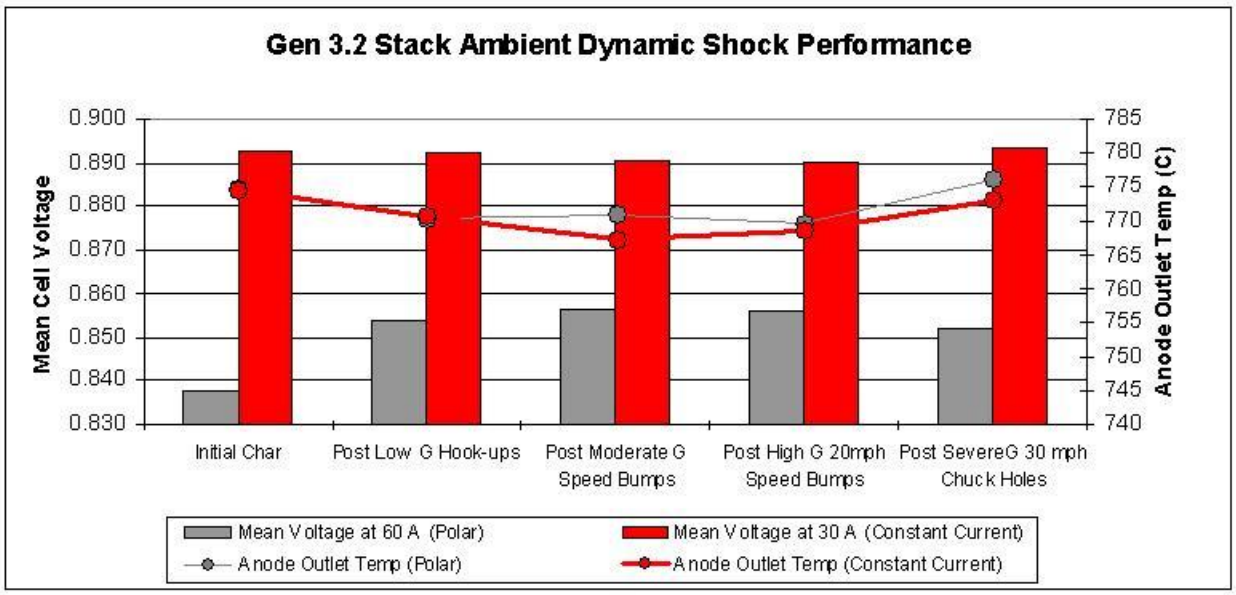

Figure 2-50: Dynamic Shock Electrochemical Performance

A Gen 4 experimental stack was removed from testing after 5,058 hours of steady state, constant current operation, and represents the longest durability exposure of the Gen 4 design to date (Figure 2-51). Ten unique design combinations were included in this 30-cell stack. The design factors varied included the following:

- Anode Attachment Method and Material

- Cathode Attachment Method and Material
- Anode Attachment Pattern
- Conductive Paste Weight
- Anode Interconnect Plating Method

The stack current was adjusted at 100 hours, forced by the low performance of a single repeating unit within the stack. This stack underwent an end of test autopsy to identify the mechanisms of degradation associated with the ten unique design combinations. Those observations have been made and have been fabricated into the latest stacks to be durability tested. Two of those stacks are currently on test, with promising performance results to date.

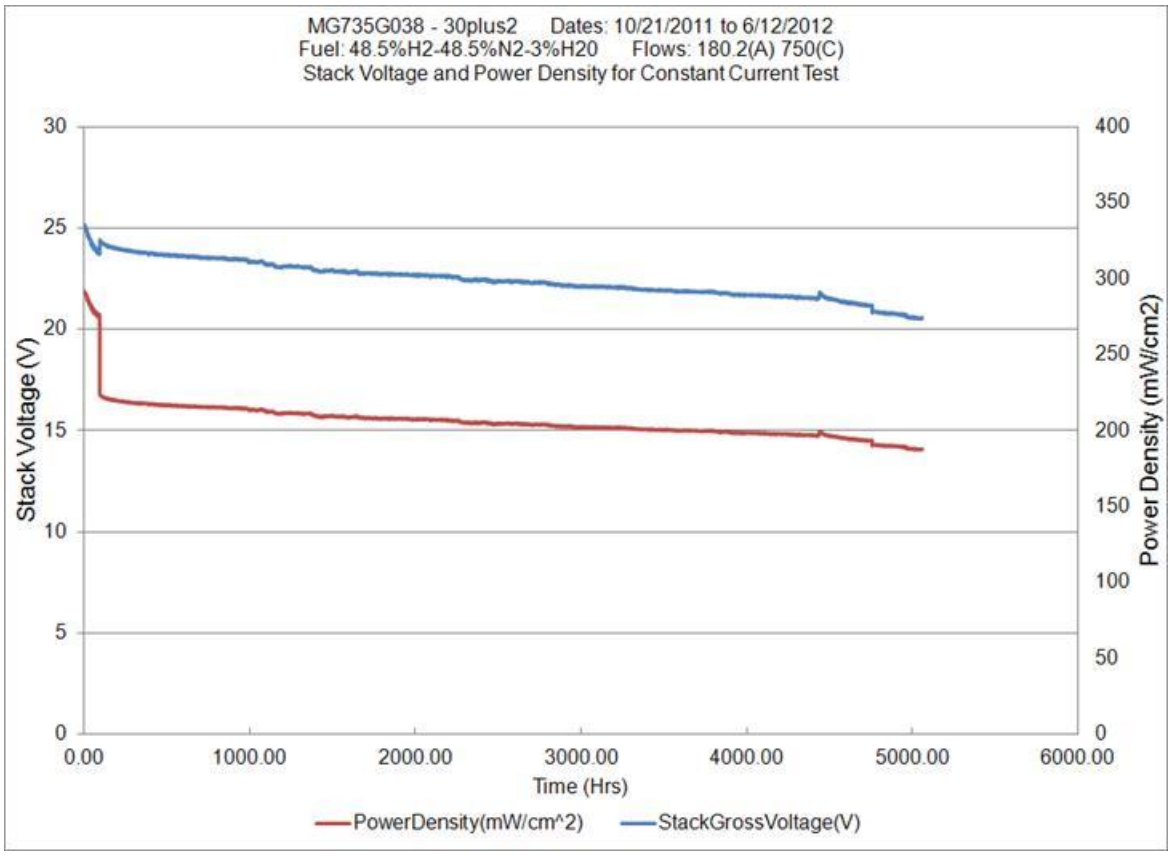

Figure 2-51: Constant current durability data for 5058 hours

Stack Test at UTC

Four 40-cell Gen 4 stacks were fabricated for the 25kW test article to be tested at UTC. Upon stack fabrication, each stack was performance tested at Delphi, prior to delivery of the set of four to UTC. By example, Figure 2-52 below is a plot of the stack voltage and power density on 48.5H2-48.5N2-3H2O at a 140 amp constant current test.

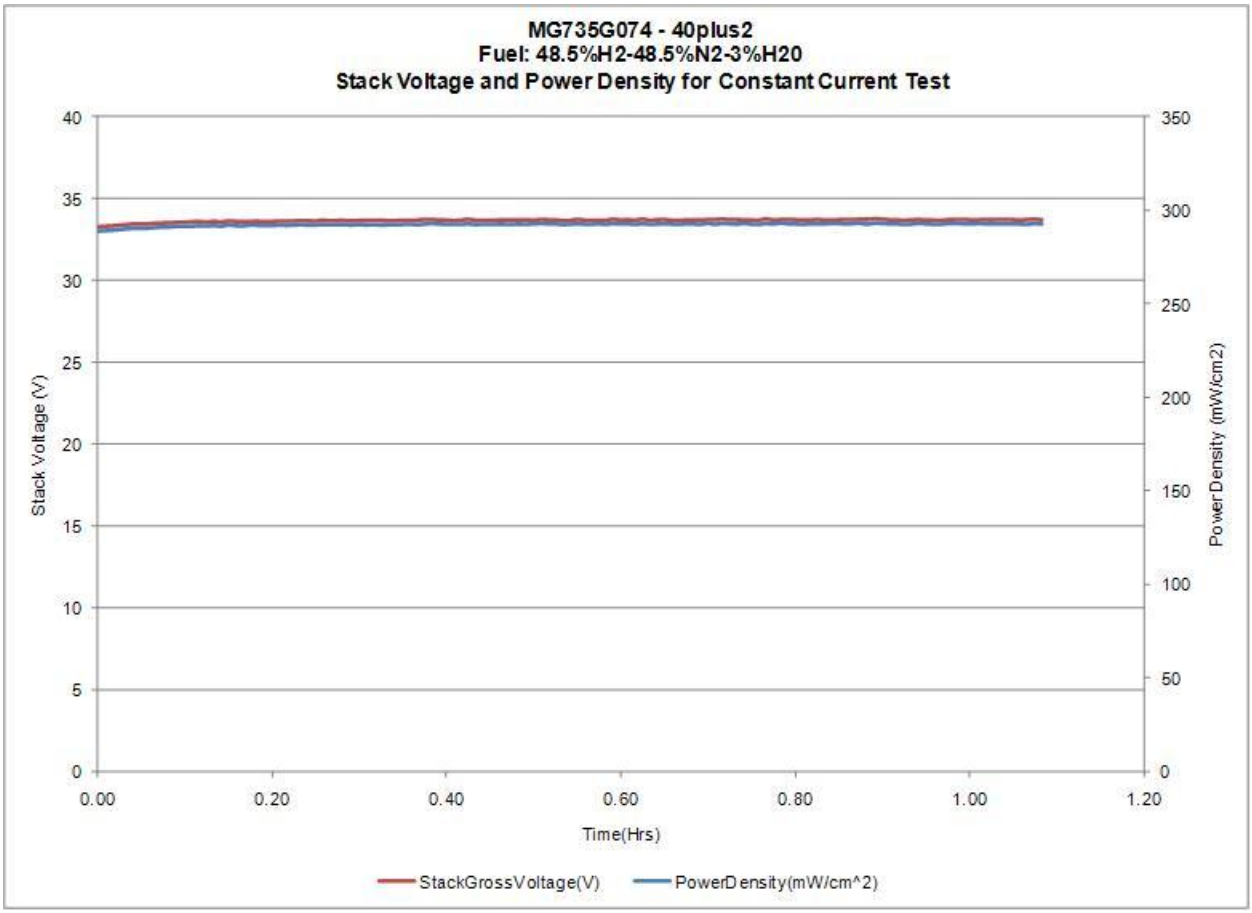

Figure 2-52: 40 Cell Stack performing at 140A Constant Current

The 25kW test article was initially operated, uninterrupted, through the first quarter of 2012 with a single stack installed on the test article. The stack operated at 60 amps for approximately 1200 hours with very stable performance, see Figure 2-53. The stack generated 1.9 kW for approximately 1200 hours with little to no change in stack voltage. The test article then underwent disassembly and was prepared for Phase II and the full complement of four stacks.

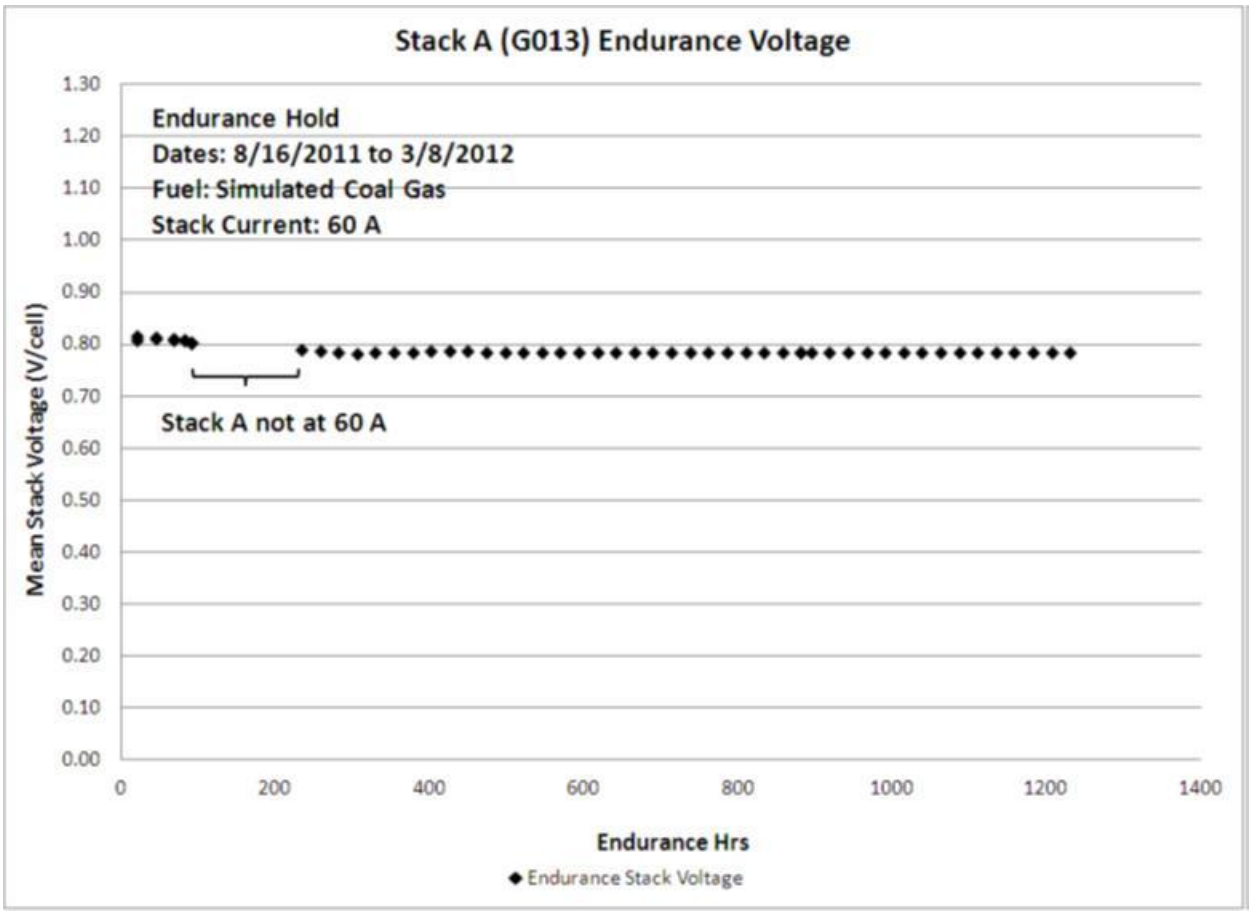

Figure 2-53: Durability Data of Stack G013

The 25kW test article was in operation with two stack assemblies and two jumper assemblies when a component, one of the anode heaters of the test stand suffered a failure and the test shut down on July 19th. Upon recovery and restart of the system the stacks displayed reduced performance, see Figure 2-54. Upon further review the data suggests the stack located in the "A" position on the manifold no longer exhibited the typical endothermic reaction temperature profile, see Figure 2-55. Figure 2-56 displays the increasing amount of methane at the exit of the stack in the "A" location on the manifold, which confirms the lack of internal reforming that was exhibited by the change in the temperature profile.

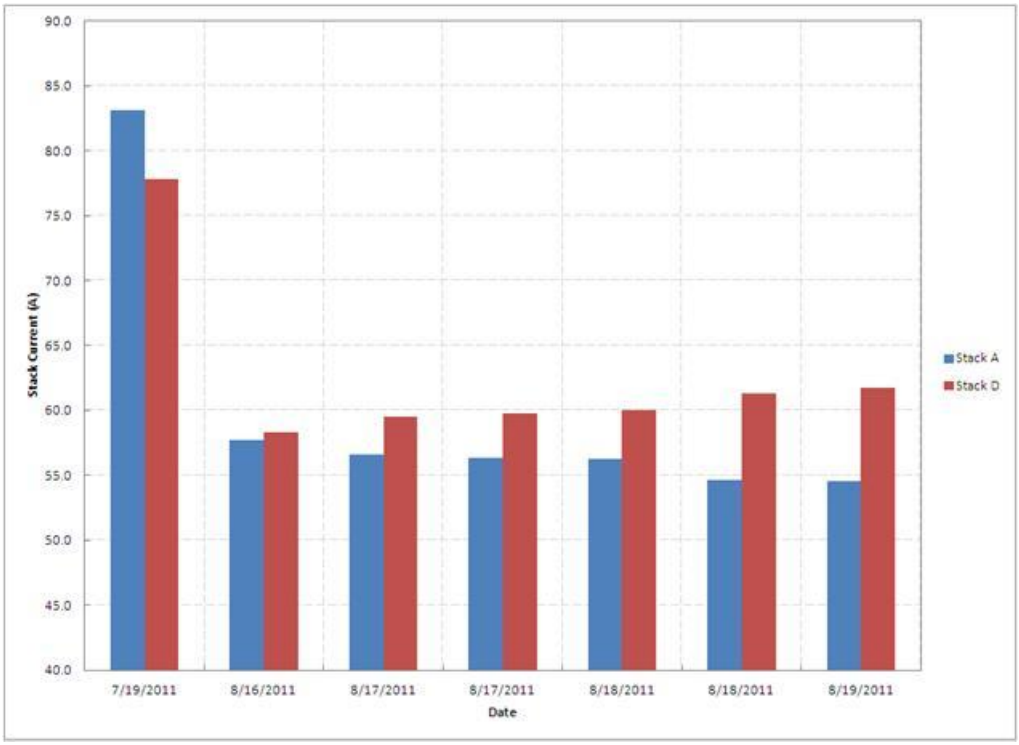

Figure 2-54: Stack Performance

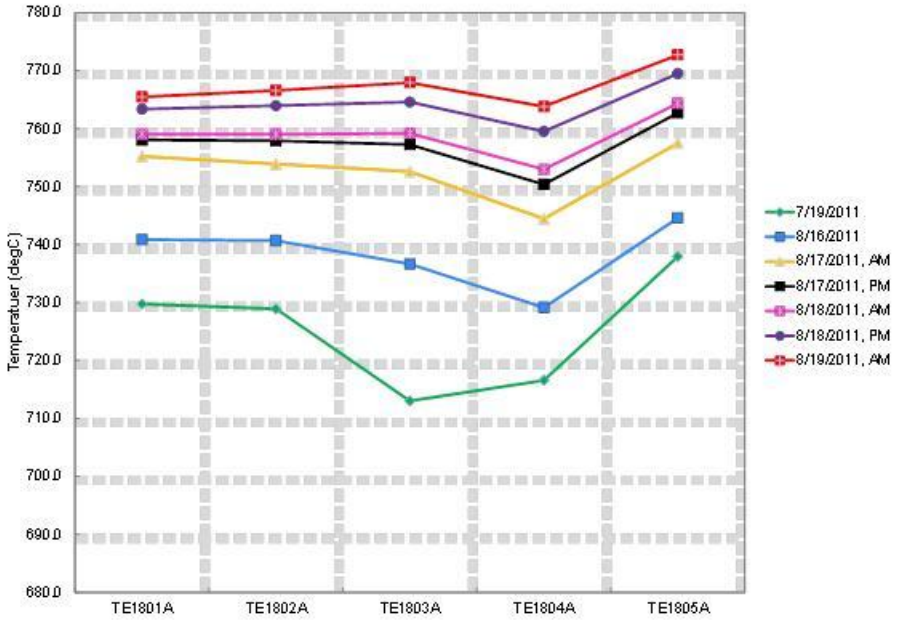

Figure 2-55: Thermal Profile

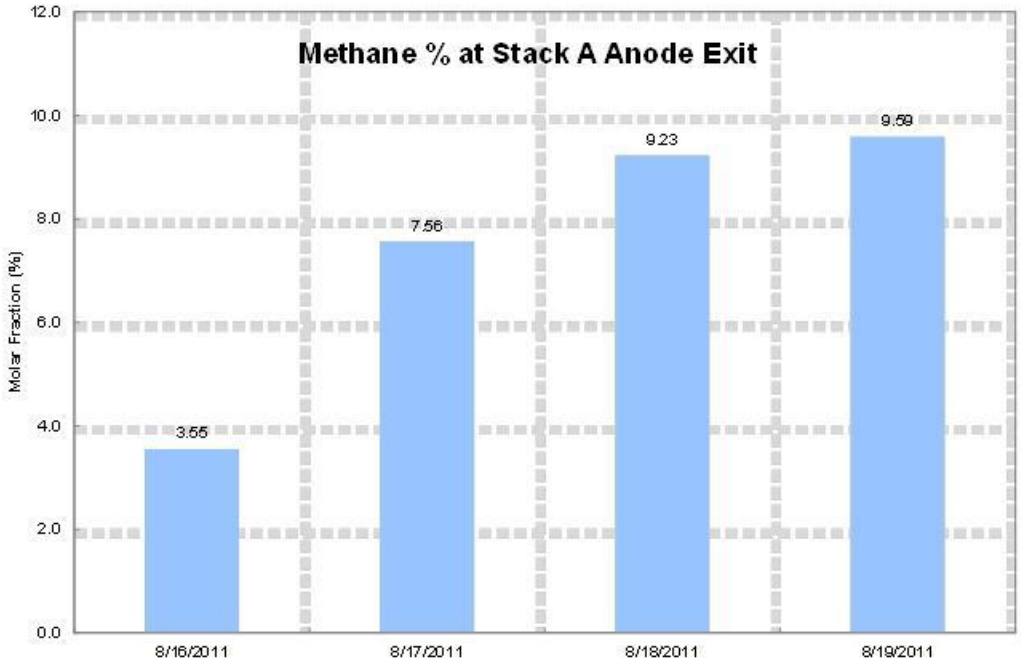

Figure 2-56: Methane at Stack A Exit

The loss of methane conversion in two stacks that were tested at UTC in Phase II of the SECA CBS coal-based IGFC project was then investigated. A 5-cell Gen 3.5 stack was tested to determine whether the anode conductive paste, printed between the anode interconnect and the separator plate, reduced the methane conversion ability of the cell. Poisoning of the anode was previously found to be responsible for the initial 10% power loss of the stack, and so the anode contact paste was changed to a material which did not contribute to anode poisoning. The stacks tested at UTC were built before the change in anode paste was made.

Figure 2-57 shows the cell voltage and the stack-outlet methane concentration as a function of time using a coal-gas feed stream that matched the testing at UTC. The cell voltage drops over the first 50 hours of testing, as expected due to the poisoning of the anode, while the methane concentration at the outlet increases by 50%.

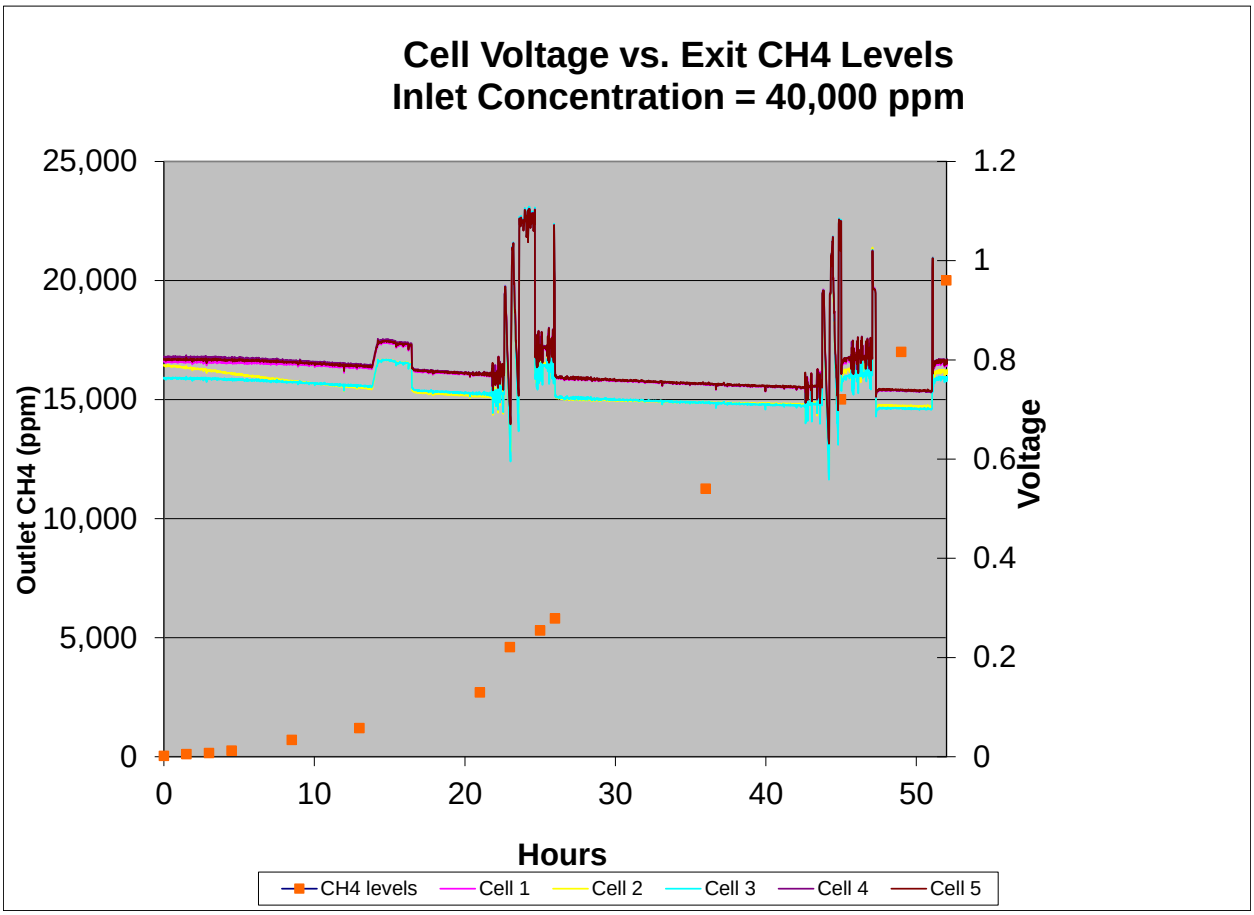

Figure 2-57: Cell voltage and methane concentration as a function of time in coal gas

Figure 2-58 shows the electrochemical impedance of cell 2 from zero hours to 144 hours. The first arc of the impedance plot, representing the chemical activation process, is increased after 24 hours indicative of a poisoning mechanism. The second arc of the impedance plot, representative of the mass transport process, is also increased indicative of reduced H_2. The reduction in H_2 is theorized to be caused by the impeded internal reforming reaction.

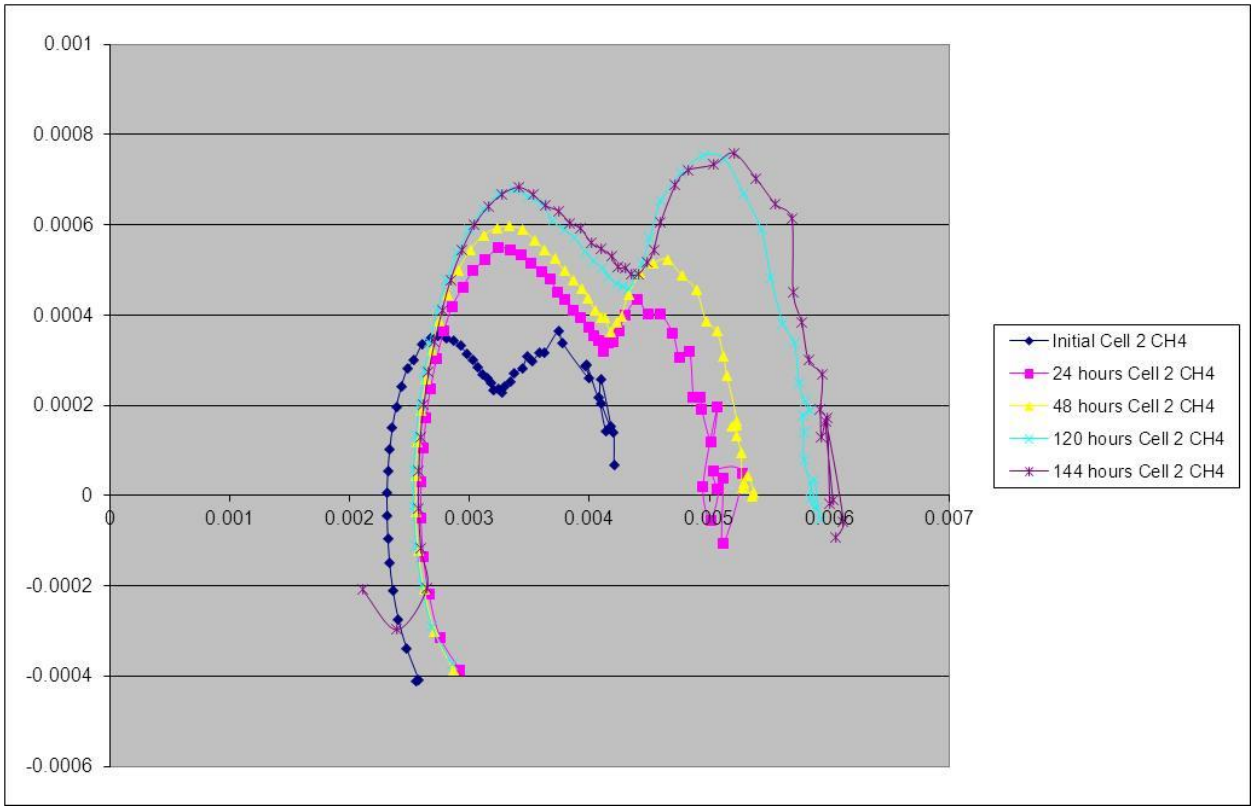

Figure 2-58: Electrochemical impedance of cell 2 from zero hours to 144 hours in coal gas

Figure 2-59 shows the impedance plots of cell 2 over the same time period, except with H_2/N_2 as the feed gas. Here, the mass transport arc is not increased, indicating that the poisoning impeded the methane reforming reaction, as opposed to physical blockage of the anode.

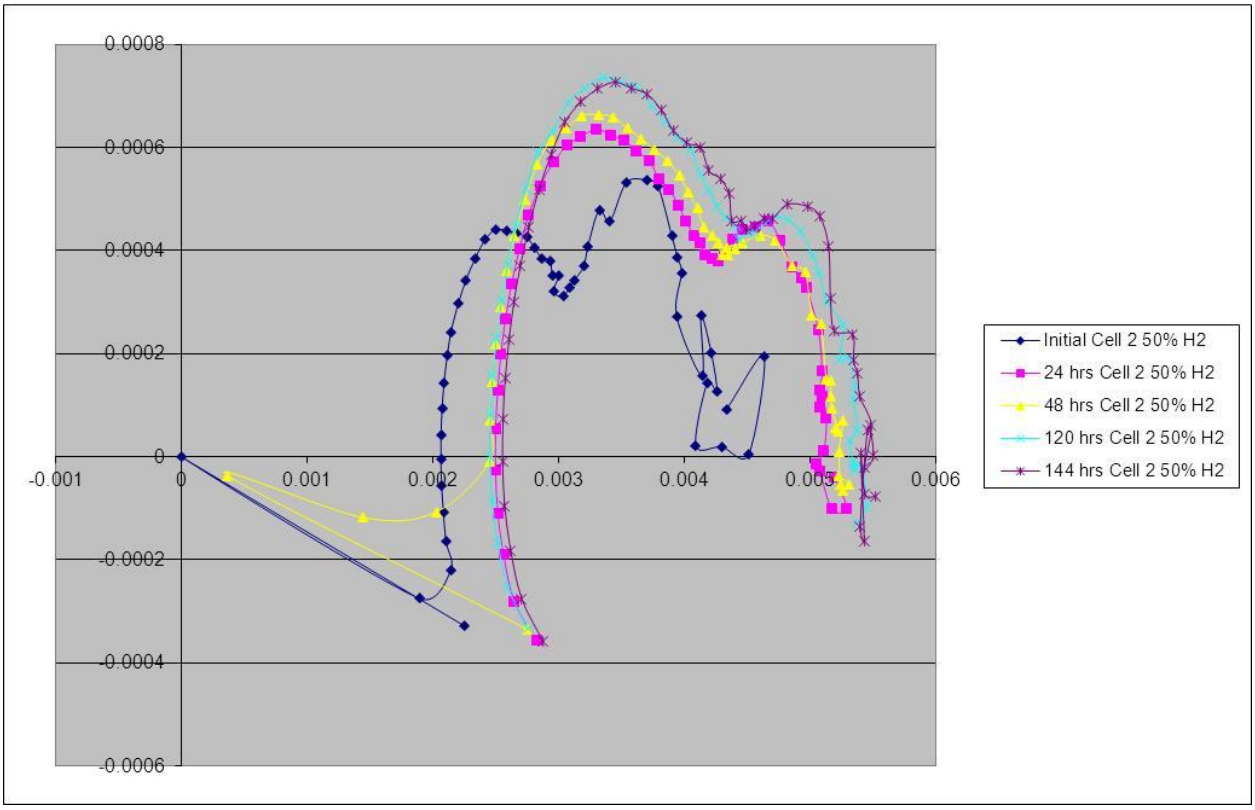

Figure 2-59: Electrochemical impedance of cell 2 from zero hours to 144 hours in H_2/N_2

Additional stacks have been tested with the newest anode contact paste to compare with the poisoned stack results for methane conversion. They have confirmed the performance stability of the newest contact pastes.

Stack Internal Reforming

1) Test an instrumented Gen 4 stack on simulated, methane-containing coal gas blends, to characterize the stack's ability to "stably" internally reform the methane
2) Identify the root cause for any characterized instability
3) Identify a set of operating conditions for stable operation of the Gen 4 stack using a high (~ 12%) methane content fuel blend

A 10-cell Gen4 G-061 stack was tested with five (5) different fuel feeds to determine the conditions for stable operation (Table 2-3). Figure 2-60 is a plot of cell voltage versus time for this stack at the various fuel feeds shown in Table 2-3 in the order listed. The methane conversion rate was not measured during this test. Note the linear degradation for the first 275 hours with the 12% methane feed. The methane was then reduced to 0% for 65 hours resulting in a stabilized voltage. The methane was then increased to 3% and no voltage degradation was seen for 90 hours. Increasing the methane to 6% and 9% resulted in degrading cell voltages. Due to the somewhat reversible response when methane is eliminated from the feed, it is theorized that this type of voltage degradation is caused by carbon deposition at steam/carbon

ratios below 3/1. Future stack tests are planned to further define the operating space of the fuel cell in coal gas, measuring the methane conversion, and utilizing electrochemical impedance spectroscopy to distinguish between cell poisoning and mass transfer limitations caused by carbon deposition.

Table 2-3: Varying coal gas feeds for Gen4 stack G-061

Molar/Volume Form								
H2	CO	CO2	CH4	H2O	N2	Steam/Carbon	O/C	LHV (100 slpm)
24%	0%	47%	12%	17%	0%	1.417	1.88	14.40 kW
45%	0%	40%	0%	15%	0%	0	2.38	14.77 kW
52%	0%	28%	3%	17%	0%	5.67	2.35	18.70 kW
42%	0%	35%	6%	17%	0%	2.83	2.12	17.05 kW
33%	0%	41%	9%	17%	0%	1.89	1.98	15.73 kW

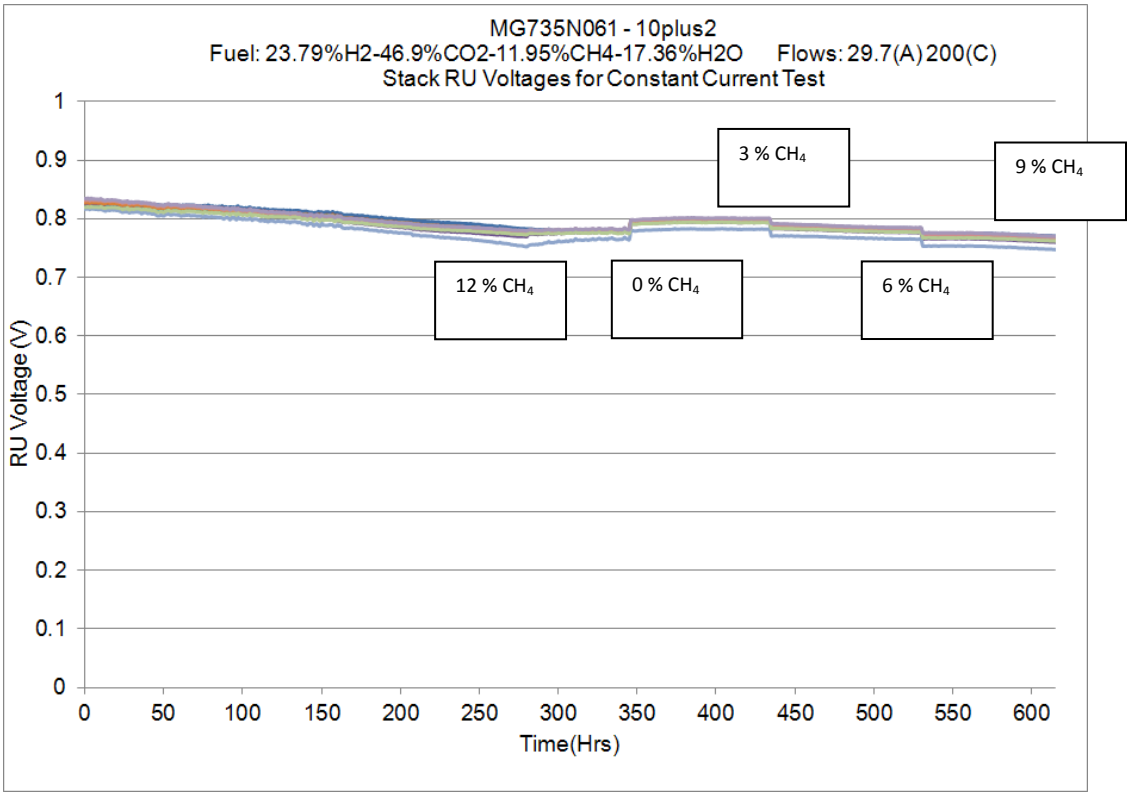

Figure 2-60: Stack G-061 voltage versus time for varying coal gas feeds

Cost Reduction

1) Sheet metal components from more “productive” tooling
2) Metal coatings from lower cost, production capable processes
3) Lower cost process for formation of repeat unit seals
4) Lower cost supply of anode, electrolyte, and (potentially) seal tapes

5) Lower cost supply of nickel oxide powder

Metal coatings from lower cost, production capable processes:
Part of the cost reduction effort for the Delphi SOFC stack program is to evaluate alternate aluminum coating processes for the cell retainer and separator plate. Currently, the aluminum coating is applied by a PVD process. The base material used for Delphi's SOFC cell retainer and separator plate is 441SS. While 441SS offers significant advantages (e.g., low material and manufacturing cost, high thermal conductivity, and high temperature oxidation resistance), there are challenges which can hinder its utilization in SOFC systems. These challenges include Cr volatility and reactivity with glass ceramic seals. To overcome these challenges, a protective coating for the surface offers a barrier to Cr volatilization and prevents the reaction of Cr and the glass ceramic seal.

One alternative to the current process is the cathodic arc process. This is a faster process that comes with a reduced cost. Another advantage of the cathodic arc process is the potential elimination of the coating diffusion step prior to cell brazing. The cathodic arc Gen4 retainer, as coated, can be sent through a cell braze furnace and simultaneously diffuse aluminum into the base material. The Reactive Air Aluminizing (RAA) process also has the potential of a lower cost for high volume.

Figure 2-61 shows a Gen4 cell braze joint employing a cathodic arc coated retainer plate. The retainer plate was coated and then brazed to the YSZ surface of the cell without intermediate processing. Upon shear testing the brazed joint interface, the YSZ cell material remained adhered to the retainer. In addition to good cell braze adhesion, the braze cell passed leak testing and showed low porosity (Figure 2-62).

RAA has been developed as another alternative to Al PVD. The RAA coating requires a post diffusion cleaning operation to remove loose oxide scale to achieve a good adhesion to glass ceramic seals and good braze joints with leak-free retainers. The cleaning process needs to be developed for high volume.

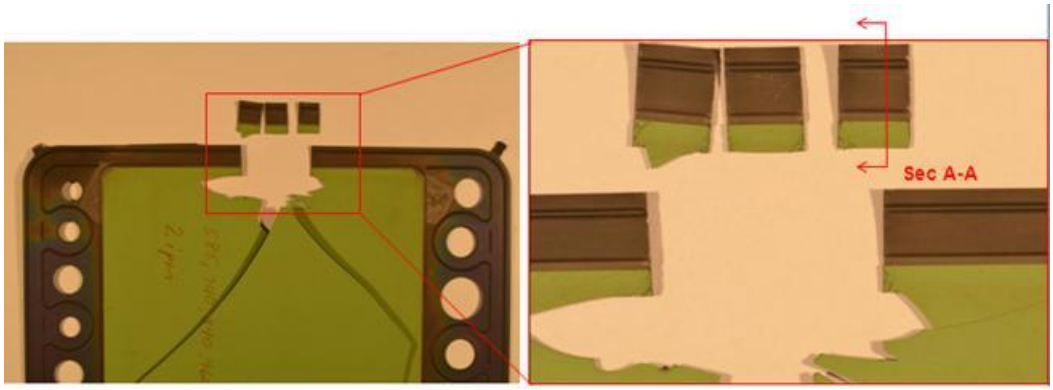

Figure 2-61: Cell braze to Aluminum cathodic arc Gen4 retainer

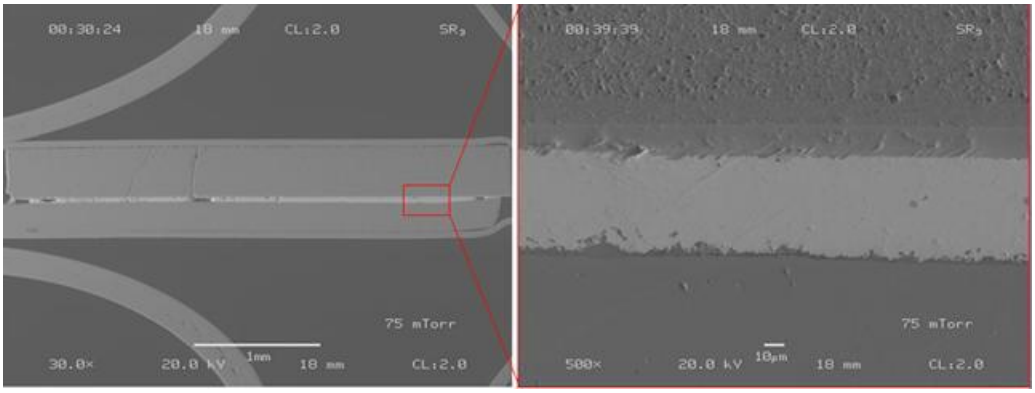

Figure 2-62: Porosity was low after cell brazed to Cathodic Arc Gen 4 retainer

Delphi has identified a second supplier of cathodic arc coatings for the aluminizing of retainers and separator plates. Delphi has received as-coated coupons and glass shear samples for a coating study. The next step is to send as-coated coupons to the material lab to prepare cross sections for coating thickness and adhesion studies. In a parallel path some of these coupons will be sent out for diffusion processing.

Lower cost process for formation of repeat unit seals

Cost reduction of repeat unit seals is being pursued using a dual-path approach. Path 1 focuses on reducing the amount of material used for the current tape-cast production method. The current process die cuts the final glass seal from a continuous sheet of glass tape, discarding the center section. The material reduction is accomplished by building a "picture frame" blank and then die-cutting the desired seal. This reduces material required by approximately 50%. Figure 2-63 shows the die-cut glass seal on top of the laminated picture frame.

The picture frame consists of three layers of thin glass tape arranged with overlapping butt-joints (Figure 2-64). The picture frame is then laminated under heat and pressure to form a continuous, thick glass seal. The lamination process knits the butt-joints together so that no leak path remains (Figure 2-65).

A small stack using the Gen 3 design has been successfully completed testing of the picture frame concept, and a 40 cell Gen 4 stack has completed 130 thermal cycles in this quarter, shown previously in Figure 2-45.

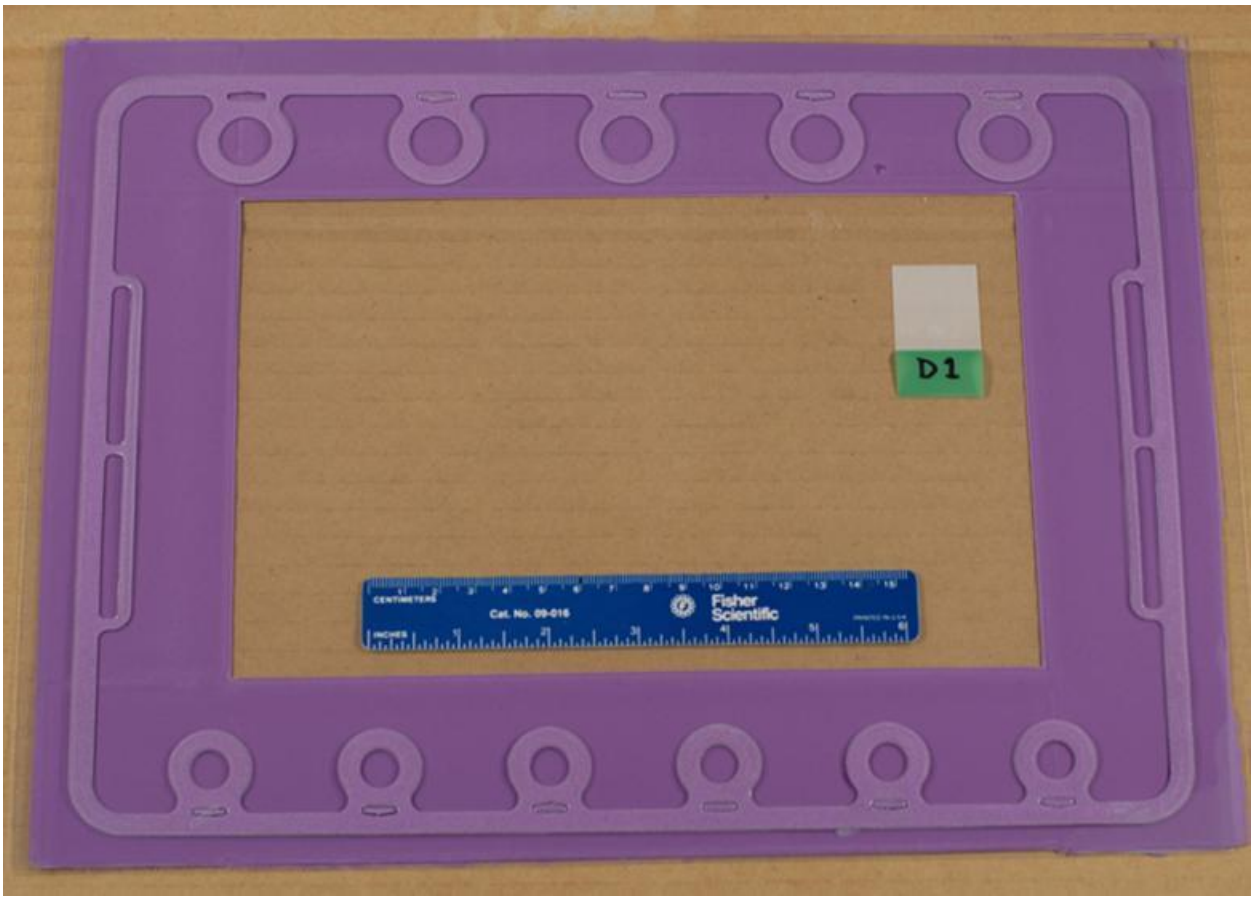

Figure 2-63: Die cut glass seal on top of glass seal picture frame.

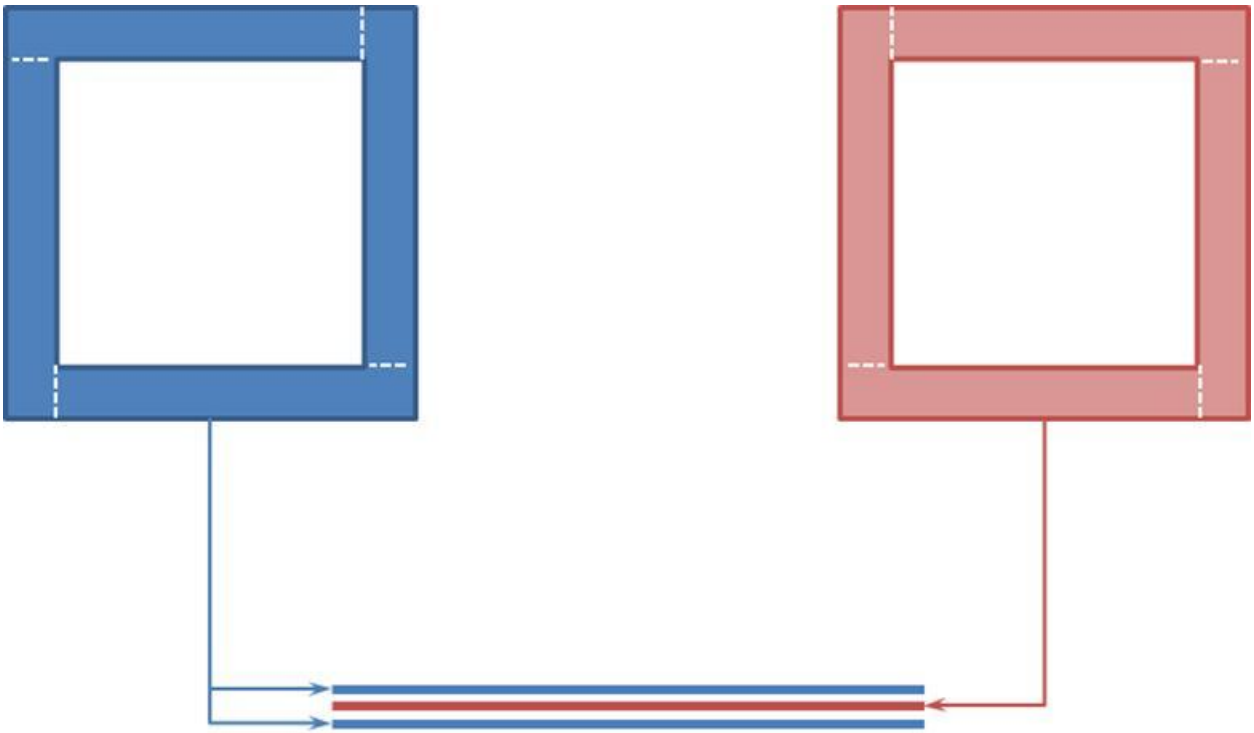

Figure 2-64: Picture frame lay-up of glass seal tape

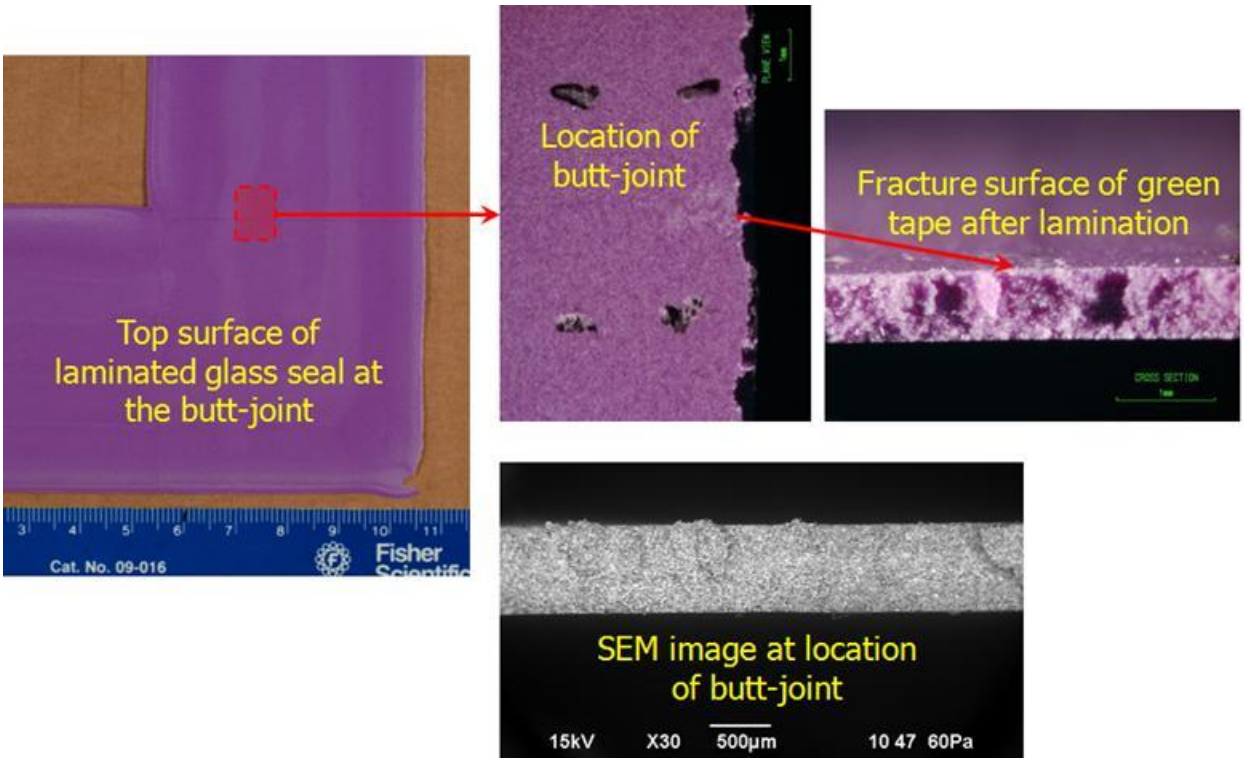

Figure 2-65: Glass seal butt-joint after lamination

Path 2 investigates alternatives to tape-casting. Two alternatives have been identified. The first uses screen print processing to achieve a net shape seal. This approach is pushing the boundaries of conventional screen print methods in order to achieve the desired part thickness for the seals. Due to the many defects associated with the printing of the glass seals, this concept has been removed from consideration.

The second alternative uses compression molding techniques. Prototype tooling has been fabricated after seeing positive results from lab testing. Initial screening tests indicate adequate room temperature shear strength of a part that is much more rigid than tape cast parts. A visual example of the compression molded material is shown in Figure 2-66.

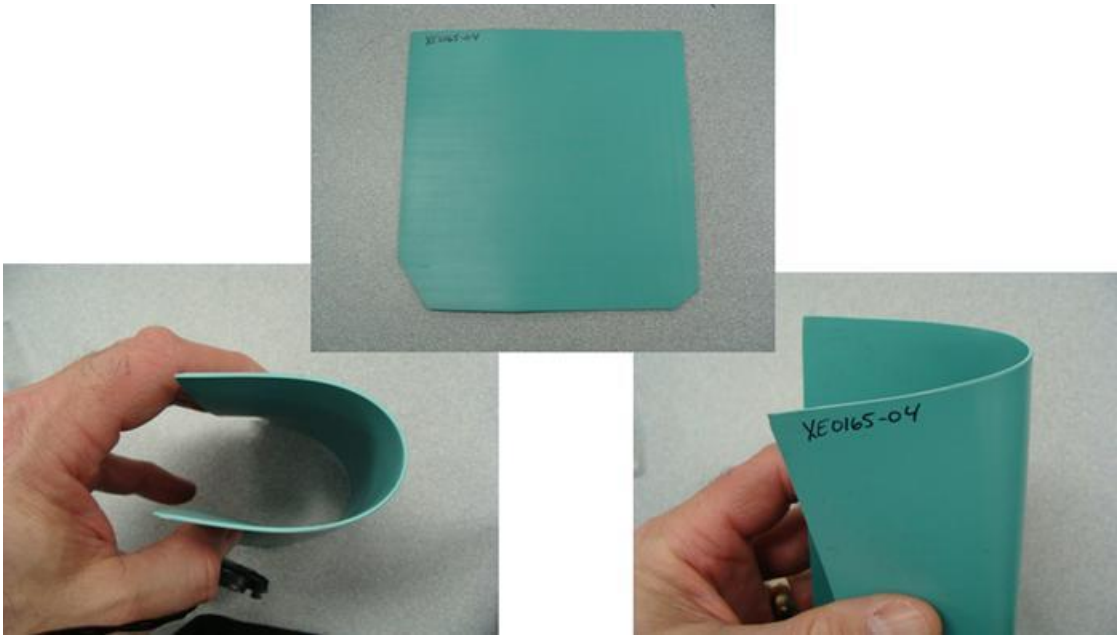

Figure 2-66: Example of compression molded seal material

An experimental stack was fabricated with seals made from the compression molding process. Seal quality, on teardown analysis, was determined to be similar to that of the current repeating unit seal material. Further testing of compression molded seals is planned in continuous current durability and thermal cycling modes.

Lower cost supply of anode and electrolyte:
Delphi also continues to work with a low cost supplier of thin tape cast (coated) films for the solid oxide fuel cell. Efforts to date have focused on electrolyte and active anode films both which are included in a co-firing operation. Since the last reporting period, Delphi has fabricated over 75 bilayers from thin tapes manufactured by the low cost supplier. Parts have been scribed into Gen4 and Gen3 footprint cells/repeating units. Delphi has worked closely with the tape supplier to characterize any defects found in the fired electrolyte. The supplier has proposed short term and long term changes to the manufacturing process to help in removing detectable defects. One step is to change the source of the Mylar carrier to a higher quality product. Also,

process changes have been implemented to reduce the number of fiber contaminants in the room and on the coating machine.

Process conditions including web speed, drying temperature, and air flow are being optimized to increase throughput while also reducing the amount of defects. The last trial provided lessons learned regarding drying temperature which is critical to the process. It is critical to the product that drying conditions provide enough heat to remove process solvents while are maintained low enough to yield a product that still contains enough plasticizer (a low temperature polymer that aids in the lamination process). Trial 3 and Trial 4 results have shown that coating machine dryer temperatures were too high and the resulting tape was starved of plasticizer. These results are shown in Figure 2-67 which compares the level of organic materials in the coated products as measured by thermal gravimetric analysis (TGA). Changes have been proposed to correct the problem and have been put in place for Trial 5 which is scheduled for first half of 2013.

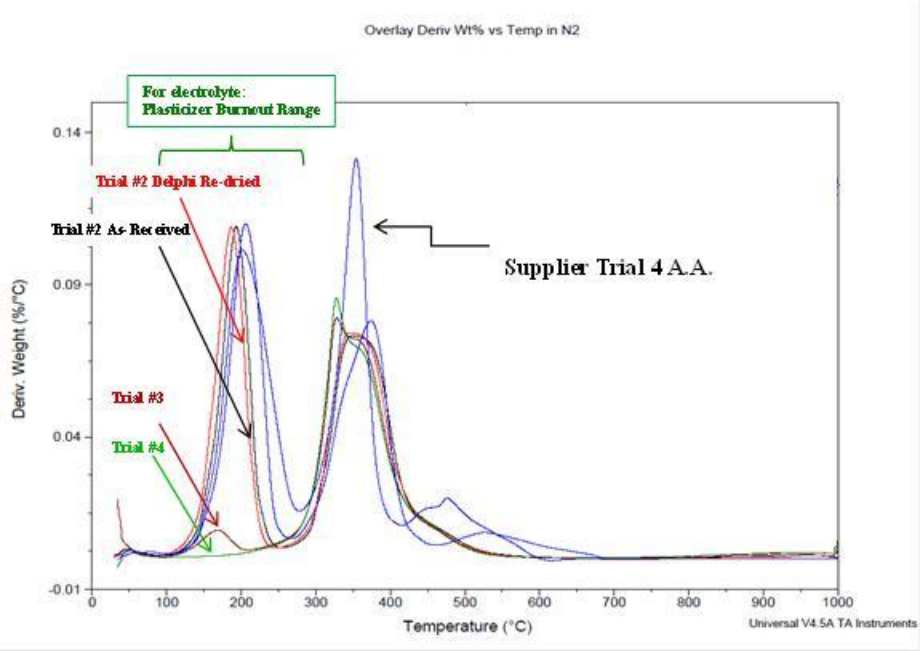

Figure 2-67: TGA Analysis of Electrolyte and Active Anode Tapes from Production Trials

Lower cost supply of nickel oxide powder:
Delphi continues to work with a commercial supplier of lower cost NiO powder to impact the cost of the raw material set being prepared for production. The goal is to substitute this NiO product in place of the current baseline material to lower overall cost and also complete the task of having two sources of NiO powder available from production intent processes. The lower cost powder has been evaluated in the solid oxide fuel in all components that contain NiO powder; these include the active anode, bulk anode and the NiO backing layer.

Figure 2-68 below shows an overall view of the +270 mesh fraction of the low cost NiO powder and the powder that has been magnetically separated from the lot. If the powder was fully oxidized, no material would have been able to be separated magnetically. Figure 2-69 shows optical cross sections of the magnetically separated fraction of powder. As is clearly visible, many of the particles have cores which are not fully oxidized. EDX analyses of the sections confirmed that these cores are comprised of unoxidized nickel metal. These metal cores tended to flatten and widen during milling of the powders and cause filter plugging problems during subsequent tape casting operations.

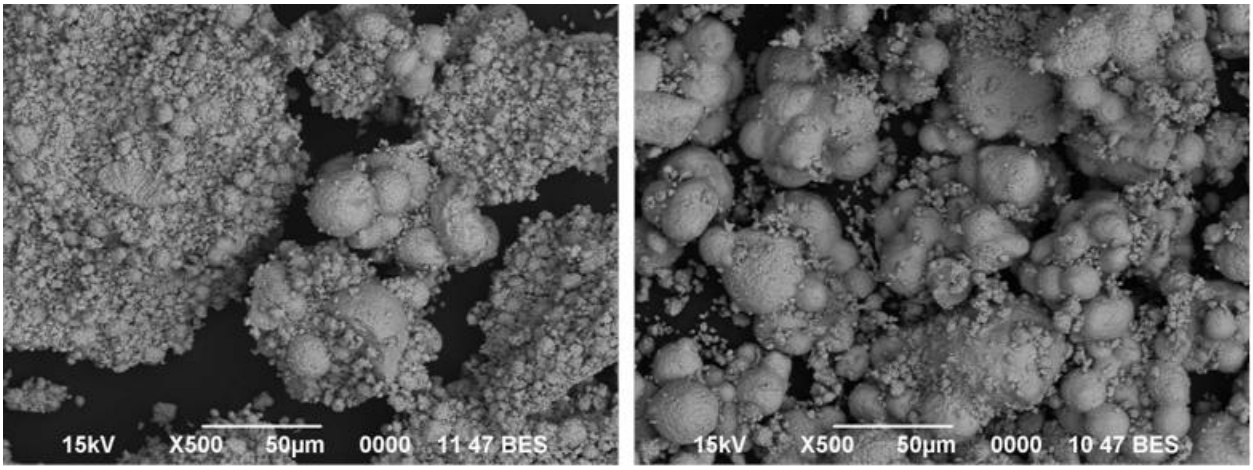

Figure 2-68: Low Cost NiO Powder Fractions

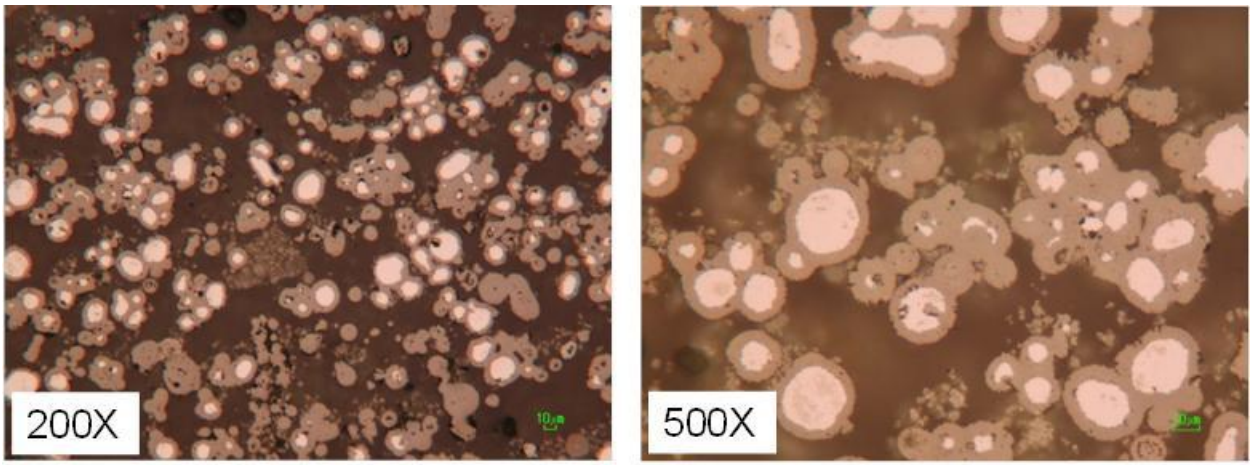

Figure 2-69: New NiO Powder Lot Sieved +270 Mesh, Magnetically Separated, Optical Micrographs

Since the last reporting period, the low cost NiO powder was integrated into an experimental batch of active anode composition power blend that was taken to a commercial supplier for grinding equipment evaluation. The idea was to either identify the equipment necessary to perform the scaled up grinding operation in-house or to develop the company as an outside supplier and use them for toll grinding of powders to assist in the production tape cast processes. The powders that were ground by this company remain contained in the grinding solvent and are ready for further characterization.

This quarter, the low cost NiO powder was also used in slurry that was cast by a second tape supplier that is currently being developed. The film from that casting trial is ready for further evaluation of quality and performance. The goal is to experience a smooth transition from the more expensive product to the lower cost product by the end of 2013.

3. Stack Materials and Process Development – UTRC

Objective:

From October 2008 through the end of 2009, United Technologies Research Center (UTRC) developed stack materials and processes in support of the stack development effort led by Delphi. The objective of this effort was to provide concept development and feasibility studies to Delphi and UTC Power. Under Delphi's direction, UTRC focused on key technical challenges for stack scale-up and durability. Specifically, the effort was devoted to the evaluation of coated alloys, the development and evaluation of advanced seal concepts and materials and the development of coating materials and processes for multiple stack components.

The team agreed that UTRC would perform three tasks. The first task would focus on the evaluation of coated alloys for the fabrication of cost-effective stack components. The purpose of that effort was to provide Delphi and UTCP with recommendations and/or independent verification on alloy material and coating selection for meeting the >40,000 hour life goal. The second effort was to develop and evaluate self healing glass (SHG) seal concepts and materials. The third and final task was to develop coating materials that can be applied by cost-effective, high-volume manufacturing processes to minimize oxidation, improve conductivity and mitigate chromia volatility so the coated components would meet the >40,000 hour life goal.

Experimental methods:

Alloy Evaluation

In early 2009, detailed characterization of $(MnCo)_3O_4$ (MCO) spinel coated Crofer 22 APU, Plansee ITM and Haynes 230 alloys was carried out after long term oxidation tests. Initial Area Specific Resistance (ASR) measurements of MCO coated Crofer 22 and stainless steel 441 were completed, and long term oxidation of coated samples from Delphi was initiated.

Oxidation behavior of the coated alloys was investigated by monitoring sample weight changes and conducting detailed post-exposure microstructural characterization. Coating adherence was assessed via rapid thermal cycling experiments. Both as-processed and aged samples (500 h in air at 800°C) were tested. The thermal cycling tests were carried out in a drop-bottom furnace that move samples in and out the hot zone, which allowed the specimen to remain at 750°C for 2 h and at room temperature for 2 h repeatedly

During Q3 2009, the long term exposure tests were completed while the ASR measurements were ongoing. During Q4 2009, the area specific resistance (ASR) measurement of coated alloy coupons was completed.

Seal Development

Thermal cycling tests were carried out to evaluate a self-healing glass seal material, interaction between the glass materials and alloys was investigated, and crystallization behavior of the glass materials were characterized using high temperature x-ray diffraction.

During Q2 2009, additional subscale leak testing and characterization of the crystallization behavior were performed on the two self-healing glass compositions.

By the end of Q3 2009, additional subscale leak testing of glass seals after a high temperature exposure was carried out to investigate the effect of crystallization on seal performance.

Coating Material and Manufacturing Process Optimization

In early 2009, a dip coating process was developed for the MCO coating. Thin, dense and uniform coating layers were achieved on alloy coupons and coating process scale-up for stack components was initiated. In parallel, an alternative method of forming a protective spinel layer was investigated. Coupon trials were completed to determine aluminizing processing parameters.

During Q2 2009, thin dense and uniform MCO coating coatings were achieved on alloy coupons using dip coating process. The coating process scale-up for stack components was completed. In parallel, alternative low cost coating process to form a protective spinel layer was being developed. Process optimization for the aluminizing processing was completed.

In Q3 20009, cost effective coating processes for both conductive and non-conductive coatings were scaled-up. Delphi stack components were coated and delivered to Delphi for visual examination and evaluation.

Parallel to coating process development, advanced characterization techniques were explored for better understanding of the coating / alloy interfacial reaction. Coatings and interfaces for SOFC are commonly investigated by traditional EDS/WDS line scan techniques in scanning electron microscopy (SEM), with a resolution limit of ~1 μm due to excitation. The resolution limit was improved to 10 nm utilizing transmission electron microscopy on a thin section sample prepared using focused ion beam (FIB)

Overall, UTRC's three material development tasks were completed per the agreed to Statement of Work by the end of 2009.

Results and discussions:

Alloy Evaluation

Various components can be made of metal alloys for SOFC stacks operating at temperatures of about 800°C. Alloys offer the potential for lower material cost, ease of fabrication and joining by established metal forming processes, excellent thermal conductivity, and commercial availability. Cell interconnects provide cell-to-cell electrical connection. Specifically, a cathode interconnect shall be oxidation resistant and provide a conductive interface between interconnect and cathode. Oxidation resistant chromia-forming alloys are suitable materials for SOFC applications due to high electric conductivity and protective nature of the chromia scale formed at operating temperatures. However, coatings are still needed for improving oxidation resistance and/or mitigating cathode poisoning and loss in performance resulting from volatile chromia species released from the cathode interconnect.

The subtask focused on evaluating $(MnCo)_3O_4$ (MCO) spinel coated Crofer 22 APU, Plansee ITM, and Haynes 230 alloys. Oxidation kinetics of the coated alloys was studied via long term high temperature exposure tests while coating adherence performance was examined by thermal cycling tests.

Weight gain of the coated coupons were recorded and plotted as a function of time. An Arrhenius plot was used (Figure 3-1) to calculate oxidation rate constants.

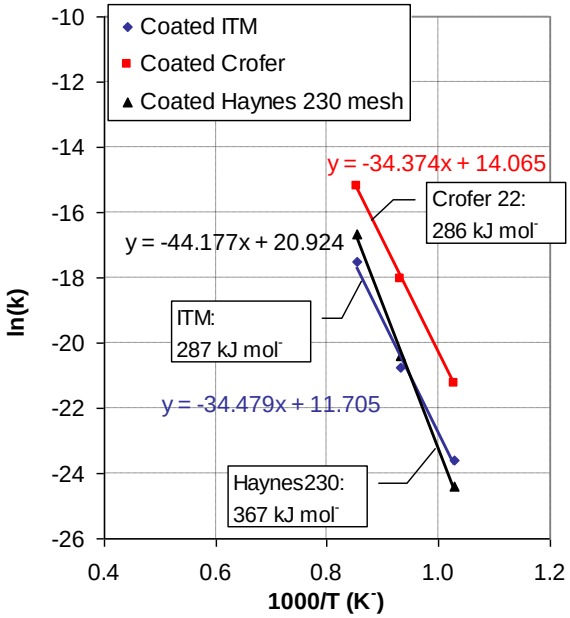

Figure 3-1: Oxidation Arrhenius plots

The oxidation rate constants of MCO coated Crofer 22 were an order of magnitude higher than those of ITM alloy and Haynes 230 mesh at respective temperatures. The MCO coating resulted in ~17 times reduction in the oxidation rate constant for ITM and 5.5 times reduction for Crofer 22, whereas the oxidation rate constant of coated Haynes 230 remained the same as bare Haynes 230. The activation energies for Crofer 22 and ITM alloys are approximately the same (~287 kJ mol^{-}). The activation energies for these ferritic steels are in agreement with that (250 kJ mol^{-}) associated with Cr^{3+} diffusion in Cr_2O_3, indicating similar mechanism likely dominates oxidation of the coated alloys. On the other hand, coated Haynes 230 exhibited a higher activation energy of (367 kJ mol^{-}) that is in agreement with that of bare Haynes 230. The efficacy of coating on inhibiting oxidation of the ferritic steels was remarkable, whereas the coating serves primarily as a chromia barrier for Haynes 230.

Weight change of coated alloy specimens upon thermal cycling is shown in Figure 3-2. Changes in coating weight after 35 rapid thermal cycles ranged from -0.2% to 0.2%. Such small changes are considered negligible from the perspective of coating spallation. Hence, it is believed that the MCO coating adhered well to all three alloys.

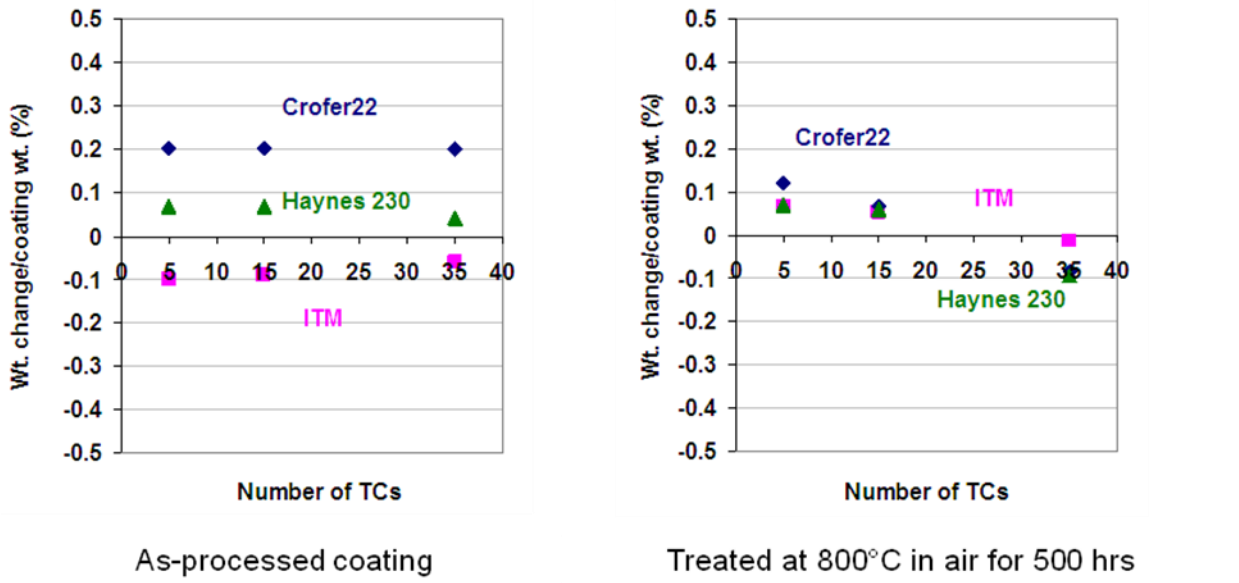

Figure 3-2: Oxidation weight change

The coated alloy coupons subjected to exposure test at 800°C in flowing air for 250 h and 1000 h were cross-sectioned and prepared for microstructural characterization. The coating / alloy interfacial chemistry was examined using an electron probe micro-analyzer (EPMA). Figures 3-3 to 3-5 are elemental concentration profiles across the interfaces. The Cr profiles exhibited a finite penetration into to the MCO coating for all three alloys, indicating the effectiveness of Cr containment during the exposure tests. Cr penetrated into the coating for up to ~3 µm after 1000 hours at 800°C. Some differences in the progression of element distribution in the three alloys were observed. The Cr profile of coated H230 exhibited a slight depressed trend with increasing oxidation time. It appears that inward diffusion of Mn and Co may have contributed to the depression in the Cr profile. The Cr profile for ITM remained unchanged over the exposure time. On the other hand, Cr in the coated Crofer 22 appeared to diffuse outward more rapidly. It is not well understood how the base alloys affect Cr transport mechanism in the MCO coating. However, the Cr diffusion seems to correlate with oxidation resistance of the coated alloy, i.e. higher oxidation resistance resulting in lower Cr concentration in the coating.

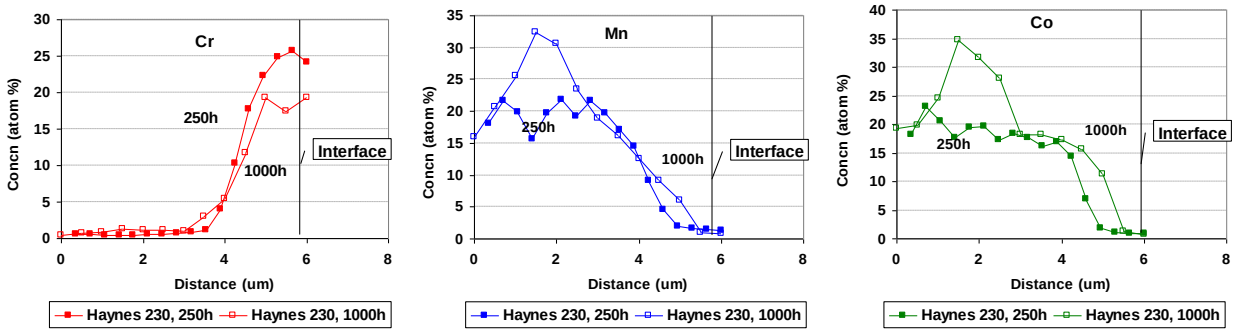

Figure 3-3. Cr, Mn and Co profiles in MCO coating on H230 after 250 h and 1000 h exposure in air at 800°C

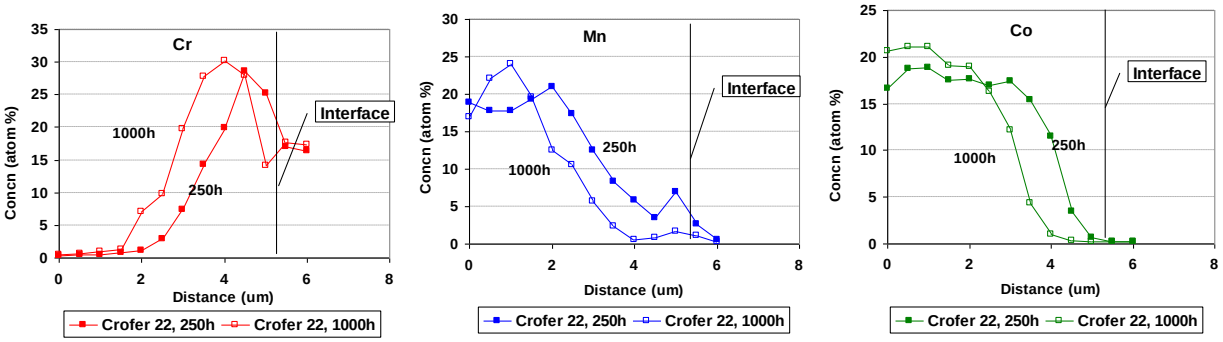

Figure 3-4. Cr, Mn and Co profiles in MCO coating on Crofer 22 after 250 h and 1000 h exposure in air at 800°C

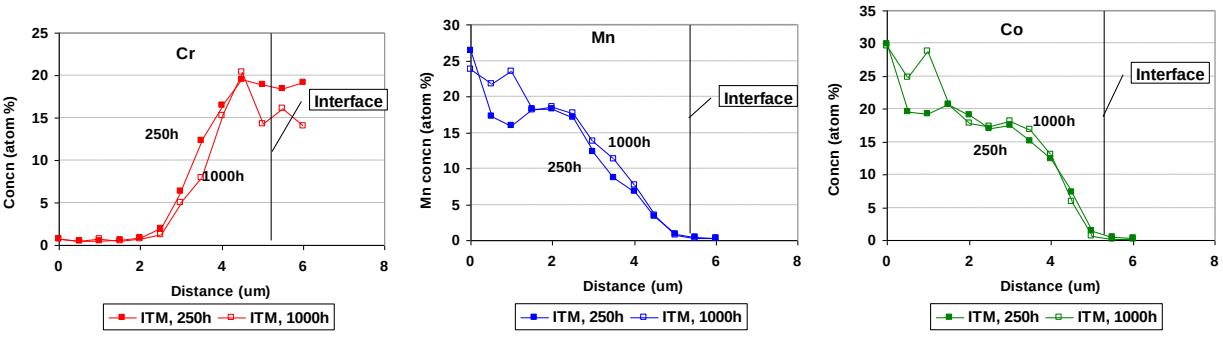

Figure 3-5. Cr, Mn and Co profiles in MCO coating on ITM after 250 h and 1000 h exposure in air at 800°C

Long Term Oxidation Test of PVD Co and Ce-MCO Coated Alloys

Long term oxidation tests of PVD cobalt coated alloys (Crofer 22H, ITM and 441SS) at 800°C were completed. In addition, vacuum diffused PVD Co coated 441SS coupons were tested at

900°C. Oxidation test of Ce-modified MCO coated alloys (Crofer 22 H, ITM and 441SS) prepared by the Pacific Northwest National Laboratory (PNNL) were also evaluated at 800°C and at 900°C

The first set of PVD Co-coated alloys provided by Delphi comprises diffusion treated and as-coated specimens. It was noticed that weight increase for those samples without the diffusion treatment was higher than those with diffusion treatment during the initial oxidation period, as shown in Figure 3-6. Spallation of the PVD Co coating was observed during the 500-hour inspection for 441SS samples without the diffusion treatment and testing of these samples were terminated. In contrast, PVD Co coating appeared to be adherent on Crofer 22H and ITM even without the diffusion treatment. Samples that survived the 1000-hour exposure tests exhibited parabolic oxidation behaviors. The oxidation rate constants are reported in Table 3-1. Samples with the diffusion treatment exhibited lower oxidation rates. PVD Co coating without diffusion treatment did not improve the oxidation resistance of Crofer 22 (oxidation rate constant 8×10^{-8} mg^2/cm^4 s at 800°C for uncoated alloy). The diffusion treatment appeared to improve coating adherence on 441SS. Overall, the PVD Co coating on 441SS was prone to spallation. Even with the diffusion treatment, PVD Co coated 441SS exhibited severe spallation after 200-hour exposure at 900°C.

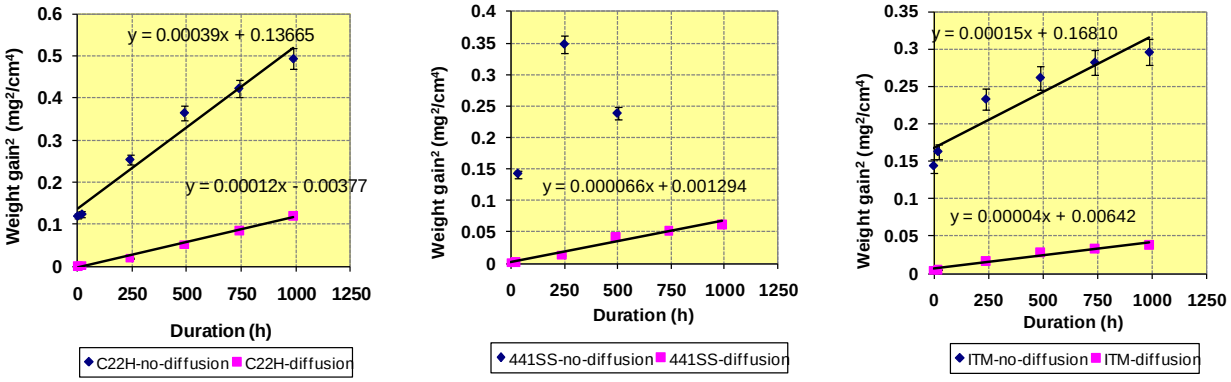

Figure 3-6. Weight gain of PVD Co coated Crofer22H, 441SS and ITM alloys as a function of exposure time at 800°C.

Table 3-1. Oxidation rate constants of PVD Co coated Crofer22H, 441SS and ITM alloys at 800°C.

Coating-alloy	k_g (mg^2/cm^4 s)
Co CF22 diffusion	3.33E-08
Co CF22 no diffusion	1.08E-07
Co 441 diffusion	1.83E-08
Co ITM diffusion	1.11E-08
Co ITM no diffusion	4.17E-08

Long term oxidation tests of Ce-modified MCO coated alloys at 800°C and 900°C were completed and the results on weight gain are shown in Figure 3-7 and 3-8. Coatings with the Ce stoichiometry being 0.02 and 0.05 were compared. Ce addition did not appear to influence oxidation kinetics of coated Crofer 22H and ITM but effected coating adherence on 441SS. The Ce0.02-MCO coating on 441SS spalled off during the first 200-hour exposure while the Ce0.05-MCO survived the 1000-hour exposure. Overall Ce-MCO coated ITM alloy exhibited much lower weight gains than the Ce-MCO coated Crofer 22H and 441SS at the temperatures tested. Oxidation rate constants of the Ce-MCO coated alloys were determined based upon the weight gain measurement and are reported in Table 3-2**.** The Ce-modified MCO coating appeared to be more effective than PVD Co coating on inhibiting base alloy oxidation with lower rate constants.

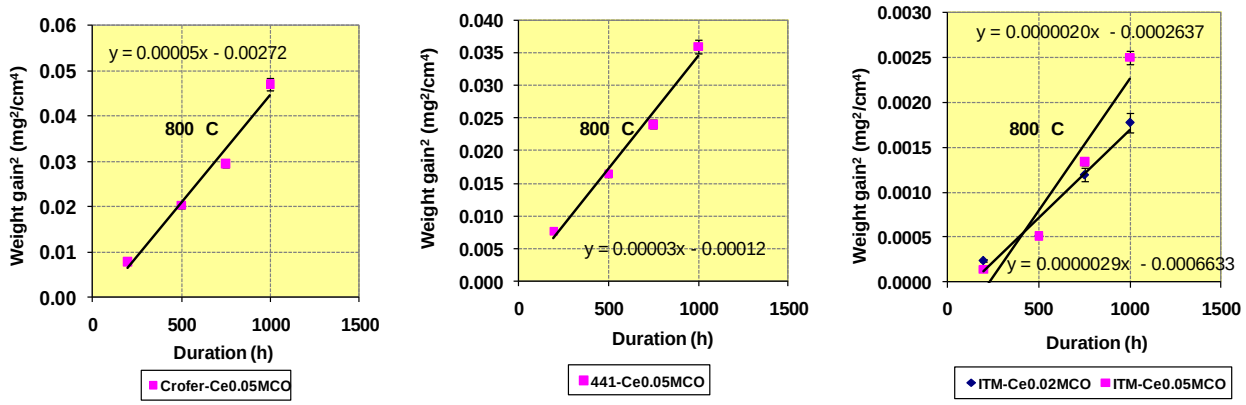

Figure 3-7. Weight gain of Ce-MCO coated Crofer22H, 441SS and ITM alloys as a function of exposure time at 800°C.

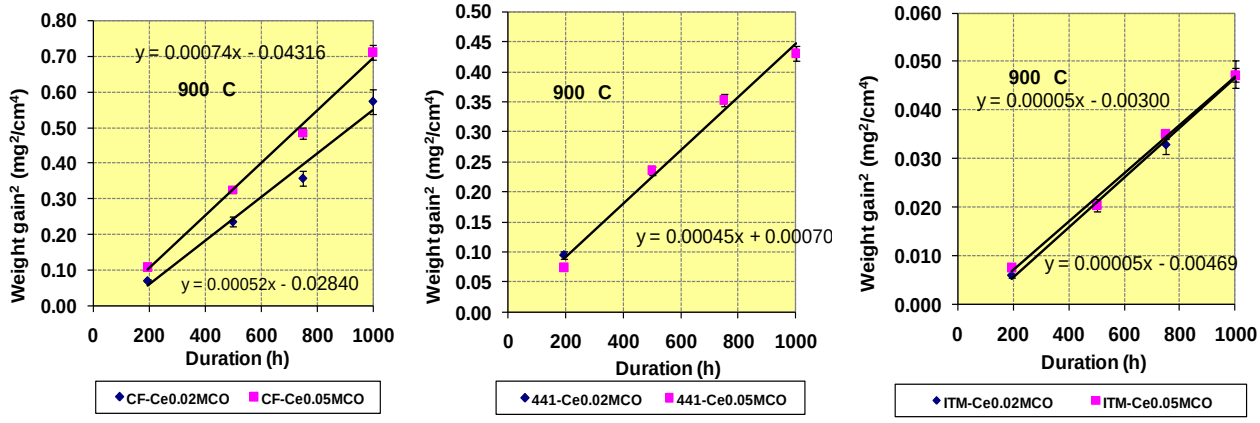

Figure 3-8. Weight gain of Ce-MCO coated Crofer22H, 441SS and ITM alloys as a function of exposure time at 900°C.

Table 3-2. Oxidation rate constants of Ce-MCO coated Crofer22H, 441SS and ITM alloys at 800°C and 900°C.

Coating-alloy	kg (mg^2/cm^4 s)	
Temp.	800 ºC	900 ºC
Ce0.02MCO-Crofer	N/A	1.4E-07
Ce0.05MCO-Crofer	1.1E-08	1.9E-07
Ce0.02MCO-441	N/A	Spallation
Ce0.05MCO-441	8.33E-09	1.4E-07
Ce0.02MCO-ITM	4.72E-10	1.4E-08
Ce0.05MCO-ITM	5.83E-10	1.4E-08

ASR Measurement

A DC four-probe two-point technique was used to measure ASR of coated alloys. ASR measurement was conducted at 800°C in air. ASR values of PVD Co coated 441SS, Ce-MCO coated Crofer 22 (1 duplicate) and MCO coated Haynes 230 are shown in Figure 3-9. The second break in the measurements was due to an unplanned furnace cool down. The step increases in ASR values immediately following the cool-down was probably unrelated to intrinsic conductivity values of the coatings. The PVD Co coated 441SS exhibited a decreasing trend of ASR over time while the Ce-MCO coated Crofer 22 exhibited an opposite trend. Among these coated alloys, the MCO coated Haynes 230 showed the most stable trend.

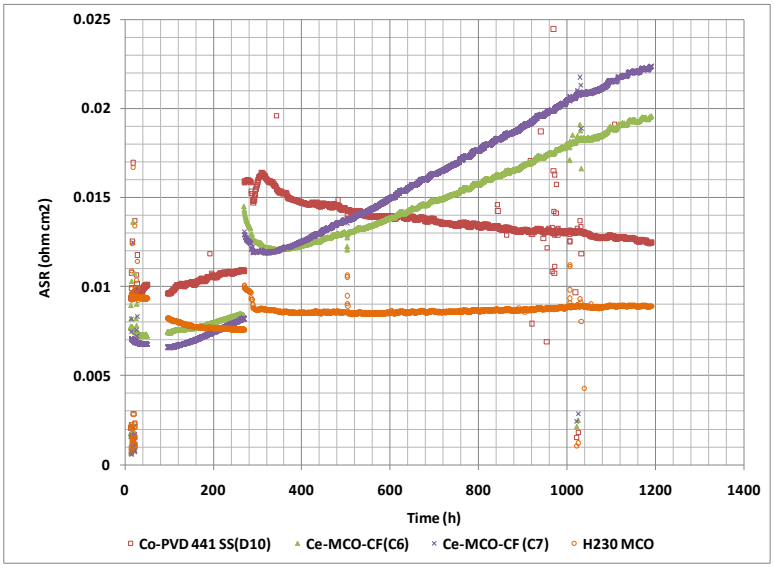

Figure 3-9. ASR of PVD Co coated 441SS, Ce-MCO coated Crofer 22 (1 duplicate) and MCO coated Haynes 230 measured at 800°C.

5.3.2 Seal Development

Sealing of planar SOFCs is challenging because the seal needs to provide a good thermal expansion match with other stack components and structural integrity under operation and thermal cycling conditions. Specifically, the seal must be stable for 40,000 hours of operation, be non-contaminating, have a strong ceramic to metal bond, have a good thermal expansion match (CTE) and be robust to thermal cycling. UTRC has been developing new seal design and materials to address these requirements. Two primary concepts were evaluated; a multi-strip seal concept and a self-healing glass material.

The multi-strip seal concept consists of three parallel strips—Ag/Cu, a glass tape, and another strip of Ag/Cu. The purpose of the multi-strip design is to prevent the Ag/Cu from being exposed to both oxidizing and reducing environments and also to prevent any volatile glass contaminants from affecting the electrochemical performance of the cell. Leak tests were carried out and no detectable leak was observed even after 10 thermal cycles.

A high expansion glass composition to be used alone or in conjunction with the multi-strip seal design was also evaluated. The first composition considered is a borosilicate glass with barium. The composition was chosen due to its compatibility with SOFC and low softening point of ~715°C. The subscale leak test using a 0.2" wide strip of glass showed no detectable leak at the operating temperature of 750°C. As the sample was thermal cycled, there was a small amount of leak measured at lower temperatures (~200°C) but due to the self-healing nature of the glass, the leak rate decreased to zero as the same was heated up to temperature during each cycle.

Further characterization of SHG (self healing glass) -1 continued during first quarter of 2009 as well as the identification of another self-healing glass composition (SHG-2). SHG-2 is a calcium borosilicate glass which is believed to be more resistant to chromate formation than SHG-1.

Crystallization Study Using High Temperature XRD

High-temperature x-ray diffraction (HT-XRD) was used to determine the degree of crystallinity of SHG-1 and SHG-2 as a function of temperature. The glass powder was heated in air and the temperature was held constant for thirty minutes at a range of temperatures to determine when a crystalline phase develops. The onset of crystallization occurs at 950°C in SHG-1 as shown in Figure 3-10. The typical heat treatment temperature of this glass is 850°C and the operating temperature is 750°C. Based on these results, SHG-1 is expected to remain amorphous during operation. SHG-2 showed onset of crystallization at 860°C (Figure 3-11).

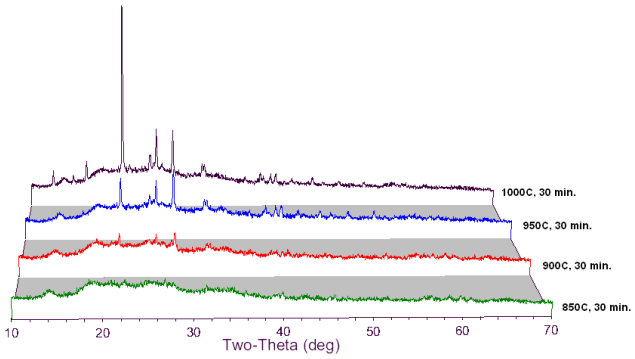

Figure 3-10. HT-XRD data for SHG-1.

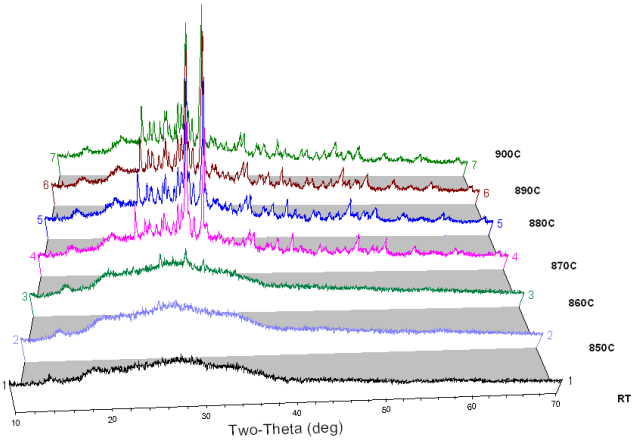

Figure 3-11. HT-XRD data for SHG-2.

Glass-Alloy Interaction

In order to understand the interaction of the glass seal materials with the substrate, 500 hour exposure tests were performed on coupon samples. Cross sectional SEM analysis of the SHG-1 sample showed no indication of crystallization and a thin oxide scale on alloy surface (Figure 3-12).

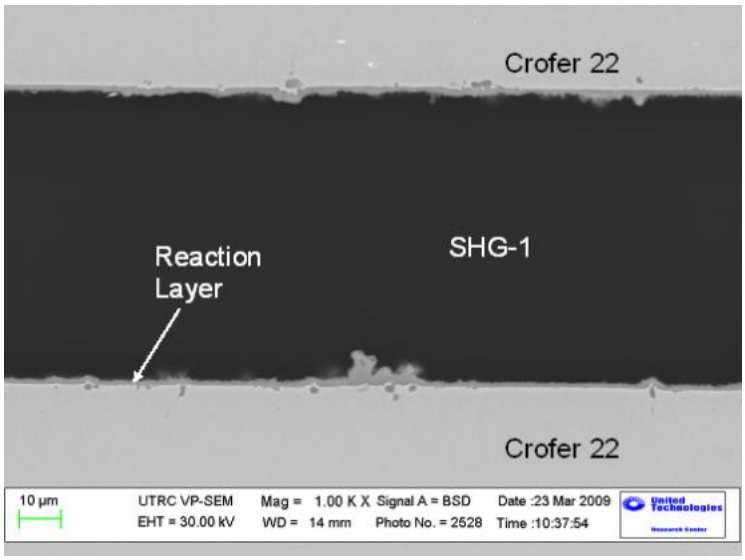

Figure 3-12. SHG-1 sandwiched between Crofer 22 held at 800°C for 500 hours.

Thermal Cycling Test

Subscale leak test data was taken as the samples were cycled from 750°C to 200°C. The test was repeatedly cycled from 750°C to 25°C and increasing the number of thermal cycles from 10 to 25. The results are shown in Figure 3-14. SHG-1 showed minimal leak at room temperature and exhibited self-healing behavior as it was heated up to operating temperature. The compressive load was decreased to 10psi and the test was repeated. The results plotted in Figure 3-15 shows leakage >10% at room temperature and an increased leak rate with thermal cycling. Although the overall room temperature leak rate is high, it should be noted that self-healing behavior is observed as the glass is cycled.

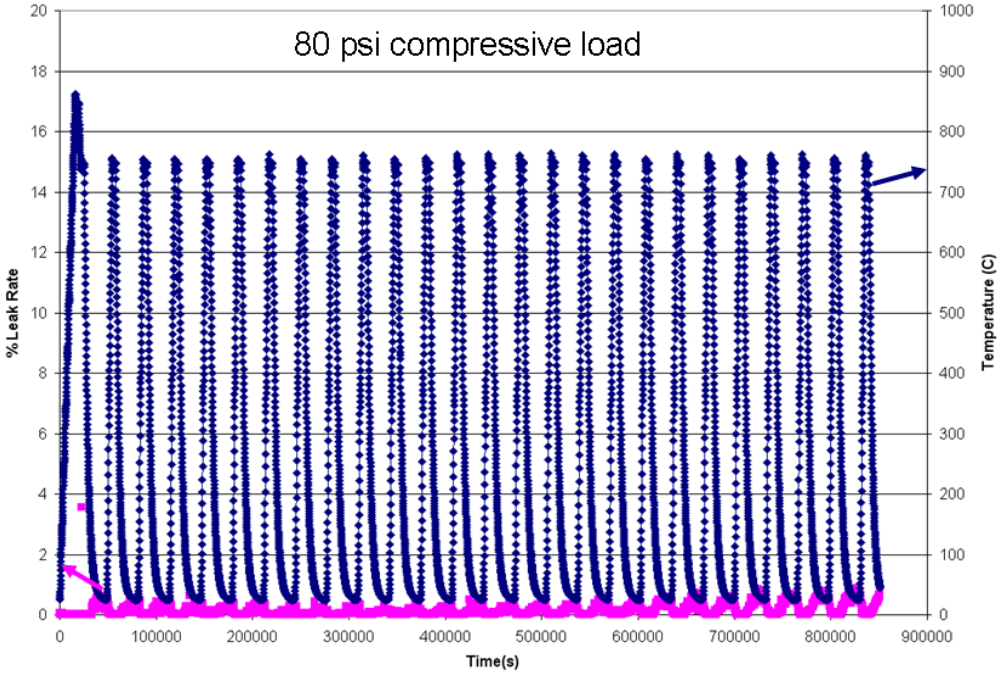

Figure 3-14. Subscale leak test with SHG-1 under 80 psi compressive load with 25 thermal cycles to room temperature.

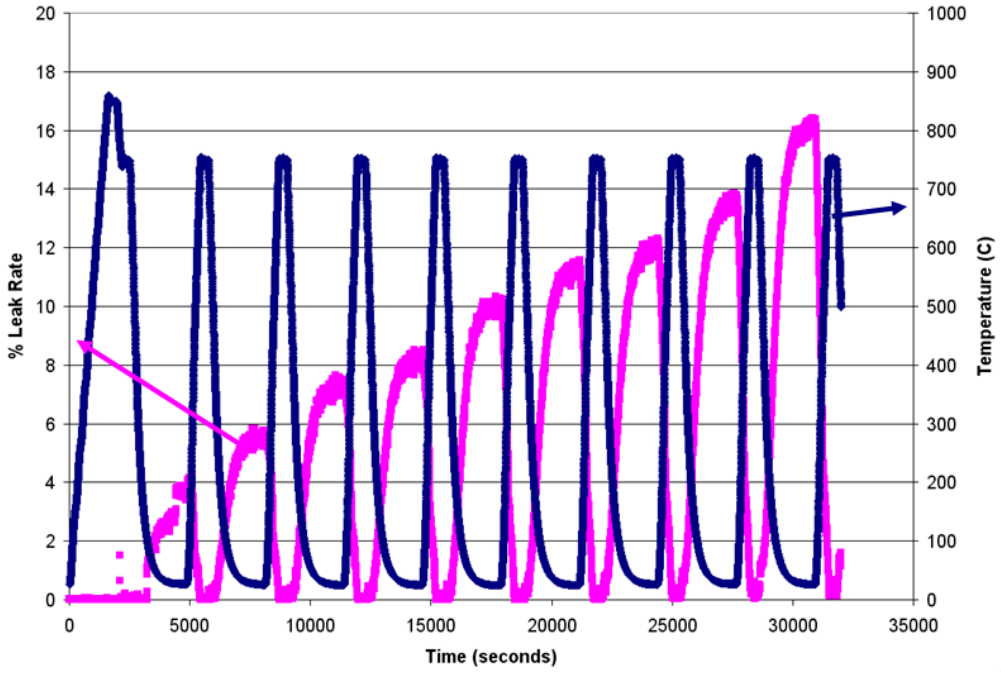

Figure 3-15. Subscale leak test with SHG-1 under 10 psi compressive load with thermal cycles to room temperature.

In order to better define the necessary axial load, a subscale leak test at 20psi compressive load was carried out. As shown in Figure 3-16, ~8% leak was observed at room temperature while there was no detectable leak at 750°C. Although the leak rate at room temperature is significant, the self-healing behavior of the glass allows the leak rate to be below 1% at only 300°C. This test indicated that 20psi compressive load was adequate.

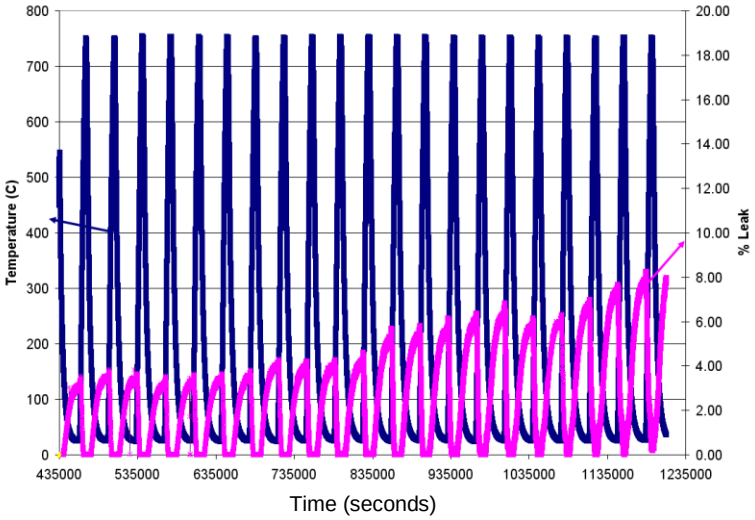

Figure 3-16. Subscale leak test with SHG-1 under 20 psi compressive load with 25 thermal cycles from 750°C to room temperature.

Subscale leak testing was performed on SHG-2 under 10psi and 20psi compressive loads. In the case of 10psi compressive load, significant leakage was observed after 11 thermal cycles as shown in Figure 3-17 indicating cracking or formation of leak pathways. With a compressive load of 20psi there was no detectable leak through the course of the 25 thermal cycles as shown in Figure 3-18.

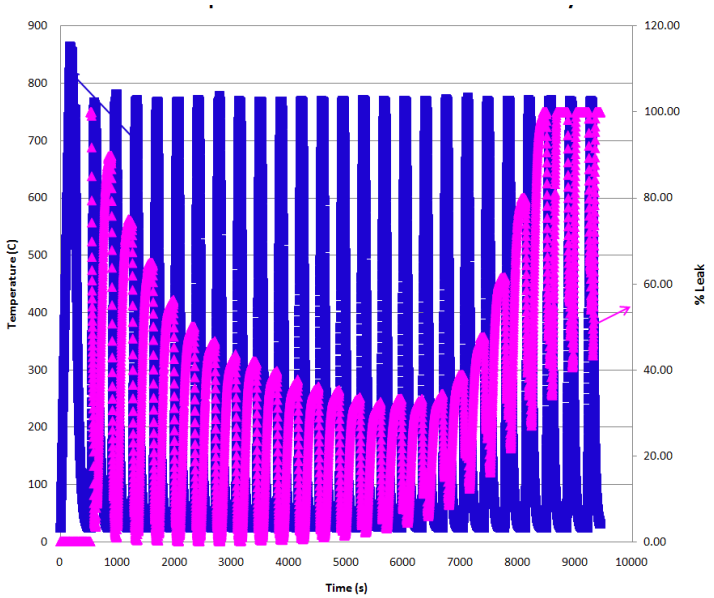

Figure 3-17. Subscale leak test with SHG-2 under 10 psi compressive load with thermal cycles from 750°C to room temperature.

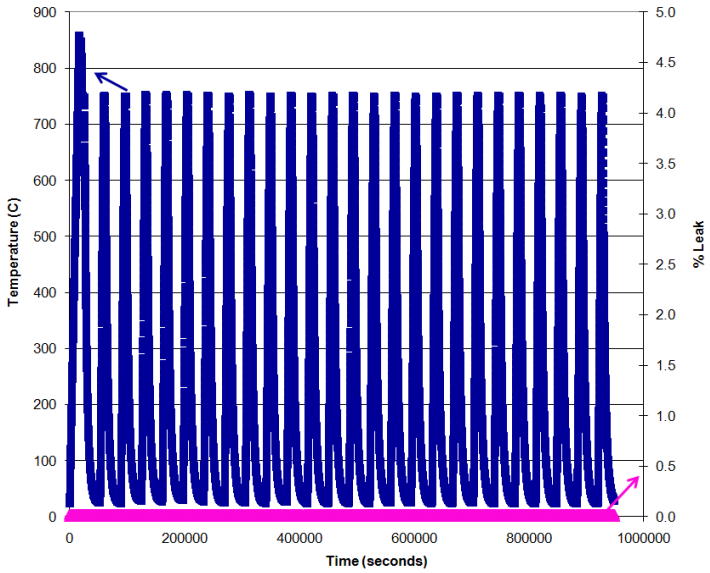

Figure 3-18. Subscale leak test with SHG-2 under 20 psi compressive load with thermal cycles from 750°C to room temperature.

Coating Material and Manufacturing Process Optimization

The goal of this subtask is to develop coating materials that can be applied by cost-effective, high-volume manufacturing processes to minimize oxidation, improve conductivity and mitigate chromia volatility so the coated components will meet the >40,000 hour life goal. Both

conductive and non-conductive coatings will be investigated. Various coating processes were investigated and evaluated. The most promising candidate processes were scaled-up and optimized for stack components. Initial efforts were devoted to (1) coating process optimization for cathode interconnect, striving for a dense, thin and electrically conductive coating that effectively reduces the diffusion of Chrome out of the interconnect, and (2) cathode interfacial material and process to achieve a mechanical bonding hence reducing performance degradation during thermal cycling.

Electrophoretic Deposition (EPD) was evaluated as a cost effective and scalable process that has the potential to improve green density and quality control. In EPD, colloidal particles are suspended in a liquid medium and migrate from the slurry to the electrode under the influence of an electric field and are deposited onto an electrode. Any colloidal particles that can be used to form stable suspensions and that can carry a charge can be used. This process, unlike electroplating, does not involve ion reduction. The fact that the deposition is charge driven leads to the possibility of more uniform and complete coverage. Thin films can be processed through this method by controlling the deposition rate via voltage, time, charge and loadings. The EPD process has shown promise in making thin homogenous films. Both flat plates and mesh substrates were tested.

Dip coating is well known as an established process to deposit particles onto a substrate through a slurry route. Particles are suspended in a liquid medium at varying loadings and deposited onto the substrate as it is dipped and removed from the slurry. There are many variables in processing a slurry for dip-coating including: powder particle size, size distribution, surface area, solvent, binder, pH, homogenization method, etc. Initial dip-coated samples showed very good coverage over the entire area, including all tight radius components. The thickness was optimized to about 5µm. The coating process was1-cell electrochemical tested for over 800 hours.

Initial FIB and TEM work was performed on MCO coated Haynes 230 coupon which was oxidized at 900°C for 1000 hours. The Haynes 230/Cr_2O_3/MCO interface was clearly seen using this method. EDS line scan across the interface revealed an intermediate Cr-Mn-Co-O phase between the pure Cr_2O_3 scale and the MCO coating, indicating interfacial reaction between the coating and the base alloy. FIB / TEM techniques offers insight into such complex interfaces and should be utilized in future efforts.

The cathode interfacial material has multiple functional requirements in a SOFC stack. The interfacial material is responsible for electrical collection from the cathode to the interconnect, maintaining a physical bond between the cathode and interconnect over thermal cycling, and maintaining an adequate porosity to allow sufficient gas flow. In addition, the interfacial material must be chemically compatible with the cell and the coated interconnect. A new interfacial material, developed at UTRC, was tested. Samples were made to test the shear strength of the interfacial material. The test sample consisted of a SOFC cell, the interfacial paste and the mesh interconnect tacked onto a piece of the bipolar plate. The test sample was heat treated following the same profile as initial stack heat up cycle. The bond strength was tested by a lap shear method. The new interfacial material exhibited a bonding strength >150

lbs/in^2 and was stronger than that of the cell it was bonding too. The coupon cells typically failed within the SOFC cell. This was a significant improvement over the commonly used perovskite-based interfacial material, which typically exhibits a bonding strength <2 lbs/in^2 after the same heat treatment step. The new interfacial material, along with the scaled up dip coating process for the interconnect was electrochemical tested in a 1-cell repeat unit. 0.83% performance degradation was measurement over 5 thermal cycles.

MCO Dip Coating Process Development

The dip-coating task focused on developing thin and dense coatings that will coat larger SOFC SS 441 components for a Delphi stack. Due to limited availability of 441SS material, Crofer 22 was used for most of the coating trials. During initial dip coating trials, a homogenous coating layer was achieved across the entire surface of the coupon. As shown in Figure 3-19, the coating was relatively thick and ~20 μm in thickness. Compositional profiles across the coating / alloy interface are shown in Figure 3-20. A dense dual-layer structure was formed between the porous MCO coating and the Crofer 22 substrate. The dense dual layer exhibited a chromia rich layer adjacent to the alloy substrate and underneath a dense reaction layer containing Cr, Mn and Co, consistent with observations reported in literature. The MCO coating layer remained to be relatively porous. Attempts were made to reduce the thickness of the porous MCO layer. Figure 3-21 shows that the dense interfacial layer was maintained while we scaled down coating thickness to ~5 μm. The chromia rich layer was maintained to be less than 1 μm as shown in Figures 3-22.

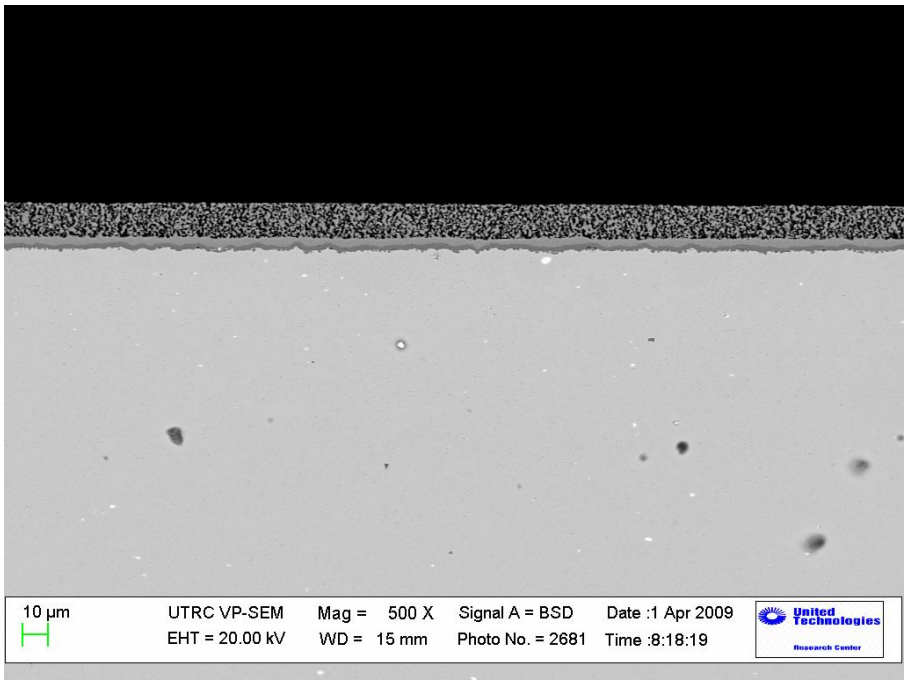

Figure 3-19. Long range coating homogeneity on dip-coated Crofer 22.

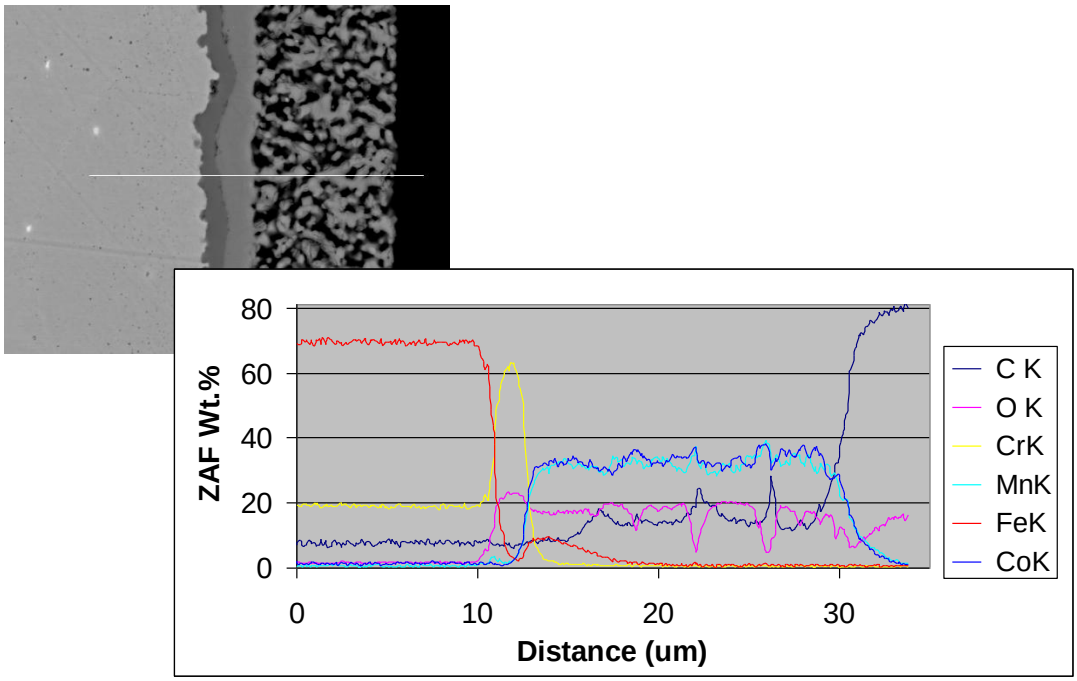

Figure 3-20. Linescan across the Crofer 22 / coating interface.

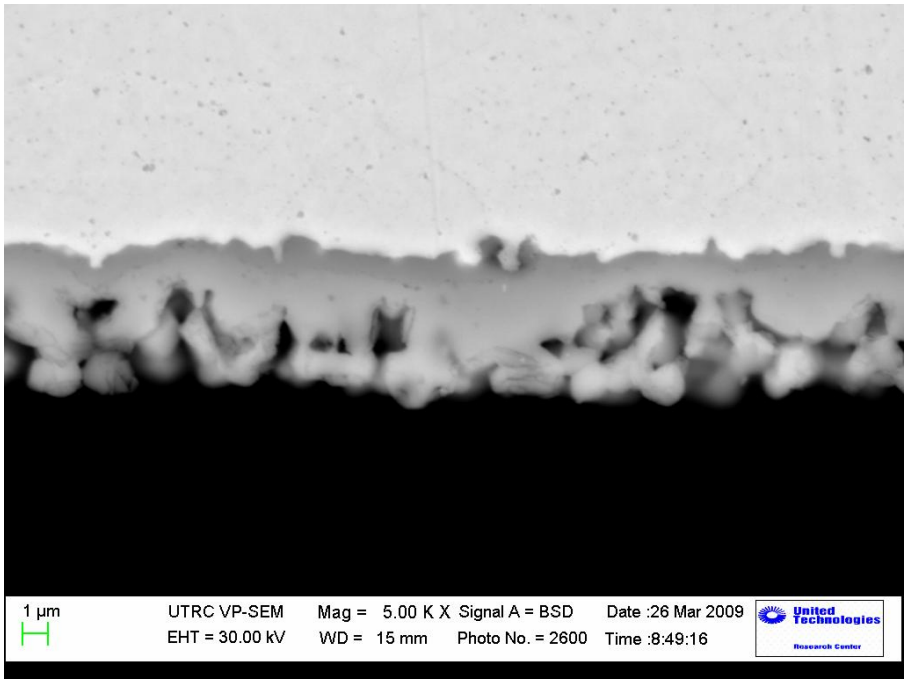

Figure 3-21 Thin coating on Crofer 22

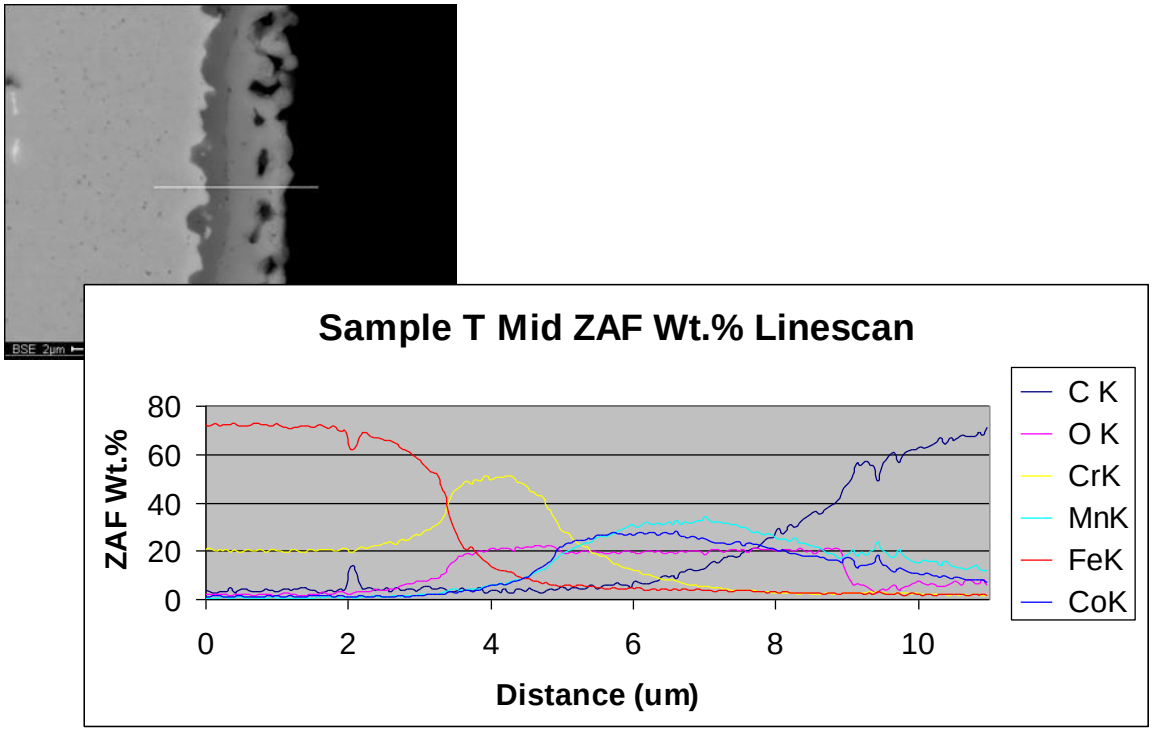

Figure 3-22. Linescan of coating on Crofer 22 showing dense interlayer maintained in thinner coating.

Later efforts were focused on developing thin and dense coatings on Delphi stack components. A Design of Experiment was carried out to identify processing conditions providing the optimal coating quality. A dense coating which had been repeated with varying film thickness had been demonstrated, as shown in Figure 3-23. The dip coating process has been scaled and applied to the Delphi separator plate as shown in Figure 3-24. The part was first masked for the dip coating process, and the masking material was removed following film drying. The MCO coated Delphi components were processed in conjunction with the aluminide coating. Because there was a 2 mm overlap between the two coating materials at the periphery of the conductive coating area, coupon tests were carried out to ensure chemical compatibility and coating adherence.

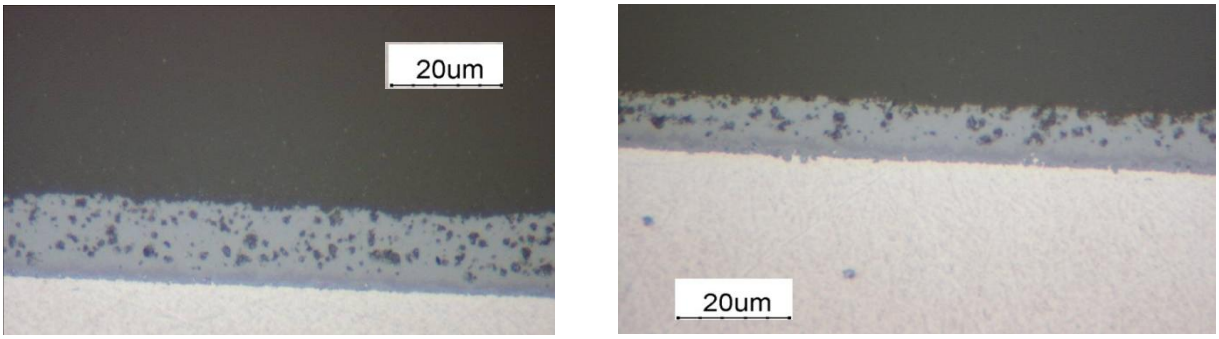

Figure 3-23. Thin dense MCO coating on Crofer 22.

Figure 3-24. Dip coating on Delphi stack component (separator plate).

Electroplating Cobalt

Cobalt electroplating was studied at UTRC as an inexpensive alternative coating for interconnects. By oxidizing an electroplated Co coating it was possible to form a spinel phase on the interconnect surface. Initial Co-plating work performed showed significant promise. An initial round of evaluations was performed which examined different plating thicknesses and diffusion treatment temperatures. Electroplating tests were performed on Crofer 22 APU (CR-22) and Stainless Steel 441 (SS-441). Ten 2”x1” coupons of each material were cut and polished down to a 6 μm diamond finish. Figure 3-25 shows backscattered electron micrographs of the

plated coupons. Two plating thicknesses were deposited, 10 coupons of each thickness were created for further diffusion treatment studies.

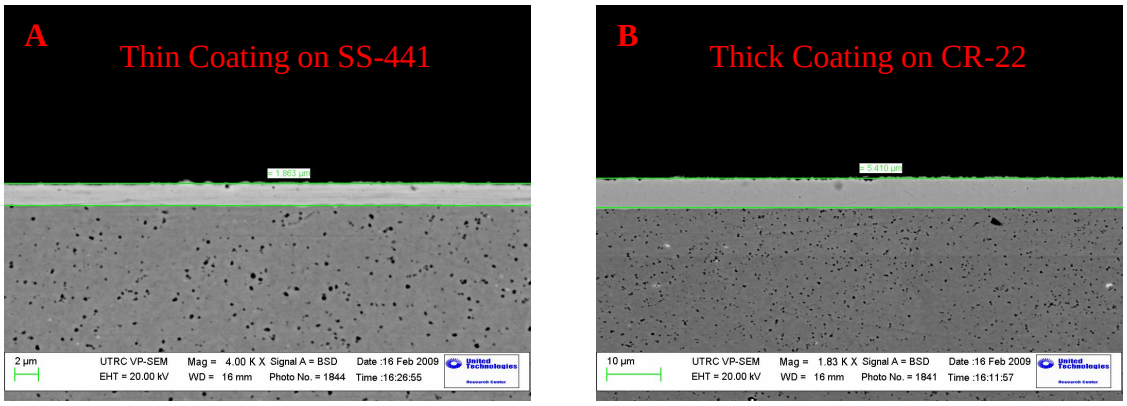

Figure 3-25. Backscattered electron images of as-plated cobalt. Note that the "thin" coatings are ~1.8 µm thick (A) and the "thick" coatings are ~ 5.4 µm thick (B).

The as-plated coupons showed a very consistent thickness; however there did appear to be some de-lamination of the coating on the edges of some of the coupons. In addition, gas bubbles could be seen on the surface of the plated coupons. This is a known phenomenon that can occur in electroplating when there is insufficient solution agitation during the plating process. It is thought that a Co diffusion treatment is an essential step to facilitate bonding of the coating and substrate as well as limit rapid oxidation of the pure Co plating. Figure 3-26 shows images of both as-plated coupons and Co plated coupons that underwent a subsequent diffusion treatment. Note the appearance of the coupons changes from dull in the as-plated condition to a bright, shiny surface after the diffusion treatment.

Figure 3-26. Photo on left is as-plated Co on CR-22 (left in both pictures) and SS-441 (right in both pictures) (B). The same coupons after diffusion treatment at 1000º C/4 hours under high vacuum are shown in the photo on right.

A sensitivity study was performed at 800ºC for 250 hours to determine the effect of Co diffusion on oxidation resistance. It was observed that the coating layer oxidized at a much faster rate in regions where the layer was delaminated and diffusion did not occur than coated regions where diffusion occurred. This indicates that diffusion is a necessary step in producing an adherent spinel coating from electroplated Co layer. Figure 3-27 is a backscattered electron micrograph showing the difference in oxide scale thickness between a diffused and undiffused region.

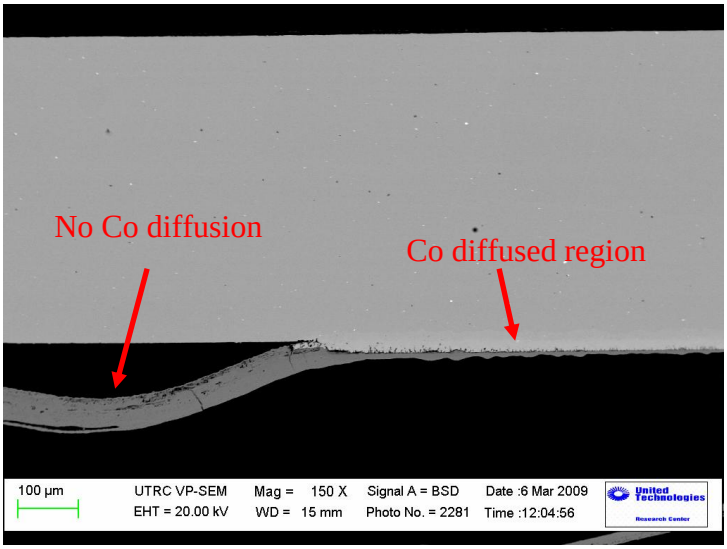

Figure 3-27. Backscattered electron image of a SS-441 sample oxidized at 800º C in air for 250 hrs. Note the difference in oxide thickness between diffused and undiffused (pure Co) regions.

The oxidation products formed during the 800º C/250 hr. heat-treatment were examined via scanning electron microscopy (SEM) and energy dispersive spectroscopy (EDS) linescans. The results of this preliminary analysis showed a complex layered structure consisting of an underlying Cr_2O_3 scale with a Cr-Fe-Co-rich oxide on top. Figure 3-28 shows SEM cross section and EDS linescan of an SS-441 coupon with a Co diffused coating (1000º C/ 4 hrs.) oxidized at 800º C for 250 hours. This coupon was produced from a thick (≈5 µm) Co plated sample. For comparative purposes, the same sample prior to oxidation is shown in Figure 3-29. Note Co diffuses 15-20 µm into the surface of SS-441. Similar profiles were observed for CR-22 samples under identical diffusion conditions.

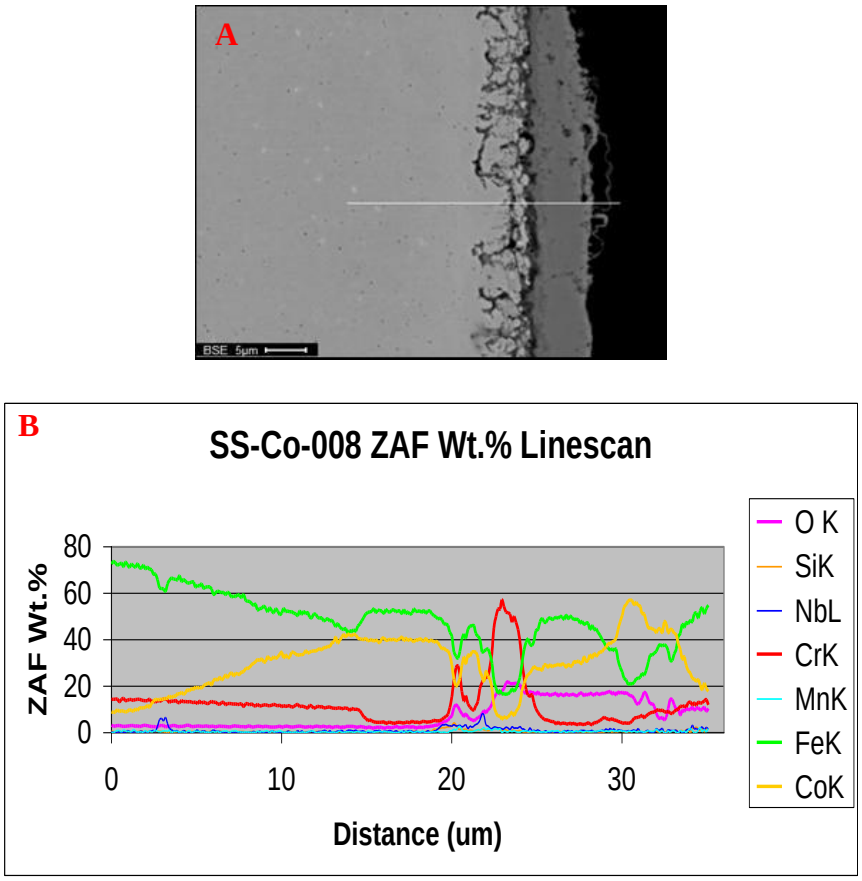

Figure 3-28. (A) Backscattered electron image showing Co diffused sample oxidized at 800ºC for 250 hrs. (B) Corresponding EDS linescan taken from the line indicated in the image in (A).

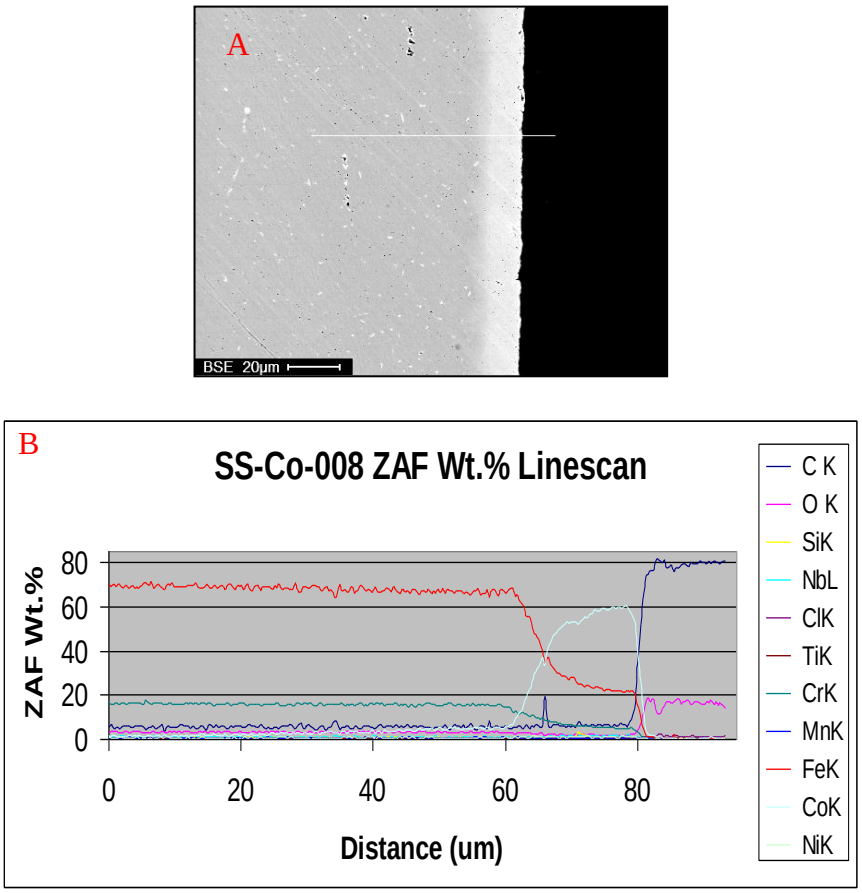

Figure 3-29. (A) Backscattered electron image SS-441 plated with Co (5 µm) and diffused at 1000º C/4 hrs. in vacuum. (B) Corresponding EDS linescan shows 60 wt.% Co at the surface.

UTRC also carried out electroplating cobalt in-house to eliminate plating defects and edge effects observed in coatings provided by vendors. The in-house plating on 1"x2" Crofer 22 and stainless steel 441 coupons was very successful and there was no evidence of edge effects or delamination with these small coupons. In addition, a series of diffusion studies were carried out in vacuum to better understand the effect of plating thickness and diffusion temperature on cobalt concentration. Figure 3-30 is a representative cross sectional image of a 1"x2" coupon that was cobalt electroplated at UTRC.

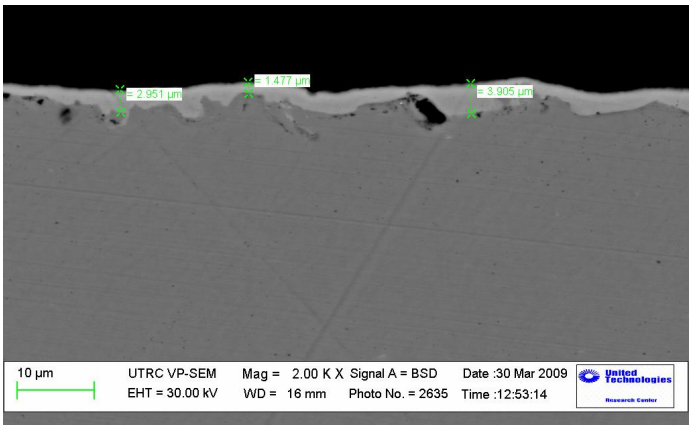

Figure 3-30. A backscattered electron image of a coupon plated at UTRC for 60 minutes with a constant current of 0.09 A.

Cobalt diffusion properties were measured on stainless steel 441 coupons with both thick (~ 5.4 µm) and thin (~1.8 µm) initial electroplating thicknesses. Diffusion of cobalt into the alloy is a necessary processing step. As reported previously, the absence of a diffusion treatment prior to high temperature exposure in air leads to rapid spallation of the coating. Diffusion treatments were carried out at 850 °C and 925 °C for 5 hours in a vacuum furnace. These diffusion profiles were compared to the initial diffusion heat-treatment performed at 1000 °C for 4 hours. Figure 3-31 shows the results of numerous EDS elemental linescans. Only the cobalt concentrations are shown in the figure.

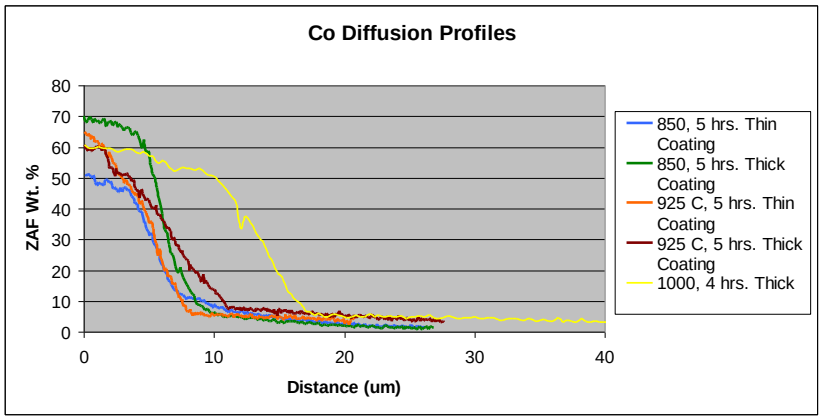

Figure 3-31. Cobalt diffusion profiles obtained from EDS linescans by varying plating thickness and diffusion temperature. The alloy surface is on the left (distance = 0).

Note from Figure 3-31 that the initial plating thickness plays a large role at lower temperatures. At lower diffusion temperatures, cobalt concentration at the alloy surface can be tailored by varying the initial plating thickness. To further verify this effect, coupons with 15 minutes, 30 minutes and 60 minutes plating time were prepared and examined. For this set of experiment, diffusion heat-treatments were carried out at a low temperature (800 °C) for 5 hours in a vacuum furnace. The resulting cobalt profiles obtained from EDS linescans and corresponding SEM backscattered images are shown in Figure 3-32. The surface composition varied from 35 wt.%

Co to 55 wt.% Co by varying the initial plating thickness. In addition, surface of the samples were examined in SEM prior to and after the diffusion treatment. Plan view EDS analysis shows that a plating time of 15 minutes at 0.09 amps is not sufficient enough to cover the entire surface of the sample, but the 30 and 60 minute plating times provide complete coverage. Figure 3-33 shows electron images of the 30 minute sample in the as-plated condition (A) as well as the post-diffused condition (B). The cobalt crystallites change in morphology from needle-like crystals in the as-plated condition to equi-axed crystallites in the post-diffusion condition. Similar studies were conducted to examine the effect of varying diffusion time at a given temperature. It should also be noted that successful diffusion was carried out in a standard retort furnace in flowing argon.

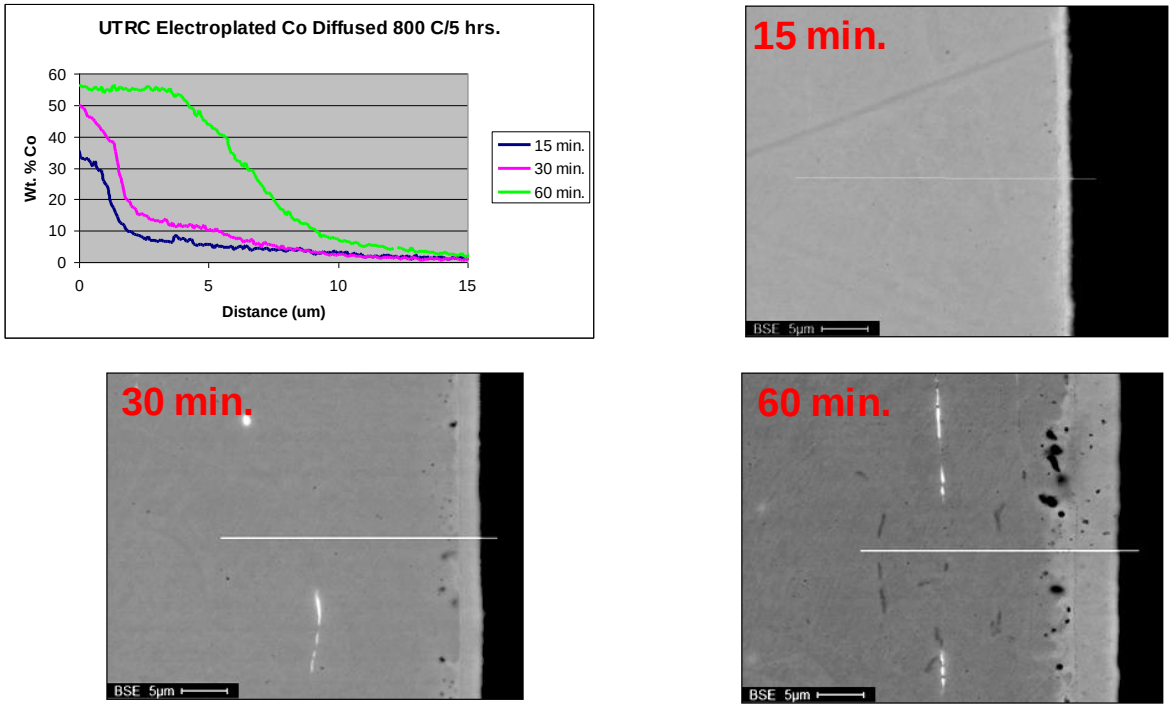

Figure 3-32. Cobalt profiles and cross sectional images taken from samples with varying plating times followed by a diffusion treatment at 800º C for 5 hrs.

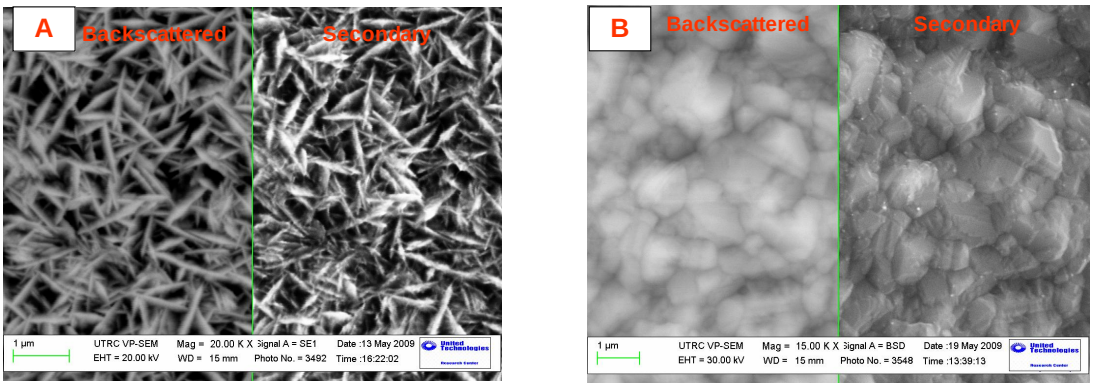

Figure 3-33. (A): Backscattered and secondary electron images of a coupon plated for 30 minutes and (B) Backscattered and secondary electron images of the same coupon after being diffused at 800º C for 5 hours.

To scale up this low cost manufacturing plating process for stack components, a large 6"x6" sheet of Crofer 22 was electroplated and diffused, as shown in Figure 3-34. The majority of the sheet showed a consistent plating and good coating adherence after diffusion. Some minor adhesion issues were observed at the lower edge of the sheet, likely due to higher current densities that are known to present at the edges of the sample being plated (cathode). Approaches to solve this problem included using larger anodes or using "dummy" plates around the edge of the part being plated to eliminate high current densities on the actual parts.

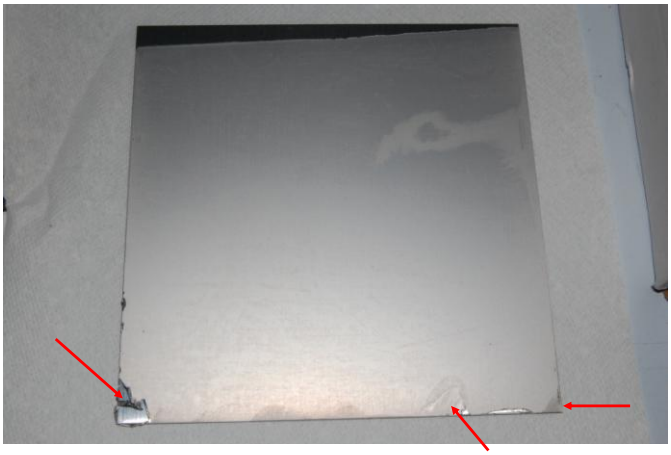

Figure 3-34: A large 6"x6" sheet of Crofer 22 after being Co electroplated for 1 hr. at 1.125 A and diffused at 800º C for 5 hrs. Arrows indicate regions near the edge with adhesion issues.

Aluminide Coating

Nonconductive coatings were also examined for barrier layers to minimize the interaction between glass seals and metallic frame materials. Aluminides have been recognized by the SOFC community as an attractive material for this application. Traditionally, aluminide coatings are applied using chemical vapor deposition (CVD) or physical vapor deposition (PVD). Both

processes are relatively expensive, requiring high vacuum conditions and complex masking for regions that do not require coating. UTRC previously developed an inexpensive slurry aluminizing process that does not require a vacuum system. The purpose of this thin alumina scale is to act as a barrier layer which limits any chemical reaction between the glass and the metal frame.

Coupons of SS-441 and CR-22 were cut to 1"x1" and polished to a 6 μm diamond finish. Figure 3-35 is a backscattered electron image showing an aluminide coating formed on SS-441. Note the thickness of the coating is ≈ 30 μm.

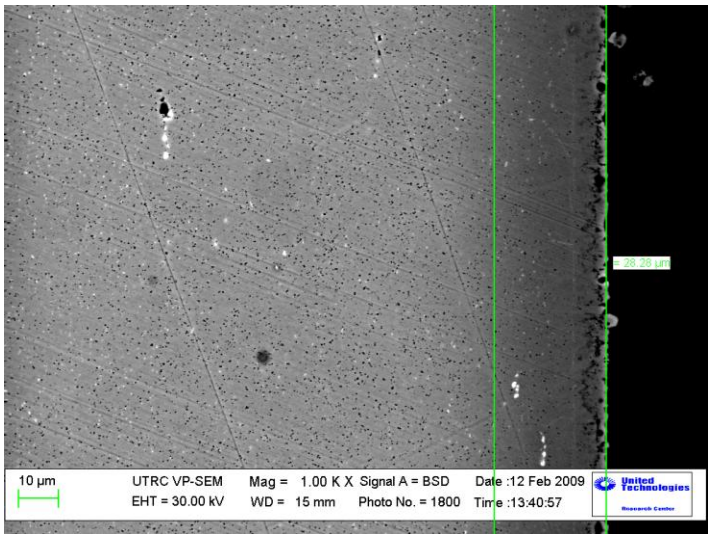

Figure 3-35. A backscattered electron image of a slurry aluminide coating formed on SS-441, heat treated in argon at 800º C for 5 hrs.

The aluminide coatings were then oxidized to form a dense Al_2O_3 protective scale. This scale was chemically stable and acted as the barrier layer between the glass seals and the ferritic stainless steel frames. Figure 3-36 shows the dense alumina scale formed on a slurry aluminide coating by heat treating at 1000º C for 1 hour.

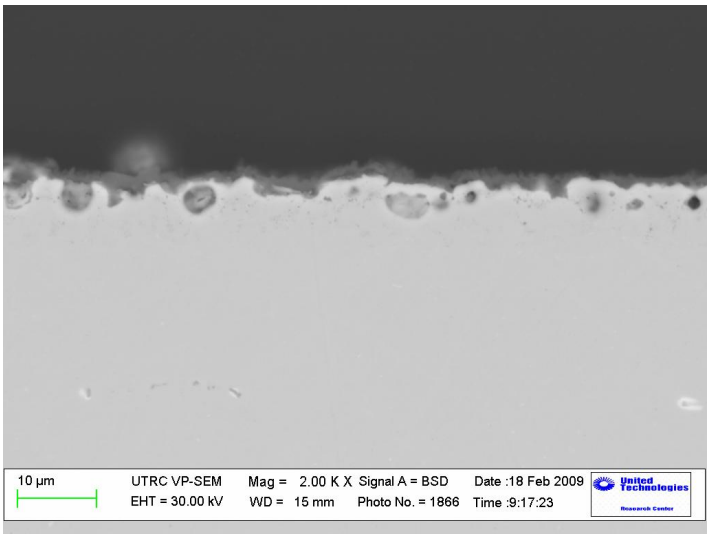

Figure 3-36. A dense alumina scale is formed on the aluminide surface after heat treating in air at 1000º C for 1 hour.

In order to get a better understanding of the coefficient of thermal expansion (CTE) values, thermal mechanical analysis (TMA) is being carried out on coated coupons. Three coupons were initially tested. It was noted that the CTE value of the aluminide coated SS-441 is much higher than the un-coated SS-441.

Thermal cycling tests from 830°C to room temperature were performed to study the effect of thermal mismatch between the coating and the base alloy. Two samples were tested. One coupon was slurry aluminized in argon and the other was aluminized at the same conditions and then oxidized in air. Both coupons exhibited well-adhered oxide scales and showed no signs of spallation after 25 thermal cycles, as seen in Figures 3-37 and 3-38. Note that the coupon that was not oxidized prior to thermal cycling shows an oxide scale of roughly 10 µm while the pre-oxidized sample has a very thin 1-2 µm scale. This is very likely due to the fact that the pre-oxidized aluminide coupon has a thin, protective Al_2O_3 coating that prevents further oxidation. This emphasizes the necessity for forming the continuous Al_2O_3 scale prior to exposure to stack operating conditions.

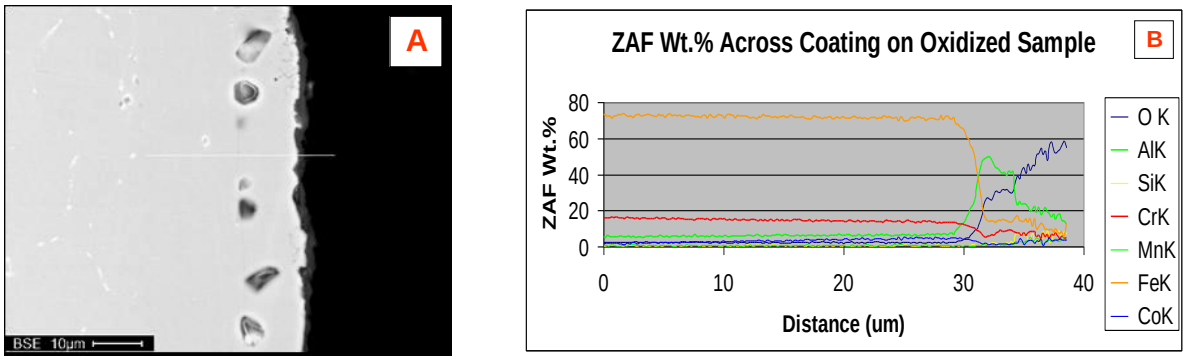

Figure 3-37. (A) Backscattered electron image of a pre-oxidized aluminide coating after 25 thermal cycles and (B) Corresponding EDS linescan showing the chemistry across the interface.

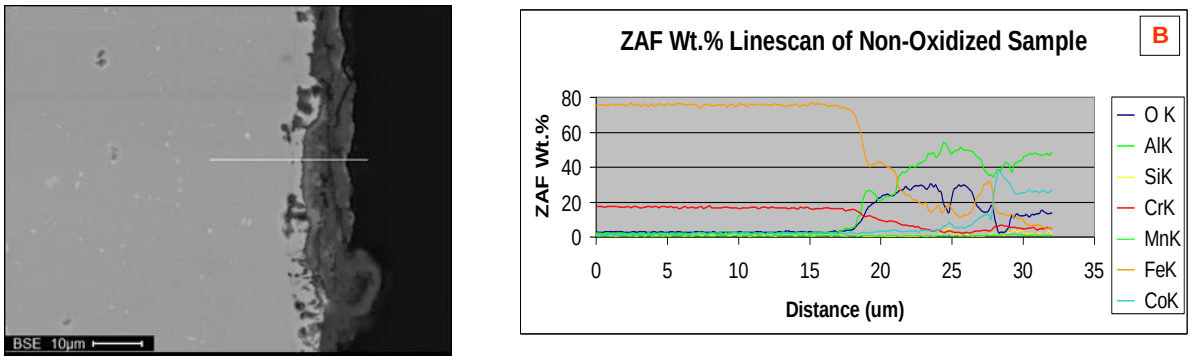

Figure 3-38. (A) Backscattered electron image of a non-oxidized aluminide coating after 25 thermal cycles and (B) Corresponding EDS linescan showing the chemistry across the interface.

A thickness study was performed by keeping the diffusion temperature constant at 800 °C and varying the diffusion time. Diffusion was carried out on 1"x1" coupons at 1 hour, 3 hours and 5 hours in an argon atmosphere. Figure 3-39 shows EDS linescan profiles for the three heat-treatment times. The aluminum diffusion distance did not drastically change between 1 hour and 5 hour heat-treatments. This indicates that the gas phase reaction and subsequent outward diffusion of Fe and Cr species is very rapid at 800°C.

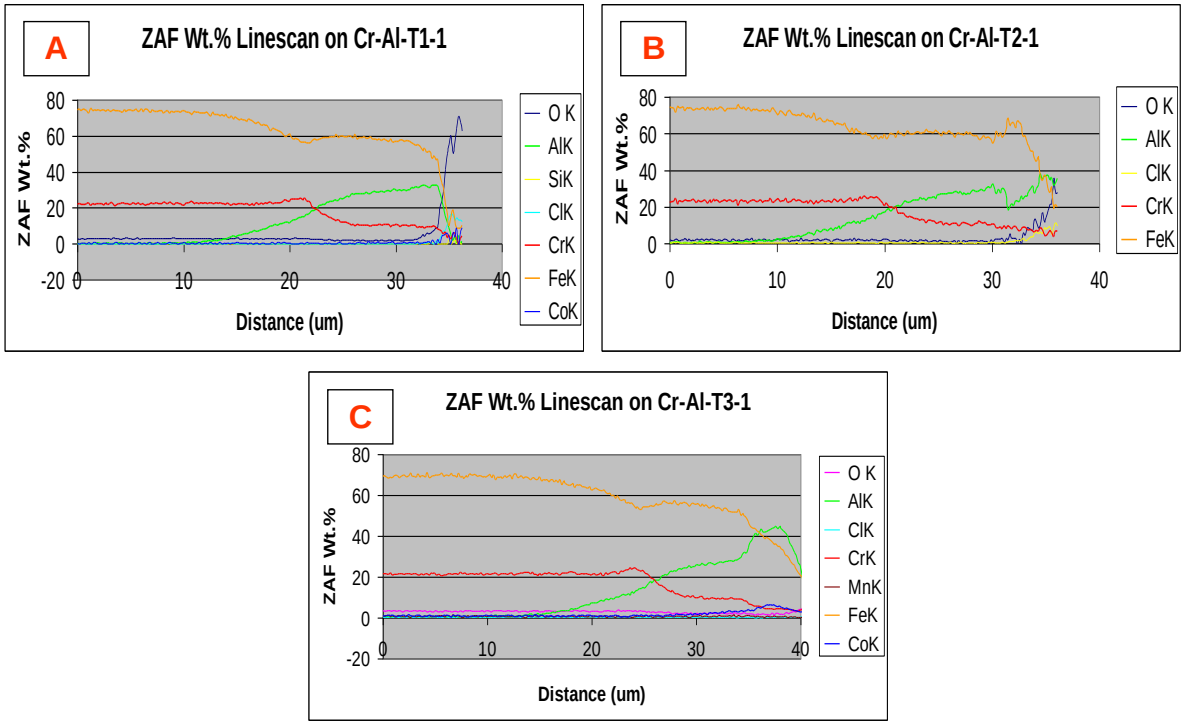

Figure 3-39. EDS linescans of aluminide diffusion profiles for coupons heat-treated at 800 °C in argon for (A) 1 hour; (B) 3 hours and (C) 5 hours.

Conclusion:

Alloy Evaluation

Oxidation studies of uncoated H230, ITM and Crofer 22 indicate that H230 exhibits the slowest oxidation kinetics. Testing of coated interconnect alloys with a standard MCO coating showed that the effectiveness of the MCO coating was highly dependent on the base alloy. This is thought to be due to differences in Cr diffusion rates in the different alloys studied. Further work in this area should focus on interconnect alloy and coating interactions as these interfaces may prove to be even more important than the starting properties of the coating (i.e. electrical conductivity and thermal expansion coefficient).

PVD cobalt and Ce-modified MCO coatings were also evaluated and run in short-term ASR tests. The PVD Co coatings were eventually abandoned due to adhesion and issues with the coating. While diffusion treatments prior to oxidation did improve the adhesion, it was found that after a couple hundred hours of oxidation the coatings started to de-bond from the alloy substrate. The prime path for long-term SOFC durability appears to be an MCO coated H230 alloy or an alloy with equivalent oxidation resistance. Additional long-term testing up to 5,000-10,000 hours is needed in order to understand the implications of alloy/coating reactions and how they affect long-term oxidation and ASR properties.

Seal Development

Two sealing concepts were evaluated in this study—a multi-strip seal design and a high expansion glass seal. The multi-strip seal concept consisting of three parallel strips Ag/Cu, a glass tape, and Ag/Cu was shown to have no detectable leak after 10 thermal cycles. Two high expansion glass compositions were evaluated to determine their viability as a seal material either in the multi-strip concept or as stand-alone seals. SHG-1 (self healing glass) is a borosilicate glass with barium and a low softening point of ~715°C. SHG-2 is a calcium borosilicate glass which was chosen based on its resistance to chromate formation.

Minimizing the amount of compressive load is important to prevent excess stress on the stack. A compressive load of 20psi was found to be adequate for both glasses. Under a compressive load of 20psi and 25 thermal cycles, SHG-2 showed no detectable leak while SHG-1 showed a small amount of leakage at room temperature but no detectable leak at operating temperature.
Both are viable options at an operating temperature of 750°C. They can be used in a multi-strip design or as standalone seals. In comparing the two compositions, SHG-1 shows an onset of crystallization around 950°C versus the onset of crystallization in SHG-2 at 860°C. Longer term studies are needed to determine if crystallization of SHG-2 will impact durability of the seal.

Coating Material and Manufacturing Process Optimization

UTRC developed low cost processes for depositing both conductive interconnect coatings (MCO and electroplated Co) and non-conductive coatings (slurry aluminide). A dip coating process was successfully developed for the MCO coating which initially resulted in 20 μm thick coatings, and was further optimized down to 5 μm dense coatings. A parallel approach to using a spinel coating is to electroplate the alloy surface with Co and oxidize it to form a protective spinel over the surface. The key to this approach was found to be the vacuum diffusion treatment of Co prior to oxidation. The main technical barrier appears to be controlling the amount of Co deposited and CTE mismatch which can occur due to oxidation of the Co. Future work in this area should focus on creating alloy compositions with the correct Co concentrations to eliminate the electroplating and vacuum diffusion treatment processes. This is similar to the alloy development approach used to design Crofer 22 APU to form a spinel coating above the chromia scale.

Slurry aluminide coatings were successfully developed and coated hardware was delivered to Delphi. UTRC's expertise in development of aluminide coatings for aerospace applications was used in order to optimize the coatings for lower temperature ferritic stainless steel substrates. The key technical barrier for aluminide coatings is a depletion of the aluminum reservoir in the alloy which can lead to eventual failure and spallation of the alumina scale. In order to use these lower temperature aluminide coatings in SOFC applications, additional long-term durability tests are necessary.

4. Cell & Stack Procurement and Delivery – TOFC

Objective:

The objective of this task was the delivery and evaluation, including testing, of a Topsoe Fuel Cell (TOFC) multi-cell SOFC stack. This evaluation would familiarize UTC Power and DOE with the characteristics of TOFC's stack technology and facilitate early verification of potential stack performance differences associated with different design approaches to scale up. No R&D was supported in this activity. The cost of the task was only the material purchase from TOFC. All test plans, testing, analysis and recommendations on the TOFC stack(s) was to be documented and provided to TOFC and UTCP. UTC took appropriate actions to prevent IP cross over between Delphi and TOFC including isolating files and personnel as appropriate and in accordance with standard procedures. Topsoe's IP was protected as agreed to by DOE, TOFC and UTCP in the Protected Data and Limited Rights Data provisions of the cooperative agreement.

Program Logistics and Outcome:

In late 2008 and the first quarter of 2009, UTC Power worked with TOFC to develop a Statement of Work, a Testing, Confidentiality and Non-analysis Agreement, and the terms of the Purchase Order for the 10 kW TOFC stack.

The basis of the stack design approach was to combine stacks of modest area together to create a single modular stack with a more commercially viable active area. A mock-up version of the modular stack was assembled and some technical issues were discovered with respect to the modular stack approach.

A modified version of the modular stack design was assembled prior to the cancellation of the project for schedule and budget considerations. The stack was never tested owing to the cancellation of the project.

Details of the project were previously reported in an EPAct protected report from TOFC.

5. Cell & Stack Manufacturing Facility - Delphi

Delphi's SOFC sites have been developed to meet internal and SECA's manufacturing development and volume needs. Our technical centers are in Michigan and New York, as shown in Figure 5-1. The latest addition is the facility in Fenton, Michigan, as shown in Figure 5-2. Cell fabrication and cell scale up from Gen 3 to Gen 4 has occurred at this facility.

SE Michigan

- Cell Fabrication
- Manufacturing Development
- Electrochemical Testing
- Material Characterization and Analysis
- 33K ft^2, added Q3 2008
- Capacity up to 8 MW in 2011

Rochester, New York

- Stack Build and Development
- System Integration & Perform. Lab
- Reformer Development Lab
- Catalyst Durability Lab
- BOP Development

Figure 5-1: Delphi SOFC Technical Centers

Figure 5-2: Manufacturing and Development Facility in Fenton, Michigan

Some of the equipment which has been added to the facility is shown in Figure 5-3. Manufacturing equipment such as lasers, screen printers, and high temperature kilns has been used for cell fabrication. Analytical tools such as a scanning electron microscope and laser

interferometer have been added, and have provided valuable information in our cell and stack development projects.

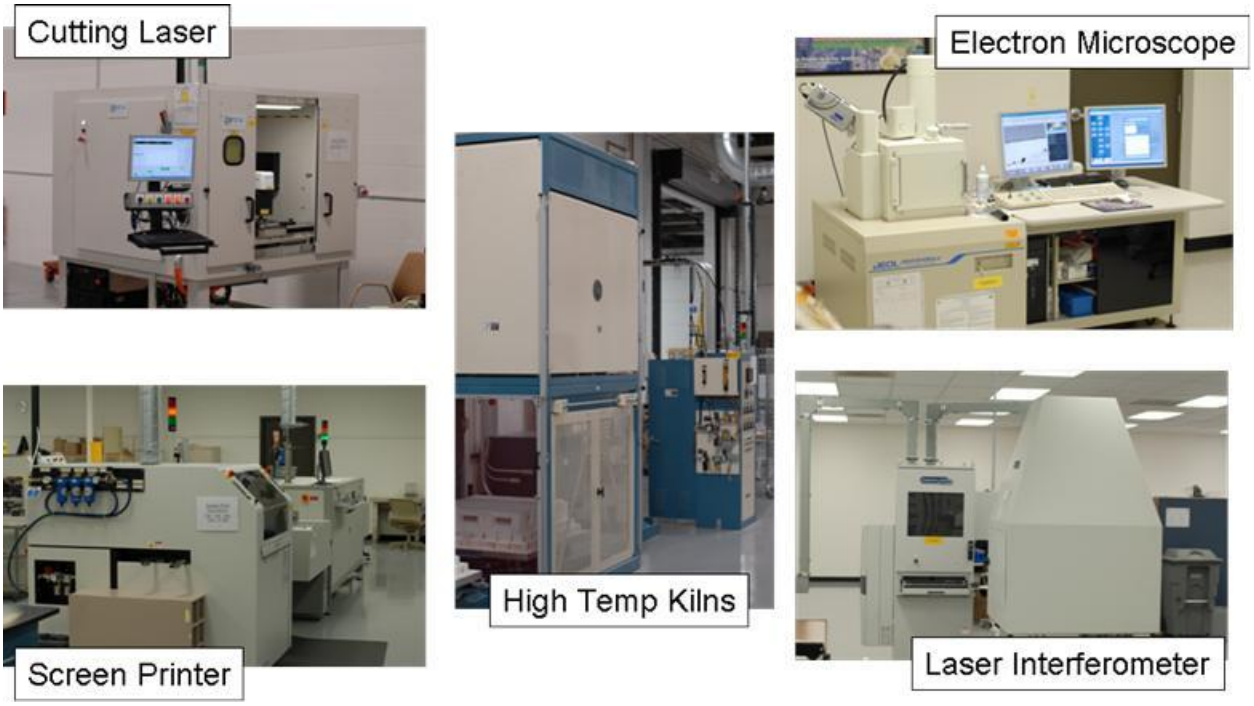

Figure 5-3: Capital Equipment Added to Fenton, Michigan Facility

As a roadmap for Delphi's manufacturing development process, a manufacturing "system" is developed. That roadmap begins with customer technical requirements and lays out the support required to satisfy those requirements. The basics of that roadmap are shown in Figure 5-4. Delphi has managed the SOFC cell and stack development as any other development project in the portfolio. Therefore, the supporting manufacturing rigor has been developed. Supporting documentation includes process flow diagrams, PFMEAs, process control plans, work instructions, process monitoring forms, cell and stack databases, standard cell documentation, and gate charts.

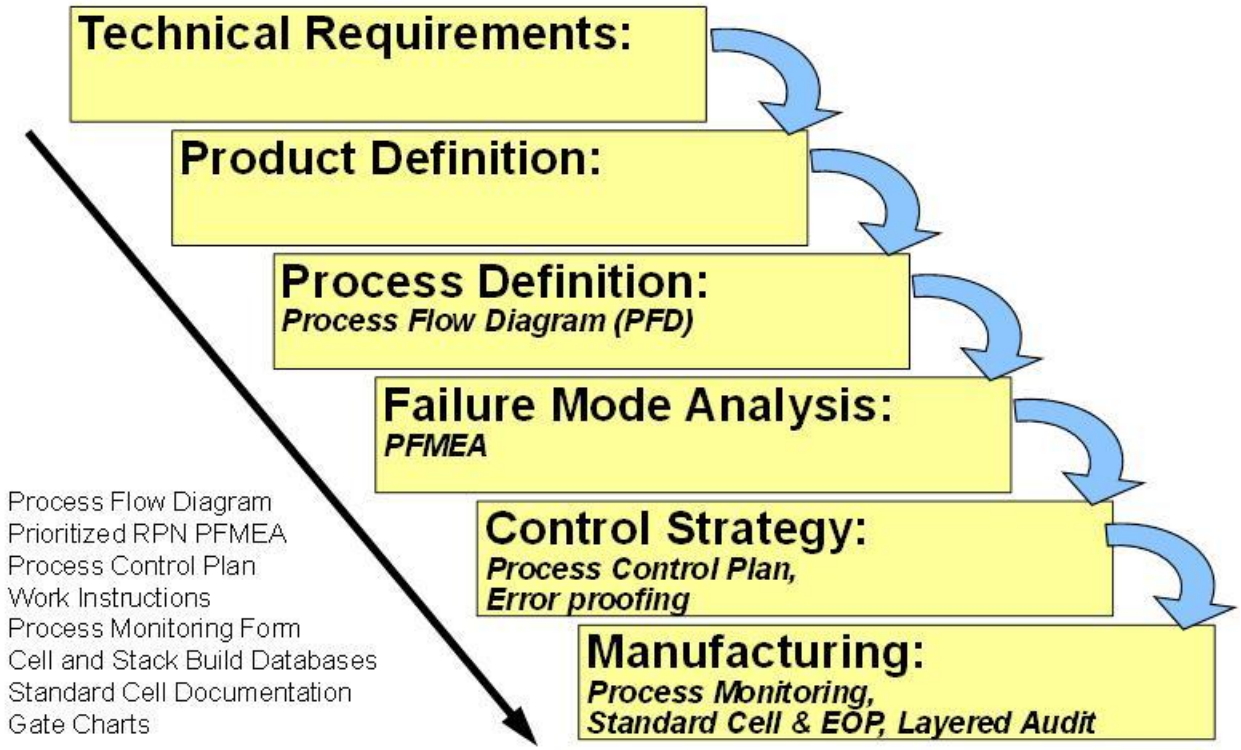

Figure 5-4: Delphi Manufacturing System Development

Scale-up of Stacks for Large Stationary Systems

In order to scale up from single stack power systems to multi-stack coal based power systems, multiple Gen 4 stacks need to be manifolded together. The initial design of the manifold for the large, coal based stationary power plant, was completed (see Figure 5-5). A few key objectives were accomplished with the design, such as cost reduction, coupling, mass, and flow distribution. The manifold is designed to be a cast stainless steel, with minimal post-machining to achieve the dimensional targets, therefore assisting with cost reduction and able to achieve production quantities. The design includes feature(s) creating a flange connection for each of the repeating stack assemblies, establishing sensible and simple seal geometry (see Figure 5-6). The mass of the manifold was minimized by means of removing any excess material, while preserving the strength and rigidity to support the mass of the stack assembly above. The air and fuel delivery geometries produce an equal flow distribution while minimizing flow degradation. The footprint and cell interface geometry are consistent with other application needs (see Figure 5-7).

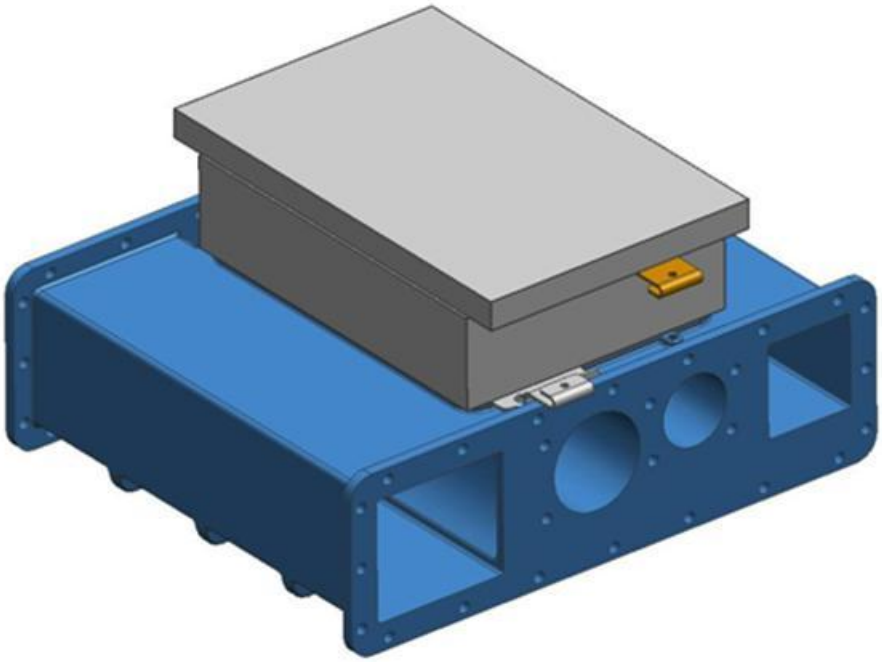

Figure 5-5: Scalable Manifold Design for Large Systems

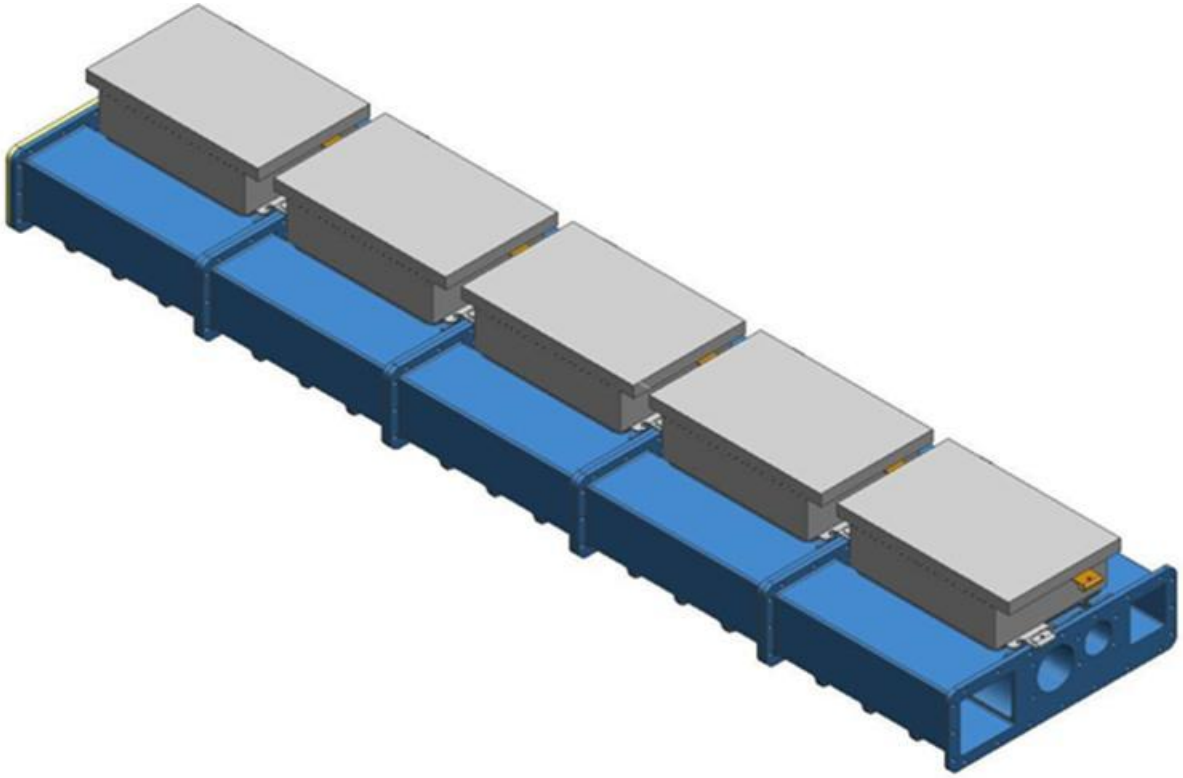

Figure 5-6: Proposed Manifolding for 25kW System

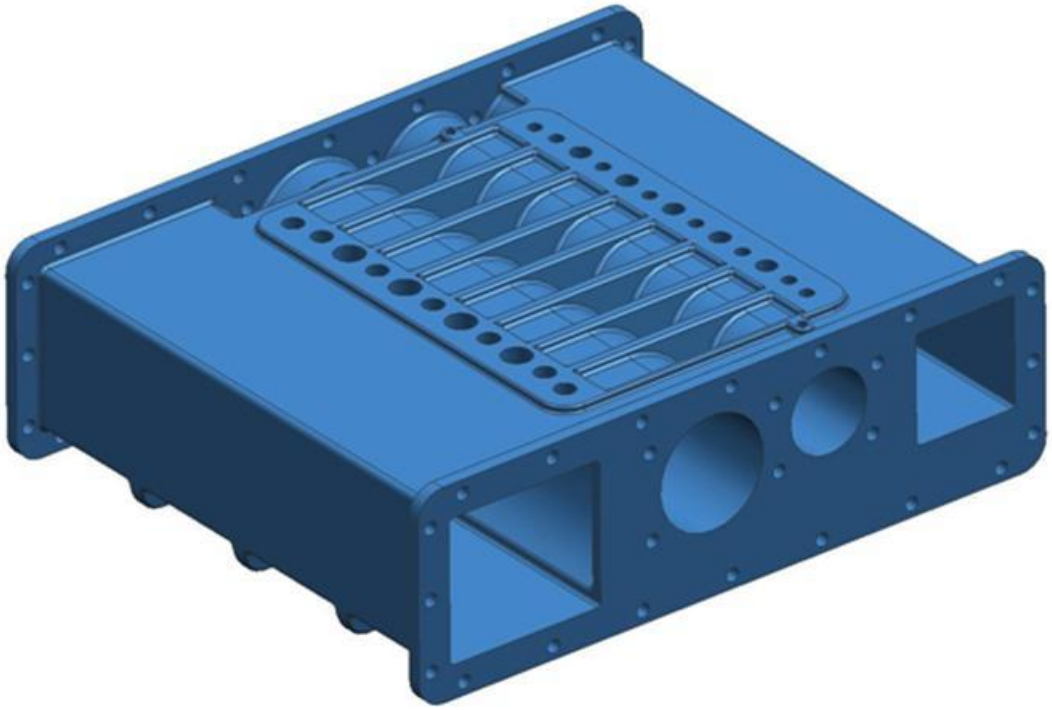

Figure 5-7: Manifold Design

The stationary power plant design concept has been developed to meet volumetric requirements for a stationary fuel cell power plant.

Design iterations were completed on a newer design of power plant, based on some of the concept(s) from the previous power plant. The new design takes advantage of a reduced volume manifold and a new arrangement of the stacks. The reduced volume manifold was possible because the required area for fuel flow was reduced by approximately 58%, which reduced the overall size of manifold (see Figure 5-8). The reduction in the area of the required anode (fuel) chamber was the result of the number of linked stacks decreasing from eight to four, therefore decreasing the amount of fuel required. The power generated from a single stack with fifty repeating units, calculated with a conservative power density, is estimated to be 9 kilowatts. If there are four stacks linked together in a single row, that row is capable of producing 36 kilowatts (see Figure 5-9). A key design feature of the stationary power plant is the symmetrically shared cathode plenum, which enables use of two faces of the cathode plenum. The combination of the new designed manifold, arrangement of stacks, and the cathode plenum the stationary power plant has a volume of 135 ft^3 and capable of generating 502 kW, 3.7kW/ft^3 (see Figure 5-10).

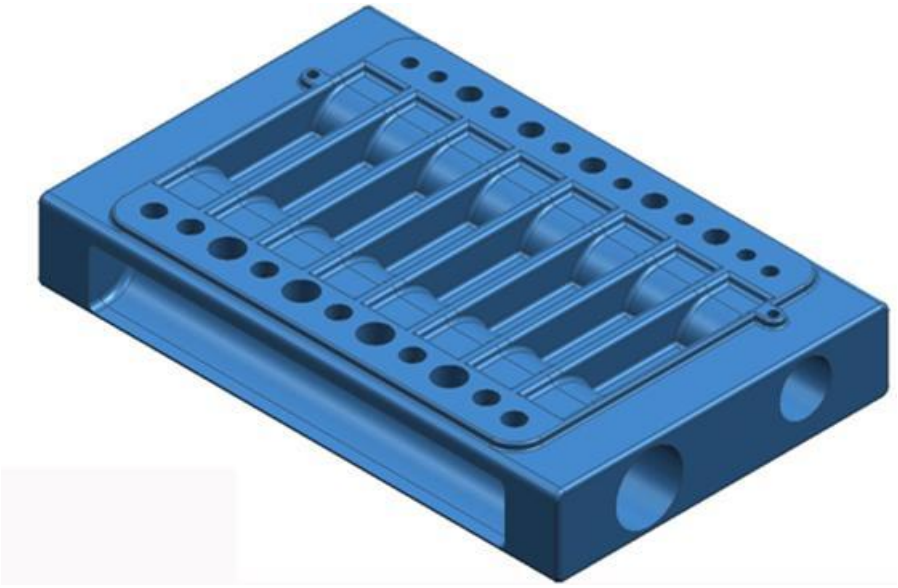

Figure 5-8: Stationary Power Plant Manifold

Figure 5-9: Stationary Power Plant Manifold

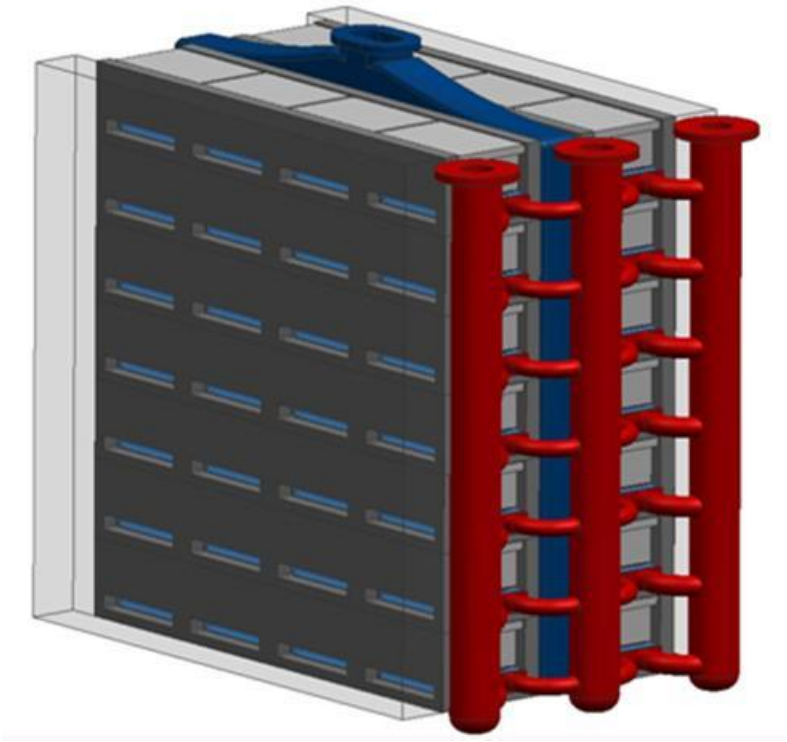

Figure 5-10: Stationary Power Plant Manifold

6. Verification Testing – UTC Power

Objectives:

Phase I: 50 kW Test Stand
The objective of this subtask is to design, procure and build an SOFC test stand capable of testing SOFC stacks up to 50 kW. The test stand will be located inside UTC Power's testing facilities and shall be capable of running on simulated syngas per the test plan and as agreed to with DOE. The effort includes establishing test stand specifications including environmental and safety specifications, conducting conceptual design of the test stand to identify test stand / facility interface requirements and evaluation of purchasing options. This task shall include the installation and final commissioning.

Phase I: Stack Test Plan
The objective of this subtask is to develop a test plan describing the demonstration of the coal-based stack design. The test plan shall be prepared in accordance with the guidance provided in the SECA Minimum Requirements. DOE approval of the test plan is required prior to initiation of testing.

Phase I: Test of Delphi ≥ 25kW Stack

The objective of this subtask is to test the Delphi stack in the SOFC test stand at UTC Power. The goal of the test is to **achieve 1500 hours of operation during Phase 1**. A test report will be prepared and submitted to DOE in accordance with the SECA Minimum Requirements as a deliverable in this subtask.

Phase I: Test of TOFC Stack
The objective of this subtask is to test the TOFC stack in the SOFC test stand at UTC Power. The goal of the test is to **achieve 1500 hours of operation during Phase 1**. A test report will be prepared and submitted to DOE in accordance with the SECA Minimum Requirements as a deliverable in this subtask.

Phase II: Test Stand Preparation
The objective of this subtask is to make modifications to the existing test stand to support breadboard testing. The breadboard will be integrated into the test stand utilizing the existing data acquisition and safety systems. Controls will also be provided where necessary. The test stand load system may be utilized to simulate an external load. The test stand will be modified such that verification of thermally self-sustaining breadboard operation is confirmed.

Phase II: Breadboard Test Plan
The objective of this subtask is to develop a test plan describing the demonstration of a breadboard incorporating the SOFC stacks and operating on natural gas. The test plan shall be prepared in accordance with the guidance provided by DOE and be sufficient to demonstrate thermal self-sufficiency. DOE approval of the test plan is required prior to initiation of testing.

Phase II: Testing of Breadboard
The objective of this subtask is to test the breadboard for a period of 3000 hours (1500 hours by the end of Phase II) including thermally self-sufficient operation. A test report will be prepared and submitted to DOE as a deliverable in this subtask.

Experimental methods:

1 October 2008 – 31 December 2008

During this reporting period, the functional requirements for the test stand were drafted and internally reviewed at UTC Power with the functional teams (mechanical, systems, software, safety, etc.). Evaluation of the environmental, health and safety (EH&S) impact associated with the anticipated operation conditions of the test stand was initiated. In addition, a model simulation of an existing UTC Power catalytic steam reformer (CSR) was carried out to identify a viable approach for producing a simulated coal gas composition.

1 January 2009 – 31 March 2009

During this reporting period, a project schedule was developed, functional leads were assigned to the project and a Task Ticket was created that defines the manpower, schedule and cost of the

Test Stand. The functional requirements for the test stand were also updated, preliminary mechanical P&I and electrical diagrams were developed, the location of the Test Stand was finalized, and a preliminary Facilities Test Stand Layout was generated.

Testing of a 30-cell TOFC stack was initiated at UTRC for the purpose of gaining experience with TOFC stack technology in anticipation of testing the larger TOFC test article in FY10.

1 April 2009 – 30 June 2009

During this reporting period, the test stand design team continued to refine both the functional requirements and the conceptual design for the test stand through recurring technical exchanges with both Delphi and TOFC. Preliminary test plan and controller functional requirements documents were developed. The team also continued to refine the mechanical P&I and electrical diagrams as it conducted a failure modes and effects analysis (FMEA). A Conceptual Design Review was held.

1 July 2009 – 30 September 2009

During this reporting period, the test stand design team continued to refine the functional requirements for the test stand through recurring technical exchanges with both Delphi and TOFC. The mechanical and controller groups also completed their peer reviews which are required to begin their detailed design phases. The remaining groups are expected to complete their peer reviews early in Q1Yr2.

1 October 2009 – 31 December 2009

During this reporting period, the test stand design team issued bid packages for the fluid management skids. Several large components, including the UPS and the load bank were ordered. The final selection of several key components such as the cathode heater and recuperative heat exchanger remain open. The controller functional requirements document was issued and the test stand design team continued to refine the functional requirements for the test stand through recurring technical exchanges with Delphi.

1 January 2010 – 31 March 2010

During this reporting period, the test stand design team issued purchase orders for the fluid management skids, the cathode heater and the recuperative heat exchanger. Agreement was reached on the flange design connecting the test stand with Delphi's 25kW test article and the interface control document for the Delphi stack was released. Weekly technical exchanges continued between the teams to ensure that the installation of the test article is as seamless as possible and the test stand shakedown period is as brief as possible.

1 April 2010 – 30 June 2010

During this reporting period, the test room, the fluid management skid, the cathode and anode heaters, the recuperative heat exchanger, several electrical enclosures, the hot flex lines and the hot box were all received. The performance of the cathode heater and the anode non-combustible heater were verified at the vendor facility. A protective aluminide coating was applied to the recuperative heat exchanger using a PVD process, and the heat exchanger was successfully tested for mechanical integrity using a pressure decay test. The test room was installed in the test facility and most of the facility connections were completed. The retrofit of the afterburner was completed, including installation of the dual burner and the new controller. The emissions permit was received from the Connecticut DEP, allowing the fluid skid to be connected to the facilities gases. Good progress continues on the controller and operator interfaces. Weekly technical exchanges continued between the teams to ensure that the installation of the test article is as seamless as possible and the test stand shakedown period is as brief as possible.

1 July 2010 – 30 September 2010

All major test stand components were installed and pressure tested. The methane supply skid was installed on site, a readiness review completed and the facility connection was completed. Insulation of high temperature plumbing in the test room was started. The test article hot box, consisting of an insulation plate and removable enclosure, were received and the test article manifold was installed to confirm fit. The insulation plate and manifold had been connected to the test stand to confirm alignment. The lifting fixture used to maneuver the hot box was modified to address handling issues.

Software system and safety checks were started. This included both the area PLC's which controls safety systems and the operator interface which controls stack testing related parameters. Approximately 80% of the alarms passed test with only minor issues identified with the remaining ones. Testing of the control loops and truth table will follow in the next quarter. Weekly technical exchanges continued between the teams to ensure that the installation of the test article is as seamless as possible and the test stand shakedown period is as brief as possible.

1 Oct 2010 – 31 December 2010

The test stand was completed and passed a final readiness review. This deems the stand safe to operate allowing system check to proceed with all gas and electrical feeds active. Insulation of high temperature plumbing in the test room had been completed. A temporary jumper pipe was used in place of the stack to allow the test stand to test heaters and flow gases. Figure 6-1 to 6-4 below illustrates the status of the test stand commissioning.

Software system and safety checks had been completed. This included both the area PLC's which controls safety systems and the operator interface which controls stack testing related parameters. All of the alarms had passed test. Testing of the control loops and truth table had started. The stack manifold was planned to be installed next to verify pressure drop and thermal performance. This will be followed by installation of a debug stack to verify product protection systems. Weekly technical exchanges continued between the teams to ensure that the installation

of the test article is as seamless as possible and the test stand shakedown period is as brief as possible.

Figure 6-1: Test Stand Side View

Figure 6-2: Test Room before Insulation

Figure 6-3: Test Stand Fluid Skid

Figure 6-4: Test Stand Afterburner

1 January 2011 – 31 March 2011

The 50kW capable test stand at UTC Power is fully functional. A debug stack has been installed into the test stand and operated on various gas compositions and at various temperatures and pressures to confirm test system operation. Some limited stack diagnostics have been performed to verify data acquisition systems and test stand controls. The test stand was ready for installation of the larger stack module.

As part of the final check of test stand systems, the load system was checked by operating the debug stack at various power levels. The debug stack was tested at power levels only up to 5kW while it is expected that the stack module will produce >25kW. The load system could not be tested at those power levels with the debug stack.

The test stand completed several days of stack testing included an extended hold over several days in unattended operation mode. The test stand controls and safety systems performed as expected during that time.

A gas analysis system was brought online to verify anode and cathode gas compositions fed to the stacks. Figure 6-7 shows the location of the gas analysis system in the test stand. The data showed fuel gases including hydrogen, nitrogen, carbon dioxide and methane were being mixed at the test stand in the proper proportions required by the fuel cell stack. Cathode gas analysis was also functioning as expected.

Figure 6-7: Rear End of Test Stand (Gas Analysis System)

1 April 2011 – 30 June 2011

UTC commissioned the 50kW capable test stand at UTC Power. A debug Gen 4 stack was installed into the test stand and operated on various gas compositions and at various temperatures and pressures to confirm test system operation. The test stand completed several days of stack testing including an extended hold over several days in unattended operation mode. The test stand controls and safety systems performed as expected during that time. A gas analysis system was brought online to verify anode and cathode gas compositions fed to the stacks. The data showed fuel gases including hydrogen, nitrogen, carbon dioxide and methane were being mixed at the test stand in the proper proportions required by the fuel cell stack. Cathode gas analysis was also functioning as expected. Limited stack diagnostics was performed to verify data acquisition systems and test stand controls. Post verification of test stand functionality a larger stack module was installed in the test stand and 1500hr endurance test was initiated.

Figure 6-8 Test room in the test stand with and without the test article installed

1 July 2011 – 30 Sep 2011

UTC started 1500hr endurance testing with 2 stacks in a parallel configuration. The fuel composition was coal gas blend: (23.79%H_2-46.9%CO_2-11.95%CH_4-7.36%H_2O). The goal was to understand impact on system design and operation. Stack module was successfully ramped up to the NOC point of 0.8V/cell. Figure 6-9 shows the operating current, voltage and output power for the 2-stack module. The test was aborted after ~10hrs due to an anode process heater (HTR380) failure.

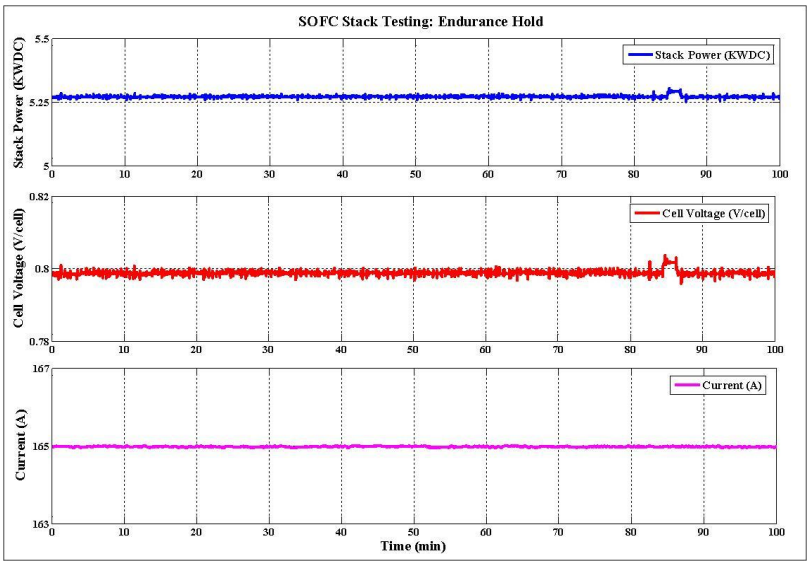

Figure 6-9: Two-Stack Module Power, Voltage and Current

UTC and OSRAM, the heater vendor, engaged research scientists with heater failure #4. UTC engaged material science technology fellows from its sister division (Pratt & Whitney) to help with the failure. Microscopic analysis of heater element samples from previous failures determined that all failures had the same morphology. Oxide and bulk structure was normal at low temperature (~<1100C) regions. However, high temperature regions showed no Al in bulk to form protective oxide. High P_{N2} coupled with low (≈0) P_{O2} resulted in Al-nitride formation with Non-homogenous bulk, 2-phase FeCr formation. The Cr-O is not protective and is very unstable. This resulted in spilling of the material from the heater causing material loss, necking and eventual failure.

1 Oct 2011 – 31 Dec 2011

UTC continued 1500hr endurance testing with 2 stacks in a parallel configuration after resolving HTR380 issues. The fuel composition was coal gas blend: (27.79%H_2-46.9%CO_2-8%CH_4-7.36%H_2O). The goal was to understand impact on system design and operation. Stack module was successfully ramped up to the NOC point of 0.8V/cell. Figure 6-10 shows the operating current, voltage and output power for the 2-stack module for ~ 24 hrs duration. The test was aborted after ~25hrs due to an anode process heater (HTR380) failure.

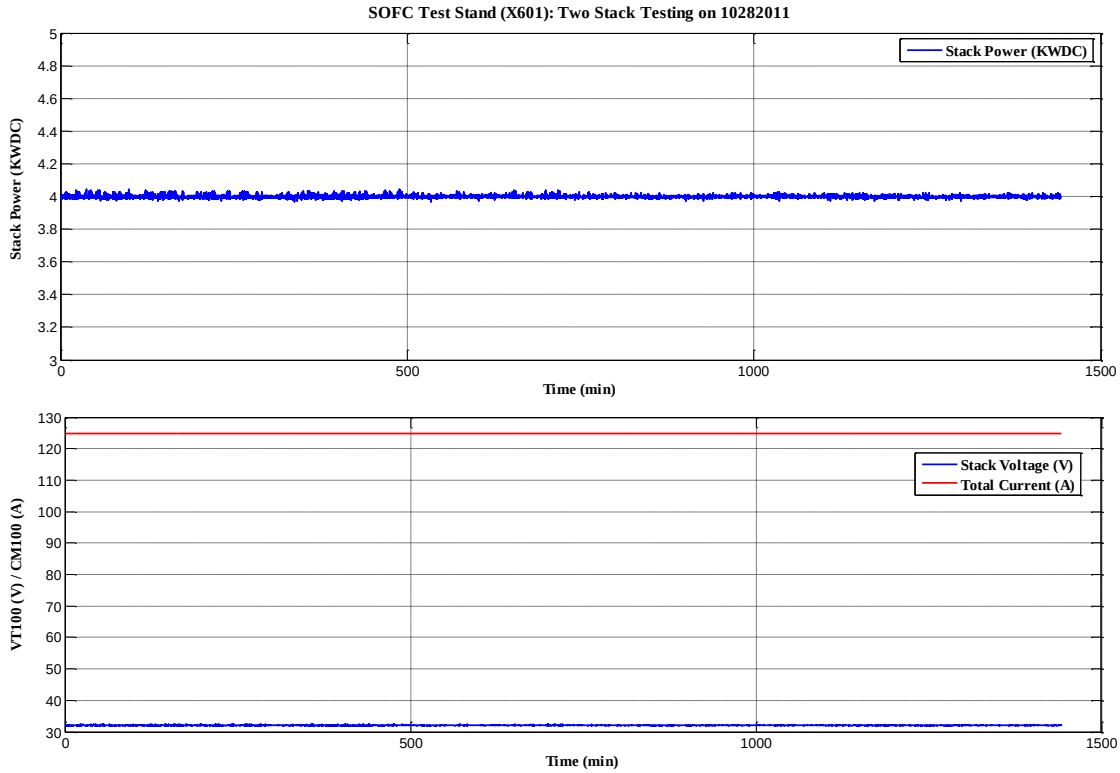

Figure 6-10: Two-Stack Module Power, Voltage and Current

The root cause activity determined that during heat-up and diagnostic modes, the nitrogen process fluid was reacting with the alumina scale and at the high temperatures (above 1150°C) forming more thermodynamically favorable aluminum nitrides. After completing the typical heat-up and diagnostic cycles, analytical testing showed that most aluminum in the Fe-Cr-Al was bound in stable, but un-protective, nitride form. Upon switching to carbon dioxide flows for endurance testing, breakaway corrosion was occurring, resulting in decreased element cross-sectional area and localized hot spots. Further studies led to an assessment that 60°C element temperature reduction would prevent alumina degradation and subsequent nitride formation. To accomplish this temperature reduction, the heater was designed using dual stage elements with a higher power density stage in the low temperature region, coupled with a lower power density in the hot region stage to lower maximum element temperature. Testing at the vendor location showed a maximum element temperature of over 80°C from the single stage design. On October 31st the stand was restarted and on heat-up the heater experienced its 5th failure in the form of a rapid uncontrolled "run away" condition and was immediately shut off. Disassembly revealed that the live center element power return connection had moved and shorted on the casing. This failure was attributed to a deficient dielectric isolation design. This design relied purely on air gap between unsupported return wires and heater casing. To address this deficiency, the heater vendor lengthened the dielectric structural alumina center support rods and mechanically fastened the return wire to them. They also removed metal from the casing edges closest to the return wire exit and replaced it with a dielectric alumina filler to add an additional layer of protection. The heater was reinstalled into the test stand and failed again on November 23rd after

15 hours runtime. Subsequent removal and disassembly showed melting of all three elements at the inlet, a completely different failure mode than previously seen. The hypothesis was that this failure had resulted from a loss of flow to the heater during operation. Test stand data logging at UTC did not support this hypothesis. Investigation showed that the oxidation rig used by the heater vendor after manufacturing had continuous temperature control, but no continuous data logging, leading to the belief that flow loss could have inadvertently occurred during oxidation process. As it is not possible to verify element condition after assembly, any possible defects could not be detected. This failure resulted in a vendor oxidation and inspection process change. Going forward the oxidation shall be performed individually on the bench with high temperature monitoring. This change allows independent control of oxidation for the first and second stages as well as visual inspection before final assembly into the heater. Independent oxidation of the element stages in free air is an improvement because it allows more consistent scale formation due to uniform temperatures and real time monitoring of element temperatures to eliminate overheating concerns. As an additional quality check, changes in the heater element are quantified by taking resistance measurements before and after oxidation as well as after installation into the casing. A design change was also made which moved one of the high limit thermocouples from the second stage hot spot to observed first stage hot spot. High temperature limits remain fixed to the second stage high temperature spots on the other two elements. This change is believed to increase heater over temperature protection robustness while retaining the current, proven, control system. The re-worked heater with the additional post-oxidation quality control documentation is expected to be delivered to UTC in the second week of January, 2012.
In parallel to pursuing design changes to improve OSRAM immersion heater life, UTC Power has also designed an indirect, electric tube furnace-type heater. The benefit of this solution is that it allows full control over process gas-tube metal interactions and the use of higher durability heating elements which cannot normally be used due to cell stack catalyst contamination concerns. The primary design difficulty is minimizing physical changes to the test stand due to long lead time and high expense on new piping assemblies. In addition to space concerns, designs are set to exactly replicate the temperature and pressure drop performance of the current heater to minimize controls and tuning changes.

1 Jan 2012 – 31 Mar 2012

UTC completed Phase I endurance testing with a 1 stack module. The fuel composition was coal gas blend: (27.79%H_2-46.9%CO_2-8%CH_4-7.36%H_2O). The goal was to understand impact on system design and operation. Stack was successfully ramped up to the NOC point of 0.8V/cell. UTC competed 1220hrs out of the total 1500hrs stipulated for the endurance test. ~800hrs of the 1220 hrs was a continuous run with no system shutdowns. This was made possible by rigorous efforts to improve test stand reliability related to the anode heater and other critical components.

Phase I testing resumed during second week of Jan 2012 after receiving HTR380 from OSRAM. Test article during this part of testing consisted of one stack. Test stand startup was initiated on Jan 12, 2012. After resolving a couple of test stand related reliability issues, achieved endurance hold on Jan 24, 2012. Test stand continued endurance hold till Mar 08, 2012 before incurring a

shutdown due to a test stand dew point sensor failure. As part of this endurance hold in Q1 2012, test stand accrued about 1000 continuous load hours.

1 Apr 2012 – 30 Jun 2012

No update this reporting period.

1 July 2012 – 30 September 2012

In the last quarter, the SOFC test stand from Phase I was upgraded for successful integration of the breadboard. Significant changes were made in the test stand, including the fluid skid, heaters, electrical system, blowers, ventilation, and test stand controls while maintaining existing data acquisition and safety systems. In parallel with the completion of these test stand upgrades, the breadboard fabrication was completed and it was installed in the test stand. While the breadboard was being installed, input/output (I/O) checks were completed using the test stand controller software I/O shell. The breadboard is shown at the fabricator's facility in comparison to its design model in Figure 6-11 below:

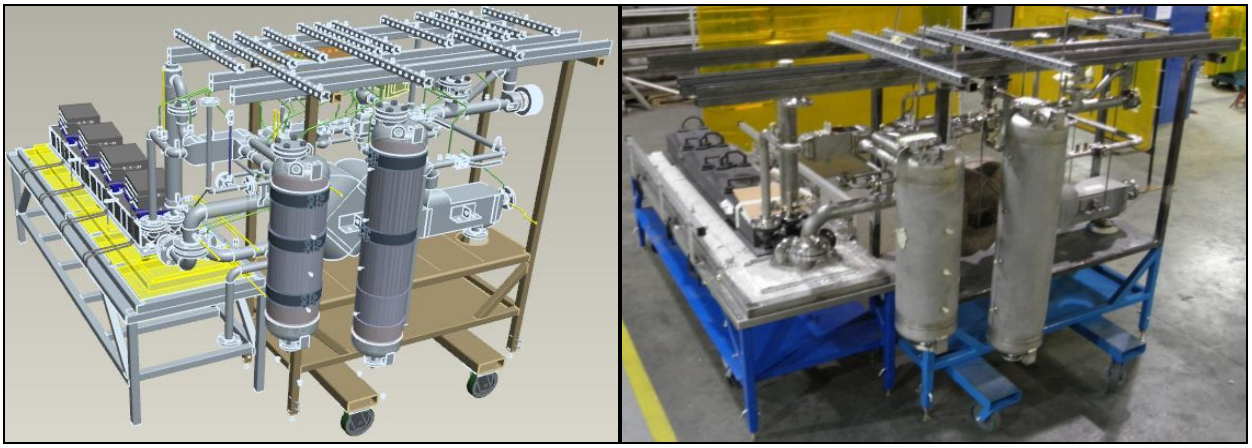

Figure 6-11: Breadboard Test Article

After completing I/O and end-to-end checks, checkout of Life Safety Truth Table (LSTT) and Product Protection Truth Table (PPTT) was initiated to ensure safety critical and product critical control actions are executed as per requirements. The LSTT is comprised of critical life safety shutdowns that are triggered by hard-wired circuit signals such as Emergency Stop (E-Stop), thermal switches, smoke detectors, controller watch-dog timers and loss of ventilation. In addition, life safety shutdowns are also triggered by H2, CO and CO2 gas sensors, signals which are wired to a Safety Controller and/or lockout enunciator. By contrast, the PPTT is comprised of shutdown events initiated by the test stand controller software due to abnormal conditions in the breadboard power plant such as, high anode inlet temperature, stack cross pressure, fuel flow demand not satisfied, etc.

UTC Power also completed the design, development and implementation of the control strategy for the breadboard. In an effort to improve system reliability, extensive lab testing of the control software was done by Systems and Software team. The control software was then transitioned from the lab testing environment to the test stand for stability testing in the final configuration. Several issues were identified during stability testing and resolved in parallel with the breadboard insulation effort.

1 Oct 2012 – 31 Dec 2012

The majority of the SOFC Breadboard and test stand checkout using debug stack was completed that included gas flows, heater function, pressure drop confirmation, instrumentation calibration and check-out, facility life safety truth table testing, test stand life safety truth table testing, and product protection truth table testing. Subsequently, the Breadboard with debug stack was tested on load using 50% H2/N2 and Natural Gas.

1 Jan 2013 – 31 Mar 2013

At the beginning of this quarter, the breadboard had just completed testing using the debug single stack running on forming gas (50% hydrogen and 50% nitrogen). The power plant was successfully transitioned to natural gas and the stack performance was consistent with expectations. The breadboard ran in this configuration for approximately one week in a largely unattended mode without significant performance decay.

After completing satisfactory functional testing using the debug stack, four new stacks were installed by Delphi personnel into the breadboard toward the end of January. The breadboard resumed testing with the new stacks in early February. The breadboard was successfully tested on load using forming gas and natural gas. On February 20, 2013 the breadboard was operating stably at 6.5kW on natural gas when a small oil leak was discovered in the blower assembly. The leak was small but significant enough to warrant remediation which could only be accomplished by shutting down the breadboard. The breadboard was shutdown on February 21st to fix the oil leak.

On February 22, 2013 ClearEdge Power, who acquired UTC Power on February 12, 2013, informed DOE by letter that it would no longer be able to continue with the program and expressed a desire to work with DOE and Delphi to transition the program by March 22, 2013. As a result of this decision, breadboard testing was ceased in the week of February 25th, 2013 and plans were prepared to safe the breadboard for an indefinite storage period. Some residual charges to the program were, and will be, incurred for proper storage of the test stand/breadboard and writing the final report.

Since the program was discontinued in this quarter, progress towards the 1500hr and 3000hr endurance objectives has ceased. At the point the program was stopped, the breadboard had accrued 250 load hours using the debug stack for initial proof of satisfactory operation and then

another 110 load hours with the full complement of four stacks. Of the load hours noted, 192 hours were logged while operating with natural gas as the fuel.

Results and discussions:

Phase I Testing using Simulated Coal Gas:
Summary of Phase I testing metrics including load hours accrued during Q2 - Q3 2011and Q1 2012 are shown in Table 6-1.

Table 6-1: Summary of SECA Phase I Testing Metrics

Metric	Total (Note 1)	2011 Q3 and Q4	2012 Q1
Test Stand Hot HRS (Note 2)	1881	755	1126
Test Stand Load HRS (Note 3)	1242	236	1006
Test Stand @ NOC for Endurance (HRS)	1216	215	1001
Total Number of Shutdowns	11	7	4
Notes: 1. Start time is 7/1/2011 with two stack module 2. Accumulated hrs whenever stack temperature > 160 C. Includes heat up, load hrs and shutdown 3. Total load hrs that includes current ramp and endurance hold			

Majority of the test stand shutdowns during 2011 were related to HTR380 failures and those during 2012 were related to test stand component failures that have since been addressed. The 1000 hrs of testing at NOC achieved in Q1 2012 was continuous operation using simulated coal gas. During this operation no significant decay was observed in the stack voltage.

Phase II SOFC Breadboard Testing:
The following breadboard testing milestones were achieved during Q4 2012 and Q1 2013.

1. Natural Gas testing of the breadboard with debug stack
    a. Current: 50 A; Power: 1.6 kW; Average V/cell: 0.81
2. Four stack install and integration into the breadboard.
3. Heat up and on-load steady operation of the breadboard using 50/50 gas
    a. Total current: 250 A; Power: 8.2 kW; Average V/cell: 0.83
4. Transition to Natural Gas and on-load operation steady operation
    a. Total current: 200 A; Power: 6.5 kW; Average V/cell: 0.82

Heat-up of the breadboard with the debug stack was initiated and transitioned to load using natural gas on 1/15/2013. Prior to that, it was ensured that the system could achieve steady unattended operation on hot standby and on load using 50/50 N2/H2 mix. After achieving steady operation on natural gas at the conditions shown above, the system was left for lights-out operation for one week, 1/15/2013 to 1/21/2013. Table 6-2 shows the testing summary metrics of the breadboard checkout testing carried out using the debug stack.

Table 6-2: Summary of SECA Phase II Testing Metrics - Debug Stack (Note 1)

Metric	Test Data (50/50)	Test Data (NG)	Expected Value (NG) (Note 5)
Stack Power (KWDC)	1.7	1.6	1.87
Stack Current (A)	50	50	60
Min / Avg / Max Cell Voltage (V/cell)	0.72 / 0.83 / 0.85	0.66 / 0.79 / 0.82	0.69 / 0.78 / 0.80
One-Pass H2 Utilization (%)	(< 14)	(< 26)	42
External H2 Utilization (%)	14	26	42
Reformer CH4 Conversion (%)	NA	40	NA
Stack CH4 Conversion (%)	NA	35	< 10
Test Stand Hot HRS (Note 2)	660		
Test Stand Load HRS (Note 3)	250		
Test Stand on NG Lights Out (HRS)	165		
Total Number of Shutdowns (Note 4)	7		

Notes:
1. Includes testing in Dec 2012 and Jan 2013
2. Accumulated hrs whenever stack temperature > 160 C. Includes heat up and load hrs
3. Includes load hrs during current ramp
4. Includes 3 planned shutdowns
5. End of Phase I endurance data

Figure 6-13 shows the operation of SOFC Breadboard with the debug stack on 50/50 H2/N2. The plot shows the debug stack power, voltage and current as a function of time in mins. After achieving operating temperature, the load was ramped up to 50 A in order to maintain an average cell voltage of 0.8 V/cell. The step down in load between 900 and 950 mins is due to a transition to lower load for overnight unattended operation.

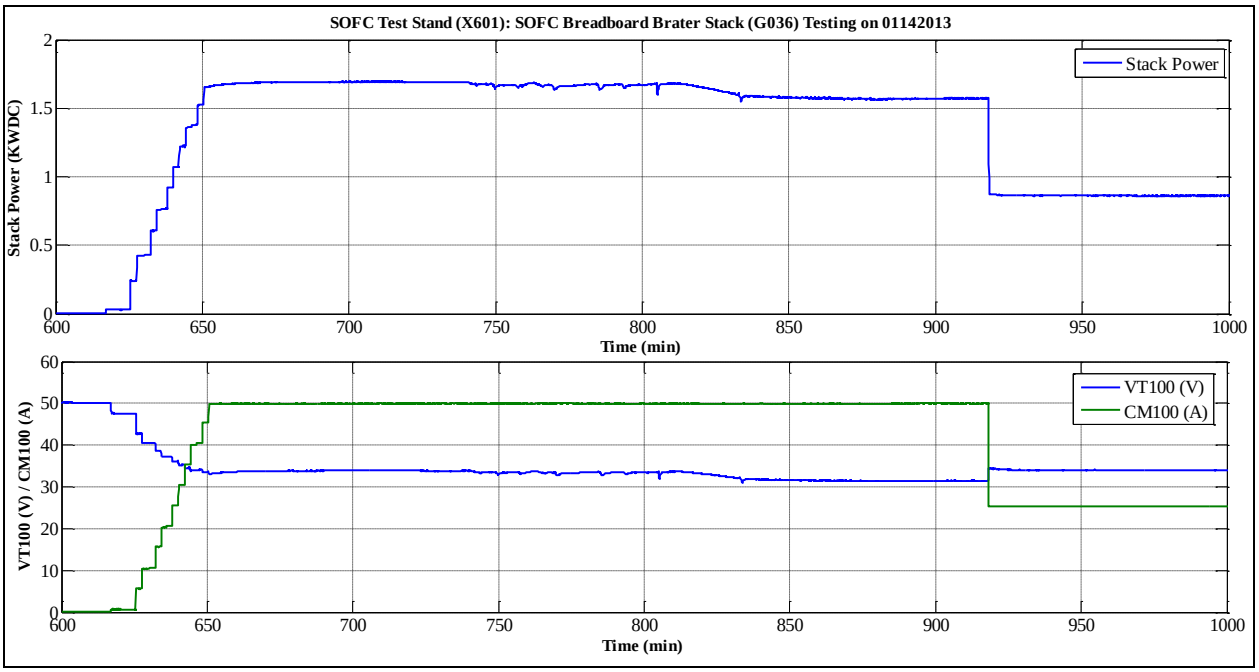

Figure 6-13: SOFC Breadboard with Debug Stack on 50/50 Gas

Figure 6-14 shows the operation of SOFC Breadboard with the debug stack on Natural Gas on 1/21/2013. The plot shows the debug stack power, voltage and current as a function of time in mins. The Breadboard was shutdown and cool down was initiated on this day after achieving continuous lights-out operation from 1/15/2013. This is shown in the figure by the step change between 600 and 800 mins. Similar to the operation on 50/50 H2/N2 gas, the debug stack was operated at 50 A load to in order to maintain an average cell voltage of 0.8 V/cell.

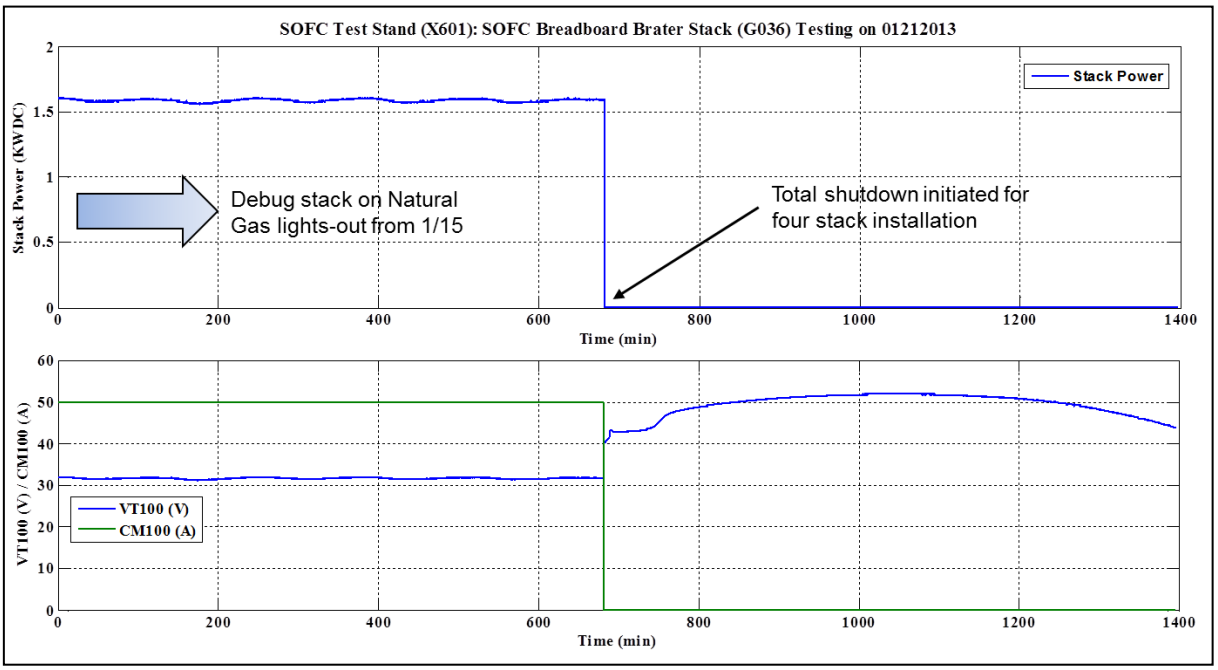

Figure 6-14: SOFC Breadboard with Debug Stack on Natural Gas

The following items were verified during the lights-out operation on debug stack

1. Using gas analysis system confirmed reformer conversion met design requirements.
2. Using gas analysis system confirmed methane conversion inside the debug stack was within the expected value from Phase I testing.
3. No Cr at cathode inlet. As per the action taken by UTC Power during the semi-annual review meeting on 10/29/2012, a Cr sampling apparatus was set up at cathode inlet (with gas sample from AP100 and operated from 1/15 – 1/21. Lab analysis of the acid trap showed no Cr present in the sample, confirming that Cr was below detectable limits at cathode inlet.

The following issues were identified during the operation of the breadboard with the debug stack:

1. Thermocouple failures:
During test stand checkout and initial debug stack testing, multiple thermocouples installed upstream of the anode and downstream of the stack assembly failed. The anode thermocouples were found to read correctly at low temperatures and then read erratically at elevated temperatures. These failures were unexpected because there were no thermocouple failures during the 1000 hours of Phase 1 testing, and 4 failures during 100 hours of Phase 2 testing.

All thermocouples selected for use in the breadboard were double-junction ungrounded Type K. The rationale behind selection of double junction sensors was that it ensured each location had two temperature measurements in the event of failure. In the event of failure the connector could be swapped from the failed junction to the integral redundant. The selected thermocouples also had flying leads covered with 750C wire insulation to allow routing of all thermocouple wires through the hot box to common bulkhead panels. These selections were different from Phase 1 in that the Phase 1 thermocouples were all single junction (still ungrounded) with integral connectors since connection was immediately outside the pipe insulation.

The initial cause of these thermocouple failures were thought to be mechanical stresses in the sheath related to high temperature exposure. Dual junction thermocouples use 24 gauge (0.020") wires whereas single junctions use 22 gauge (0.025") wires. This size difference means that single junction thermocouples are 156% stronger in axial loading (tension/compression) and 244% stronger in bending. The initial hypothesis was that thermal stresses were causing failures not seen in Phase 1 because of the stronger wires. To combat this problem, the team procured single junction thermocouples. Due to time constraints, thermocouples with fiberglass-insulated leads and stainless steel overbraid were selected (instead of the original fiberglass lead insulation and overbraid).

Disassembly of the breadboard during 4-stack installation showed the mechanical stress hypothesis to be incorrect for thermocouples located at the anode inlet. When insulation was removed, the failed thermocouples were found void of insulation (it appeared that all had burned off) with positive and negative lead wires in contact. This investigation showed that the thermocouple insulation was not suitable for the environment. All failed thermocouple wires were within view of HTR300's outer casing which operates at temperatures nearing 1000C. Figure 6-15 shows the location of the wire for one of the anode inlet heater thermocouples.

The team's belief is that radiation heat transfer to the thermocouple increased insulation temperatures above the 750C rating, causing it to break down. Replacement units with stainless steel insulation overbraid and a 950C rating should resolve this problem. Initial 4-stack breadboard running showed no failures in replacement thermocouples.

Figure 6-15: Anode inlet thermocouple wire placement.

The overall learning from these failures is that thermocouples within view of extremely hot objects (HTR300 for example) should have wire selected to withstand temperature increase due to radiation heat transfer and that thermocouples subject to stresses on installation (bending, etc) should be single junction for maximum mechanical strength.

2. Stack Cross Pressure:

   While the system was transitioned to natural gas from 50/50 N2/H2 mix, the anode pressure drop was significantly lower than the cathode. This is due to (i) low back pressure on anode due to anode exhaust plumbed directly to the test stand afterburner and (ii) low flow rates due to the debug stack operating at 50 A (1.6 kW) while maintaining 0.8 V/cell.

   To mitigate stack cross pressure issues while operating lights-out, N2 was added as an inert diluent into the anode loop. This helped maintain the stack cross pressure at its set point of 3 kPaD.

3. Dew Point Sensor Measurements:

   During the debug stack operation, it was observed that the dew point sensor was not reading correct values. Investigations revealed that the dead-ended sample line was leading to condensate formation in turn making the sensor read incorrect values. The Mechanical Balance of Plant group recommended installing a condensate trap and vent line. The vent line was subsequently modified to lead into the fluid skid ventilation system due to the presence of H2 and natural gas. A Swagelok valve was also installed to regulate the flow rate through the sample line.

The system was shut down by performing a planned Total Shutdown of the test stand on 1/21/2013 for cool down and preparation for the four stack installation. The following tasks were

accomplished between 1/21/2013 and 2/11/2013 when the heat up of the breadboard with the four stacks was initiated

1. Installation and integration of four production stacks from Delphi. See Figure 6-16 for a picture of the test stand with four stacks installed on the gas manifold.

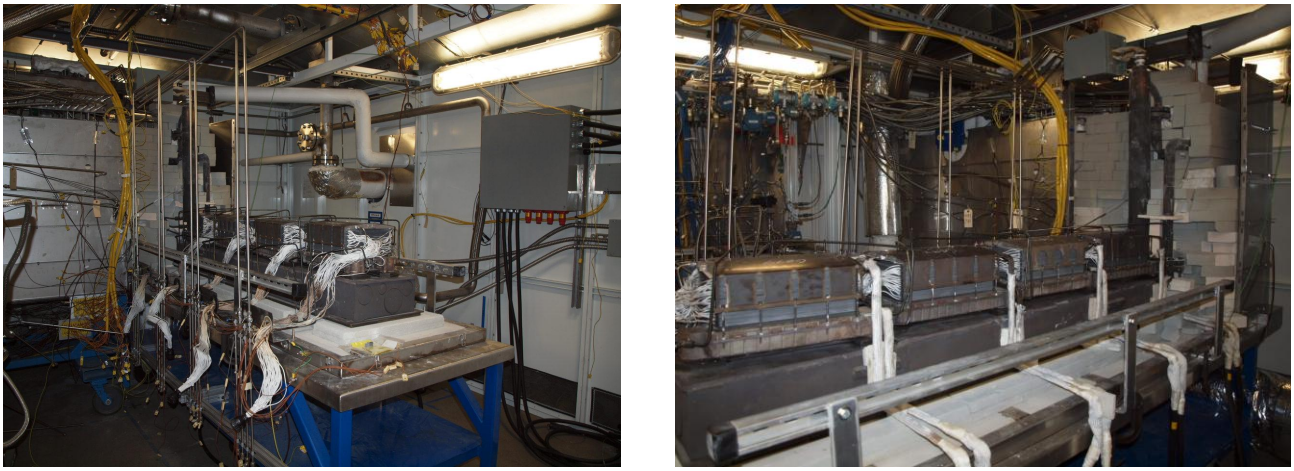

Figure 6-16: SOFC Breadboard with Four Stacks

2. Replaced all failed thermocouples, except TE311. This thermocouple, not a critical one, is located in the exit pipe of the pre-reformer that is buried inside the insulation. FPS and MBOP team agreed that the pre-reformer bed exit thermocouple (TE313C/313CR) can be indirectly used for evaluating the performance of the heat exchanger downstream of the pre-reformer (HEX300).

3. Updated test stand controller software with (i) lessons learned from natural gas debug stack testing, and (ii) control loop tunables to achieve optimal heat up and steady state controllability issues. The Systems team performed a thorough checkout of the changes on the software bench.

4. UTC Power's Systems, Test and Program groups agreed to perform an audit of the Life Safety and Product Protection Truth Tables using the updated test stand controller software. The audit was completed on 2/4/2013.

5. While attempting to initiate a heat up on 2/5/2013 it was observed that the ground fault detector circuit (Bender) was indicating a ground fault on the system at room temperature conditions. A review of debug stack data showed the same readings. The ground fault was ignored and overridden on the debug stack due to the fact that the debug stack was part of the dielectric isolation failure with four stacks electrically in series during Phase I testing (May 2011).

However, with four new stacks, the ground fault Bender device should have been indicating good isolation of the stack assembly. The team at UTC Power initiated a root cause and the following issues were identified and resolved

a. Wiring of the ground fault Bender circuit. The Bender circuit had been wired to monitor just the –ve current collector (CC) of stack C. Electrical group resolved the wiring to monitor ground fault between +ve CC of stack A and –ve CC of stack D.
b. A hard ground wire installed on the –ve bus. This was inside the load cable assembly box. Figure 6-17 shows the location of the box.

Figure 6-17: Load Cable Assembly Box inside SOFC Test Article Room

c. Identified ground in wiring assembly of the Load Bank load set point signal. This is a 0-10 V analog signal from the test stand controller to the Load Bank.

Subsequent to resolving wiring issues in the SOFC test stand, the breadboard heat up was initiated on 2/11/2013. The ground fault measurements were monitored throughout the heat up. UTC Power and Delphi teams reviewed the data and agreed to move forward with on-load operation of the four stacks.

The SOFC Breadboard with four stacks was operated using 50/50 H2/N2 gas and Natural Gas. The maximum load achieved on Natural gas was 6.5 kW before the Breadboard was shut down due to a minor oil leak. The oil leak was fixed after the Breadboard cool down. However, a

restart was not initiated due to ClearEdge Power management decision to discontinue SECA program.

The breadboard system achieved steady, on-load operation with four stacks on 2/19/2013 using 50/50 N2/H2. In the interim, the system experienced shutdowns due to pre-reformer bed inlet and exit thermocouples. This is due to (i) slow heat up of the stack assembly thermal mass, (ii) slow increase of anode exit temperatures, (iii) anode recycle flows and (iv) thermal lag inside the pre-reformer catalyst bed. The Systems and FPS groups reviewed the data and FPS group agreed to increase the shutdown to continue testing.

Subsequently, the SOFC Breadboard was transitioned to Natural Gas operation and achieved 6.5 kW on 2/20/2013. The system was shut down on 2/21/2013 after detecting a oil leak from BLO320 assembly.

Figure 6-18 shows the operation of SOFC Breadboard with Delphi's four stack assembly on 50/50 H2/N2. The plot shows the ramp up of load to 250 A, steady state operation and subsequent step down to 100 A and 0 A for overnight hold in hot standby mode.

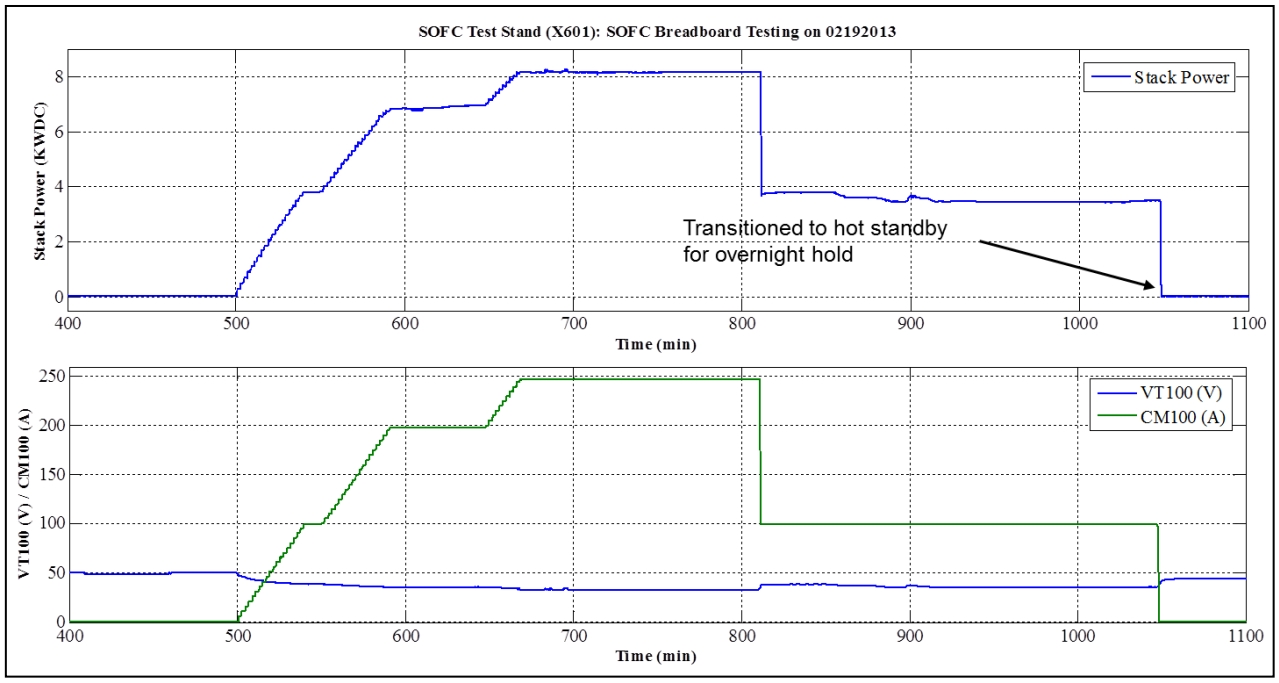

Figure 6-18: SOFC Breadboard with Four Stack Assembly on 50/50 Gas

Figure 6-19 shows the operation of SOFC Breadboard with Delphi's four stack assembly on Natural Gas. The plot shows the steady state operation from 2/20/2013 overnight hold to 2/21/2013. The system was held at 6.5 kW and 200 A of load. The blower oil leak was observed on 2/21. A Total shutdown was initiated based on Mechanical group's recommendation after a preliminary root cause effort. During the root cause effort, steady state data and gas samples

were collected to evaluate the key component performance metrics – reactor conversions, stack utilizations and stack internal reforming.

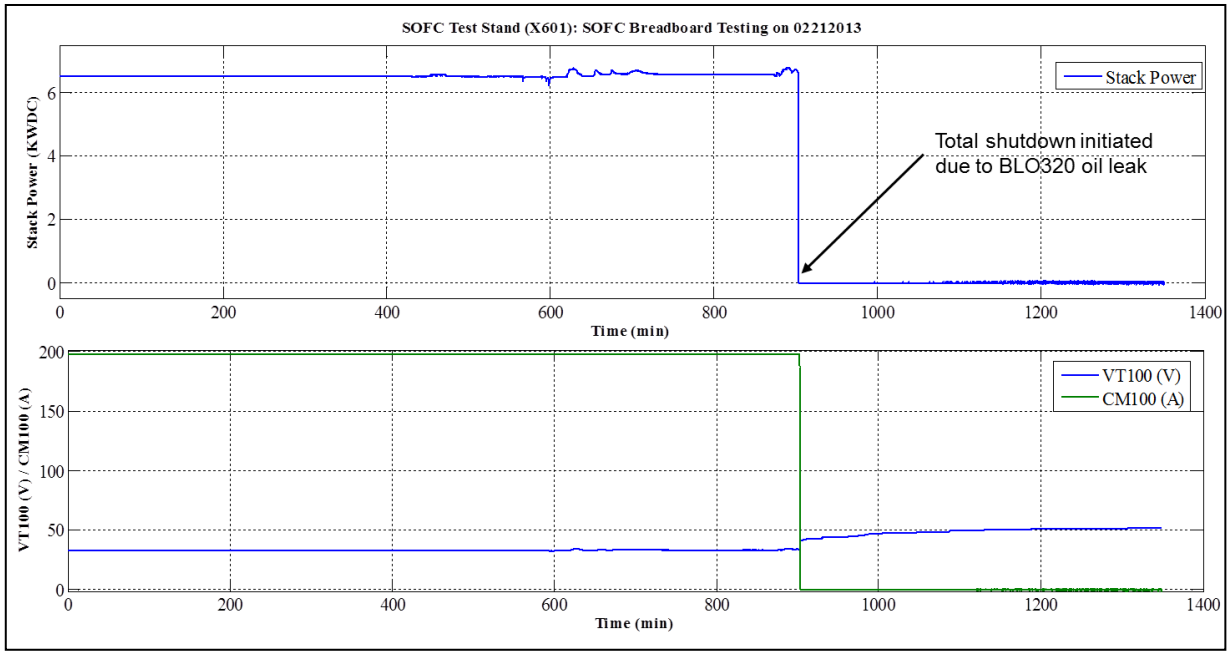

Figure 6-19: SOFC Breadboard with Four Stack Assembly on Natural Gas

As part of SOFC breadboard testing and lessons learned, the following updates were made to the test stand and its components

1. Installed a drip leg and a vent for dew point sensor (DWP320) sample line inside the fluid skid.
2. Replaced multiple dual junction TCs that failed during debug stack operation.
3. Installed emergency air and forming gas bottles as required for breadboard cool down (with 4 stacks) upon emergency shutdowns.
4. Changed orientation of hand valve of the stack differential pressure instrumentation assembly.
5. Changed set point for air pressure regulator (PRV102) from 344 kPag (50 psig) to 150 kPag in order to reduce sensitivity of cathode air flow through flow control valve (FCV100).

Conclusions:

The objective of this part of the program was to design and build a test stand capable of testing a 50 kW SOFC stack module and a 25 kW SOFC Breadboard power plant.

UTC Power successfully design and built a test stand. Initially, the test stand functionality and reliability were verified using a debug stack. Subsequently, a four stack assembly from Delphi was installed and tested. During the initial phase of testing, shorts in stack thermocouples resulted in damaging three out of the four stacks. Testing was continued with two stacks initially and subsequently with one stack. A total of about 1200 hours of endurance was achieved using the one-stack and two-stack module. During the continuous endurance hold using one stack (~ 1000 hrs), no appreciable decay was observed in the stack voltage. A plot with this endurance data is shown in Figure 2-55 above.

During Phase I verification testing starting from Q3 2011 to Q1 2012, the test stand accumulated a total of about 1881 hrs of operation. During this time, several improvements were done in the test stand controller software to optimize the operation of the test article including heat up and cool down. Upgrades were also done to some of the test stand hardware that was identified as low reliability components.

During the total run time the test stand incurred a total of eleven shutdowns. Majority of the shutdown (6 out of 11) were due to failure of the anode heater (HTR380). A detailed analysis and root cause was already presented under Q3 2011 description above.

During Q2 and Q3 2012 the Phase I test stand was upgraded to support 25 kW SOFC Breadboard power plant operation on natural gas. UTC Power team successfully designed and integrated the Breadboard and SOFC stack module inside the test stand in Q3 2012. The Breadboard power plant was extensively tested using a debug stack before a four-stack module was integrated. The SOFC Breadboard power plant was successfully tested using 50/50 H2/N2 at 8.2 kW and using Natural Gas at 6.5 kW. Further testing to achieve design operation (25 kW) and endurance testing (1500 hrs by end of Phase II) were discontinued due to sale of UTC Power to ClearEdge Power and ClearEdge Power management’s decision to discontinue SECA program.

The SOFC Breadboard power plant achieved a run time of 165 hrs with debug stack and about 27 hrs with four stacks on Natural Gas. The test stand accumulated about 950 hours of test time between Q3 2012 and Q1 2013.

In conclusion, even with a limited run time, the team was confident of achieving design conditions (25 kW) and thermal self-sufficiency on the SOFC Breadboard power plant. In addition, the SOFC Breadboard system design of the DUO P concept has promising features and potential for scale-up to meet product-level requirements of stationary fuel cell power plants.

Table 6.3 summarizes the status of the Phase I and II deliverables pertaining to the objectives defined at the front end of the section "Verification Testing".

Table 6-3: Phase I and II Deliverables Status

Phase / Subtask #	Verification Testing Deliverables	Status (% Complete)	Comments
Phase I / 6.1	Design and build test stand capable of testing 50 kW SOFC stack module	100	
Phase I / 6.2	Define test plan for stack module testing	100	
Phase I / 6.3	Test Delphi stacks and achieve 1500 hrs of endurance testing	100	Achieved a total of 1200 hrs before discontinuing for test stand upgrades
Phase II / 3.1	Upgrade test stand to support SOFC Breadboard testing	100	
Phase II / 3.2	Define test plan for SOFC Breadboard verification testing	100	
Phase II / 3.3	Test SOFC Breadboard to achieve 1500 hrs of operation by end of Phase II	20	SECA program discontinued by ClearEdge Power

The purpose of the subsequent description below is to document the remainder items of the SOFC Breadboard verification test plan (Phase II, Subtask 3.3 in Table 6.3) and action items that need to be addressed before re-initiating the Breadboard startup.

Test Stand Hardware Updates

1. Inspect and fix CHV300: While performing oxidation of HDS bed catalyst it was identified that check valve CHV300 in test stand fluid skid is partially stuck closed. The check valve shall be replaced before restarting breadboard testing.

Test Article Hardware Updates

1. Integrate Delphi stack assembly and re-insulate the Breadboard
2. Install a PT cart to house all the pressure and pressure differential transmitters that are to be connected to the Breadboard

Test Stand Controller Software Updates

1. Table 6-4 lists the major test stand controller software updates that are required before restarting breadboard testing.

Table 6-4: Controller Software Change Summary (Future Items)

SOFC Breadboard Controller Software Action Items		
Item	**Change Description**	**Rationale**
1	Changes to H2 flow (MFC601 and MFC610) and Natural Gas flow (MFC012) control	To ensure interaction between fuel flow (anode side) and cathode inlet temperature (TE101FT) along with catalytic burner over temperature protection
2	Changes to cathode startup heater (HTR100) control	To ensure HTR100 does not ramp down till catalytic burner is fully active
3	Changes to cathode startup heater (HTR100) air flow control (FCV130)	To ensure stack cross pressure control during shutdown when air flow is through HTR100 and not catalytic burner
4	Change stack cross pressure shutdown limit	Delphi communication on 2/19/2013
5	Change control tunables as identified	Achieve optimal startup and heat up

Remainder Testing Milestones

After the test stand and breadboard installation are complete, the following are the remainder verification test milestones as part of the DOE SECA contract DE-NT0003894.

1. Restart and achieve peak power (25 kW) on Natural Gas
    a. Demonstrate breadboard thermal self sufficiency
    b. Evaluate key performance metrics of Breadboard components
2. Ramp down to 15 kW for endurance hold
    a. Evaluate Breadboard thermal self sufficiency
    b. Evaluate key performance metrics of Breadboard components
3. Achieve 3000 hours of endurance hold
    a. Evaluate and monitor stack voltage decay and key performance metrics of Breadboard components

7. System Concepts, Stack and Breadboard Integration – UTC Power

Objectives:

Phase I

The objective of this task in Phase I was to develop the concept design for a 250-1000 kW power module and the notional concept design of a 5MW POC based on integrating power modules into a stand-alone power system.

Design of a 250-1000 kW Ambient Pressure Power Module (Task 7.1)
The objective of this subtask was to perform studies of several SOFC power module concepts. The power module was to be capable of delivering regulated power and use syngas as the input fuel. The design defined the internal and external characteristics of the module, the operating conditions for each component during startup, steady state operation, transient operation, shutdown, and restart. Cost estimates for the module in large scale production were to be prepared in support of the Baseline IGFC System Concept Development and the System Cost Analysis tasks. Failure mode and effects analyses were developed to guide the design.

Design of 5 MW Ambient Pressure POC (Task 7.2)
The objective of this subtask was to perform notional concept studies of several 5 MW POC configurations. The 5 MW POC configurations were to be representative of the Baseline IGFC system power block configuration and be capable of delivering regulated AC power using ”clean” coal syngas as the input fuel. Several alternate configurations were studied.

Baseline IGFC System Concept Development (Task 7.3)
In consultation with DOE, UTC established a system model for a >100MW IGFC system capable of ≥50% efficiency from coal (HHV coal to AC power). This model served as the basis for the power block cost estimate.

System Cost Analysis (Task 7.4)
The objective of this subtask was to develop a system factory cost model in accordance with the guidance provided in the SECA Minimum Requirements. A report was developed and audited in accordance with the SECA Minimum Requirements.

Phase II

Breadboard System and Stack Integration
The objective of this task is to perform the engineering design and build a 15-25 kW thermally self-sustaining system based on integrating stacks and balance of plant components into a breadboard. The existing stack module was to be utilized in the breadboard.

Design of a 15-25kW Breadboard (Task 4.1)

The objective of this subtask was to develop a breadboard configuration based on existing system models. The breadboard would operate on reformed natural gas, used as a surrogate for coal gas, and be thermally self-sustaining. The design would define the internal and external characteristics of the breadboard, the operating conditions for each component during startup, steady state operation and shutdown.

Component Selection (Task 4.2)
The objective of this subtask was to select and verify suitability of components for breadboard integration. This task included all components except the Fuel Processor. Component requirements were derived from the design task. Suitability was determined by analysis or testing as appropriate.

Reformer Development (Task 4.3)
The objective of this subtask was to design a fuel processing system in accordance with the requirement from the design task. The system was to be capable of taking natural gas as input and provide fuel at conditions suitable for SOFC stack testing.

System Integration (Task 4.4)
The objective of this subtask was to fabricate and assemble the individual components and modules developed into a breadboard. This included integration of controls and data monitoring systems. A final system check including safety review was performed before the start of testing.

Experimental methods:

Design of a 250-1000 kW Ambient Pressure Power Module

1 January 2009 – 31 March 2009

The steady-state model library upgrade was completed and documented. Using this library, steady-state system models for the Natural Gas (NG) and Coal Gas (CG) based power modules were assembled. The previous 400kW NG system design was scaled up/down to three additional power levels (250, 700 and 1000kW) and simulation results were generated to define operating conditions for component mechanical design. For the CG system, simulations were performed to study the impact of the one-pass fuel utilization. A preliminary dynamic model of the NG power module was developed in support for future transient analysis and control design.

1 April 2009 – 30 June 2009

New cell performance on a methane-free CG composition was estimated from test data provided by Delphi and was used to update the cell performance model. In the system design, the cell voltage is increased from 730 to 800 mV based on a recommendation by Delphi to mitigate chromia poisoning and thus cell degradation. Trade-studies were performed to increase the cell power density by varying the system operating parameters. Simulations show that the power

density can be increased to about 400 mW/cm^2 with acceptable cost of system efficiency when the per-pass fuel utilization is reduced to 60 percent or the steam-to-carbon ratio at the CSR inlet is reduced. Two new process flow diagram configurations are being considered to lower the recycle blower temperature and improve HDS operation by adding two heat exchangers. Simulation results show that the blower's inlet temperature can be reduced by approximately 150°C and the steam concentration in the HDS can be lowered resulting in improved sulfur removal.

1 July 2009 – 30 September 2009

Several process design options for desulfurization of the natural gas fuel were evaluated. The water content of the ZnO adsorber was also increased for the baseline design due to the higher recommended H_2 concentration for the HDS reactor. Because this reduces the ZnO bed's ability to retain sulfur, two design options were investigated to limit the steam content.

1 October 2009 – 31 December 2009

For the power module operating on natural gas, system concepts with CSR recycle were studied and a new S/C definition without counting CO in the calculation was considered. For the power module operating on coal gas, studies focused on analyzing influence of operating parameters and the fuel's methane content on the anode steam concentration and cathode flowrate. Lower methane content in the coal gas results in less steam in the anode and higher cathode flowrate due to the reduced internal reforming cooling effect. Decreasing the per-pass fuel utilization also helps to lower the steam concentration on the anode. The cathode flowrate is reduced because of more internal reforming activities and higher anode flowrate. Design results for the hydrodesulfurizer, the catalytic steam reformer, as well as the air and recycle blowers are reviewed.

1 January 2010 – 31 March 2010

For the Power Module operating on natural gas, the performance of seven system concepts were compared on a common basis. The Mono I design offers the best combination of recycle blower inlet temperature, desulfurization performance, and heat exchanger area. To investigate the part-load performance and operation control, an off-design model has been developed for the Mono II system.

The cell V-I performance model is being updated based on experimental performance data provided by Delphi in March 2010. We found that the previous model over-predicts the cell voltage for given current density at the same conditions. Preliminary corrections were applied to ensure the V-I model matches the available data. Simulations show that this updated performance model results in a 12 percent increase in the number of cells in the Mono II design to maintain a fixed 400 kW net AC power output.

1 April 2010 – 30 June 2010

Several updates to the system models were performed. A physics-based 1-D ejector model was developed to support the Power Module and IGFC simulations. To support off-design studies of the Power Module, the stack model was modified by assuming identical anode and cathode outlet temperatures, replacing the use of a heat transfer coefficient between the anode bulk flow and solid walls. The cell V-I model was revised and calibrated to match experimental performance data provided by Delphi. To support sizing and off-design predictions of the HDS reactor a kinetic model of the HDS reaction was developed based on experimental data.

For the Power Module, turn-down strategies for the Mono I & II systems were developed. Process designs were revised with additional actuators as needed to operate at all power levels from rated to net zero output while satisfying all operating constraints provided by Delphi. A new system concept - Mono L - was developed that has a lower anode recycle blower inlet temperature than the Mono I design. Its key distinguishing feature is a liquid heat exchanger that facilitates safe external cooling of the recycle blower inlet stream. Using the ejector model, a trade study on cathode recycle was performed. Cathode recycle is of interest because it reduces the cost of the cathode heat exchanger. If reliable hot recycle blowers were available there may be a benefit to cathode recycle depending on the cost of the blower versus the cost of the heat exchanger. The use of an ejector is not recommended because the increased operating power of the blower negates the costs benefit of a smaller cathode heat exchanger.

1 July 2010 – 30 September 2010

To support sizing and off-design predictions of the hydrodesulfurization reactor, a kinetic model of the HDS reaction was developed. The hydrodesulfurization model was incorporated into a standalone model that can be integrated with the existing Power Module system models. This was the prerequisite for modeling the heat-up control strategy from ambient to hot standby which is in progress.

1 Oct 2010 – 31 December 2010

Nothing reported.

1 January 2011 – 31 March 2011

The turn-down strategy of the Mono L system concept was revised to reduce the cathode heat exchanger peak temperature; also, peak parasitic heater power was reduced from 35 kW down to 9 kW. These changes resulted in a less expensive and more efficient system. The Mono I control strategy was completed with full heat-up from ambient capability. Quasi steady-state simulations are used to analyze and design the system start-up process. External forming gas storage and cathode heat exchanger bypass were added, respectively, for anode protection and stack temperature ramp rate control during heat-up.

1 April 2011 – 30 June 2011

UTC/UTRC developed three Power Module concepts after detailed investigation of several competing designs. All three systems were designed for 400 kW net AC and achieve efficiency in excess of 60% based on fuel Lower Heating Value (LHV). Heat-up and power ramp studies were performed on all systems to define internal and external characteristics. **Figure 5.7-1** shows a Coal gas Power Module concept.

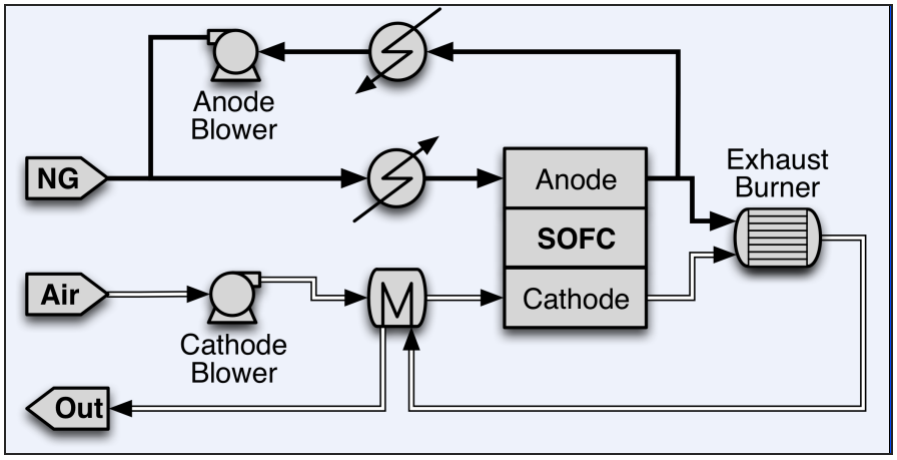

Figure 5.7-1 Coal gas Power Module concept

Design of 5 MW Ambient Pressure POC

1 July 2010 – 30 September 2010

Design of the 5 MW Ambient Pressure Proof-of-Concept system was completed. A total of four systems were designed, each achieving an efficiency of >58% based on HHV of coal gas and net AC power between 5.1 and 5.4 MW. All systems have a bottoming cycle. Two systems use a conventional steam cycle; two systems use an Organic Rankine Cycle. The systems are designed to use either an oxy-burner for carbon separation, or a conventional exhaust gas burner combining anode and cathode exhaust.

1 Oct 2010 – 31 December 2010

Nothing reported.

1 January 2011 – 31 March 2011

Based on the natural gas fueled 400 kW Power Module concepts, a Coal-Gas Power Module system concept was developed. The design achieves an efficiency of 60% based on the coal-gas

LHV. Because coal gas is cleaned-up and conditioned by upstream processes in the gasification and acid gas removal islands, the system has a simplified fuel processing train requiring neither desulfurization nor pre-reforming. Coal-gas feed is assumed available at ambient temperature and pressure and the same composition as used in the IGFC power block.

Operating conditions are identical to the IGFC power block (cell voltage, per-pass utilization, and steam-to-carbon ratio). Two heat exchangers are used to lower the recycle blower's operating temperature and to preheat the coal gas to the desired anode inlet temperature. A full heat-up and power ramp strategy from ambient to nominal load conditions was developed. Additional hardware, including start-up fuel, forming gas for anode protection, external steam generator, cathode HX bypass, and in-line electric recycle heater were added to assist system start-up and shut-down.

Baseline IGFC System Concept Development

1 January 2009 – 31 March 2009

System design activities were initiated by analyzing performance of the pressurized IGFC design from the proposal for operation on methane-rich coal gas from a catalytic gasifier. The results indicate that the high-methane content significantly reduces the stack cooling requirement because of the endothermic nature of the reforming reaction. To prevent O_2 starvation on the cathode caused by a reduction in cathode flowrate, a combination of cathode pre-heat and cathode recycle is currently being investigated as an option. This modified system meets the SOPO requirements, i.e., it produces > 100 MW net AC at > 50% HHV, and captures more than 90 percent of the carbon input to the system.

The system studies performed to date were generated based on a library of gPROMS models. gPROMS is an equation-oriented modeling system used for building, validating and executing first-principles models. To better support the ongoing system design studies, the model library was updated and refined to be compatible with recent software updates made to the gPROMS modeling language. This work involved revising five key models of the power module simulation:

- SOFC stack
- Catalytic steam reformer
- Catalytic burner
- Fresh air and anode recycle blowers
- Heat exchangers

SECA Coal-Based Systems – UTC Power

1 April 2009 – 30 June 2009

System design activities were focused on designing IGFC systems with the SOFC power block operating at ambient pressure. Preliminary analysis of two atmospheric system configurations has been completed. The first system provides cathode air by means of a fresh air blower and has a steam bottoming cycle. This system produces >100 MW net AC at approximately 49 percent HHV, and captures more than 90 percent of the carbon input to the system. The second atmospheric system is based on a Pratt & Whitney FT8 Twin PAC power system. This modified system meets the SOPO requirements, i.e., it produces >100 MW net AC at greater than 54 percent HHV, and captures more than 90 percent of the carbon input to the system. Models for the FT8 system have been updated to reflect operating points for optimum operation of the gas turbine. The steam cycle model of the bottoming cycle was improved by modeling two different configurations: Both a simple turbine cycle and a 3-stage turbine cycle with reheat were analyzed.

1 July 2009 – 30 September 2009

System design activities were focused on developing component models for the gasification island (air separation unit, gasifier, Selexol & Claus processes) and on upgrading and simulating the power block models. A gasifier model has been developed and extensively tested using DOE/NETL performance data for conventional and catalytic gasifiers. The predictions of the UTC model are in good agreement with published data for gasifier performance. Models for ASU and coal gas clean-up processes have been developed to estimate the parasitic loss in these components and describe a simplified high-level sulfur removal and recovery process. The models are derived primarily based on the information and data reported by DOE [1]. Comparisons show good agreement between the model prediction and DOE's results. A revised water removal model was developed that greatly reduces the parasitic cost of drying the CO_2 product.

System analyses of two atmospheric and one pressurized system have been completed. All three systems produce > 100 MW net AC power at >50% electrical efficiency (based on coal HHV) and capture more than 90 percent of the carbon input to the system. The simpler of the two atmospheric systems uses an air blower to feed fresh air and a steam bottoming cycle. This system produces 130.8 MW net AC at 50.7% HHV efficiency. The second atmospheric system uses a Pratt & Whitney FT8 gas turbine instead of an air blower—this system produces 143.5 MW net AC at 55.7% HHV efficiency. Using the same FT8 gas turbine, a pressurized system can be designed that achieves approximately twice the power density of the atmospheric system at a slightly higher efficiency of 56.2% HHV.

1 October 2009 – 31 December 2009

IGFC design activities were focused on integrating the previously developed gasifier, ASU, acid gas clean-up, and Power Block models into an integrated simulation model. Three such models

were developed for the two atmospheric and the pressurized power block designs. The integrated models were validated against the original component models and yield the same results.

1 January 2010 – 31 March 2010

IGFC system design activities were focused on heat integration for the three power systems. The syngas expander was integrated and heat integration was optimized. The final design achieves an approximately five percentage point gain over the non-heat integrated models previously reported on. All three systems produce greater than 120 MW net AC power at an efficiency greater than 50 percent HHV. The IGFC system with steam turbine and air blower achieves approximately 51 percent HHV efficiency, while the gas turbine systems achieve greater than 57 percent HHV efficiency.

1 April 2010 – 30 June 2010

Design of the IGFC systems was completed. An alternative atmospheric design was developed that reduces the theoretical oxyburner flame temperature to below 1000°C, while maintaining the same system performance. Results from the ejector model were integrated into the IGFC models resulting in an approximately one percentage point efficiency gain. Finally, a sensitivity analysis was carried out demonstrating that all three IGFC designs maintain their key performance requirements over a comfortably wide range of key operating parameters.

1 Oct 2010 – 31 December 2010

Nothing reported.

1 April 2011 – 30 June 2011

UTC/UTRC developed three IGFC design concepts, two atmospheric and a pressurized system. All three concepts were designed to achieve greater than 100 MW net AC power at efficiency greater than 50% Higher Heating Value (HHV) and capture greater than 90% carbon. UTC also developed a library of models for gasifier, SOFC, gas turbine, steam turbine, oxygen combustor, ASU and coal gas clean-up. Sensitivity analyses were carried out demonstrating that the designs maintained their key performance requirements over a wide range of key operating variables.

Figure 7-1 shows an atmospheric power block design that integrates an SOFC with an air blower, a steam bottoming cycle, and a refrigeration plant. The SOFC system operates at 1.1 bar.

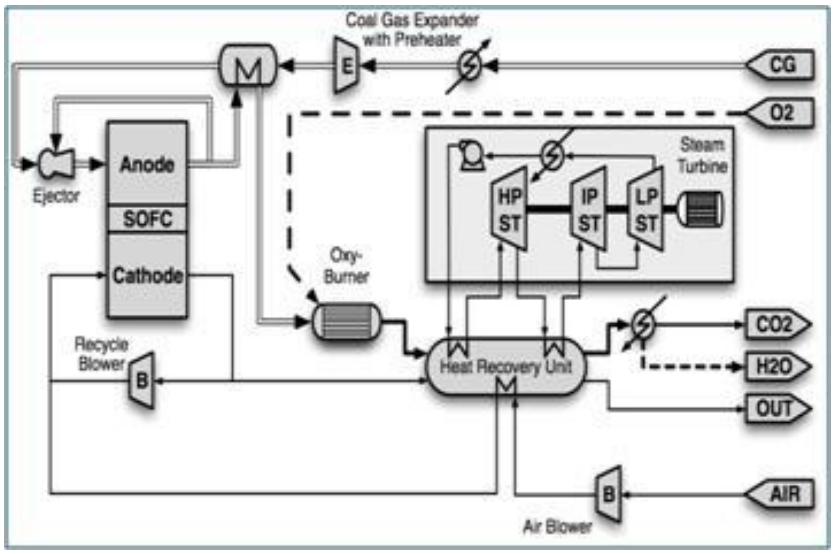

Figure 7-1 Atmospheric SOFC Power Block concept with air blower

The efficiency of the simple atmospheric design with the blower is improved by adding a gas turbine as shown in **Figure 7-2**. This system is based on a Pratt & Whitney FT8 power system. The rest of the system is the same as the atmospheric design with the blower.

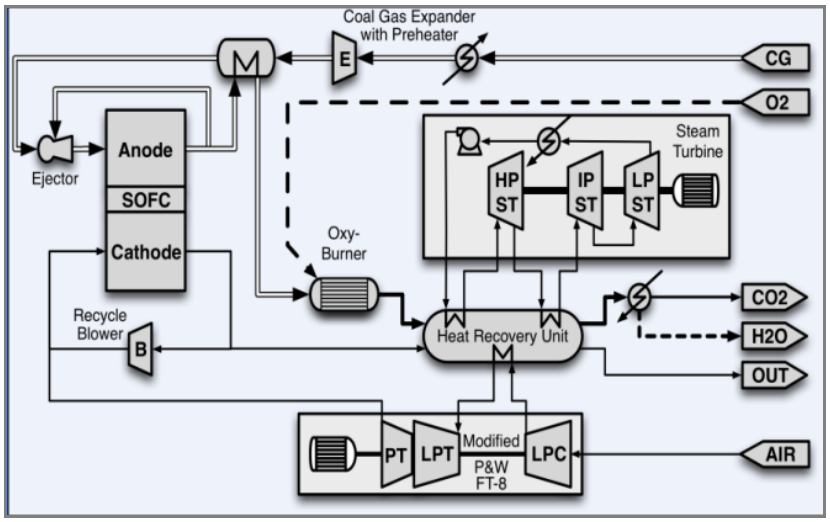

Figure 7-2 Atmospheric SOFC Power Block concept with gas turbine

System Concepts and Stack Design Integration

Several design case studies based on the natural gas 400 kW design were performed for a coal gas feed. The coal gas based system design is simpler than the natural gas based system design because the coal gas entering the power module will have been cleaned-up and conditioned by upstream processes, allowing the HDS and steam reformer to be eliminated. Among the

interesting results obtained was the observation that coal gas based systems have a lower air flowrate than their equivalent natural gas based systems. Because of the reduced methane content in the anode when operating on coal gas, and the therefore reduced amount of internal reforming, a higher cathode airflow could be expected for thermal management. This is not required however, because the anode mass flow is much larger when operating on coal gas thus compensating for the reduction in cooling through the endothermic reforming reaction.

System Cost Analysis

Cost analysis of the power block hardware for the IGFC power plant was completed and shows a cost of $685/kW in 2007 dollars with a 90% confidence interval, which meets the SECA cost requirement of $700/kW.

Design of a 15-25kW Breadboard

1 July 2011 – 30 Sep 2011

In Phase II, UTC Power will fabricate a 25 kW class breadboard power plant with all MBOP components required to demonstrate thermal self-sufficiency with focus on three key components with high technical risk; the high temperature heat exchangers, the catalytic burner and the high temperature anode recycle blower. Cost reduction of the MBOP components is very important to be considered in the conceptual design for future commercialization of SOFC power plans. UTC Power will focus design and analysis activities on the cost effective MBOP components.

System Design

Figure 7-3 shows the tasks that have been completed under the Detailed Design and Test phase. Early in this reporting period, the breadboard checkouts including debug stack Natural Gas testing and lights-out operation were completed. The breadboard verification test was only partly completed (~ 25%) before ClearEdge management made the decision to discontinue the DOE SECA program at ClearEdge. Hence the Breadboard Verification Test and Endurance Hold are incomplete.

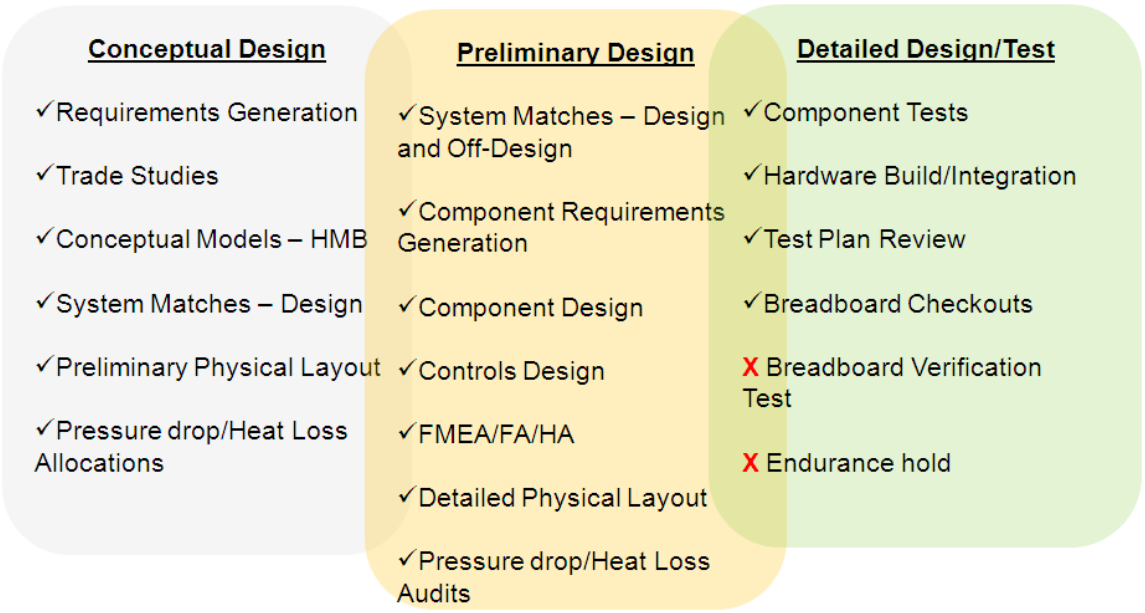

Figure 7-3: UTC Product Development Process Overview

Design of a 15-25kW Breadboard

An assessment of the heat loss from the Breadboard power plant was done using the steady state operation at 6.5 kW on Natural Gas. Figure 7-4 shows the layout of the Breadboard and the stack assembly hot box and Table 7-1 shows the appropriate dimensions and the surface area calculations.

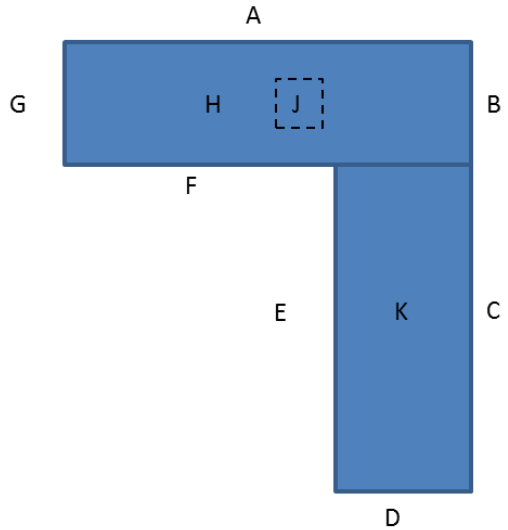

Figure 7-4: SOFC Breadboard and CSA Hot Box Layout

Table 7-1: Hot Box Dimensions and Surface Area

		Width		Depth		Height		Area	
		in	mm	in	mm	in	mm	sq in	sq mm
A	Rear MBOP	101	2565			45	1143	4545	2932252
B	Right MBOP			27	686	45	1143	1215	783869
C	Right CSA			91	2311	26	660	2366	1526449
D	Front CSA	31	787			26	660	806	519999
E	Left CSA			91	2311	26	660	2366	1526449
F	Front MBOP	67	1702			45	1143	3015	1945157
G	Left MBOP			27	686	45	1143	1215	783869
H	Top MBOP	101	2565	27	686			2727	1759351
J	Bottom MBOP	101	2565	27	686			2727	1759351
K	Top CSA	31	787	91	2311			2821	1819996
							Totals:	**23803**	**15356743**

Table 7-2 shows the heat loss results for Breadboard hotbox and CSA hot box separately. Estimates for the same from Detailed design are 1.4 and 2.2 kW, respectively. Total heat loss from the system (3.78 kW) is less than the allocation of 4 kW from Concept design.

Table 7-2: Hot Box Dimensions and Surface Area

MBOP			
Convective Losses		Radiation Losses	
SA (m2)	9.96	eps	0.075
hc (W/m2.K)	10	sig	5.70E-08
Ts	39	Area (m2)	9.96
Tb	23	Ts	39
		Tb	23
Qloss (kW)	1.59	Qloss (kW)	0.09
Total MBOP Heat Loss (kW)		1.68	

CSA Hot Box			
Convective Losses		Radiation Losses	
SA (m2)	5.39	eps	0.075
hc (W/m2.K)	10	sig	5.70E-08
Ts	57.5	Area (m2)	5.39
Tb	23	Ts	57.5
		Tb	23
Qloss (kW)	1.86	Qloss (kW)	0.25
Total MBOP Heat Loss (kW)		2.10	

The heat loss results show that the overall heat loss meets requirements and there is good agreement for stack assembly hot box. Heat loss estimate of 2.2 kW for stack assembly hot box

is from Phase I test data. Heat up data from four stack testing during Phase I was used to estimate this value (2.2 kW). Hence, there is good agreement between the latest result (= 2.1 kW) and the estimated value.

On the other hand, heat loss from MBOP hot box (1.68 kW) is higher than the estimated value of 1.4 kW. The rational for this is as following: heat loss estimate from Detailed design did not take into account the leak paths due to instrumentation and gas sample tubing. Hence, estimate that a Breadboard designed with minimum instrumentation, ≤ 1.4 kW heat loss from MBOP can be achieved.

Some of the major findings and lessons learned from the design of the Breadboard are

1. Breadboard insulation process is laborious and time consuming
    a. Opportunities for improvement: Optimize system design to achieve box-type insulation, similar to CSA hot box. Trade study required to evaluate heat loss and thermal interactions of components for optimal design
2. Structural analysis conclusions for bellows design unverified due to lack of test data
    a. Breadboard designed with one bellow between cathode heat exchangers. Six of seven bellows from concept design were removed subsequent to structural analysis during detailed design phase

Component Selection

1 July 2011 – 30 Sep 2011

In the initial conceptual design, MBOP components have been studied based on 200 kW Mono I system. For the breadboard design, however, the heat exchangers and the catalytic burner will be designed for the 25 kW system based on the conceptual design. The heat exchangers and the catalytic burner will be evaluated through breadboard testing for future large scale power plant design. These components should be relatively easy to scale-up. However, the anode recycle blower will be designed for a larger scale power plant and used with flow bypass on the breadboard due to the difficulty of future scale-up.

Heat Exchangers and Catalytic Burner Development

UTC Power has conducted an initial conceptual design for heat exchangers and the catalytic burner based on Mono I system shown in Figure 7-5. Mono I requires four heat exchangers, Cathode HEX, Anode HEX, CSR HEX, Recycle HEX and one catalytic burner. The SOFC requires reactant gas inlet temperatures of at least 700ºC. For the cathode side, this is accomplished through the use of a catalytic burner in addition to the cathode heat exchanger. The catalytic burner will be located downstream of the cell stack and be used to consume unburned fuel to reduce emissions and to increase the system efficiency. Anode exhaust gases are mixed with cathode exhaust air and burned in the catalytic burner to raise the gas

temperature. The high temperature gas then exchanges with room temperature cathode air in the cathode heat exchanger to provide the required high temperature gas to the SOFC cathode inlet. A bypass line for the catalytic burner using Cathode Splitter will be used to modulate the adiabatic temperature in the catalytic burner. For the anode side, three heat exchangers are used to recover/preheat the anode gas for the stack and the reformer in the recycle loop. Compared to the cathode side, these three heat exchangers will be smaller due to lower flow rates and less risky from the lower operating temperature. The high temperatures experienced by these heat exchangers could exceed the capabilities of conventional heat exchanger materials. The hot gas inlet temperature will exceed 800ºC except for Recycle HEX which operates at lower temperature around 300 – 600ºC. In particular, the hot gas inlet temperature of Cathode HEX will exceed 900 ºC, which, if the current design approach is applied, requires the use of exotic and expensive materials such as Ni base alloys to address high oxidation rate, cracks due to thermal cycling, creep and also chromium evaporation which will degrade the SOFC stack performance. However, the use of exotic materials is undesirable as it increases the cost of power plant components. Moreover, the temperature difference between the hot inlet temperature and the cold inlet temperature becomes more than 850 ºC which could cause a significant thermal stress on the heat exchanger. The expected risks for these components are summarized as shown below.

- High oxidation rate at high temperature and moisture
- High thermal stress for Cathode HEX due to large temperature gradient
- Cr evaporation for Cathode HEX at high temperature
- Catalytic burner performance degradation due to high temperature

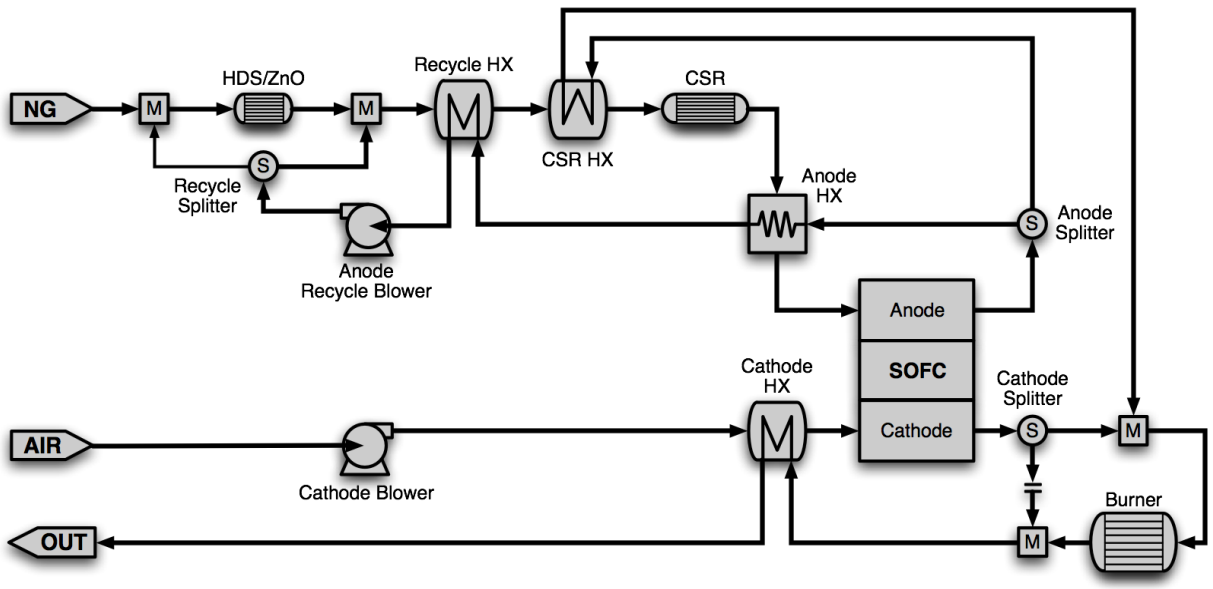

Figure 7-5: Process Flow Diagram for Mono I

UTC plans to use a multi-phase, cross flow plate fin type heat exchanger to reduce the risk associated with high temperature and high thermal gradient. Another option to reduce the impact of the high operating temperature is to use a catalyzed wall heat exchanger. In this configuration, one side of the heat exchanger will be coated with combustion catalyst to burn reactants while the other side is cooled, combining two functions into one unit. In order to minimize the Cr evaporation at high temperature, the cold side channels of components will have an aluminized coating.

1 Apr 2012 – 30 Jun 2012

Mechanical Balance of Plant

In this report, we'll focus on two key components. The first component is the anode recycle blower. As represented in previous reports, UTC Power is developing a recycle blower that can be scaled up to support a 200kW size SOFC system and still be cost competitive. The design and development of the blower assembly, including the oil loop for lubrication and the air loop for cooling, have been completed. Figures 7-6 and 7-7 show a schematic of the blower assembly as well as the actual unit. In addition, a separate test rig (Figure 7-7) consisting of a heater and heat exchanger circuit, together with the associated controls circuitry, was developed to test the performance and endurance capabilities of the blower apriori to its installment in the breadboard. The blower is currently undergoing performance and endurance testing on this test rig.

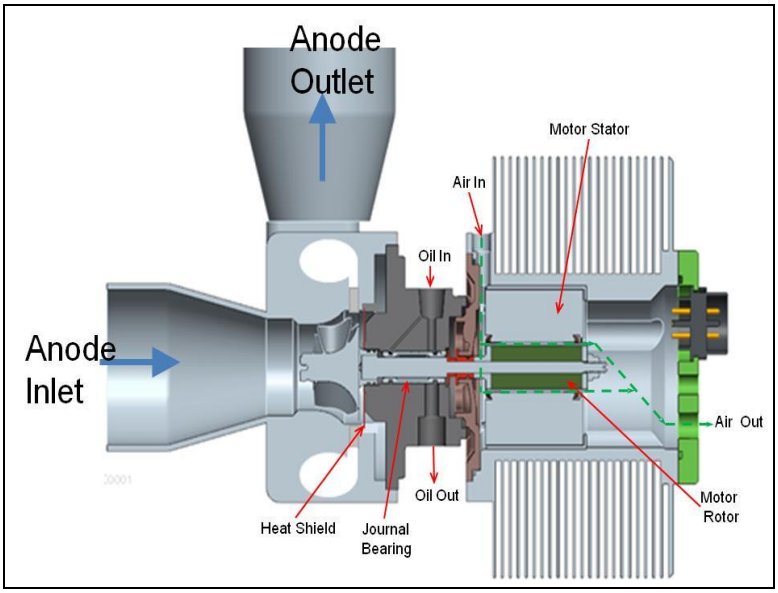

Figure 7-6: Schematic of Recycle Blower Assembly

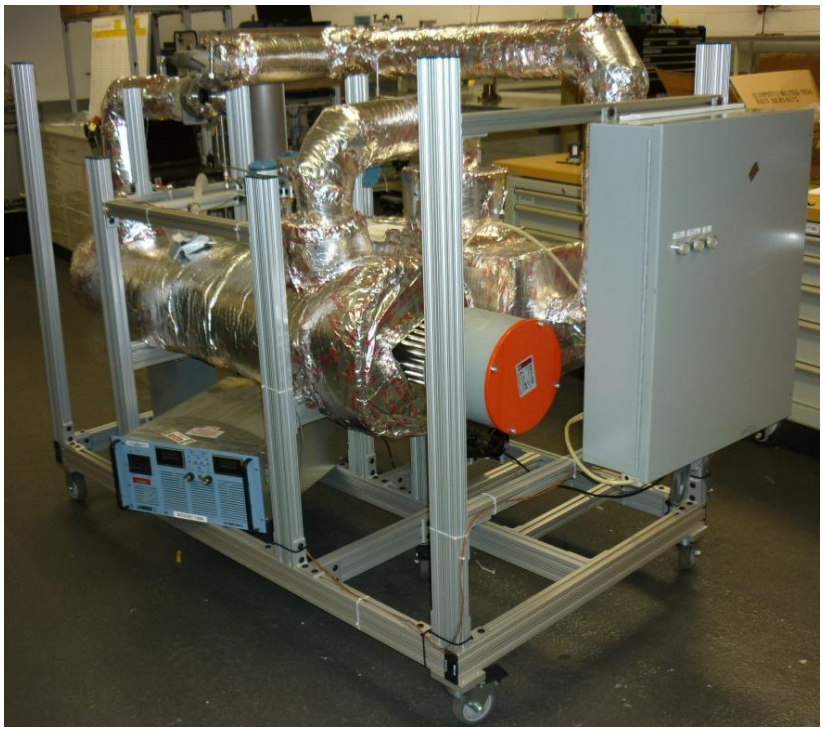

Figure 7-7: Recycle Blower Test Rig

The second component we want to focus on is the anode heater. This is a particularly critical component for the breadboard given the history of anode heater failures experienced in Phase I. Given the lower power requirements for the breadboard, UTC Power opted to design a radiative heater by leveraging some of its experience from the PC50 Phosphoric acid fuel cell program. Figure 7-8 shows a schematic of the heater. The heater has an annular tube design with the heater element installed into the center of an annular vessel. The vessel is Alloy 800 construction (common with piping) with stress calculations done per API 530-2008. The heater element is made out of Silicon Carbide (SiC) which is an off-the-shelf element, mature technology. The vessel is integrated into the piping system to reduce leaks. The design allows for separation of process from element and element change without vessel removal. It works by radiation heat transfer to inner tube surface and by convection to the fluid.

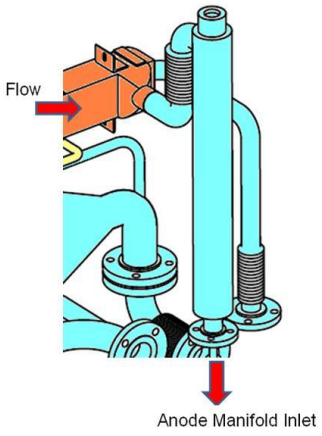

Figure 7-8: Schematic of Anode Inlet Heater

1 July 2012 – 30 September 2012

Fourth quarter MBOP work focused again on the anode recycle blower and the anode inlet heater. The turbo-driven recycle blower endurance test was conducted using a high temperature test rig at 15kW SOFC power plant (PPLT) operating conditions where it will be operating at 95% of the time. The blower successfully completed the 1048 hours of testing without any decay in performance. The motor-driven recycle blower was also tested in the fourth quarter. It encountered start-up issues related to the motor drive and required significant tuning. During drive tuning, a mechanical issue related to the thrust bearing was discovered. Preliminary analysis suggests rotor balance issues that would require rework. Given the acceptable performance of the turbo-driven recycle blower, it was decided to put further motor-driven blower development on-hold.

The anode inlet heater detailed design work was completed in the quarter. The heater was subsequently fabricated and installed in the breadboard. The anode inlet heater is a low power, high temperature heater which sees maximum duty during startup and handles temperature trim, if necessary, during steady state power generation conditions. The heater is of an annular tube design with a heater element installed in the center of the inner tube and all flow passing through the annulus. The design allows for isolation of the heater element from the process. This feature is important as it enables the use of both superior vessel casing materials and mature heater element technology.

In Phase II, UTC Power is fabricating a 25 kW class breadboard power plant with all mechanical balance of plant (MBOP) components required to demonstrate thermal self-sufficiency with a focus on four key components with high technical risk:

- High temperature heat exchangers

- Catalytic burner
- High temperature anode recycle blower
- Anode inlet pre-heater

Cost reduction of the MBOP components is very important for future commercialization of SOFC power plans. UTC Power has focused its design and analysis activities on cost effective MBOP components. The component selection and development has been conducted based on UTC Power's stage gated product development process.

During this quarter, even though the system has not been set up in the final configuration, the preliminary performance evaluations for key components in the anode loop have been conducted using the four stacks system running with natural gas. The detailed evaluation should be conducted in the future with the final configuration in the nominal operating condition.

Heat Exchangers and Catalytic Burner Development

In the last quarterly report, the preliminary performance evaluations were conducted for the catalyzed wall heat exchanger (HEX100A) and the counter flow cathode heat exchanger (HEX100B) during the heat up and the hot standby mode using the debug stack installed in the breadboard. The results showed that these cathode heat exchangers were working as they were expected. In this quarter, the anode heat exchangers have been evaluated using four stacks installed into the breadboard. There are three heat exchangers in the anode loop including the anode heat exchanger (HEX300), the recycle heat exchanger (HEX320) and the HDS heat exchanger (HEX000) shown in the Figure 7-9. All heat exchangers used in the breadboard are the plate fin type made of austenitic stainless steel. The pictures of these heat exchangers installed into the breadboard are shown in Figure 7-10. Table 7-3 shows the heat exchangers specifications at the design point of 25 kW EOL operation. The operating conditions in this table have small discrepancies from the latest gProms match because the heat exchangers design point was defined in the old version of the gProms match. The effect of the discrepancies on the system operation, however, would be negligible since the system can compensate for these discrepancies. There is another heat exchanger in the anode loop, the blower recycle heat exchanger (HEX104), which was not evaluated in this report since this heat exchanger was not fully utilized in the preliminary testing, and not so important as others working in the main loop.

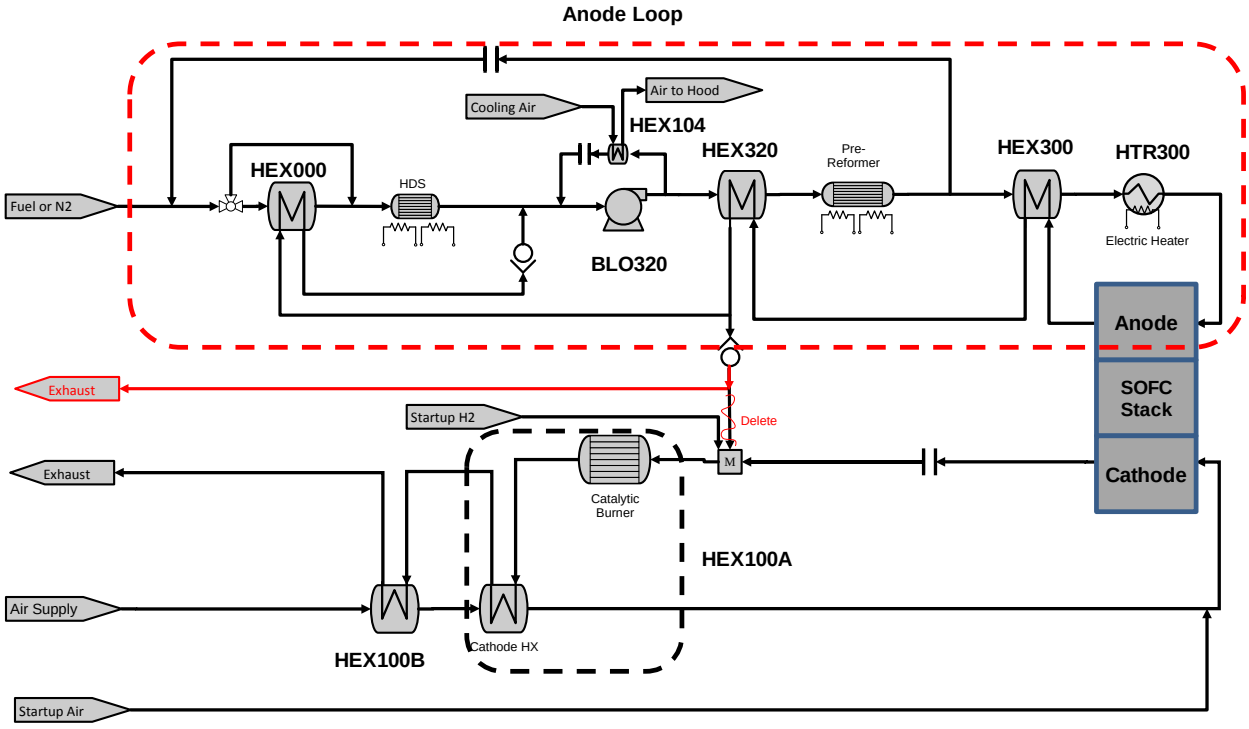

Figure 7-9: SOFC Breadboard Process Flow Diagram

HEX300 Anode Heat Exchanger

HEX320 Recycle Heat Exchanger

HEX000 HDS Heat Exchanger

Figure 7-10: Anode Heat Exchangers in Breadboard

Table 7-3 Anode Heat Exchangers Specifications

Name of HEX		Anode HEX300		Recycle HEX320		HDS HEX000	
HEX Type		Plate Fin		Plate Fin		Plate Fin	
Flow Pattern		Coutner Flow		Coutner Flow		Cross Flow	
		Hot Side	Cold Side	Hot Side	Cold Side	Hot Side	Cold Side
Fluid		Anode Gas	Anode Gas	Anode Gas	Reformate	Anode Gas	Natural Gas
Mass Flow Rate	g/s	10.6	7.9	10.6	8.3	7.1	1.2
Inlet Temperature	C	838	398	568	410	469	131
Outlet Temperature	C	569	718	470	522	419	333
Ooperating Presure	kPa	108.3	110.6	107.3	114	106	105.9
Pressure Drop	kPa	0.9	0.8	0.9	1	0.3	0.06
Heat Duty	kW	5.0		1.74		0.6	
Net Thermal Rating	kW/C	0.035		0.033		0.003	
Heat Transfer Area	m^2	0.9	0.8	0.72	0.79	0.11	0.1
Number of Fin Layer		9	8	7	6	5	4
Design Pressure	kPa	10.8	16.2	10.8	16.2	10.8	7.4
Design Temperature	C	887	791	680	652	498	423
Fouling Factors	m^2K/W	0.0035	0.0035	0.0035	0.0035	0.0035	0.0035
Ramp Rate	C/min	< 5		< 5		< 5	
Core Size	mm	100 W x 125 H x 300L		100 W x 97 H x 300L		75 W x 74 H x 75L	
Weight	kg	28		21		9	
Material		NAR-AH-7 (Fin Core), SS310		SS310		SS310	

The anode heat exchangers evaluation was conducted under a steady state operation using natural gas. The heat duties and the pressure drops are the factors to be focused on at this phase. Figure 7-11 shows the temperature distributions in the HEX300 as a function of time. The test conditions such as flow rates, pressure drops, etc. are also shown in this figure. The stack output power was 6.5 kW with 200A current. As shown in this figure, the system achieved a full steady state operation. Figures 7-12 and 7-13 also show the temperature distributions for the HEX320 and HEX000. These temperatures and the flow rates were used to evaluate the performance of heat exchangers. It should be noted that the flow rates are the calculated results based on the gas compositions and the natural gas flow rate due to no direct measurement. Compared to the design point, the flow rates are smaller due to the lower output power. The hot inlet temperature of HEX300 was 770 C which was much lower compared to the design point (838 C).

For the heat exchanger performance evaluation in the anode loop where the gas compositions vary with the locations, it is important to estimate the fluid properties accurately for both sides of heat exchangers since they affect the heat exchanger performance. In this analysis, the gas compositions as well as the flow rates were estimated based on the GC analysis data and the natural gas compositions data provided by the gas supplier. The GC data were taken at three different locations, the reformer inlet, the reformer outlet (anode inlet) and the anode outlet shown in P. XX to P. XX. Table 7-4 shows the estimated gas compositions used in the heat exchangers analysis.

The heat exchangers were evaluated using simple heat exchanger models based on Log-Mean-Temperature Difference (LMTD) method. All dimensional data as well as j-f factors of fins used in the models were provided by the heat exchanger supplier. The models were tuned by the heat exchanger specification data without considering heat losses.

Table 7-4: Estimated Gas Compositions

	HEX300, HEX320 HEX000 Hot Side	HEX320 Cold Side	HEX300 Cold Side	HEX000 Cold Side
Gas Analysis Port	Anode Exit (Wet)	Reformer Inlet (Wet)	Reformer Exit (Wet)	Estimation No GC Analysis
CO2	0.305	0.330	0.331	0.190
CH4 methane	0.001	0.040	0.010	0.420
C2H4 ethylene	0.000	0.000	0.000	0.000
C2H6 ethane	0.000	0.000	0.000	0.013
C3H8 propane	0.000	0.000	0.000	0.001
Ar	0.000	0.000	0.000	0.000
O2	0.000	0.000	0.000	0.000
N2	0.028	0.030	0.032	0.020
CO	0.048	0.044	0.040	0.023
H2	0.107	0.109	0.229	0.130
H2O	0.510	0.447	0.358	0.204
Total	1.000	1.000	1.000	1.000
Molecular Weight	25.004	25.524	23.657	20.214

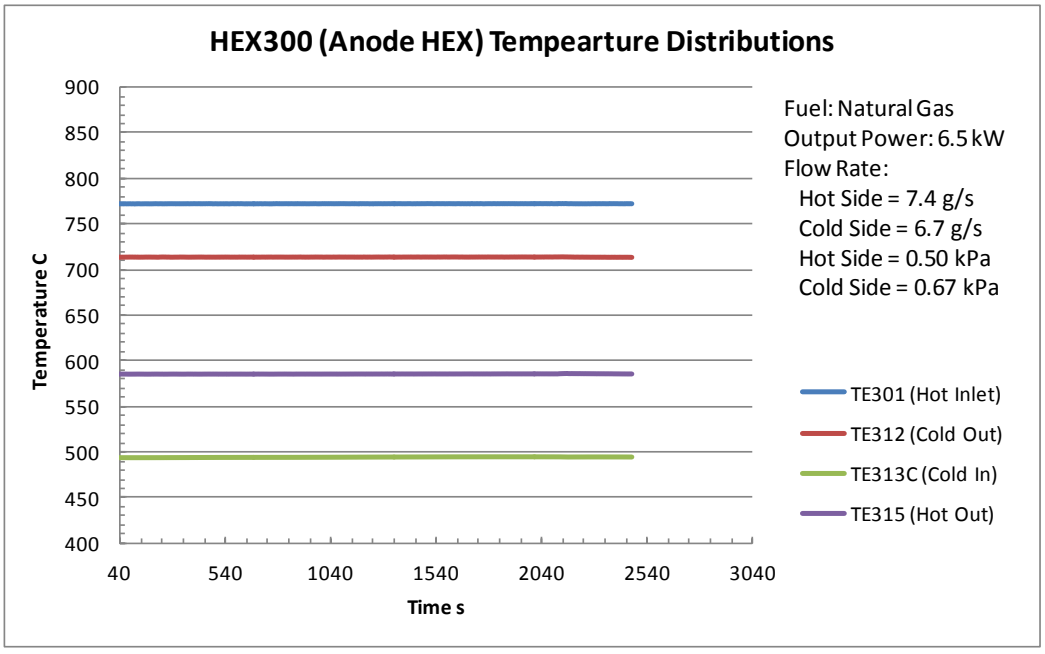

Figure 7-11: Temperature Distributions for HEX300 (Anode Heat Exchanger)

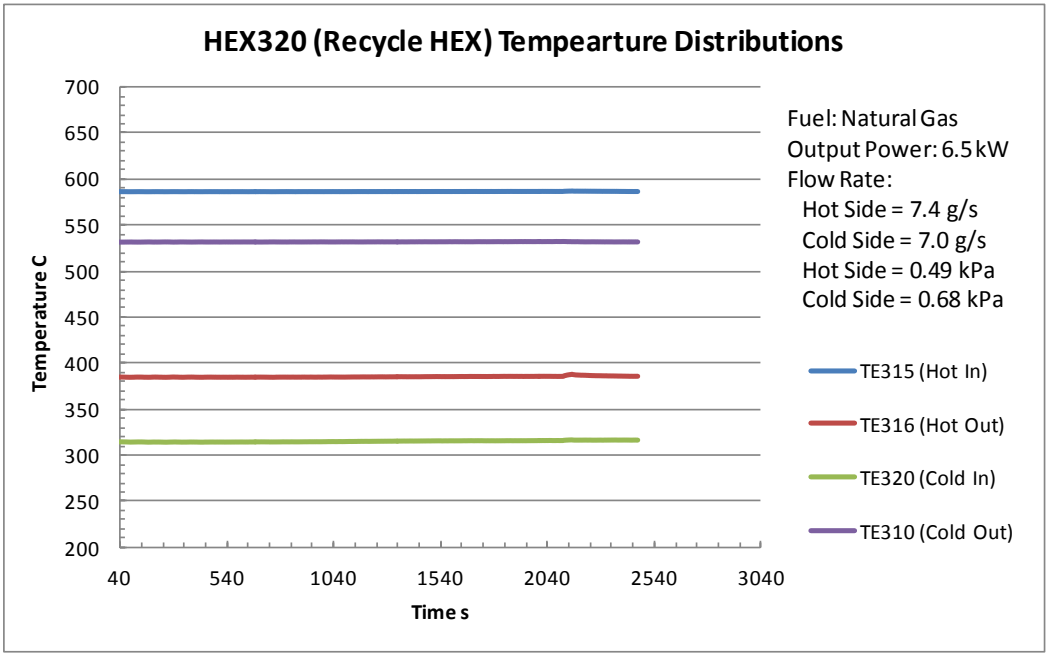

Figure 7-12: Temperature Distributions for HX320 (Recycle Heat Exchanger)

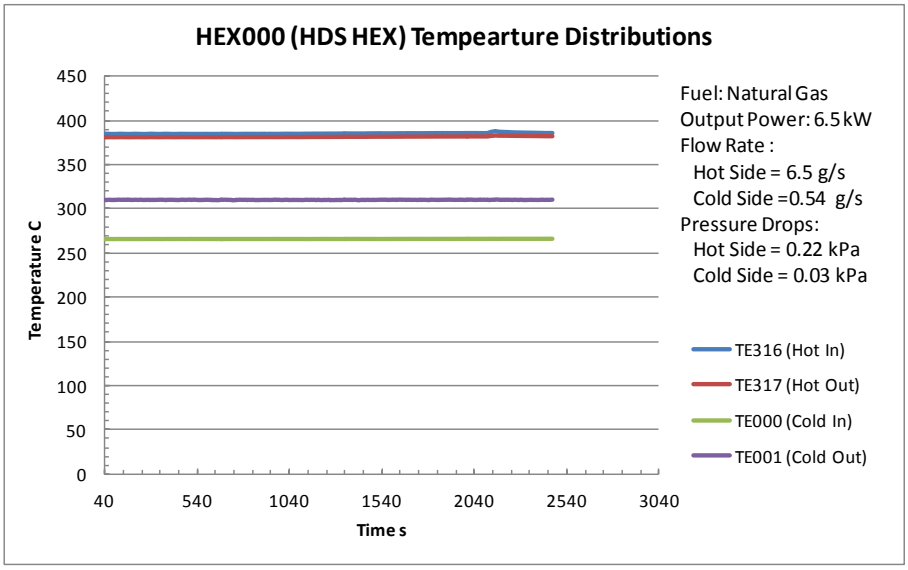

Figure 7-13 Temperature Distributions for HEX000 (HDS Heat Exchanger)

Table 7-5 to Table 7-7 show the results of heat exchangers performance evaluation. The heat duties in the test data between the hot side and the cold side almost matched together for all heat exchangers, indicating that the estimation of flow rates and gas compositions were reasonable.

For HEX300 and HEX320, the model results fairly agree with the averaged heat duty with some conservative numbers. These heat exchangers will have some margin for the thermal performance. However, HEX000 test data showed more than 50% lower heat duty than it was expected by the model, showing that the heat exchanger seemed to be underperforming at this test condition. This may be because the heat duty was too low. Compared to the heat exchanger specifications, the heat duty based on the test data is only 50 W which is less than one tenth of the specification (600 W). Small errors of TC reading and the flow rate estimation from GC analysis could lead such a discrepancy in the thermal performance. Further investigation for HEX000 thermal performance will be required at a higher power output operation.

For the pressure drops, all test data except for HEX320 cold side pressure drop showed a good agreement with the model results. Only HEX320 cold side was 17 % higher than it was expected. This means that the heat exchanger will not meet the target pressure drop requirement in the design point operation. However, there would be little impact on the power plant operation since the additional pressure drop should be only around 0.2 kPa, and the anode blower has an adequate margin to compensate for this additional pressure drop. Overall, the anode heat exchangers operated as expected, and will be able to meet the requirements for the design point.

Table 7-5: HEX300 Evaluation Results

	Test Data	Model Results	Discrepancy %
Hot Side Flow Rate g/s	7.39	7.39	
Cold Side Flow Rate g/s	6.69	6.69	
Hot Inlet Temp. C	772.8	772.8	
Hot Outlet Temp. C	586.1	585.7	0.1%
Cold Inlet Temp. C	494.1	494.1	
Cold Outlet Temp. C	714.4	697.1	2.5%
Hot Side Heat Gain kW	2.37	2.36	0.1%
Cold Side Heat Gain kW	2.58	2.36	9.2%
Average Heat Gain kW	2.47	2.36	4.6%
Hot Side Pressure Drop kPa	0.52	0.56	-7.5%
Cold Side Pressure Drop kPa	0.62	0.68	-9.3%
UA W/C	33.4	28.34	18.0%
LMTD C	74.0	83.43	

Table 7-6 HEX320 Evaluation Results

	Test Data	Model Results	Discrepancy %
Hot Side Flow Rate g/s	7.39	7.39	
Cold Side Flow Rate g/s	7.04	7.04	
Hot Inlet Temp. C	586.1	586.1	
Hot Outlet Temp. C	385.8	400.4	-3.6%
Cold Inlet Temp. C	314.2	314.2	
Cold Outlet Temp. C	532.5	512.3	3.9%
Hot Side Heat Gain kW	2.40	2.22	8.2%
Cold Side Heat Gain kW	2.46	2.22	10.8%
Average Heat Gain kW	2.43	2.22	9.5%
Hot Side Pressure Drop kPa	0.56	0.56	-0.3%
Cold Side Pressure Drop kPa	0.81	0.70	17.2%
UA W/C	39.1	27.79	40.5%
LMTD C	62.2	79.84	

Table 7-7: HEX000 Evaluation Results

	Test Data	Model Results	Discrepancy %
Hot Side Flow Rate g/s	6.25	6.25	
Cold Side Flow Rate g/s	0.54	0.54	
Hot Inlet Temp. C	385.8	385.8	
Hot Outlet Temp. C	381.1	374.1	1.9%
Cold Inlet Temp. C	266.2	266.2	
Cold Outlet Temp. C	310.1	366.3	-15.4%
Hot Side Heat Gain kW	0.05	0.12	-59.5%
Cold Side Heat Gain kW	0.05	0.12	-57.2%
Average Heat Gain kW	0.05	0.12	-58.3%
Hot Side Pressure Drop kPa	0.17	0.22	-20.3%
Cold Side Pressure Drop kPa	0.03	0.03	3.9%
UA W/C	0.51	2.23	-77.1%
LMTD C	93.9	51.66	

Turbocharger High Temperature Performance Test

The air-driven type anode blower has been used to recirculate the anode gas in the breadboard testing. Figure 7-14 shows the blower speed and the pressure rise as a function of time during 6.5 kW stack output power using natural gas. The blower speed was controlled by the air supply flow rate to meet the required performance. The blower speed was controlled at 85,000 rpm to provide 7.0 g/s anode gas with 8.5 kPa pressure rise to the anode loop. From this figure, the blower was found to be operating in stable condition. Small fluctuations shown in this figure is due to the air flow control to keep a steady state operation. Table 7-8 shows the blower test data

compared with the target requirements at 25 kW EOL. The anode recirculation flow rate was found to be much larger than the expected one at this power output level (6.5 kW) and similar to the target requirements. Figure 7-15 shows the estimated blower curve based on the component level test data with the test data and the target requirement. As shown in this figure, the actual flow rate provided by the blower at this operating condition was expected to be about 0.35 m^3/s (17 g/s) which is much larger than the flow rate 0.14 m^3/s (7.0 g/s) recirculated in the anode loop. In other words, more than half of the flow should be bypassing through the blower bypass loop. Thus, the air-driven blower will be able to supply the enough flow rate at the target 25 kW EOL condition. The detailed investigation including the blower efficiency, the tear down analysis, etc. should be conducted after achieving the 25 kW operation and the durability test.

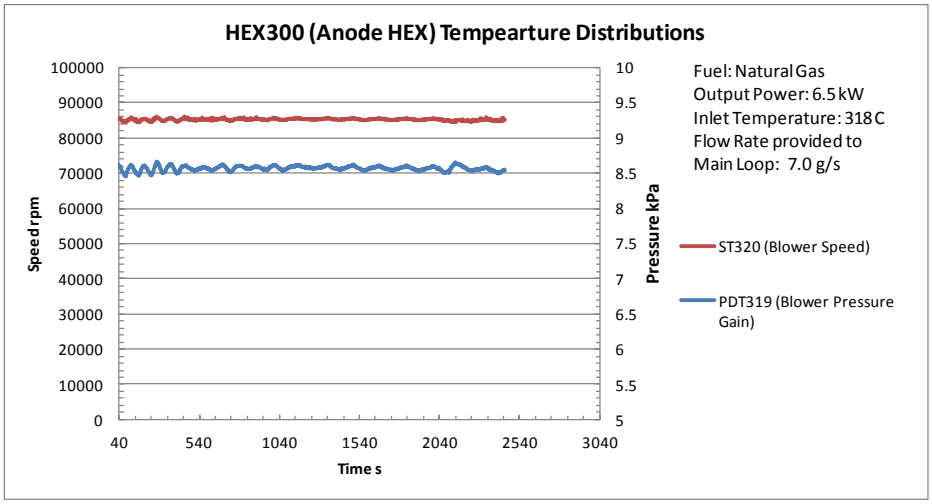

Figure 7-14: Anode Blower Speed and Pressure Rise in the Breadboard

Table 7-8: Blower Test Data and Target Requirements

	Test Data	Target Requirement
Flow Rate g/s	7.0	8.3
Pressure Rise kPa	8.65	9.21
Inlet Temperature C	318	370
Inlet Pressure kPa	94.5	105.1
Gas Density kg/m^3	0.49	0.498

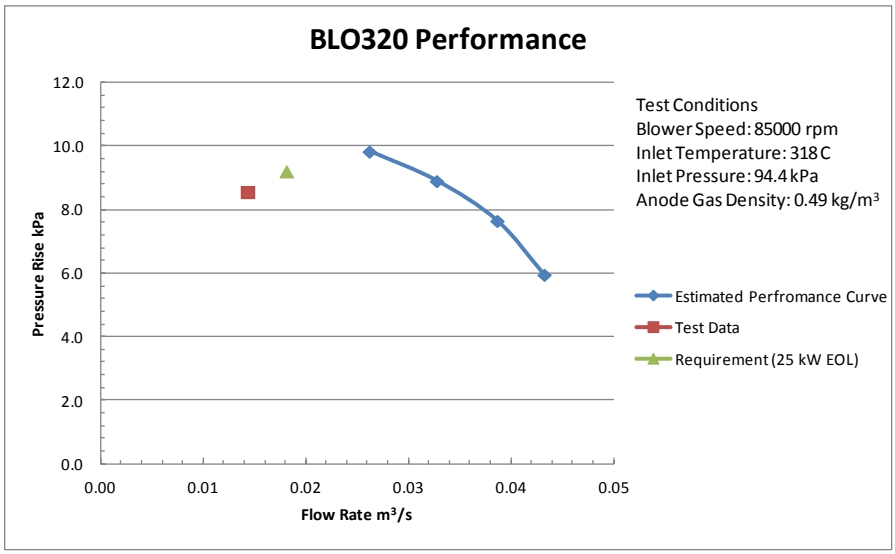

Figure 7-15 Anode Blower Flow Rate vs. Pressure Rise

During the natural gas testing, the breadboard had a lubrication oil leak from the anode blower. Although the power plant showed no difference in the operation before and after the oil leak, the team decided to shut down the power plant to avoid risks from oil contamination in the anode loop as the oil seal failure in the bearing housing was suspected as one of the cause of the issue. After the shut down, the investigation was conducted and showed that the oil return hose was cracked near the hose band at the exit of the oil outlet nozzle of the bearing housing as shown in Figure 7-16. It was found that the oil leaked from the crack. The cause of this crack was extra stress on the hose at relatively high temperature. The hose might be too much tightened by the hose cramp, and was pulled strongly with some angle to connect with the oil tank located on the floor, which caused the extra stress. The hose was replaced with a hose used in the high temperature blower test rig with a stress relief strap. It would be recommended to use a metal braid hose for the future endurance testing. Bore scope inspection inside the anode loop was also conducted just in the case that the leak occurred in the blower. It was found that the pipe inner surface was clean and there was no evidence of oil leaked.

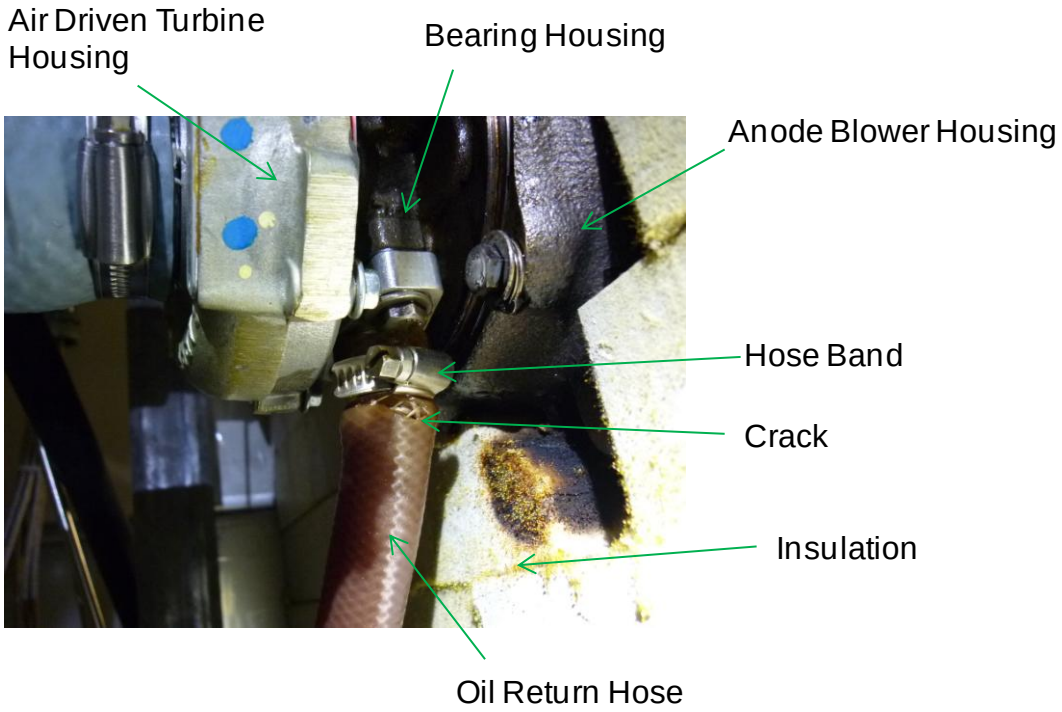

Figure 7-16: Lubrication Oil Leak from Anode Blower

Reformer Development

1 Oct 2011 – 31 Dec 2011

Figure 7-17 shows one of the conceptual designs. In this design, the incoming natural gas is mixed with the anode recycle stream. This mixed feed is then passed through the HDS system to remove sulfur. The de-sulfurized natural gas is then partially converted to CO, CO_2 and H_2 in the fuel processor.

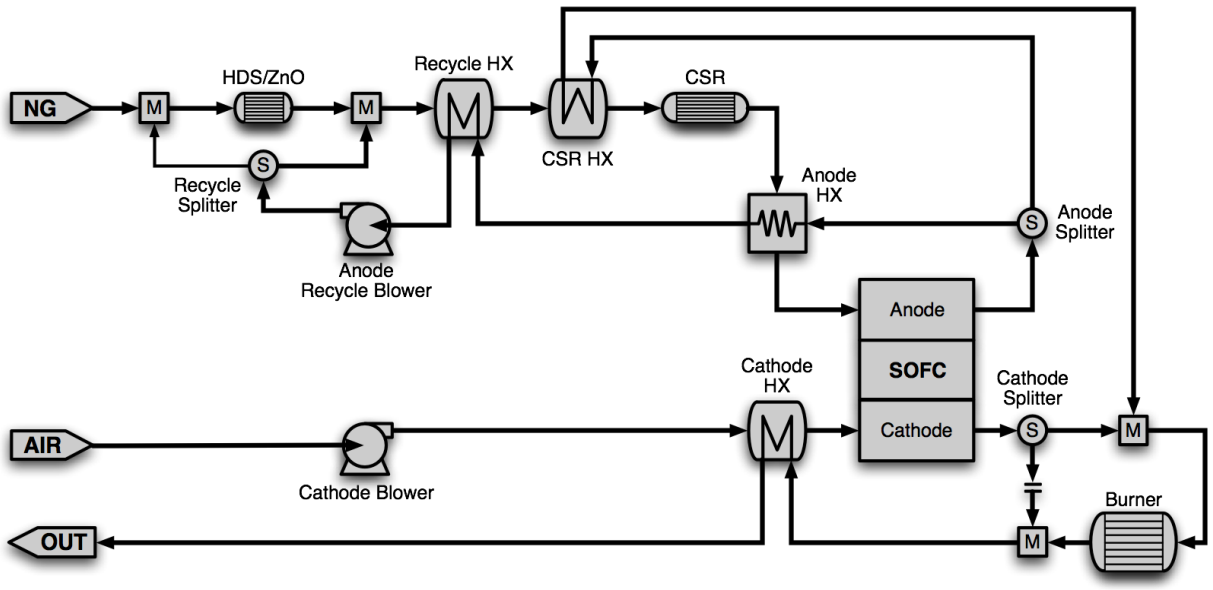

Figure 7-17: Process Flow Diagram for Mono I

There are several fuel reforming technologies such as partial oxidation (CPO), auto-thermal reforming and steam reforming that are available to generate hydrogen for SOFC from natural gas. Due to low tolerance to oxygen by SOFC anode, CPO and ATR can not to be used due to oxygen slip observed as a result of deactivation of reforming catalyst.

Natural gas steam reforming is another option but is not preferred for the breadboard due to concerns with coking at lower S/C ratios, longer residence times and size constraints. Steam reforming is an endothermic reaction and it is heat transfer limited. UTC is reviewing this and other options for developing a fuel reformer for the SOFC breadboard.

1 Jan 2012 – 31 Mar 2012

During this period three reformer catalysts were tested in an isothermal fixed–bed reactor to down select the catalyst material for the Breadboard reformer. Reforming tests were conducted at various temperatures and steam-to-carbon ratios. Data from the tests were analyzed for kinetics of the partial reforming and methane conversion. Based on the results, UTC Power FPS group recommended the final reformer catalyst selection.

1 Apr 2012 – 30 Jun 2012

Figure 7-18 shows the Duo P concept which was selected as the final configuration based on high scores for system efficiency, system reliability, controllability, development cost and cost of

future product. The Duo P design consists of a fuel system with a hydro-desulfurizer (HDS) that removes sulfur from the in-bound natural gas and a pre-reformer that converts some of the natural gas into H_2. There are three heat exchangers in the fuel system to facilitate heat recovery from the hot anode exhaust gas. A recycle blower is used to recycle some of the anode exhaust to ensure (a) heat recovery and (b) higher overall utilizations and hence higher system efficiency. The cathode system consists of a catalytic burner that is used on start-up to heat the system using a slip stream of H_2. During steady state operation the catalytic burner burns unconsumed fuel in the anode exhaust and uses the heat generated to maintain higher operating temperatures as well as facilitate exhaust management. Finally, there is a heat exchanger downstream of the catalytic burner to facilitate heat recovery from the exhaust gas exiting the power plant.

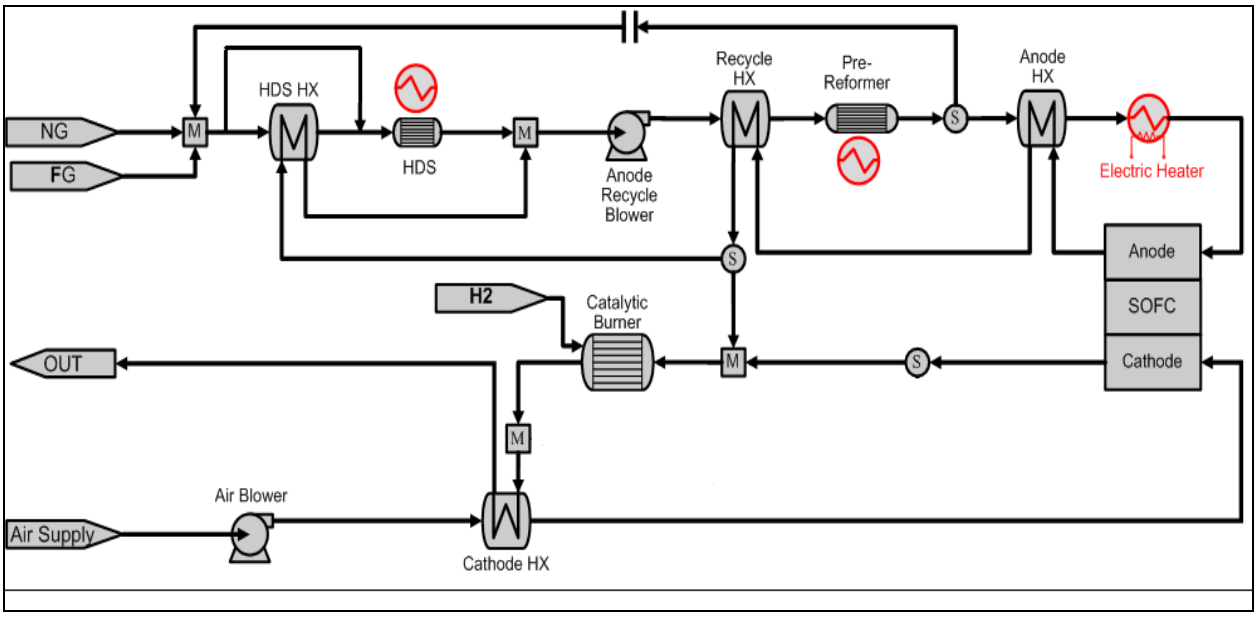

Figure 7-18: Process Flow Diagram for Duo P

Reformer performance testing:

During the second phase of testing with four stacks, pre-reformer performance was going to be tested at various power levels from 2kW-25kW. However due to intermittent program shutdown, pre-reformer performance was just evaluated at 6.5kW. The complete transition from 50-50 gas to natural gas was achieved in steps. Table 7-9 shows the summary of gas composition taken at the inlet and outlet of the pre-reformer after transition and at 6.5kW power.

Table 7-9: Summary of Pre-reformer operating conditions and GC results

Components		Sample1		Sample2		Sample3	
Composition		Inlet	Outlet	Inlet	Outlet	Inlet	Outlet
Dry in %	H2	16.46	32.86	19.64	35.64	18.28	30.43
	N2	5.59	4.30	5.42	5.01	5.10	8.25
	CO	5.32	4.80	8.02	6.19	8.66	5.72
	CO2	64.69	56.05	59.67	51.58	60.73	54.46
	CH4	7.93	1.99	7.25	1.58	7.24	1.14
$\emptyset_{Reformer}$,%		75%		79		85	

From above table it can be seen that, at 6.5kW power level, GC samples 1, 2 and 3 shows that pre-reformer was converting way more than 20% methane. This anomalous behavior of pre-reformer was may be due to lack of control on the steam/CH4 ratio in the recycle loop or may be due to the very high recycle ratio than anticipated at certain speed of the BLO320. The Steam/CH_4 ratio requirement to achieve at least 20% methane conversion is around 3.5. Higher Steam/CH_4 ratios lead to higher conversion. The dew point sensor was predicting about 62% steam content. The equilibrium model was used to predict the amount of steam present in the recycle loop to simulate the methane conversion of 80% as seen in sample 2 of Table 7-10.

Table 7-10: Simulated gas sample composition using equilibrium model

Components		Wet Simulated Sample 2		Dry Simulated sample 2	Dry sample 2 as per Table 5.4.3.1-1
Composition		Inlet	Outlet	outlet	
	H2	5.31	14	35.7	35.64
	N2	1.80	1.7	4.33	5.01
	CO	1.72	1.24	3.18	6.19
	CO2	20.87	21.52	55.12	51.58
	CH4	2.56	0.616	1.6	1.58
	H2O	**67.7**	61	0.0	

Table 7-10 shows the comparison of gas sample 2 and simulated gas sample. It can be seen that clearly there is very good match between the dry simulated outlet gas sample and dry sample from Table 7-9. Therefore it can be assumed that there was roughly 68% steam in the recycle loop which gives the Steam/CH4 ratio of 26. This explains very high conversion of methane than anticipated conversion of 20%.

Very high amount of residual steam in the recycle loop was due to the transition from 50-50 gas to natural gas. From above test data it can be concluded that during transition from 50-50 gas to natural gas, controlling the steam to CH_4 ratio is very difficult and much better steam control strategy should be developed.

System Integration

1 Oct 2011 – 31 Dec 2011

In Phase II, UTC Power will fabricate a 25 kW class breadboard power plant with all MBOP components required to demonstrate thermal self-sufficiency with focus on three key components with high technical risk; the high temperature heat exchangers, the catalytic burner and the high temperature anode recycle blower. Cost reduction of the MBOP components is very important to be considered in the conceptual design for future commercialization of SOFC power plans. UTC Power will focus design and analysis activities on the cost effective MBOP components.

In the initial conceptual design, MBOP components have been studied based on 200 kW Mono I system. For the breadboard design, however, the heat exchangers and the catalytic burner will be designed for the 25 kW system based on the conceptual design. The heat exchangers and the catalytic burner will be evaluated through breadboard testing for future large scale power plant design. These components should be relatively easy to scale-up. However, the anode recycle blower will be designed for a larger scale power plant and used with flow bypass on the breadboard due to the difficulty of future scale-up.

1 Jan 2012 – 31 Mar 2012

In Phase II, UTC Power will fabricate a 25 kW class breadboard power plant with all MBOP components required to demonstrate thermal self-sufficiency with focus on three key components with high technical risk; the high temperature heat exchangers, the catalytic burner and the high temperature anode recycle blower. Cost reduction of the MBOP components is very important to be considered in the conceptual design for future commercialization of SOFC power plans. UTC Power will focus design and analysis activities on the cost effective MBOP components.

In the initial conceptual design, MBOP components have been studied based on 200 kW Mono I system. For the breadboard design, however, the heat exchangers and the catalytic burner will be designed for the 25 kW system based on the conceptual design. The heat exchangers and the catalytic burner will be evaluated through breadboard testing for future large scale power plant design. These components should be relatively easy to scale-up. However, the anode recycle blower will be designed for a larger scale power plant and used with flow bypass on the breadboard due to the difficulty of future scale-up.

1 Apr 2012 – 30 Jun 2012

In support of the design of a 250–1000 kW SOFC Power Module, UTC Power is designing and building a 25kW breadboard that shall demonstrate thermally self-sustained operation and 3000 hours of system level endurance operation (1500 hours as part of Phase II). UTC Power performed conceptual trade-studies of 18 different system concepts for the SECA Phase II

breadboard and selected the Duo P concept as the final configuration based on high scores for system efficiency, system reliability, controllability, development cost and cost of future product. The team has completed the conception and preliminary design of a 25 kW breadboard based on the Duo P concept. A critical part of the design was related to identifying and/or designing all critical balance of plant for the breadboard. Some of the components such as the desulfurizer, fuel reformer, anode heater and anode recycle blower were designed in-house by leveraging UTC Power's expertise/prior experience in these areas. Other components were sourced from qualified UTC suppliers.

1 July 2012 – 30 September 2012

The Phase II 25 kW class breadboard power plant was fabricated with all Mechanical Balance of Plant (MBOP) components required to demonstrate thermal self-sufficiency with a focus on four key components with high technical risk:

- High temperature heat exchangers
- Catalytic burner
- High temperature anode recycle blower
- Anode inlet pre-heater

Cost reduction of the MBOP components is very important for future commercialization of SOFC power plans. UTC Power has focused its design and analysis activities on cost effective MBOP components. The component selection and development has been conducted based on UTC Power's stage-gated product development process.

During this quarter, all MBOP components including the key components were successfully installed into the breadboard power plant. This includes six heat exchangers, a catalytic burner, the anode recycle blower, the anode inlet heater, valving, the fuel processing train and instrumentation. For the high temperature anode recycle blower, the air-driven turbo charger type, which was the backup blower in the original plan, was installed instead of the motor-driven turbo charger type due to the failure of bearings during the testing. The motor-driven turbo charger effort has been put on-hold to preserve resources for breadboard testing.

1 Oct 2012 – 31 Dec 2012

During this quarter, initially, un-insulated Breadboard was integrated with the test stand. Subsequent to successfully completing the Breadboard and test stand checkout, the Breadboard was disconnected, removed from the test room, insulated and was integrated back with the test stand. Stack module with Delphi's debug stack was integrated with the Breadboard and remainder of the insulation work was completed. Subsequently, the Breadboard with the debug stack was tested with 50/50 H2/N2 and Natural Gas.

SECA Coal-Based Systems – UTC Power

1 Jan 2013 – 31 Mar 2013

After the Breadboard testing with debug stack was completed in early January, the debug stack was removed from the manifold. Delphi installed four new stacks and completed integration and end-to-end checks for the stack module before proceeding with Breadboard verification testing.

During the four stack installation period, test stand controller software was updated with lessons learned from debug stack testing.

Results and discussions:

Many milestones were achieved as part of the 25 kW SOFC Breadboard system integration during Phase II. The test stand from Phase I was upgraded to accommodate Natural Gas operation and successfully checked out. A new load bank was purchased and integrated into the test stand. The GC gas sampling system was upgraded to accommodate sample lines from the Breadboard, in addition to the sample lines from the stack module.

The Breadboard assembly was aligned and integrated inside the test stand twice: un-insulated and insulated. Figure 7-19 shows the installed configuration of the insulated Breadboard along with the stack module in the test room.

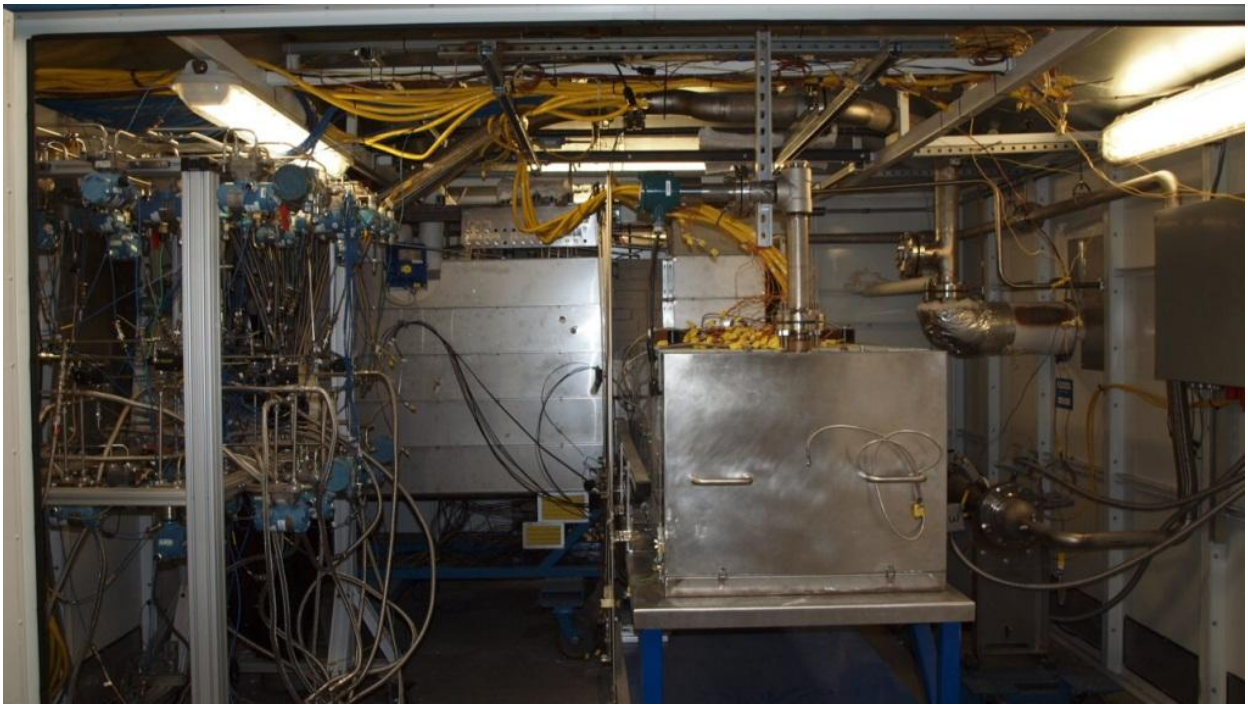

Figure 7-19: Installed Configuration of 25 kW SOFC Breadboard

Conclusion:

The objective in Phase I was to develop the concept design for a 250-1000 kW power module and the objective in Phase II was to perform the engineering design and build a 15-25 kW thermally self-sustaining system based on integrating stacks and balance of plant components into a breadboard.

During Q2 and Q3 2012 the Phase I test stand was upgraded to support 25 kW SOFC Breadboard power plant operation on natural gas. UTC Power team successfully designed and integrated the Breadboard and SOFC stack module inside the test stand in Q3 2012.

The following lessons were learned during the system integration tasks

1. Breadboard insulation process is laborious and time consuming
    a. Opportunities for improvement: Optimize system design to achieve box-type insulation, similar to CSA hot box. This warrants a trade study to evaluate heat loss and thermal interactions of components for optimal design
2. Structural analysis conclusions for bellows design unverified
    a. Breadboard was finally designed with one bellow between cathode heat exchangers. Six of seven bellows from concept design were removed subsequent to structural analysis during detailed design phase. However, due to limited testing and lack of multiple thermal cycles, the bellow design remains unverified.

In spite of limited testing time and data, the 25 kW Breadboard design, integration and operation has provided some key lessons that can be leveraged in a product-level design for SOFC-based stationary power plants.